# TRACTION DRIVES FOR ZERO STICK-SLIP ROBOTS, AND REACTION FREE, MOMENTUM BALANCED SYSTEMS

FINAL REPORT

for

NASA LEWIS RESEARCH CENTER

CONTRACT NAS 3-26897

by

WILLIAM J. ANDERSON

and

WILLIAM SHIPITALO

NASTEC, INC.

and

WYATT NEWMAN

DEPARTMENT OF APPLIED PHYSICS & EE

CASE WESTERN RESERVE UNIVERSITY

DECEMBER 1995

NASTEC, INC.

CORPORATE OFFICES:
1111 Ohio Savings Plaza
1801 East Ninth Street
Cleveland, OH 44114
(216) 696-5157
FAX (216) 781-8688

ENGINEERING & DESIGN CENTER
5310 Weat 161st. Street
Suite G
Brook Park, OH 44142
(216) 433-1555

## TABLE OF CONTENTS

## SUMMARY

Two differential (dual input, single output) drives (a roller-gear and a pure roller), and a momentum balanced (single input, dual output) drive (pure roller ) were designed, fabricated, and tested. The differential drives are each rated at 295 rad/sec (2800 rpm) input speed, 450 N-m (4,000 in-lbf) output torque. The momentum balanced drive is rated at 302 rad/sec (2880 rpm) input speed, and dual output torques of 434N-m (3840 in-lbf). The Dual Input Differential Roller-Gear Drive (DC-700) has a planetary roller-gear system with a reduction ratio (one input driving the output with the second input fixed) of 29.23:1. The Dual Input Differential Roller Drive (DC-500) has a planetary roller system with a reduction ratio of approximately 24:1. Each of the differential drives features dual roller-gear or roller arrangements consisting of a sun, four first row planets, four second row planets, and a ring. The Momentum Balanced (Grounded Ring) Drive (DC-400) has a planetary roller system with a reduction ratio of 24:1 with both outputs counterrotating at equal speed. Its single roller cluster consists of a sun, five first and five second row planets, a roller cage or spider and a ring. Outputs are taken from both the roller cage and the ring which counterrotate. Test results reported for all three drives include angular and torque ripple (linearity and cogging), viscous and Coulomb friction, and forward and reverse power efficiency.

Of the two differential drives, the Differential Roller Drive had better linearity and less cogging than did the Differential Roller-Gear Drive, but it had higher friction and lower efficiency (particularly at low power throughput levels). Use of full preloading rather than a variable preload system in the Differential Roller Drive assessed a heavy penalty in part load efficiency. Maximum measured efficiency (ratio of power out to power in) was 95% for the Differential Roller-Gear Drive and 86% for the Differential Roller Drive.

The Momentum Balanced (Grounded Ring) Drive performed as expected kinematically. Reduction ratios to the two counterrotating outputs (design nominal=24:1) were measured to be 23.98:1 and 24.12:1 at zero load.. At 250Nm (2200 in-lbf) output torque the ratio changed 2% due to roller creep. This drive was the smoothest of all three as determined from linearity and cogging tests, and maximum measured efficiency (ratio of power out to power in) was 95%. The disadvantages of full preloading as compared to variable preload were apparent in this drive as in the Differential Roller Drive. Efficiencies at part load were low, but improved dramatically with increases in torque. These were consistent with friction measurements which indicated losses primarily from Coulomb friction. The initial preload level setting was low so roller slip was encountered at higher torques during testing.

## SYMBOLS

| | |
|---|---|
| a | contact ellipse semi-major axis, mm (in.) |
| b | contact ellipse semi-minor axis, mm (in.) |
| A, a | roller or gear radii, mm (in.) |
| $x_1$ | |
| $x_2$ | |
| $y_1$ | |
| c | |
| C | spline pitch diameter, mm (in.) |
| D | diameter, mm (in.) |
| d | |
| E | modulus of elasticity, GPa, (psi) |
| F | tangential force, N (lbs) |
| f | coefficient of friction |
| G | shear modulus of elasticity, GPa (psi) |
| H | high speed shaft |
| H1 | inner high speed shaft |
| H2 | outer high speed shaft |
| I | moment of inertia, $mm^4$ ($in^4$) |
| J | polar moment of inertia, $mm^4$ ($in^4$) |
| K | stiffness, Nm/rad (inlbf/rad) |
| L | low speed shaft |
| | length, mm (in.) |
| $L_1$ | inner low speed shaft |
| $L_2$ | outer low speed shaft |
| l | length, mm (in.) |
| N | number of gear teeth |
| | normal load, N, (lbs) |
| P | power, watts (inlbf/sec) |
| | gear pitch |
| R | cluster ratio with carrier or cage stationary |
| | ratio, drive |
| S | stress, $N/m^2$ (psi) |

| | |
|---|---|
| $T, \tau$ | torque, Nm (in-lbf) |
| $\alpha$ | angular acceleration, rad/sec/sec |
| $\delta$ | deflection, mm (in.) |
| $\eta$ | efficiency, dimensionless |
| $\mu$ | traction coefficient, dimensionless |
| $\omega$ | angular velocity, rad/sec (rpm) |
| $\sigma$ | stress, GPa (ksi) |
| $\theta$ | angle, rad (deg) |

**Subscripts**

| | |
|---|---|
| B | bending |
| c | cage or carrier |
| | compressive |
| GR | grounded ring |
| H | high speed shaft |
| H1 | inner high speed shaft |
| H2 | outer high speed shaft |
| i | input |
| | element no. |
| L | low speed shaft |
| $L_1$ | inner low speed shaft |
| $L_2$ | outer low speed shaft |
| o | output |
| P | planet roller |
| R | ring roller |
| r | reaction |
| s | sun roller |
| | shear |
| T | tangential |
| x,y | coordinate directions |
| $\theta$ | torsional |
| 1P | first row planet roller |
| 2P | second row planet roller |
| 1,2 | cluster number |

# INTRODUCTION

Stick-slip problems associated with starts and stops of motors which drive robotic joints and servomechanisms in both terrestrial and spatial applications could significantly penalize the performance of such mechanisms. Control systems are not able to cope with sudden changes from static to dynamic friction without compromises in performance. Differential transmissions with continuously rotating dual inputs and the capability of providing forward, zero, and reverse output rotation should make possible improved robotic performance.

Planetary traction drives which provide smooth, backlash free torque transfer with low levels of torque ripple and noise [1][1] are ideal for such applications. In [2] two types of robotic positioner and dynamic experiment drives were investigated for use in systems which require mantenance of torque and/or angular momentum balance. Planetary traction drives which provide dual, counterrotating, matched output speeds only if the torques are equal were termed "torque matched" drives . Drives which provide dual, counterrotating, matched output speeds regardless of the output torques were termed "speed matched" drives. Geometries and sizes, kinematic, efficiency and fatigue life analyses for two torque matched drives, as well as feasibility studies of two speed matched drives were completed in [2]. In [3] designs of two speed matched drives were completed and compared with the torque matched drives designed in [2]. The torque and speed matched drives were compared on the basis of size, weight, efficiency, and fatigue life. Dual input differential drive configurations were also investigated in [3] for use as a robotic transmission requiring smooth motion transfer without stick-slip irregularities. A concept incorporating dual clusters was chosen as least risky for detail design, fabrication, and test.

The objectives of this investigation were to:

1. Complete detailed designs and manufacturing drawings for two versions of a dual input differential drive (one pure roller, and one roller-gear) with a nominal ratio of 24:1.

2. Fabricate, assemble, and check out the roller and roller-gear differential drives.

3. Complete detailed design and manufacturing drawings for a dual counterrotating output, momentum balanced roller drive with a nominal ratio of 24:1.

4. Fabricate, assemble, and check out the momentum balanced roller drive.

5. Design, fabricate, and check out a test facility for experimentally evaluating the linearity, friction, efficiency, and cogging of the two differential drives and the momentum balanced drive.

---

[1] Numbers in brackets refer to references.

6. Experimentally evaluate the linearity, friction, efficiency and cogging of all three drives.

7. Prepare a report which includes all pertinent design information, all pertinent test results, an analysis of the results, and an evaluation of each of the drives.

## DRIVE DESIGNS

### DUAL INPUT DIFFERENTIAL ROLLER-GEAR DRIVE (DC-700)

For consistency and ease of comparison with drives previously developed [3,4 and 5], the drives investigated herein were sized for an output torque capacity of 452Nm (4000inlbs), an output speed capability of 120 rpm, and a nominal ratio of 24:1 The finalized geometric arrangement for the Dual Input Differential Roller-Gear Drive is shown in figure 1. Roller-gear cluster 1 has a non-rotating ring roller-gear fixed to the housing, while cluster 2 has a rotating ring roller-gear from which the output is taken. Kinematic operation of the drive, development of roller and gear geometries, key stress and deflection calculations, assembly procedure, and inspection results at assembly will be discussed prior to discussion of test results in a later section.

#### Kinematics

To review briefly the kinematic analysis of [3], the angular velocities of the components are as follows (angular velocities of shafts are assumed positive pointing out of the drive or traansmission):

| | | |
|---|---|---|
| Cluster ratio R: | $R = (N_c / N_{y1})(N_{x1} / N_a)$ | (1) |
| Cage: | $\omega_c = \omega_{H2} / (1-R)$ | (2) |
| Cluster 1: | | |
| 2nd Planet: | $\omega_{2P1} = \omega_{H2} (1-N_c / N_{x2}) / (1-R)$ | (3) |
| 1st Planet: | $\omega_{1P1} = \omega_{H2} (1+N_c / N_{y1}) / (1-R)$ | (4) |
| Cluster 2: | | |
| 2nd Planet: | $\omega_{2P2} = \omega_{H2} [1/(1-R) - (1/(1-R)(R)(N_c / N_{x2})] + (\omega_{H1} / R)(N_c / N_{x2})$ | (5) |
| 1st Planet: | $\omega_{1P2} = \omega_{H2} [1/(1-R) + (1/(1-R)(R)(N_c / N_{y1})] - (\omega_{H1} / R)(N_c / N_{y1})$ | (6) |
| Rotating Ring: | $\omega_{R2} = \omega_o = (\omega_{H2} - \omega_{H1}) / R$ | (7) |

If the inputs $\omega_{H1}$ and $\omega_{H2}$ are of opposite sense, then the output speed will be greater than

either input speed divided by R. Both input torques will be in the direction of the inputs (positive) and there will not be any recirculating power loss. In a robotic application that is not the purpose of employing a differential, so that will not be the mode of operation.

When $\omega_{H1}$ and $\omega_{H2}$ are of the same sense, then the output speed will be less than the greater input speed divided by R. One of the two input torques will be negative (that input will be a power absorber or brake rather than a driver). There will then be a recirculating power loss. This will be the operating mode of the differential drive. It will be used with two unidirectional variable speed inputs to produce low magnitude bidirectional output speeds, with a non-rotating output achievable without having to stop either input. This eliminates the stick-slip uncertainties associated with starts and stops.

The input power to the drive (disregarding signs) will be

$$P_i = \omega_{H2} T_{H2} + \omega_{H1} T_{H1} \qquad (8)$$

For equilibrium of the cage or planet carrier

$$T_{H2}(R-1) = -T_{H1}(R-1) \qquad (9)$$

Equation (9) confirms that one of the torques must be negative.

The output power will be

$$P_o = (\omega_{H2} - \omega_{H1}) T_{1i} \qquad (10)$$

The efficiency (neglecting friction losses) will be

$$\eta = (1 - \omega_{H1} / \omega_{H2}) / (1 + \omega_{H1} / \omega_{H2}) \qquad (11)$$

Efficiency (as influenced by recirculating power loss, neglecting friction losses) is shown as a function of the ratio of input speeds in figure 2. It illustrates dramatically how the input speeds influence efficiency. From eq. 8 it is obvious that recirculating power losses can be kept low by reducing input speeds when the desired output speed is low or near zero.

For purposes of gear stress calculations (from [3])

$$T_{R1} = -T_{H2} R \quad \text{(reaction torque at non-rotating ring roller-gear)} \qquad (12)$$

$$T_{R2} = -T_{H1} R \quad \text{(output torque)} \qquad (13)$$

The output and reaction torques will be equal to the input torques multiplied by the cluster ratio.

## Cluster Geometry

The Hinge Joint Drive (NA-300A), with a gear system designed by the method presented in [4], and final designed, fabricated, and tested in [5] was considered a candidate gear design for the Dual Input Differential Roller-Gear Drive. Four other gear arrangements were developed using the method of [4] for comparison. These are shown in Table I. Each of the four designs shown is more compact than the Hinge Joint and three of the four have ratios slightly closer to the 24:1 ratio of the Dual Input Differential Roller Drive. However, the smaller diameter sun roller-gears posed a problem with the required hollow configuration of the input side sun roller-gear to allow passage of a quill shaft to the output side sun roller-gear. The roller-gear configuration of the Hinge Joint Drive was therefore chosen for the Dual Input Differential Roller-Gear Drive, since its size permits retrofitting into the same housing as the Dual Input Differential Roller Drive.

Gear data for each of the roller-gear clusters is shown in Table II. A detailed development of the cluster geometry by the method of [4], and calculation of gear stresses by the methods of [6] are presented in APPENDIX A. Data for the rollers which act in conjuncton with the gears is shown in Table III. Rollers are sized to transmit 20% of the torque assuming a traction coefficient of .06 at the sun-first planet contacts. Included in Table III are roller sizes, normal and tangential forces, Hertz contact widths, stresses, amd deformations. Also shown are the ring roller radial deflections at the contact points with the second row planets, and inner fiber stress resulting from ring bending [7].

The quill shaft through which torque is inputted to the output side sun roller-gear must pass through the input side sun roller-gear (see figure 1). This results in some thin sections and potentially adverse stress conditions. Stress studies were made of the quill shaft and splines, as well as roller fits to establish that stress and deflection conditions were satisfactory. A summary of the calculations is presented in APPENDIX B.

It was not necessary to make stress calculations for parts other than the gears and rollers which comprise the clusters, and the sun roller-gears, quill shaft, and splines.

## Drawings

The Dual Input Differential Roller-Gear Drive is defined by assembly drawing DC-700. Individual parts are detailed on drawings DC-700-01 through DC-700-36. Each of the part drawings provides complete material and processing information necessary for manufacture.

The Assembly Fixture is defined by drawings DC-700-37, DC-700-39 and DC-700-40.

## Assembly

**Assembly Procedure**.- Prior to completion of parts fabrication, an Assembly Procedure was worked out. During and after assembly it was modified to incorporate the changes that hands on experience indicated would facilitate easier assembly. The revised Assembly Procedure is given in APPENDIX C.

**Assembly Notes**.- Measurements were made between pins on the Ring Gears (print dimension is 9.2981/9.3010in.)

| | | |
|---|---|---|
| Ring Gear No. 1 | | |
| Short dowel side: | 9.2989 | |
| | 9.2983 | |
| | 9.2986 | average |
| Long dowel side: | 9.2994 | |
| | 9.2992 | |
| | 9.2993 | average |
| Overall average | 9.29895 | |
| | | |
| Ring Gear No. 2 | | |
| Short dowel side: | 9.2988 | |
| | 9.2985 | |
| | 9.2993 | |
| | 9.2989 | average |
| Long dowel side: | 9.2985 | |
| | 9.2985 | |
| | 9.2981 | |
| | 9.2984 | average |
| Overall average | 9.29865 | |

Both Ring Gears were within print.

Roller-gear clusters assembled quite easily, following the Assembly Procedure and using the Assembly Fixtures, to the point of mounting the ring gear. That proved to be very difficult. When finally assembled, the cluster was so tight it couldn't be rotated. At that point the ring

gear was removed for detailed measurements of all gears. Measurements over pins were made on sun gears, first planet pinions, first planet gears, and second planet gears. All of these gears had been nitrided. Results of the measurements were as follows:

a) Sun "a" gears (print dimension .9768/.9757in.)
Both sun gears measured .9772in. (.0004in. over the high limit).

b) First planet "y1" pinions (print dimension .8423/.8414in.)
Measurements on the sixteen pinions ranged from .8418 to .8426in. (-.0005 to +.0003in. relative to the high limit).

c) First planet "x1" gears (print dimension 1.9961/1.9947in.)
Measurements on the eight gears ranged from 1.9968 to 1.9978in. (+.0007 to +.0017 relative to the high limit).

d) Second Planet "x2" Gears (print dimension 3.6975/3.6963in.)
Measurements on the eight dual gears ranged from 3.6977 to 3.7000in. (+.0002 to +.0025 relative to the high limit).

It was obvious from these measurements that the gears had grown from the nitriding. Not checking the pin dimensions after nitriding was a costly error. Growth of the "a" and "y1" gears was minimal, and they were accepted. The "x1" and "x2" gears were sent back to the gear shop for rework. The "x1" rollers had to be destructively removed by EDM, and made over again after reworking the gears. Assembly was stopped for the rework, and was resumed after a ten day delay.

Gear measurements after rework are shown on Table IV. Also shown are the Index Errors between the "y1" and "x1" gears (these were measured at the gear shop), and the cluster (#1 or 2) into which each planet and ring gear was assembled.

Roller measurements, taken earlier, are shown on Table V. All roller diameters were within print dimension limits.

The location of all planet roller-gears in both clusters is shown in Figures 3a and 3b.

After the gear rework, assembly went smoothly (ring gears went on easily) up to the point of shrinking the ring rollers into place in the two roller clusters. After the ring rollers were in

place, we noted gear cogging. There were eighteen well defined cogs per revolution of either input, indicating that the ax1 mesh was bottoming. We decided to continue assembly to ascertain that no other problems existed, and then to do detailed calculations of backlashes in all the gear meshes (based on actual pin measurements), and to recheck the ring roller fitup over the planet rollers.

Assembly was completed and 20oz of Santotrac 50 was installed. The drive was run at speeds to 660 rpm on the Bridgeport, with each input driven separately in both forward and reverse. No torque was applied to the output. The drive functioned satisfactorily

Assembled weight was 120 lbs.

**Post Assembly.**- Backlash levels were calculated based on measurements over pins without considering compression of the cluster due to roller preloading. Values of backlash for operation at the theoretical pitch circle were as follows:

| | |
|---|---|
| ax1 mesh: | .0009 min. to .0018in. max. |
| y1x2 mesh | .0016 min. to .0018in. max. |
| y2c mesh | .0021 min. to .0022in. max. |

These seem to be satisfactory, although four of the eight ax1 meshes were .001in. or less, which is too tight prior to roller preloading.

Next the ring roller fitup was chcked using actual roller measurements. Roller load, contact stress, and deflection data are shown on Table VI. It was found that the ring roller inside diameter was .004in. too small for a roller compression capable of transmitting 20 percent of the rated torque. The major source of gear cogging appears to be the error in ring roller fitup. It was decided to increase the inside diameter of the ring rollers to achieve, by trial and error if necessary, the ring roller fitup that allows cog-free gear action.

Ring Rollers were reworked to 9.3730/9.3734 in. but gear action was still a little tight so the dimension was reset to 9.3740/9.3744 in. With that Ring Roller fitup, gear action was cog free and smooth. Only an occasional slight catch was felt when the Sun Roller/-Gear was rotated by hand. The final Ring Roller diameter corresponds to a roller torque level of 12 to 14 percent.

## DUAL INPUT DIFFERENTIAL ROLLER DRIVE (DC-500)

The Dual Input Differential Roller Drive was also sized for an output torque capacity of 452Nm (4000inlbs), an output speed capability of 120 rpm, and a nominal ratio of 24:1 The finalized geometric arrangement for the Dual Input Differential Roller Drive is shown in figure 4. Roller cluster 1 has a non-rotating ring roller fixed to the housing. The sun roller of cluster 1 is directly driven from an external spline connection., Cluster 2 has a rotating ring roller from which the output is taken. Its sun roller is driven by a quill shaft which passes through the cluster 1 sun roller. The cluster carrier and both sets of planet rollers orbit as a solid body, although the angular velocities of the two sets of first and second row planet rollers can be, and usually are, quite different.

Kinematic operation of the drive, development of roller geometries, key stress and deflection calculations, assembly procedure, and inspection results at assembly will be discussed prior to discussion of test results in a later section.

### Kinematics

The kinematic analysis of the Dual Input Differential Roller Drive (presented originally in [3]) closely parallels that of the Dual Input Differential Roller-Gear Drive with roller radii used in place of numbers of gear teeth. The angular velocities of the components then become as follows:

| | | |
|---|---|---|
| Cluster ratio R: | $R = (c/y_1)(x_1/a)$ | (14) |
| Cage: | $\omega_c = \omega_{H2} / (1-R)$ | (15) |
| Cluster 1: | | |
| 2nd Planet: | $\omega_{2P1} = \omega_{H2}(1-c/x_2)/(1-R)$ | (16) |
| 1st Planet: | $\omega_{1P1} = \omega_{H2}(1+c/y_1)/(1-R)$ | (17) |
| Cluster 2: | | |
| 2nd Planet: | $\omega_{2P2} = \omega_{H2}[1/(1-R) - (1/(1-R)(R)(c/x_2)] + (\omega_{H1}/R)(c/x_2)$ | (18) |
| 1st Planet: | $\omega_{1P2} = \omega_{H2}[1/(1-R) + (1/(1-R)(R)(c/y_1)] - (\omega_{H1}/R)(c/y_1)$ | (19) |
| Rotating Ring: | $\omega_{R2} = \omega_o = (\omega_{H2} - \omega_{H1}) / R$ | (20) |

As previously discussed for the Dual Input Differential Roller-Gear Drive, if the inputs $\omega_{H1}$ and $\omega_{H2}$ are of opposite sense, then the output speed will be greater than either input speed divided by R. Both input torques will be in the direction of the inputs (positive) and

there will not be any recirculating power loss. In a robotic application that is not the purpose of employing a differential, so that will not be the mode of operation.

When $\omega_{H1}$ and $\omega_{H2}$ are of the same sense, then the output speed will be less than the greater input speed divided by R. One of the two input torques will be negative (that input will be a power absorber or brake rather than a driver). There will then be a recirculating power loss. This will be the operating mode of the differential drive. It will be used with two unidirectional variable speed inputs to produce low magnitude bidirectional output speeds, with a non-rotating output achievable without having to stop either input. This eliminates the stick-slip uncertainties associated with starts and stops.

Equations for input power, output power, torques and efficiency are the same as given for the Dual Input Differential Roller-Gear Drive (equations 8 through 13) As before, efficiency (as influenced by recirculating power loss, neglecting friction losses) is shown as a function of the ratio of input speeds in figure 2.

## Cluster Geometry

Results of the computer program which sizes the rollers and establishes approximate cluster geometry were presented in [3]. Table VII summarizes roller radii and, for the full output torque conditions of 452Nm (4000inlbs.), normal forces, contact ellipse dimensions, Hertz stresses and Hertz compressions. Hertz compressions are required to determine effective roller radii under load and ring roller radii for desired preloading.

Other than the cluster rollers and the quill shaft driving the cluster 2 sun roller, none of the parts are subjected to stress levels that require detailed stress analysis. As shown on Table VII, the ring roller maximum bending stress under full torque conditions is .153GPa (22,200 psi). That stress level precludes the use of a through hardened alloy, so a case carburized steel is used. A stress analysis of the sun roller quill shaft was not done because its geometry and the torque carried are the same as those of the quill shaft in the Dual Input Differential Roller-Gear Drive. That analysis is presented in APPENDIX B.

## Drawings

The Dual Input Differential Roller Drive is defined by assembly drawing DC-500. The assembly drawing includes a listing of commercial parts as well as a listing of all fabricated parts. Individual parts are detailed on drawings DC-500-01 through DC-500-34. The roller drawings include coordinate tables for NC machining and metrology. Each of the part drawings provides complete material and processing information necessary for manufacture.

## Assembly

**Assembly Procedure**.- Prior to completion of parts fabrication, an Assembly Procedure was worked out. During and after assembly it was modified to incorporate the changes that hands on experience indicated would facilitate easier assembly. The revised Assembly Procedure is given in APPENDIX D.

**Assembly Notes.**- Sun and planet rollers were gaged for the record and to ascertain conformance with print dimensions. Gaging was done on an optical comparator. X-coordinates were measured from a shoulder with an estimated accuracy of +/- .001in.. This would make the accuracy of gage diameter measurement approximately +/- .0002in. Measurements are summarized on Table VIII. Sun roller "a" diameters were slightly undersized, varying from -.00035 to -.0008in. First planet "x1" diameters varyed from 0 to +.0003in., and "y1" diameters varied from -.0001 to +.00035in.. Second planet "x2" diameters varied from -.00035 to +.00045in.. These diameters are acceptably consistent.

Cross radius checks were made on selected "y1" and "x2" surfaces. On first planet number 8 the 10.4in. radius was measured as 10.03in. On second planet, stationary ring roller, number 4, plain side, the -14.9in. radius was measured as -14.62in. On second planet, rotating ring roller, number 1, long end, the -14.9in. radius was measured as -15.04in. Overall roller geometries were quite acceptable.

The arrangement of first planet and second planet rollers in the two cluster assemblies is shown in figure 5. Referring to assembly drawing DC-500, the following were measured:

Input side X DIM. = 1.060/1.070in.

Output side X DIM = 1.075/1.085in.

A .010in. span is shown in each because of the difficulty of picking up the point at which solid ring roller contact is made with the second planets.

From these measurements and calculations of second planet-ring roller engagement, the Preload Fitted Shims, DC-500-23, should be as follows for 100% preload:

Input side = .106in.

Output side = .091in.

Problems were immediately encountered in Assembly Procedure steps (20) and (21) in attempting to preload the roller clusters (they became very tight), so we decised to postpone preloading until we could recalculate the relationship between cluster preload (torque capacity) and ring roller shim thickness. Assembly of the roller clusters without shims in place results in a cluster preload level of about 50 percent.

For the input side assembly, Brg Hsg, Input, DC-500-31 and Seal Carrier, DC-500-29 were mated with the Sun Roller and Cluster Carrier bearings without the Input Housing, DC-500-01. This proved easier than working with the entire assembly.

The most difficult part of the entire assembly was mating the Sun Roller Brg. Housing, DC-500-11, with the sun roller and the cluster carrier bearings. We worked without the Output Spindle, DC-500-12, in place. Then, after DC-500-11 was mated, we removed the cup nut and the jam nut and installed the sun roller locknut. The cup nut and jam nut were reinstalled, followed by the output spindle. Finally the Output Housing, DC-500-10 was mated with the output spindle. The seal carrier was removed for installation of the locknut on the output spindle. The seal carrier was then reinstalled.

Seals and pipe plugs were not installed, nor was the unit charged with Santotrac 50 fluid. These were withheld until the preload situation could be resolved.

Final dry weight was 95 lbs.

**Post Assembly.**- The averages of planet roller dimensions obtained at asembly were used to recalculate the second planet-ring roller engagement points. Roller dimensions were corrected for Hertzian deformations at 0, 25%, 50%, 75% and 100% preload levels. Figure 6 illustrates roller spacing at the different levels of preload. The dimensions represent $a+x_1$, $y_1+x_2$(with $y_1$), z, and $x_2$(with c). Figures 7a through 7f are the second planet-ring roller engagement diagrams for the initial setup, the initial engagement point, zero load, and the four levels of preload. From the diagrams of figure 7, a curve of preload level as a function of ring roller travel is constructed. This is shown in figure 8. The calculated ring roller travel from zero to 100% preload is .1438in.

The values of the X DIM for the input and output side clusters (given above) were then used together with the results of the engagement diagrams to obtain curves of required shim thickness vs. preload level. These are shown on figure 9 for the input side and output side clusters. For 100% preload the following shims would be required:

Input side shim = .0738/.0838 in.

Output side shim = .0588/.0688 in.

For assembly without shims the preload levels are:

Input side = 30 to 37%

Output side = 45 to 50%

As a compromise to reduce the drive tare torque slightly, the drive was assembled with .060 in. shims on the input side and .045 in. shims on the output side. These shims produce a preload level of approximately 88%. Plastic shim stock with thicknesses of .005, .010, and .015 in. was used in the assembly.

It is quite probable that tare torques would decrease as the drive is run in, but testing would be required to verify that.

## GROUNDED RING (MOMENTUM BALANCED) DRIVE (DC-400)

The conventional way to achieve dual counterrotating speed matched outputs from a single input is to utilize a dual roller or roller-gear cluster arrangement [2]. One cluster has a non-rotating cluster carrier or cage and rotating ring rollers, while the second cluster has non-rotating ring rollers and a rotating cage. One output is taken from cluster 1 ring rollers, and the second from cluster 2 cage. The two clusters are designed with ratios R and R+1 to achieve equal and opposite output speeds.

The Grounded Ring Drive represents a novel approach to achieving dual counterrotating outputs with a significant reduction in size and weight (approximately 40%) as compared to the conventional dual cluster design. The finalized geometric arrangement for the Grounded Ring Drive is shown in figure 10. Outputs are taken from the rotating ring rollers and from the rotating cage.The grounded ring is non-rotating and absorbs reaction torques which depend in magnitude on the two output torques. Kinematic operation of the drive, development of roller and gear geometries, key stress and deflection calculations, assembly procedure, and inspection results at assembly will be discussed prior to discussion of test results in a later section.

## Kinematics

A complete kinematic development is given in [3]. To review briefly (see figure 11):

Cluster ratio: $R = (c/y_1)(x_1/a)$ (21)

If the two output speeds are equal and opposite, i.e., $\omega_{L1} = -\omega_{L2}$. Then

$$\omega_{L1} = -\omega_H/(2R-1) \quad (22)$$

$$\omega_{L2} = \omega_H/(2R-1) \quad (23)$$

To achieve a non-rotating grounded ring it is necessary that

$$y_2 = x_2(c-x_2)/(2c-x_2) \quad \text{Then} \quad (24)$$

$$c_2 = c-x_2+y_2 \quad (25)$$

$$a_2 = c_2-2y_2 \quad (26)$$

where $a_2$, $y_2$, and $c_2$ are the grounded sun, planet, and ring radii.

A torque balance on the drive requires that:

$$T_H + T_{L1} - T_{L2} -/+ T_{GR} = 0 \quad (27)$$

When the drive is torque balanced:

$$T_{L1} = ((R-1)/R)T_{L2} \quad (28a)$$

and $T_{GR} = 0$ (28b)

when $T_{L1} = ((R-1)/R)T_{L2}$ it is shown in [3] that

$T_{L1}$ can be expressed as

$$T_{L1} = ((R-1)/R)T_{L2} +/- T_{GR} \quad (29)$$

From equations (27) and (29)

$$T_H -(1- (R-1)/R )T_{L2} = 0 \quad (30)$$

The input power to the drive is

$$\text{Input power} = T_H\omega_H \quad (31)$$

The output power from the drive is

$$\text{Output power} = T_{L1}\omega_{L1} + T_{L2}\omega_{L2} \quad (32)$$

The conclusion reached in [3] was that there would be phantom power loss when the output torques are not in the ratio as given in equation (28a). A further examination of the torque relationships as presented here shows that not to be the case. Neglecting friction losses, the output power will always be equal to the input power, so there will be no loss in efficiency due to phantom or recirculating power.

The DC-400 drive has a cluster ratio R=12.5 to achieve an input-output speed ratio (with equal and opposite output speeds) of +/- 24. Regardless of the imbalance in output torques, neglecting roller creep losses

$$\omega_{L2} = -\omega_{L2} = \omega_H/24 \quad (33)$$

It should be noted that in the DC-400 drive the three shaft connections are kinematically coupled so that none of the three can be constrained without constraining all three. This is in contrast to the DC-700 and DC-500 drives, in both of which torque and motion transfer can occur between any two shaft connections with the third shaft connection constrained or locked. In the DC-400 drive torque and motion transfer between any two shaft connections can only occur with the third connection free.

## Cluster Geometry

Results of the computer program which sizes the rollers and establishes approximate cluster geometry were presented in [3]. Table IX summarizes roller radii and, for the full output torque conditions of 452Nm (4000inlbs.), normal forces, contact ellipse dimensions, Hertz stresses and Hertz compressions for both the rotating (power transfer) and grounded ring clusters. Hertz compressions are required to determine effective roller radii under load and manufactured roller radii for desired preloading.

Stress and deflection analyses were done for the rotating cluster ring roller and the grounded ring cluster sun and ring rollers. None of the other parts is subjected to stress levels that require detailed stress analysis. As shown on Table IX, the rotating cluster ring roller maximum bending stress under full torque conditions is .148GPa (21,400 psi). That stress level precludes the use of a through hardened alloy, so a case carburized steel is used. For the grounded ring cluster, both the sun and ring roller bending stresses are very nominal ( on the order of .0295 GPa (4,270 psi) so that the material chosen could be either through hardened or case carburized. Sun and ring roller bending deflections are small ( on the order of .005mm [.0002in.]), but were still factored into the manufactured radii.

## Drawings

The Grounded Ring (Momentum Balanced) Drive is defined by assembly drawing DC-400. The assembly drawing includes a listing of commercial parts as well as a listing of all fabricated parts. Individual parts are detailed on drawings DC-400-01 through DC-400-36. The roller drawings include coordinate tables for NC machining and metrology. Each of the part drawings provides complete material and processing information necessary for manufacture.

## Assembly

**Assembly Procedure**.- Prior to completion of parts fabrication, an Assembly Procedure was worked out. During and after assembly it was modified to incorporate the changes that hands on experience indicated would facilitate easier assembly. The revised Assembly Procedure is given in APPENDIX E.

**Assembly Notes**.- Sun and planet rollers were gaged for the record and to ascertain conformance with print dimensions. Gaging was done on an optical comparator. X-coordinates were measured from a shoulder with an estimated accuracy of +/- .001in.. This would make the accuracy of gage diameter measurement approximately +/- .0002in. At the first preassembly inspection of rollers, almost all rollers were found to be grossly oversize. Errors had been made in setting up the coordinates for finish grinding. We adjourned to have the rollers reworked to size. Rework of the rollers consumed approximately two weeks. After rework all rollers were acceptable except for the grounded ring. Measured roller dimensions are shown on Table Xa. The 5.7296 in. diameter on the grounded ring was measured as 5.7305. That was considered usable but outside tolerance so the vendor agreed to make a duplicate. Assembly of the drive was postponed until completion of the second grounded ring. On the second grounded ring the 5.7296 in. diameter was measured as 5.7295 in.

Planet roller dimension were used to calculate the second planet-ring roller engagement points in the rotating cluster. Roller dimensions were corrected for Hertzian deformations at 0, 25%, 50%, 75% and 100% preload levels. Figure 12 illustrates roller spacing at the different levels of preload. The dimensions represent $a+x_1$, $y_1+x_2$(with $y_1$), z, and $x_2$(with c). Figures 13a through 13e are the second planet-ring roller engagement diagrams for the initial setup, the initial engagement point, zero load, and the four levels of preload. From the diagrams of figure 13, a curve of preload level as a function of ring roller travel is constructed. This is shown in figure 14. The calculated ring roller travel from zero to 100% preload is .109 in.

The arrangement of planet rollers in the rotating cluster is shown on figure 15. The value of the X DIM across the ring rollers at zero preload (see assembly drawing DC-400) was measured as .975 in. The nominal gap between the Load Ring (DC-400-20) and the Ring Roller Carrier (DC-400-09) when assembled inside the Clamping Lugs (DC-400-5A-C) is .904 in. The preload level without shims was therefore approximately 60% (figure 14 at .975-.904=.071 in. ring roller travel). A shim of .038 in. was added to produce a preload level of 100%.

For the grounded ring cluster, the value of the Y DIM across the idler sun rollers at zero preload (see assembly drawing DC-400) was measured as .747 in. As shown on figure 16, the nominal value is .7547 in. Figure 16 shows the initial engagement point and the final engagement point at 100% preload. The idler sun rollers are 3° cones so the contact points between them and the planet shafts remains at the 3° slope point on the 4.1 in. cross radius p;anets. The idler sun rollers must approach each other a total of .7547-.6792 = .0755 in. for 100% preload. The nominal shim required is .679-(2*.250) = .179 in. For this assembly the idler sun roller shim was ground to .171 in.

The parallelism of the axes of the second row planet shafts and the drive axis is felt to be an important parameter in the DC-400 drive. The z dimension in the cluster setups was calculated using averages of the measured roller dimensions for the rotating and grounded ring clusters.The calculated values were:

| | |
|---|---|
| For the rotating cluster | z= 2.393699 in. |
| For the grounded ring cluster | z = 2.393475 in. |
| | Δz = .000224 in. |

Within the accuracy of calculations, the axes should be parallel.

In assembling the cluster it was found that control of concentricity between the cluster carrier axis and the roller cluster axis was critical. The inner output spindle must be fastened to the cluster carrier before starting assembly of the roller cluster. When the ring rollers are in place, the outer output spindle should be engaged with the ring roller carrier to insure that concentricity between the roller cluster, cluster carrier and output spindles is not lost. The assembly procedure was modified to incorporate these procedures.

Assembly was completed with the addition of 17 oz. of Santotrac 50 traction fluid. Assembled weight was 58 lbs.

**Post Assembly.-** Breakaway torques were measured with deadweights applied to the input. With both outputs free to rotate the tare torque was 8.65Nm (76.5 in-lbf). This torque is 24% of the full torque rating of 36.17Nm (320in-lbf). The magnitude of the tare torque illustrates the disadvantage of full preloading- high friction losses at low output torques.

A check of drive kinematics was conducted by rotating the input 25 revolutions. This resulted in a 370° rotation (1.028 revolutions) of the inner output, and a 372° rotation (1.033 revolutions) of the outer output. These reduction ratios are 24.3 and 24.2. The calculated

cluster ratio is 12.5 or 24 with both outputs rotating equally and opposite, so the measured ratios compare quite well with theory.

**Post Failure Reassembly .** Details of the failure which occurred shortly after the start of tests are given under **TEST RESULTS, GROUNDED RING (MOMENTUM BALANCED) DRIVE (DC-400).** A new set of Planet Rollers, 1ST Row (DC-400-26) was made, the alternate Grounded Ring (DC-400-03) replaced the Grounded Ring used in the first asembly because the latter had a slightly scored roller track, and several other parts were refurbished for the new assembly. Measurements of the new set of Planet Rollers, 1ST Row are given on Table Xb. The X DIM was measured as .995 in. A ring roller shim of .015 in. would have been required for 100% preload, but in view of the very high tare torque obtained in the first assembly, it was decided to assemble with 80% preload, which required no shimming. For the grounded ring cluster, grounded ring loading was recalculated with the new grounded ring and the .171 in. idler sun roller shim used in the first assembly. It was found to be 830 lbf (3,694N) which is very close to the 100% preload design value of 844 lbf (3,756N). We then assembled with the .171 in. idler sun roller shim. The new values of the z dimension which determine parallelism between the drive axis and the axes of the second row planet roller shafts were:

| | |
|---|---|
| For the rotating cluster with 80% preload | z= 2.393691 in. |
| For the grounded ring cluster | z = 2.393975 in. |
| | Δz= - .000284 in. |

As for the first assembly, within the accuracy of calculations, the axes should be parallel.

As with the first assembly, breakaway torque was measured with deadweights applied to the input. With both outputs free to rotate the tare torque was 1.36Nm (12 in-lbf). This torque is 3.8% of the full torque rating of 36.17Nm (320in-lbf), and is significantly lower than that obtained in the first assembly. This indicates that there may have been several faults in the first assembly.

A check of drive kinematics was conducted by rotating the input 24 revolutions. This resulted in exactly 360° rotation (1 revolution) of both the inner and outer outputs (within the accuracy of measurement). The drive seemed very smooth with little or no perceptible cogging.

## TEST FACILITY

A test facility capable of applying and reacting torques, and of accurately measuring torques, angular shaft positions, and rotational speeds was designed to evaluate the performance characteristics of all three drives. The instrumentation incorporated in the test facility made possible measurement of angular and torque ripple, viscous and Coulomb friction, and forward and reverse power efficiency. The arrangement of components is shown quarter scale on drawings DC-800 SK, sheet 1 for the differential drives and sheet 2 for the momentum balanced drive. Fabricated parts for the test facility are defined by drawings DC-800-01 through DC-800-29. These are listed, together with major commercial parts, on drawing DC-800 SK sheet 1. Schematics of the component arrangements are shown in figure 17a for the differential drives and in figure 17b for the momentum balanced drive. Figure 18 shows photos of the test setups.

A notably challenging aspect of the test stand design was the need to drive concentric inputs (or outputs). To do so, it was necessary to utilize a hollow drive shaft, torque transducer, torque motor, and encoder for the outer shaft. Limited space for coaxial shafts made some compromises in angular stiffness necessary.

Components used in the test stand included: three drive motors, three torque transducers, 3 precision encoders, a load transmission, a multiprocessor motor control and data acquisition system, and a variety of mechanical fixtures.

### MOTORS

The most important components in the test stand were the drive motors used to power the transmissions. The drive motors included two Compumotor KHX-740 ac servo motors and one Uniq Mobility SR-180 brushless dc motor. For the DC-700 and DC-500 transmission tests the Compumotor electronic drives were modified such that the motors could be operated in three different modes: linear PD servo feedback, torque-controlled mode, or synchronous mode. These motors were capable of providing the full 19 N-m (170 in-lbf) desired "input" (high-speed) torque, but were limited in speed to approximately 135 rad/sec (1300 rpm). These motors were capable of both supplying and absorbing power up to these torque and speed limits. Because of the Compumotors' speed limitations, the maximum power these motors could source or sink was limited to approximately 2.5kW. Thus, the DC-700 and DC-500 transmission tests were primarily limited to roughly half the transmissions' rated speed and power (except for limited cases in which both Compumotors acted as maximum power

sinks).

The third drive motor, the Uniq Mobility SR-180, was required for its relatively rare quality of offering a hollow armature. This design permitted driving the outer shaft of each of the transmissions. The inner shaft of each transmission was driven via a shaft extension, which passed through the center of the Uniq motor, as well as its associated torque sensor and encoder. The Uniq motor was much more powerful than the Compumotors. It was capable of no-load speeds up to 570 rad/sec (5450 rpm), intermittent low-speed torque up to 34 N-m (300 in-lbf), and intermittent power up to 12kW (16hp). The associated controller was built for full 4-quadrant operation, with regeneration to zero speed. The higher speed, torque and power capabilities of the Uniq motor were exploited under conditions for which both Compumotors were running at full speed and power. The Uniq motor was able to balance double the speed of the two Compumotors and was able to balance the combined power of the two Compumotors. Under this condition only, full rated speed and power of the DC-700 and DC-500 transmissions were tested.

A limitation of the Uniq motor was its inability to provide well-regulated power absorption and its poor controllability at low speeds. This motor was capable of regenerating power down to low speeds, as specified. However, the power absorption occurred in sharp pulsations, making it unusable as a precision power sink for efficiency tests. As a result, the Uniq motor was always used as a power source for all efficiency tests of the DC-700 and DC-500 transmissions. For the DC-400 transmission, it was used primarily as a power source for efficiency tests, though some limited testing was conducted with this motor acting as a power sink. The consequence of this limitation for the DC-400 tests was that efficiency data was taken primarily with the transmission acting as a speed increaser rather than the more normal sped reducer mode.

It was also observed that the Uniq motor did not provide smooth torque production at speeds below about 35 rad/sec (335rpm). Thus, efficiency tests did not include cases for which transmission shaft H2 (outer input shaft of DC-700 and DC-500) ran at speeds less than 35 rad/sec. This restriction included zero speed, as the Uniq motor could not servo to a fixed angle.

Yet another limitation of the Uniq motor was its inability to interface to computer controls. Although the logic power supply of the Uniq driver was described as decoupled from the motor drive power, the electronic controls were not compatible with computer outputs. This problem could be solved using analog isolator modules, though this should not have been necessary. Ultimately, the Uniq motor was controlled manually via the control pendant

provided by the motor manufacturer. The Compumotors were controlled by the computer, and final load adjustments were made manually with the Uniq motor.

Synchronous-mode control of the Compumotors was used almost exclusively in the tests of the DC-700 and DC-500 transmissions. This control mode enabled precise speed regulation of two of the three shafts of each transmission. The Uniq motor was used as a torque source. In fact, the control interface available for the Uniq motor was a velocity command, which would seem to be in conflict with velocity control of the two Compumotors. However, the Uniq motor controller utilized a weak, proportional-only velocity-error feedback controller internal to the power amplifier to regulate motor torque. As a result, the Uniq motor, under load, would not achieve its commanded velocity. Rather, the velocity-controlled Compumotors would constrain the speed of the Uniq motor. Velocity commands to the Uniq motor higher than the shaft velocity imposed by the Compumotors resulted in a velocity error in the Uniq controller, resulting in a proportional torque response. As a result, the Uniq motor could be utilized as a torque source by varying its velocity command. The Compumotors responded accordingly to react to the torque introduced by the Uniq motor, but synchronous control of the Compumotors maintained a regulated speed. In this manner, it was possible to establish various combinations of shaft speeds and torques, subject to the restrictions noted on maximum speeds of the Compumotors and the requirement that the Uniq motor act as a power source.

For the DC-400 tests the Compumotors were driven in two different modes. The Compumotor driving the input shaft (shaft H) was driven in synchronous mode. Synchronous mode control enabled precise regulation of input speeds. Since the low speed shafts (L1 and L2) were dependent on the input speed, the motors on shafts L1 and L2 were controlled as torque sources, not as speed sources.

For the DC-400 transmission tests, utilizing the Uniq motor as a torque source involved depending on its relatively "soft" velocity servo stiffness. Since the velocity-controlled Compumotor constrained the speed of the Uniq motor (within torque limits of the Compumotor), the speed of shaft H was precisely regulated, and the speed of shaft L2 followed by kinematic constraint Velocity commands to the Uniq motor higher than the L2 shaft velocity resulted in a velocity error in the Uniq controller, inducing a proportional torque response. In this manner, the Uniq motor could be utilized as a torque source by varying its velocity command slightly above or below the regulated velocity of shaft L2.

The Compumotor on shaft L1 was also torque controlled. As the torque of shaft L2 (Uniq motor torque) was adjusted, the torque on shaft L1 was adjusted as well, to keep the two

output torques relatively close. Most desirable operation of the DC-400 drive occurs when the outputtorques are kept comparable--within approximately 30% of each other.

By varying the velocity of shaft H, the torque load on shaft L1 and the torque load on shaft L2, the space of valid loading conditions could be evaluated.

## TEST STAND GEARING

For the DC-700 and DC-500 tests, the motors used were appropriately sized for direct drive of the high-speed transmission shafts. However, to source or sink power at the low-speed shaft(s), it was necessary to reduce the speed and increase the torque of the motors. Two additional transmissions were used for this.

For the single low-speed shaft L of transmissions DC-700 and DC-500, a Nastec model NAS-300A transmission was used. This transmission had a ratio of 29.23:1, and exceeded the torque, speed and power ratings of the DC-series transmissions under test.The 29.23:1 ratio was a good match for the 29.23:1 and 24:1 ratios of transmissions under test. In all cases, the NAS-300A transmission was driven by a Compumotor at its high-speed shaft, and the low-speed shaft was connected in series with a 2804T (4-3) Himmelstein reactionless torque meter (Figure 17). Both input and output shafts of the NAS-300A were coupled via Thomas flexible couplings. Due to its high linearity, low friction and good efficiency as both a speed reducer and speed increaser, the NAS-300A transmission was well suited for performing as a component within both a power source and a power sink.

For the DC-400 transmission tests the Compumotor used for shaft H was under-sized for direct drive of this high-speed shaft. Neither the maximum speed nor the maximum torque of the Compumotor could attain the rated limits of the DC-400 input shaft. However, the speed and torque limits of the Compumotor were reasonably balanced with respect to the DC-400 constraints, and thus direct drive of shaft H was preferable to the addition of an input transmission.

Shafts L1(inner output) and L2(outer output) of DC-400, on the other hand, called for torque loading far in excess of that which could be supplied by the motors, albeit at a much lower speed. To match the electromechanical drives to the task, load transmissions were required.

For shaft L1 of DC-400, a Nastec model NAS-300A transmission was used. This

transmission exceeded the torque, speed and power ratings of the DC-400 transmission under test. The 29.23:1 ratio was a reasonable match for the (nominal) 24:1 ratio of the DC-400. The NAS-300A transmission was driven by a Compumotor at its high-speed shaft, and the low-speed shaft was connected in series with a 2804T (4-3) Himmelstein reactionless torque meter. Both input and output shafts of the NAS-300A were coupled via Thomas flexible couplings. The NAS-300A transmission was well suited for performing as a component within both a power source and a power sink.

For shaft L2 of DC-400, a second speed reducer was needed. A constraint on this transmission was that it had to permit torque measurements of the outer output shaft (shaft L2) while providing a through hole for passage of the inner output shaft (shaft L1) extension . A harmonic drive, Harmonic Drive model HDC-8M with a 60:1 ratio was used for this. The ratio of 60:1 was not as well matched as the 29.23:1 NAS-300A transmission, but the higher speed range of the Uniq motor, with which the harmonic drive was used, made the harmonic drive a viable candidate.

In practice, the harmonic drive presented a more severe limitation than expected. When the harmonic drive's wave generator was driven in excess of approximately 3,000 rpm, the wave generator was not stable. At these speeds, the wave generator would "walk" axially along the concentric shaft L1, and would bind against components it contacted. Consequently, measurements were restricted to input speeds between plus and minus 105 rad/sec (approximately 1,000 rpm), corresponding to approximately 262 rad/sec (2,500 rpm) of shaft L2. This speed restriction further limited the range of data (both speed and power) that could be measured.

## TORQUE SENSORS

Torque measurements were performed using Himmelstein torque meters. Each torque meter had been calibrated at the factory, and is nominally rated for 0.1% linearity and hysteresis. Compatible Himmelstein torque-meter signal conditioners (model 6-201) were used.

For each transmission, two reactionless rotating torque meters and one reaction-type torque meter were used. Reactionless torque meter Himmelstein model 2402T (35-1), with a full-scale range of 40N-m (350 in-lbf), was used in each case to measure a high-speed shaft torque of transmissions DC-700 and DC-500. The range of this torque meter was

approximately twice the rated input torque of each of the transmissions. This meter was connected in series with a Compumotor and shaft H1 using Thomas flexible couplings. Torques could be measured with this meter while the shaft was rotating, and the meter introduced no perceptible additional torque loading. However, this type of meter uses a solid shaft, which does not accommodate concentric differential shafts. Thus, torques from shaft H2 of DC-700 and DC-500 could not be measured with this type of meter.

Low-speed shaft torques (shaft L of DC-700 and DC-500) were measured using Himmelstein reactionless torque meter model 2804T (4-3). This meter had a full-scale output of 450 N-m (4,000 in-lbf). This capacity matched the output rating of the transmissions, and was thus optimally ranged for highest precision. The meter was connected in series between the low-speed, high-torque shaft L, and a torque load (a geared-down Compumotor) using Thomas flexible couplings.

The third torque, in each case, applied to the outer input shaft of the dual, concentric shafts of DC-700 and DC-500, was measured using a reaction-type torque meter. For these transmissions, torque was provided to shaft H2 from direct drive of the Uniq motor. The applied torque was measured using Himmelstein reaction torque meter model 2030 (6-2), with a range of 68 N-m (600 in-lbf). The range of this meter was not optimal for the application, since the span was 350% of the torque range to be applied. This meter did, however, provide the required through-hole dimensions. In addition, it could adequately support the cantilever moment produced by the 21 Kg (47lbm) Uniq motor. The reaction torque meter was bolted on one side to the case of the DC-700 or DC-500 transmission, and the other flange was bolted to the stator of the Uniq motor. The Uniq motor was not supported by any other means. Thus, rotor torques from the Uniq motor reacted equal and opposite on the stator, which was supported solely by the reaction torque meter. By this arrangment, torques applied to shaft H2 could be measured accurately with a non-rotating torque transducer, and this construction allowed for unimpeded passage of a shaft extension from shaft H1.As stated the range of the model 2030 (6-2) meter was suboptimal, being 350% higher than the desired measurement span. Consequently, there was some compromise of precision in measuring the torques of interest in the DC-700 and DC-500 tests.

For the DC-400 tests, a reactionless torque meter Himmelstein model 2402T (35-1), with a full-scale range of 40N-m (350 in-lbf), was used to measure high-speed shaft torque (H). The range of this torque meter was well matched to the rated input torque of the DC-400, although the Compumotor drive was not capable of producing torques to this torque level. This reactionless torque meter was connected in series between a Compumotor and shaft H using Thomas flexible couplings.

Low-speed shaft torques (shafts L1 and L2 of DC-400) were measured using one reactionless torque meter and one reaction-type torque meter. Himmelstein reactionless torque meter model 2804T (4-3), with a full-scale output of 450 N-m (4,000 in-lb), was well matched to the torque range of the output shafts, but, due to this meter's solid shaft, its use was restricted to shaft L1. This meter was installed between shaft L1 of DC-400 and the high-torque/low-speed shaft of the NAS-300A load transmission using Thomas flexible couplings with keyways.

The third torque of DC-400, that of shaft L2, was measured using a reaction-type torque meter. A Himmelstein model 2060 (1-4) reaction-type torque meter, with a range of 1,130 N-m (10,000 in-lbf), was bolted on one side to the case of the DC-400 transmission. The drive package for shaft L2 (consisting of the harmonic-drive transmission coupled to the Uniq motor) was bolted to the other flange of the torque meter. No other supporting structure was provided for the motor/harmonic drive. Thus, all torques from shaft L2 reacted through the reaction torque meter to the case of the transmission. Although there were frictional losses in both the motor and speed reducer, these losses acted only as internal moments. The net torque acting on shaft L2 was accurately sensed via its reaction torque with respect to the transmission case, independent of internal losses in the electromechanical drive package.

The range of the model 2060 (1-4) meter was suboptimal, being 250% higher than the DC-400 transmission's rated maximum torque output. (The torque range oversizing was worse still with respect to the torques which could be achieved in the tests). Consequently, there was some compromise of precision in measuring the torques of interest in the DC-400 tests. Use of this torquemeter was nonetheless necessary, due to the large cantilever loads it was required to support as well as the relatively large axial through-hole required.

## ANGULAR POSITION SENSORS

For measuring transmission ratio linearity, high-precision encoders were used. For the inner input shaft and output shaft of DC-700 and DC-500 (shafts H1 and L), identical encoders, BEI series 143, were used. These solid-shaft encoders provided 360,000 counts per revolution, offering a resolution of 6.28 mrad (0.001 deg). For the third shaft (H2) of the DC-700 and DC-500 transmissions, an angular sensor with a through hole was required. A similar BEI encoder, model 5VL677, also with 360,000 counts per revolution, was acquired for this purpose. This encoder provided a hollow shaft with a 2-inch bore.

A design modification from the original plan was required to use the hollow-shaft BEI encoder. The mount between this encoder and the Uniq motor did not originally incorporate a flexible coupling. Since the Uniq motor was cantilevered from a reaction-type torque meter, its mount had significant flexibility. The resulting misalignment with respect to the rigid coupling of the encoder made the encoder unusable. A coupling modification was made, in which the outer spline to shaft H2 (part numbers DC-800-10 and DC-800-18 for the DC-700 and DC-500 drives, respectively) was mated to a modified Thomas flexible coupling. The other side of this coupling was modified to fit the interface flange (part number DC-800-23) of the BEI encoder. A consequence of this modification was that the Uniq motor had to be removed to install the hollow-shaft BEI encoder. However, this was not a limitation for the linearity or cogging tests, since under these tests, the input shaft was rotated manually.

In the DC-400 tests, for shafts H and L1, BEI encoders, series 143, were used. For shaft L2, the BEI encoder, model 5VL677, also with 360,000 counts per revolution, was used. This encoder provided a hollow shaft with a 2-inch bore.

The high-precision encoders were used only in low-speed, manually-driven torque-ripple and angular linearity tests. For all motor-driven tests, only velocities (not high-precision angles) were needed. For friction and efficiency tests, velocities were known from the drive frequency in synchronous mode, and these velocities were verified using lower-resolution, higher-speed encoders on the Compumotors.

For linearity tests, the load transmissions were removed, and the encoders were coupled directly to shafts . This enabled precision angular measurements unaffected by imperfections of the load transmissions.

## MECHANICAL COUPLINGS

Most mechanical couplings for rotating parts used Thomas flexible couplings. These couplings accommodate minor shaft misalignments, both translational and rotational, yet are stiff and backlash free in torsion. In most instances, the Thomas couplings were coupled to shafts using Fenner-Manheim "Trantorque" friction/expansion couplings. Couplings made with the Trantorques were stiff and backlash free.

A number of problems arose with the original coupling designs. These necessitated ad-hoc design changes. First the coupling between the high-speed shaft of the NAS-300A load transmission and its Compumotor drive was via rigid shaft adapter (part DC-800-21). This rigid coupling was found to be inadequate, and prospectively damaging to the motor and/or transmission. An additional motor mount was fabricated to enable retrofitting a flexible coupling at this interface.

The interface between the BEI encoder model 5VL677 (with hollow shaft) and the Uniq motor did not include a flexible coupling. This interface was designed to use mating keyed flanges. As noted above, this method of coupling was not adequate to allow the BEI encoder to rotate with the Uniq motor without significant binding. Flexing of the Himmelstein reaction-type torque meters due to applied motor torques caused sufficient deflection to make this coupling ineffective. Due to constraints from the length of the internal shafts (part numbers DC-800-17, DC-800-19 and DC-800-22), it was not possible to increase the axial distance between the Uniq motor and the BEI encoder. It was, however, possible to install the BEI encoder with a retrofit flexible coupling directly to the input splines (parts DC-800-10 and DC-800-18), but with the Uniq motor removed. This arrangement was used for cogging and linearity tests.

Several other couplings were more problematic. All three couplings to the DC-700 and DC-500 shafts and two of three couplings to the DC-400 shafts were via splines. These couplings could accommodate some shaft misalignment, but could not be guaranteed backlash free. Backlash in these couplings would affect measurements of angular linearity.

The Himmelstein model 2804T torque meter was coupled to the low-speed shaft (L) of DC-700 and DC-500, and to the low-speed shaft of the NAS-300A load transmission via Thomas flexible couplings. The couplings were not secured to the shafts via Trantorques, however, but via shaft keys because of diameter constraints. The shaft keys, although professionally machined with care to match each keyway, resulted in observable backlash.

The shaft keys on the 2804T torque sensor presented an additional problem in the DC-400 tests. While the keys constrained rotational motion between the output shaft L1 and the torque-meter shaft, this coupling did not prevent axial motion between the two shafts. The torque meter was secured to the fixture rail, preventing axial motion of its shaft, but the L1 shaft extension was not constrained axially. This shaft extension mated with the DC-400 transmission via a spline (which permitted axial translation), and connected to the 2804T torque meter (via a flexible coupling) secured with a key, which also permitted axial motion.

The axial freedom of the L1 shaft extension of DC-400 became a problem, since this shaft was responsible for constraining axial motion of the flex spline of the harmonic drive (via thrust washers on the L1 shaft extension). The flex spline produced unexpectedly large axial forces on the thrust washers of the L1 shaft extension. Consequently, the shaft extension would translate axially until the flex spline came in contact with the Uniq motor housing (on one side) or produced excessive frictional torques on the inner shaft (via the thrust washer on the other side). This design flaw in the test stand made data collection difficult. Data could be acquired for relatively short durations, until the L1 shaft extension displaced too far axially and had to be re-adjusted. When the flex spline displaced away from the DC-400 transmission, such displacement could be noted visually and the test would be halted. When the flex spline displaced towards the DC-400, however, significant frictional torques between L2 and L1 could develop, and this condition was not visually obvious. Under conditions of such internal binding, the losses are indistinguishable from efficiency losses internal to the DC-400.

Finally, the mechanical coupling securing the wave generator of the harmonic drive also proved to be inadequate. The wave generator was driven by the Uniq motor via a spline. As with the L1 shaft extender, however, no axial constraint was provided. Consequently, the wave generator was capable of translating axially under operation. This unconstrained motion was particularly problematic at higher speeds, limiting the top speed at which the DC-400 could be tested.

For the angular linearity measurements, the 2804T torque meter and its keyed shaft couplings were removed, so as not to influence the measurements. However, the shaft connection to the output (e.g., part DC-800-20, output shaft for the DC-700 and DC-500 drives) had a mating spline on one end, and a keyway on the other. Backlash associated with the key of this required part was problematic for angular linearity measurements.

For linearity and torque-ripple tests of DC-700 and DC-500, one shaft at a time was fixed stationary, one shaft was rotated, and the input torque of the driven shaft and angles of the driven and free shafts were measured. To secure one shaft at a time, the chosen shaft was coupled via a Trantorque to a stiff fixture bolted to the rail.

For the DC-400 tests it was not permissible to fix or constrain any of the three shafts. To minimize the influence of system backlash on linearity measurements, one shaft at a time was rotated slowly and smoothly (manually) without direction reversals within a given test. By rotating in a constant direction, and by avoiding inertial effects, any backlash in the system

should have approached and remained in contact with its limit. Thus, backlash effects would be removed from the linearity tests.

In retrospect, the test-stand design should have: 1) eliminated all keyway couplings in favor of backlash-free couplings such as Trantorques ( spatial constraints did not permit those to be used); 2) provided axial thrust bearings for the flexible spline of the harmonic drive; 3) provided thrust bearings restraining axial motion of the harmonic drive's wave generator. All other design features of the test stand were found to be successful.

Each component of the system was mounted to a common rail (a 2-piece, 10' aluminum I-beam, bolted to a concrete floor) using custom mounting fixtures ( drawing DC-800, sheets 1 and 2, and figure 17). The fixtures located all shaft centers nominally 19.05 cm (7.5") above the rail.

## EXPERIMENTAL PRECISION

### Angular Position Measurements.

The resolution of the encoders was plus or minus 6.28 mrad (0.001 deg). Transmission ratios were measured incrementally, reported in terms of change of input angle divided by change in output angle, fixing one shaft at a time. Measurements were recorded every 1 degree of output rotation. For high-speed to low-speed shaft measurements, error associated with the encoder resolution can be calculated. For a nominal transmission ratio of 24:1, plus or minus one increment of the output and input encoders would result in apparent ratios of 24.025:1 and 23.975:1, or 0.1% error. For a nominal ratio of 1:1 (e.g., the ratio between dual inputs or dual outputs), the error associated with encoder resolution is 0.2%, based on 1-degree angular changes.

A potentially more significant error was due to backlash in the spline couplings to the transmission, (e.g., part DC-800-20) and (more prominently) their associated keys/keyways. To attempt to remove this effect from the measurements, rotations were induced continuously in first the positive direction for one full output revolution, then in the negative direction for a full revolution. This approach should minimize the effects of backlash in the external couplings, but would also disguise any backlash internal to the transmission. Under the circumstances, backlash of the transmission could not be measured reliably, but linearity of transmission ratios should be trustworthy to within approximately 0.2%.

## Torque Measurements

The torque meters were calibrated by Himmelstein, and claimed traceable to NIST standards. The stated precision (linearity and hysteresis) is 0.2% (0.1% each) of full scale. Voltages were sampled using a 12-bit, ADC, with a span of -5V to +5V, resulting in a conversion accuracy (plus or minus one bit) of 0.05%.

The Himmelstein models 2402T (35-1) and 2030 (6-1), with 350 in-lbf and 600 in-lbf ranges, respectively, were coupled in series, torques were applied, and the readings were recorded from each. At 300 in-lbf load, the two meters agreed within 0.8 in-lbf. This variance falls within the claimed tolerance of 0.1% full scale, allowing for 0.6 in-lbf error from the 2030 meter and 0.35 in-lbf error from the 2402T meter. At lower torques, however, the discrepancy between the two meters was as high as 2.2 in-lbf (worst case, at 221 in-lbf applied torque). Such a discrepancy would translate into an efficiency error of plus or minus 1%. The discrepancy at 170 in-lbf, the rated input torque, was 2.0 in-lbf, which would produce a 1.2% error in computed efficiencies.

The high-torque meter (2804T at 4,000 in-lbf range) could not be compared directly to the lower torque meters, as their ranges were so disparate. However, this meter is a scaled up design of the 2402T, is made by the same manufacturer, is claimed to have the same relative precision, and was used used with the same signal conditioning electronics. This high-torque meter was well scaled to its application. The two low-torque meters, 2402T and 2030, were oversized by 200% and 350%, respectively, whereas the high-torque meter (2804T) was scaled to the correct 100% full range. We may thus reasonably estimate that the output meter would introduce errors comparable to (or lower than) those observed with the relative readings of the low-torque meters. With three meters in operation, efficiency measurements should be within plus or minus 2.5%, as a conservative worst case.

In measuring the output torques of the DC-400 transmission, similar, but larger torque meters were used. Himmelstein model 2060 (1-4) reaction-type torque meter, with a range of 1,130 N-m (10,000 in-lbf) was used to measure the outer-ring (L2) torque. Himmelstein reactionless torque meter model 2804T (4-3) with a full-scale output of 450 N-m (4,000 in-lb) was used to measure the inner output torque (L1). These two meters were not compared directly in series, but since they had the same manufacturer, same construction type and roughly the same ratio of torque ranges as the lower-range meter pair, comparable precision limits may be expected.

Calibrating the high-torque meters (2060 at 10,000 in-lbf range, and 2804T at 4,000 in-lbf range) with respect to the input torque meter (2402T, 350in-lbf) was impractical, due to the disparity in ranges. The manufacturer's calibration numbers had to be trusted. Given that all meters used were fabricated and calibrated by the same manufacturer, that the meters were quoted to have the same relative precision, and that all meters were used with identical signal-processing electronics, the relative errors in calibration among the meters may be presumed to be within the quoted tolerances, as confirmed by tests on the lower-range meters. With three meters in operation, efficiency measurements should be within plus or minus 2.5%, as a conservative worst case.

Another source of error in the torque measurements was electrical noise. Although the signal conditioning electronics incorporated modulation noise-suppresion techniques, the substantial electromagnetic interference produced by the switching amplifiers of the three motors did produce a noticeable bias of noise on the torque signals. With the motors on, a bias of 57mV was observed, which corresponds to just over 1% full scale. Powering the signal conditioners from an isolated line-power supply seemed to improve, but not eliminate the problem. Subsequently, the noise-induced bias torque was accounted for by assuming symmetry of the transmission behavior at positive and negative velocities. Asymmetries, assumed induced by torque-sensor noise, were removed mathematically in post-processing the data.

Finally, another source of error peculiar to the 2804T meter is possible sensor saturation. The torque meters are safe to operate up to twice their rated output. However, the analog-to-digital converter used saturated at 5V input, corresponding to the full-scale rating of each meter. Since the 2804T meter was rated for 4,000 in-lbf, matching the output rating of the transmissions, tests which slightly exceeded this torque would be incorrectly recorded as equalling this torque. Data with output torques very close to 4,000 in-lbf may, therefore, not be reliable.

## Velocity Measurements

Velocities were regulated by driving the Compumotors in synchronous mode. This produced the equivalent of electronic gearing, for which the number of mechanical revolutions per electrical revolution is a fixed integer. As a result, as long as the motors maintained synchronism, the speed was (on the average) precisely the same as the drive frequency. Loss of synchronism was obvious, as the motors would stall.

In the DC-700 and DC-500 tests two of the three motors were driven in synchronous mode. The velocity of the third (the Uniq motor) could be precisely inferred from the known (measured) transmission ratio. For efficiency computations, error associated with velocity measurements was insignificant relative to other sources of error.

In the DC-400 tests only the input motor (shaft H) was driven in synchronous mode. The velocity of the output shafts could be inferred from the known (measured) transmission ratio. The velocity of shaft L1 was measured nonetheless via an encoder on the Compumotor driving the load transmission NAS-300A. Since this load transmission had a precise gear ratio fixed by gear teeth, the speed of shaft L1 (coupled to the low-speed output of the NAS-300A transmission) could be accurately deduced. Measurements showed that the transmission ratio of the DC-400 was not constant. Under varying load, the speed ratio from shaft H to shaft L1 changed, due to roller creep. The speed of shaft L1 changed by approximately 2% as the torque increased from zero to 2,000 in-lbf. It is presumed that shaft L2 experienced comparable speed changes under load, though this could not be measured directly.

In the analyses of efficiency of DC-400, it is presumed that the speed of shaft L2 is equal to the measured speed of shaft L1, since the torques on L1 and L2 were comparable. This assumption should correct for the expected (but unmeasured) speed variations of shaft L2, making error associated with velocity measurements insignificant relative to other sources of error.

## INFLUENCE OF RESONANCES

Mechanical resonances were observed during testing. For example, for the DC-700 transmission, one such resonance was near 35 rad/sec input speed, which corresponded to one of the chosen velocity states. Resonances can produce fluctuating torques and velocities. Since the data acquisition averaged torque and velocities measurements, it did not account for possible phase differences between fluctuating signals (analogous to a power factor in reactive electrical systems). Average velocity and torque measurements under resonant conditions are correctly reported, but efficiency computations for data taken under resonant conditions may not be reliable.

Resonances observed could not be attributed to the transmissions themselves. Compliances of the flexible couplings, flexing of the aluminum rail, and magnetic cogging of the motors all contribute to the system dynamics, making transmission effects impossible to isolate under the test conditions.

## TEST RESULTS

### DUAL INPUT DIFFERENTIAL ROLLER-GEAR DRIVE (DC-700)

The DC-700 transmission was integrated into the test stand as per drawing DC-800-SK, subject to the coupling modifications noted earlier. Angular linearity, torque cogging, Coulomb and viscous friction, and power transfer efficiency were measured. Test procedures, data, and interpretation for the DC-700 drive are presented in this section.

Before presenting the data, a note on sign conventions is important. All rotations have been defined as positive pointing *out* of the transmission. A positive rotation of H1 produces a negative rotation of L, and a positive rotation of H2 produces a positive rotation of L. If H1 and H2 both rotate at the same speed in the same direction, then shaft L remains stationary. The formula for relating the shaft velocities (previously presented as eq. (7) is:

$$\omega_L = \omega_{H2}/R_{2L} - \omega_{H1}/R_{1L} \tag{34}$$

where $\omega_L$ is the angular velocity of shaft L, $\omega_{H1}$ is the angular velocity of shaft H1 and $\omega_{H2}$ is the angular velocity of shaft H2. The ratios $R_{1L}$ and $R_{2L}$ are the transmission ratios from shaft H1 to L and from shaft H2 to L, respectively. As will be shown from the data, $R_{1L} = R_{2L} = 29.23$ for the DC-700 transmission.

Ideally, torque production in the DC-700 drive could be computed as:

$$\tau = -R_{2L}\tau_{H2} + R_{1L}\tau_{H1} \tag{35}$$

Since $R_{1L} = R_{2L}$ for the DC-700, the input torques would, ideally, always be equal and opposite. Any torque imbalance between the H1 and H2 shafts would result in acceleration of the transmission until the balance condition is met. Note, though, that while the input torques should balance, there is no such constraint on the input velocities. The input torques are more nearly balanced when the input shafts deliver nearly equal power.

The torque signs have been assigned such that positive torque and positive velocity at any shaft implies power flow *into* the transmission at that shaft. The DC-700 was tested with power flows both into and out of shafts H1 and L. Since the Uniq motor was not a well-controlled power sink, shaft H2 was always driven with power in.

## Angularity Linearity

On the average, a geared transmission has a precise, integer-fraction transmission ratio, as dictated by tooth ratios. Within a revolution, however, there are small variations in the ratio of incremental input angle to incremental output angle. Such variations give rise to velocity ripple of the output for smooth rotation of the input. Velocity ripple acting on a load inertia induces torque pulsations. Transmissions with identical reduction ratios can have quite different dynamic behaviors within a system, depending on the linearity.

**Linearity Test Procedure.-** Linearity was measured with the high-precision BEI encoders on shafts H1 and L, while shaft H2 was clamped still. The input shaft, H1, was rotated slowly by hand while the computer continuously polled the encoder angles. For each 1.000-deg increment of the output (shaft L), the input angle was sampled and the incremental ratio was computed.

These tests were performed with constant positive or constant negative rotation of the driven shaft, so as to minimize the effects of backlash in the keys of the couplings. As a result, backlash in the transmission would have been disguised as well.

Ratio and linearity tests were repeated with: H1 driven, H2 fixed, L free; H1 driven, H2 free, L fixed, and H1 fixed, H2 driven, L free. In each case, the input excitation was manual.

**Data.-** Figure 19 shows the data measured for one full revolution of the low-speed shaft, L, with the inner high-speed shaft, H1, driven and the outer high-speed shaft, H2, fixed. The mean transmission ratio of 29.23:1 is superimposed on this plot for reference. The standard deviation of the incremental transmission ratio was 0.10. The maximum incremental ratio (with respect to 1-degree output changes) was 29.71, and the minumum was 28.49. The minimum incremental ratio stood out significantly from the mean, giving the appearance of a mechanical error. The incremental ratio test was repeated 6 times, and on each trial there was a single, narrow region (over 1 rev of shaft L) in which the incremental ratio deviated significantly. A second data-set from these tests appears in figure 20. For all trials, the mean ratio was 29.23:1 (to four significant digits) and the standard deviation was 0.10.

Linearity tests were repeated with H1 driven, H2 free, L fixed, and with H1 fixed, H2 driven and L free. As expected, the ratio from H2 to L was 29.23 (on the mean), and the ratio from H1 to H2 was unity. The standard deviation of the ratio from H2 to L was somewhat lower than the standard deviation of H1 to L.

**Analysis.**- The DC-700 transmission ratio of 29.23:1 matched precisely the ratio of the NAS-300A load transmission. The notable deviations in the incremental transmission ratio may indicate some mechanical damage or imperfection. The standard deviation of the incremental ratio was 0.10. This may be considered a reasonable benchmark for comparing linearity among transmissions. It should be noted that the true derivative (change in output angle with respect to change in input angle) cannot be measured directly. Rather, the incremental transmission ratio is a digital approximation of the true derivative. By choosing an output $\Delta\theta$ of 1 degree (1000 encoder counts), the resolution of the test was not better than 0.1%. The measurement error due to encoder resolution alone would account for a standard deviation of the incremental transmission ratio of 0.03. Incremental ratios computed every 1 degree of output resulted in relatively low spatial sampling rate, seeming to approach the Nyquist sampling (spatial) frequency. A zoom on the first 50 datapoints of figure 20 is shown in figure 21. Since successive datapoints are not very close together, the spatial sampling rate is somewhat low, and the computed incremental rotation may be too coarsely approximated by considering "large" output increments of 1 degree. A higher spatial sampling rate, however, would It is concluded that the chosen sampling resolution was a good compromise among competing sources of error. The linearity standard deviation of 0.10 is a reasonable representative figure of merit for linearity of this transmission.

## Cogging

Angular nonlinearity, or, equivalently, a modulated transmission ratio, results in torque ripple during operation. The influence of such torque disturbances depends on the speed of operation and on the resonances and stiffness of the coupled sytem. Another source of torque ripple is referred to as "cogging." When rotating the input shaft of a transmission by hand, torque cogging is usually evident. Tooth-to-tooth gear interactions and variable binding due to imperfect tolerances can be felt easily.

To measure cogging, the transmission shafts were rotated slowly through a torque transducer, and resulting input torque vs angle was logged.

**Cogging Test Procedures.**- Accurate measurement of cogging requires a smooth input driver. Further, such tests should be performed quasi-statically, to avoid affecting the data with dynamic terms (e.g., due to angular nonlinearity). It is not, however, necessary that the driver input enforce a steady velocity. Thus, a good choice of input driver is manual rotation.

To test inner high-speed shaft (shaft H1) cogging, shaft H1 was rotated slowly by hand, with a torque sensor in series. Separate H1 cogging tests were performed with shaft H2 locked and

with shaft L locked. In one set of experiments, the input torque was sampled every 1 degree of rotation of shaft L. In additional tests, the input torque was sampled every 3.6 degrees of input (H1) rotation. Cogging was measured for both positive and negative input rotations. Shaft H2 cogging tests could only be performed with shaft H1 free and shaft L fixed. This restriction was due to the fact that the shaft H2 torque meter was a reaction-type torque meter. It was only capable of measuring reaction forces on the stator of the Uniq motor due to torques generated electromagnetically on the rotor. In turning shaft H2 by hand, no torque reaction was induced in the static torque meter. To measure shaft H2 torques, it was necessary to install a reactionless type torque meter in series, and rotate shaft H2 by hand through the torque meter. Since the reactionless torque meters do not have hollow shafts, however, it was not possible to prevent inner shaft H1 from rotating during tests. Thus, H2 cogging data could only be obtained with shaft L fixed and shaft H1 free.

Cogging tests for the low-speed shaft (shaft L) could not be performed in this way. Shaft L exhibited significant "breakaway" torque. Upon slowly increasing the applied torque, shaft L would remain stationary until reaching a breakaway threshold, at which point the shaft would release suddenly. The rapid transients upon release resulted in transient torques which precluded measuring quasi-static cogging. Therefore, the shaft-L cogging tests were replaced with breakaway tests. In these tests, the history of torque vs time was recorded while applied torques were slowly increased until breakaway.

In all tests, the low-pass filters of the torque meter signal amplifiers were set for 100-Hz cutoff.

**Data.**- Figure 22 shows the cogging torque measured for shaft H1 with H2 fixed and L free. Data is displayed for one full revolution of the output (29 input revolutions) in both the positive and negative directions.

Figure 23 shows a higher-resolution cogging plot, sampled every 3.6 degrees of input rotation, displayed for one revolution of the input.

Figure 24 shows the cogging torque of shaft H1 with shaft H2 free and shaft L fixed. The data covers 30 spans of H1.

Figure 25 shows the cogging torque of shaft H2 with shaft H1 free and with shaft L fixed.

Figure 26 shows the time-history of applied torque to shaft L. The breakaway torque levels are apparent. In this test, both H1 and H2 shafts were free.

**Analysis.**- Shaft tests revealed torque cogging with a bias offset. The bias offset (torque mean) is attributable to Coulomb friction, and the variation about bias (e.g., standard deviation) is an indication of the cogging.

For H1 driven, H2 fixed and L free, the mean applied torque was 0.38 N-m, and the standard deviation was 0.20 N-m (based on the higher-resolution sampled data). Figure 23 gave a more trustworthy measure of cogging than figure 22. The coarser sampling rate of figure 22 gives a better overview of cogging dependence on output angle, but the coarser sampling rate of this experiment may have resulted in undersampling, missing the peak input torques. The mean applied torque for this dataset was only about 0.26 N-m, with a standard deviation of only 0.12.

For H1 driven, H2 free, L fixed, the mean applied torque was 0.51 N-m, and the standard deviation of torque was 0.19 N-m. Thus, lower friction was observed for L free vs H2 free, but the magnitude of cogging was comparable for the two cases.

For H2 driven, H1 free, L fixed, the mean applied torque at shaft H2 was 0.50 N-m, and the standard deviation was approximately 0.16. The case of H2 driven, H1 free is quite similar to the case of H1 driven, H2 free.

The breakaway torque test of figure 26 shows a release torque of roughly 12 N-m, though the breakaway torque can vary significantly, depending on the shaft angles. The rapid drop in torque seen in this figure indicates a rapid torque relief, which occurs upon breakaway of shaft L.

## Friction

Even at zero load, a transmission requires some input torque to drive a shaft. Such input torque can be reasonably modelled by measuring the driving torque vs shaft speed, and approximating the torque-speed curve by an offset (due to Coulomb friction) and a slope (viscous friction).

At no load, the efficiency of any transmission is identically zero, since power is consumed by the input, and 0% of that power is delivered to the output. While such an efficiency computation is correct, it sheds little light on the performance of the unloaded transmission.

Much of the inefficiency of a transmission can be accounted for in terms of the no-load torque required to drive an input. Tests, data and analysis for input friction are presented below for the DC-700 transmission.

**Friction Test Procedures.**- Friction tests were performed by driving one shaft at a time with a second shaft free and the third shaft held fixed (thus six combinations of driven, free and fixed shafts). The driving torque was measured for each case at selected drive speeds, both positive and negative. At each speed, approximately 5,000 samples of the drive torque meter were acquired over 5 seconds, sampled at 1kHz. The analog low-pass filter of the torque sensor drive electronics in each case was set to 1Hz. The test speeds were stepped up incrementally from near zero to maximum positive, then retraced to zero, then stepped to maximum negative, the retraced back to zero. This sequence permitted inspection of whether the data was reproducible, whether approach from higher or lower speeds had an influence, and whether the data was affected over the course of the run, e.g. due to mechanical run-in or temperature.

**Data.**- Figure 27 shows the friction data acquired for shaft H1 driven, H2 fixed and L free. Individual data points are steady-state speeds at which input torques were measured. The line Shaft H1 friction data is similarly displayed for the case of shaft H2 free and shaft L fixed, shown in figure 28.

Shaft H2 friction data is given in figure 29 for fixed shaft H1 fixed and shaft L free, and in figure 30 for shaft H1 free and shaft L fixed.

Shaft L friction, for which the low-speed shaft is driven and for which the transmission behaves as a speed increaser, is shown in figures 31 and 32. Figure 31 is the case of shaft H1 free and shaft H2 fixed, and figure 32 is the case of shaft H1 fixed and shaft H2 free.

**Analysis.**- Shaft H1 friction is relatively flat vs speed. That is, the Coulomb friction component is strong, and the viscous component is negligible. Shaft H1 friction ranges from 0.2 to 0.4 N-m, being higher with shaft L fixed than with shaft H2 fixed. The friction does not appear entirely symmetric, but the asymmetry is only approximately 0.1 % of full scale of the torque meter, which is too small to be measured reliably by the meter.

For shaft L free, the power consumed by friction to drive shaft 1 is roughly 35 W at the maximum measured speed of 140 rad/sec. With shaft L locked, the frictional power loss grew to roughly 55 W. This power loss can be expected to scale linearly with speed, since the friction torque is nearly flat.

The friction data for shaft H2 was similar. For power input to shaft H2, power output from shaft L, and shaft H1 fixed, the power loss was comparable to shaft H1 driving shaft L (roughly 30 to 35W at max measured speed). Back-driving shaft H1 via shaft H2, however,

corresponded to a power loss of about 90 to 100 W at maximum measured speed, which was less efficient than back-driving shaft H2 via shaft H1.

The "reverse" friction (torque required to drive the low-speed shaft), was approximately 5 N-m for shaft H1 free, and roughly twice as high to back-drive shaft H2. The frictional power loss to back-drive the transmission was 25W to back-drive shaft H1, and 50W to backdrive shaft H2 (at the max tested speed). This power loss would scale linearly with speed, since the friction is roughly constant vs speed.

## Efficiency

Efficiency tests were performed on the DC-700 transmission, involving extensive data collection. Torques and speeds at each of the three shafts were measured and averaged for 288 conditions of steady-state speeds and torques. The data included positive and negative rotations of all shafts, power flows both in out of shafts H1 and L, and input and output torques spanning the rated range. The chief limitation of these tests was the speed constraint on the Compumotors. The maximum power condition that could be tested was $\omega_{H1}$ = 140rad/sec, $\omega_{H2}$ = 280rad/sec, and $\omega_L$ = 4.78rad/sec at full rated torque, resulting in a power throughput of 4.6kW.

Due to limitations of the Uniq motor, shaft H2 could not tested as a power sink. In addition, since the Uniq motor was not position servo controlled, tests could not be performed with zero power transfer at shaft H2. All efficiency tests involved power sourced at shaft H2.

Efficiencies were computed on the basis of (power-out)/(power-in). Motor power from the Uniq motor thus always appeared in the denominator. However, either motor power from shaft H1 or from shaft H2 (but not both) could also appear in the denominator, if either of these shafts also sourced power to the transmission. In each computation of efficiency, the sign of the power flow at each shaft was considered to determine the correct contribution of power at that shaft to efficiency.

**Efficiency Test Procedures.**- Data was acquired at 9 steady-state velocities of shaft L: 4.79 rad/sec (140/R), 3.59 rad/sec (105/R), 2.40 rad/sec (70/R), 1.2 rad/sec (35/R), 0 rad/sec, -1.2 rad/sec (-35/R), -2.4 rad/sec (-70/R), -3.59 rad/sec (-105/R) and -4.79 rad/sec (-140/R). At each of these output speeds, 8 steady-state speeds of H1 were tested. The tested speeds of H1 were all but one of: 140, 70, 35, 0, -35, -70, -105 and -140 rad/sec. The one speed not tested

in each case was the combination of $\omega_{H1}$ and $\omega_L$ which resulted in zero speed $\omega_{H2}$. Zero speed could be tested for $\omega_{H1}$ and $\omega_L$, since the drive motors for these shafts could hold a constant position; only the Uniq motor on shaft H2 could not hold zero velocity.

At each of the above 72 combinations of speeds $\omega_{H1}$ and $\omega_L$, torque and speed measurements were taken at 4 torque levels. To accomplish this, the drive motors for shafts H1 and L were controlled in synchronous mode, enforcing a precise velocity for these shafts (the velocity of shaft H2 followed by kinematic constraint). The speed control for the Uniq motor was then adjusted to vary the load torque at all three shafts. Although the speed of the Uniq motor did not change with this adjustment, the motor torque did change in response to varying the speed command. Torque loading was adjusted in this manner for each speed combination; for each, 4 torque conditions were tested, spanning the rated torque range.

At each condition of speeds and torques (288 combinations), torques and speeds were sampled at 500Hz for 4 seconds. For these tests, the torque-meter signal-conditioning amps were set for a low-pass filter of 1-Hz. For combination of speeds and torques, the resulting 2000 samples were averaged to constitute a single data point. Efficiencies were computed for and plotted for each such point.

**Data.**- Figure 33 shows the results for the condition of stationary shaft L. For each datapoint on this plot, the Uniq motor sourced power to shaft H2, and a Compumotor on shaft H1 absorbed the power out of the transmission. Since shaft L was stationary, there was no power transfer at his port. Thus, the efficiencies were computed as the ratio of power absorbed at shaft H1 to the power sourced at shaft H2.

All plots in this section follow the same convention. Efficiencies are plotted vs the output (shaft L) torque. Individual datapoints are marked, and datapoints acquired at the same speed conditions (with varying torque loading) are connected with solid or dashed lines.

Solid lines with point markers "o", "x", "+" and "*" indicate conditions of $\omega_{H1}$ = +35, +70, +105 and +140 rad/sec, respectively. Dashed lines with point markers "o", "x", "+" and "*" indicate conditions of $\omega_{H1}$ = -35, -70, -105 and -140 rad/sec, respectively. The single dot-dash line on each plot (excluding the $\omega_L = 0$ plot ) is for the condition of $\omega_{H1} = 0$.

Efficiencies for output speeds ranging from 4.79 rad/sec to -4.79 rad/sec are given in figures 34 thru 41.

**Analysis.**- Measured efficiencies ranged approximately from 75% to 95%.

Power flow directions can be read from the plots as follows. For all plots, power flow is *into* shaft H2. For all conditions of positive $\omega_L$, a positive output (shaft L) torque implies power *into* shaft L, and a negative shaft L torque implies power *out* of shaft L. For example, figure 37 includes negative output torques exclusively and the output speed for all points on this graph is +4.79 rad/sec. Thus, all points on this graph correspond to power *out* of shaft L.

In figure 34, the output speed is positive (1.2 rad/sec). The five lines on the left half of the plot (negative shaft-L torques) correspond to power *out* of shaft L, whereas the three lines on the right half of the plot (positive shaft-L torques) correspond to conditions of power *into* shaft L.

The same logic applies to negative shaft-L velocities, for which positive shaft-L torques imply power out, and negative shaft-L torques imply power in. Figure 41 includes only data for which power is *out* of shaft L. All data points are at conditions of positive output torque and negative output velocity $\omega_L$ = -4.79 rad/sec.

For figures 34 through 37, all lines on the left (negative shaft-L torques) correspond to power *out* of shaft L, and all lines on the right correspond to power *into* shaft L. For figures 38 through 41 (negative shaft-L velocities), lines to the left (negative shaft-L torques) correspond to power *into* shaft L, and lines to the right (positive shaft-L torques) correspond to power *out* of shaft L.

The power flow direction for shaft H1 can be inferred from the graphs as well. All solid lines correspond to positive velocities of shaft H1, and all dashed lines correspond to negative shaft-H1 velocities. Due to the torque balance relationship, all positive shaft-L torques also correspond to positive shaft-H1 torques. Thus, dashed lines on the left side of the efficiency plots correspond to negative H1 velocities at negative H1 torques, implying power *into* shaft H1. Similarly, solid lines on the right half of the plots imply positive H1 velocities at positive H1 torques, again implying power into shaft H1. Conversely, dashed lines on the right and solid lines on the left correspond to conditions of power *out* of shaft H1.

The lowest efficiencies were measured at the lowest torques. At these levels, the losses due to Coulomb friction constitute the greatest percentage of power transfer, resulting in the lowest efficiencies. In fact, if two of the three shafts are unloaded, then the power consumed to drive one shaft will be lost totally due to friction, resulting in zero efficiency. Zero efficiency at low power levels is consistent with the formal definition of efficiency. However, efficiency measurements near zero power are not very enlightening, as all

transmissions drop to zero efficiency at sufficiently low powers. For low speeds and torques, the friction data presented above is more useful.

The highest efficiencies measured were obtained with power input to shafts H1 and H2, and power output from shaft L (e.g., acting as a typical speed reducer). This is consistent with the friction measurements, in which shaft H2 was shown to have higher friction than shaft H1. Thus, any power delivered to shaft H1 should be transferred more efficiently to shaft L than via shaft H2.

## DUAL INPUT DIFFERENTIAL ROLLER DRIVE (DC-500)

The DC-500 and DC-700 transmissions are similar in that two input shafts drive a single, speed-reduced output shaft differentially. Installation of the DC-500 drive in the test stand was nearly identical to that of the DC-700.

There were some notable differences from the DC-700 transmission, however. The foremost difference was that the DC-500 transmission utilized a much higher preload on its traction drive, whereas the DC-700 used a light traction preload, backed up by conventional gearing. Further, as will be described in detail below, the input shafts of the DC-500 had a lower reduction ratio than the DC-700, and, unlike the DC-700, the ratios for the two shafts were not identical (this is discussed later in the **DISCUSSION OF RESULTS** section).

The same differential velocity kinematics apply (previously presented as eq. (20) for a single ratio R):

$$\omega_L = \omega_{H2}/R_{2L} - \omega_{H1}/R_{1L}) \qquad (36)$$

but in this case, the two ratios, $R_{1L}$ and $R_{2L}$ are not identical.

Also, since the DC-500 drive had a lower transmission ratio (nominal 24:1), the NAS-300A drive, acting as a speed increaser or speed reducer at 29.23:1, limited the measurable output velocities to slightly lower values.

Another difference from the DC-700 drive was that, as a consequence of traction-drive preloading, the Coulomb friction for the DC-500 drive was significantly higher.

Due to the relatively high friction torque, tests presented here were limited to approximately 75% of rated full torque. During tests, the transmission heated up significantly. A cooling fan helped keep the temperatures down, and cool-down periods between tests were

sometimes necessary.

## Angular Linearity

One prospective advantage of traction drives is high linearity. Tests performed on the DC-700 drive were repeated for the DC-500 drive.

**Linearity Test Procedure.**- The test procedures for linearity were identical to those of the DC-700 drive. Incremental ratios were measured for: shaft H1 driven, shaft H2 fixed, shaft L free; shaft H1 fixed, H2 driven, and L free; and shaft H1 driven, shaft H2 free, shaft L fixed.

**Data.-** Figure 42 shows the incremental ratio from shaft H1 to shaft L. The mean ratio measured was 23.50:1; for reference, the mean ratio is plotted superimposed on the data. The standard deviation of the incremental transmission ratio was 0.05.

Figure 43 shows the incremental ratio from shaft H2 to shaft L. The mean ratio (shown superimposed on the data) was 24.08:1, and the standard deviation of incremental transmission ratio was 0.04.

Figure 44 displays the data for the rotation of H2 with respect to H1, with L fixed. Unlike the DC-700 transmission, this ratio was not unity. Rather, it was approximately 1.02:1.

**Analysis.-** The different ratios for L:H1 (23.50) vs L:H2 (24.08) result in a slightly different behavior from that of the DC-700 drive. For the DC-500 drive, if shafts H1 and H2 are turned at the same speed, then the output shaft, L, will not be stationary.

The different ratios were confirmed with respect to measuring the ratio of H2:H1 (1.02). In this case, shaft L was fixed, and H1 was rotated, and the angles of H1 and H2 were sampled and logged. The measured ratio of 1.02:1 is a good match to the ratio of ratios, 24.08/23.50 = 1.025.

In computing efficiencies, it is important to take into account the difference between L:H1 and L:H2 ratios.

## Cogging

Cogging tests for the DC-500 transmission were performed similarly to those of the DC-700 transmission. An important difference, though, was that the reverse (shaft L) stick-slip friction was much lower, enabling measurement of shaft-L cogging by the same method as used for shafts H1 and H2. That is, it was not necessary to resort to the break-away torque

measurements performed for shaft L of the DC-700 transmission.

**Cogging Test Procedures.-** In each case, the shaft under test was rotated smoothly and slowly in series with a reactionless torque meter. Torques were recorded at specified intervals of input angle. Mean torques and standard deviations of torques were computed for comparison with the DC-700 transmission.

**Data.-** Figure 45 shows the input torque required to smoothly rotate shaft H2 with shaft H1 free and shaft L fixed. Torques were sampled and recorded every 3.5 degrees over 2 revolutions of shaft H2. The mean torque was 1.54 N-m and the standard deviation of torque (indicative of ripple) was 0.10.

Figure 46 shows the input torque over 25 revolutions of shaft H2. This data corresponds to what would be one full revolution of shaft L (although shaft L was fixed in this test). The mean and standard deviation of the input torque were consistent with the higher-resolution data of figure 45.

Figure 47 shows the input torque required for the reverse case: H1 driven, H2 free, L fixed. The mean torque required to drive shaft H1 was 1.6 N-m, and the standard deviation was 0.14. Input torque is shown for driving shaft H1 in both the positive and the negative direction for a full revolution each.

Figure 48 shows the input torque for turning shaft H1 with H2 fixed and shaft L free. The mean H1 torque was 1.2 N-m and the standard deviation was 0.10.

Figure 49 shows the result of turning shaft H2 with H1 fixed and L free. The mean input torque was 0.95 N-m and the standard deviation was 0.50

The next two tests performed on the DC-500 drive could not be performed on the DC-700 drive, due to stick-slip friction. For the DC-500 drive, it was possible to rotate shaft L slowly and smoothly by hand. The results are shown in figures 50 and 51 for shafts H2 and H1 fixed, respectively.

The mean torque required to back-drive shaft H1 was 27 N-m, and the standard deviation was 2.0. To back-drive shaft H2 required a mean torque of 13 N-m, and the standard deviation was 5.5.

**Analysis.-** Input friction for shaft H1 driving shaft L was several times higher for the DC-500 drive vs the DC-700 drive. However, the standard deviation of shaft-H1 torque was

half that of the DC-700 drive. Thus, while the input friction was significantly higher for the DC-500 drive, the torque ripple was significantly lower. The same comparison was also true for the case of shaft H1 driving shaft H2 (shaft L fixed). For both the DC-700 and the DC-500 drives, higher torque was required to drive shaft H2 with shaft H1 than was required to drive shaft L with shaft H1. In both casess, the DC-500 drive had higher friction but lower torque ripple.

Tests with driving shaft L are harder to compare, since the DC-700 drive exhibited too much stick-slip friction to obtain cogging data. The release torque of the DC-700 drive was approximtely 12 N-m, whereas the torque required to back-drive the DC-500 drive was 27 N-m with shaft H1 free, and 13 N-m with shaft H2 free. It is noteworthy that driving shaft H2 via shaft L had roughly half the friction, but nearly three times the ripple vs driving shaft H1 via shaft L.

A similar asymmetry was noticed with the forward cases of driving shaft L via shaft H1 vs driving shaft L via H2. Driving shaft L via H1 required more torque, but had lower torque ripple than driving shaft L via shaft H2.

## Friction

Friction tests for the DC-500 drive were performed in the same way as for the DC-700 drive. Data and analysis for the DC-500 drive friction follow.

It is noteworthy that the DC-500 drive did heat up significantly during testing. Forced-air cooling and intermittant cool-down periods were required. No overheating problems were observed with the DC-700 drive, but the friction was much lower in this drive.

**Data.-** Figure 52 shows the friction data acquired for shaft H1 driven, H2 fixed and L free. Individual data points are marked corresponding to steady-state speeds at which input torques were measured.

Shaft H1 friction data is similarly displayed for the case of shaft H2 free and shaft L fixed, shown in figure 53.

Shaft H2 friction data is given in figure 54 for fixed shaft H1 and free shaft L, and in figure 55 for shaft H1 free and shaft L fixed.

Shaft L friction, for which the low-speed shaft is driven and for which the transmission behaves as a speed increaser, is shown in figures 56 and 57. Figure 56 is the case of shaft H1

free and shaft H2 fixed, and figure 57 is the case of shaft H1 fixed and shaft H2 free.

**Analysis.-** Like the DC-700 drive, the friction plots for the DC-500 drive are relatively flat vs speed. This indicates that frictional losses are dominantly due to Coulomb friction. The friction plots are also consistent with the computed mean torque at low speeds, as measured in the cogging tests.

Driving shaft L (unloaded) via shaft H1 required roughly 1.2 N-m, and driving shaft L (unloaded) via shaft H2 required only about half that torque. Similarly, back-driving shaft H1 (unloaded) via shaft L required approximately 25 N-m, whereas back-driving shaft H2 via shaft L required about 12 N-m.

Friction torque for driving shaft H1 via H2 vs driving H2 via H1 was nearly symmetric at roughly 1.5 N-m.

Note that in the tests presented earlier for the DC-700 drive, back-driving shaft H1 via shaft L required only about 5 N-m, and back-driving shaft H2 via shaft L required about 10 N-m. Oddly, with the DC-500 drive, it was easier to back-drive shaft H2 (12 N-m) than it was to back- drive shaft H1 (25 N-m).

It is noteworthy that the DC-500 drive had considerably more Coulomb friction than the DC-700 drive. For shaft H1, the DC-700 drive had a 35W loss for driving shaft H1 with shaft L unloaded at the maximum test speed. The same conditions for the DC-500 drive led to over 170W loss.

In backdriving the DC-500 drive, the power loss due to Coulomb friction at shaft L driving shaft H1 was approximately 130W at the maximum speed tested. Backdriving shaft H2 at the maximum speed tested required 55W.

The larger Coulomb friction components of the DC-500 drive influence efficiency, resulting in lower efficiencies. This is particularly true at lower torques, since the frictional torque is then a significant fraction of the total torque.

## Efficiency

**Efficiency Test Procedures.-** Efficiency tests were conducted identical to those described previously for the DC-700 drive.

**Data.** - Figure 58 shows the results for the condition of stationary shaft L.

Figures 59 through 66 show the efficiency results for 7 additional (non-zero) output speeds.

**Analysis.-** At the higher torque levels, efficiencies were measured at about 85%. Efficiencies dropped off dramatically at lower torques, since the higher Coulomb friction was then a higher percentage of the net torque. The datapoint markers and the solid vs dashed lines may be interpreted in the same manner as presented for the DC-700 transmission.

## GROUNDED RING (MOMENTUM BALANCED) DRIVE (DC-400)

The DC-400 transmision has a single high speed shaft, referred to as shaft "H", and dual counterrotating output shafts, referred to as shaft "L1" (inner output shaft) and shaft "L2" (outer output shaft). The terms "input" and "output" are used in the conventional sense in that power is typically introduced to a high speed shaft and transmitted out a low speed shaft. In such cases the transmission is used as a "speed reducer" which amplifies the torque produced by a high-speed, low torque electromechanical actuator. It should be recognized, however, that each of the three shafts can input or output power. Efficiency tests, for example, were performed with both forward and reverse power flows at both high-speed (input) and low-speed (output) shafts.

In the DC-400 transmission all three shafts are kinematically linked. If one of the shafts is locked or constrained, then the other two cannot be moved, i.e.,torque and motion transfer paths between any two shafts are not independent of the third shaft. The two output shafts (L1 and L2) counterrotate at equal and opposite speeds. This is in contrast to the DC-700 and DC-500 transmissions which allow torque and motion transfer between any two shafts with the third shaft constrained. As a consequence of its kinematic differences with the DC-700 and DC-500 units, the test procedure for DC-400 was quite different from that of the DC-700 and DC-500 units.

The DC-400 transmission was integrated into the test stand as per drawing DC-800-SK, sheet 2, subject to the coupling modifications noted above. Angular linearity, torque cogging, Coulomb and viscous friction, and power transfer efficiency are presented in this section.

Shortly after tests were initiated, a failure of the drive occurred. Disassembly of the drive revealed that it had been assembled with an incorrect locknut on the outer output shaft (part DC-400-15). The outer diameter of the locknut that was used had not been relieved as on the

Whittet-Higgins nut that was specified. As a result, the nut rubbed the inside of the Seal Carrier-Output (DC-400-18). The nut machined aluminum chips from the seal carrier, and eventually seized. Torque input to the outer output shaft unscrewed the nut allowing the Output Spindle-Inner (DC-400-16) and the Cluster Carrier (DC-400-25) to move toward the input side. The Planet Rollers, 1ST Row (DC-400-26) were forced out of alignment until two of them fractured. A new set of Planet Rollers, 1ST Row was manufactured, the locknut was machined to its specified configuration, the seal carrier was cleaned of debris, and the Ring Rollers (DC-400-22) polished to remove nicks. Some surface distress was found on the Grounded Ring (DC-400-03) so it was decided to use the alternate grounded ring in the reassembly. The drive was then reassembled for test. Details of the reassembly are given in the **Post Failure Reassembly** section of the discussion on DC-400 drive design.

## Angular Linearity

Conventional geared transmissions have exact integer-fraction transmission ratios. However, tooth-to-tooth interactions result in small variations in the ratio of incremental input angle to incremental output angle. Such variations give rise to velocity ripple of the output for smooth rotation of the input. Velocity ripple acting on a load inertia induces torque pulsations. Transmissions with identical reduction ratios can have quite different behaviors within a system, depending on their linearity.

The DC-400 transmission has no gear teeth, but instead relies on smooth rolling contact of sun and planet rollers. Consequently, such designs have the potential for smoother operation (i.e., greater linearity). Another consequence of such designs is that the transmission ratio is not precisely known a priori, as it can depend on machining tolerances of the rollers. Further, the transmission ratio can change slightly under load, as the rollers exhibit rolling creep.

**Linearity Test Procedure.-** To measure the transmission ratio and linearity, the precision BEI encoders were coupled to the DC-400 transmission. The motors, torque sensors and load transmissions were removed, so as to eliminate the influence of coupling imperfections with these elements. Shaft H (input shaft) was rotated slowly and smoothly by hand. The direction of rotation was maintained constant (to minimize any backlash effects) while encoder readings were logged by the data acquisition system. All three angles were recorded at 1-degree increments of shaft L1 (plus or minus 0.001 deg). The data was acquired over a full revolution of L1, corresponding to 24 revolutions of shaft H.

**Data.-** The raw data of input angle vs output angles is relatively uninformative, as the

dataplots are indistinguishable from straight lines. To obtain average transmission ratios, the output angles were fit to equations: H = L1*R1 and H = L2*R2, where the input angle (H) was fit to the output angles (L1 and L2) via a least-squares fit of the data, yielding correlations R1 and R2 of the effective transmission ratos.

The resulting transmission ratios were: R1 = 23.98 and R2 = 24.12. Given these average ratios, gross transmission nonlinearity could be evaluated by comparing the measured angles L1 and L2 to the ideal angles H/R1 and H/R2 respectively. Figure 67 displays the errors L1*R1-H and L2*R2-H vs input angle H. The maximum deviation of angle L1 from the ideal corresponds to approximately 1 degree of input angle, observed at nearly 2000 degrees of input rotation. The deviation of angle L2 was roughly half as large.

The incremental transmission ratio, R = (delta H)/(delta L), was computed with respect to both outputs, evaluated at increments of 1 degree of each output. The result is plotted in Figure 68. The mean incremental transmission ratios were R1=23.97 and R2=24.11, which agree closely with the least-squares evaluations of the ratios. The incremental ratio R1 varied from a minimum of 23.88 to a maximum of 24.05, and had a standard deviation of 0.03. The incremental ratio R2 varied from a minimum of 24.00 to a maximum of 24.26, with a standard deviation of 0.03.

**Analysis.-** The standard deviation of incremental transmission ratio is a reasonable figure of merit for smoothness. The standard deviation of incremental transmission ratio of the DC-400, computed at 0.03, indicates that this is a relatively smooth drive, characteristic of traction-drive designs. By comparison, the DC-700 drive (which incorporates gears) had a standard deviation of transmission ratio of 0.10, and the DC-500 drive (a traction-drive design) had a corresponding standard deviation of 0.05. It should be noted that the resolution limit of the encoders (at 0.001 degree) introduces some error in this computation. Encoder resolution artifacts can imitate incremental ratio errors approximately as large as the computed standard deviation of the DC-400 drive. While the computed standard deviation is comparable to the measurement noise, specific datapoints in the dataset exceed the variations expected from sensor discretization. Thus, the computed 0.03 standard deviation is believed to be a realistic measure of the transmission's linearity.

## Cogging

In addition to angular nonlinearity, another source of torque ripple in transmissions is cogging. Cogging is a quasi-static phenomenon that can be induced by effects such as

variable binding due to imperfect tolerances. Cogging can have both reproducible and stochastic components. For example, a flat spot on a roller would result in a reproducible torque disturbance, whereas dust or dirt between rollers could introduce torque variations that are not repeatable.

**Cogging Test Procedure.-** Accurate measurement of cogging requires a smooth input driver. Further, such tests should be performed quasi-statically, to avoid affecting the data with dynamic terms (e.g., due to angular nonlinearity). For such tests, it is not necessary that the input driver enforce a steady velocity, provided the accelerations are low. Thus, manual rotation is a good candidate input driver.

Cogging tests were performed on shafts H (input) and L1 (inner output) of the DC-400, in each case with the remaining shafts unconstrained. Shaft H was rotated for approximately 500 degrees in both the positive and negative directions. The rotation was induced by hand, in series with the input torque meter. During this rotation, the input torques were datalogged vs shaft angle.

Shaft L1 was more difficult to drive, since the friction was too high to rotate it manually. The NAS-300A load transmission was used, in this case, to amplify manually-induced drive torques. The input shaft of the NAS-300A was manually rotated, and the output of the NAS-300A drove shaft L1 (inner output shaft) of the DC-400 transmission through a reactionless torque meter. Since the NAS-300A is a relatively smooth transmission, this approach enabled slow, smooth excitation of shaft L1. Further, since the torque transducer was located between the NAS-300A output shaft and shaft L1 of the DC-400, the torque measurements did not include any imperfections of the NAS-300A. The manual rotation produced a shaft L1 rotation of plus and minus 245 degrees. Torques acting on shaft L1 were datalogged vs the angle of shaft L1.

Cogging of shaft L2 could not be measured directly. The hollow harmonic drive (load transmission) on shaft L2 did not permit a smooth enough excitation to obtain valid cogging data. The cogging of shaft L2 may be expected to be similar to that of L1.

**Data.-** Figure 69 shows the results of the positive and negative rotations of shaft H. The mean torque (plus and minus) is 1.56 N-m and the standard deviation is 0.12 N-m. There are three noticeable torque increase "humps" in the data. Windowing a section of data which excludes these relatively large, low-frequency variations results in reducing the standard deviation by half (to 0.06 N-m).

Figure 70 shows the results for shaft L1. The mean torque (plus and minus) is 36.8 N-m and the standard deviation is 4.8 N-m. Again, windowing a section of data which excludes the several relatively large, low-frequency spikes, the resulting standard deviation is significantly less at 2.6 N-m.

**Analysis.-** The data shows that torque nonlinearity is dominated by Coulomb friction. The Coulomb friction was 1.56 N-m for shaft H and 36.8 N-m for shaft L1. The cogging data showed occasional significant variations in input torque (on the order of 30%). Such variations may be due to small eccentricities of the rollers. The higher-frequency torque variations were much smaller -approximately 0.1 and 3.0 N-m RMS for shafts H and L1, respectively.

The ratio between input Coulomb friction and the Coulomb friction of shaft L1 is 23.6, which is remarkably close to the reduction ratio. This observation suggests that the friction load may be coming from a common source. In that case, one would expect to find the Coulomb friction losses distributed among the 3 shafts, rather than find additive losses for each shaft independently.

The input friction and cogging for shaft H of the DC-400 were very close to those measured on the DC-500 (dual-input) transmission inputs (with shaft L locked). The inner output friction (shaft L1) of the DC-400 was also roughly comparable to shaft-L (output) friction of the DC-500 with shaft H2 fixed. The DC-700 transmission (which incorporated gear teeth) had lower friction but greater torque ripple.

## Friction.

The cogging tests revealed the presence of strong Coulomb friction. Accounting for such friction is an important element of reconciling transmission efficiencies. Ordinarily, a transmission exhibits a speed-dependent friction term in addition quasi-static friction. Tests, data and analysis of speed-dependent friction of the DC-400 transmission are presented below.

**Friction Test Procedure**.-Friction tests were performed by driving each shaft, one at a time, with the remaining two shafts unconstrained. The driving torque was measured for each case at selected drive speeds, both positive and negative. At each speed, approximately 5,000 samples of the drive torque meter were acquired over 5 seconds, sampled at 1kHz. The

analog low-pass filter of the torque sensor drive electronics in each case was set to 1Hz. The test speeds were stepped up incrementally from near zero to maximum positive, then retraced to zero, then stepped to maximum negative, then retraced back to zero. This sequence permitted inspection of whether the data was reproducible, whether approach from higher or lower speeds had an influence, and whether the data was affected over the course of the run, e.g. due to mechanical run-in or temperature.

**Data.-** Figures 71, 72 and 73 show the friction data measured. Figure 71 is the input friction driving shaft H with shafts L1 and L2 free. Figure 72 is the friction observed driving shaft L1 (inner output) with shafts L2 and H free. Figure 73 shows the friction of shaft L2 (outer output) with shafts H and L1 free. Unlike the cogging friction tests, measurement of shaft L2 friction was possible, since input torques were averaged at each velocity, rather than logged in detail as a function of angle.

**Analysis.-** The friction plot for shaft H is somewhat anomalous. The Coulomb friction is evident at low speeds, consistent with the results from the cogging tests. However, the low-speed friction has an imbalance between positive and negative torques. This imbalance is likely due to sensor noise introduced as electromagnetic interference from the PWM power amplifiers of the motors. (The cogging tests used manual excitation, and thus did not pick up motor interference). Besides the slight imbalance in low-speed friction, the higher-speed data also shows a difference between positive and negative velocities. The positive-velocity datapoints have a velocity dependence of approximately 0.005 N-m/(rad/sec). The negative velocities, however, showed no consistent velocity-dependent friction. It should be noted that the positive velocities were tested first, followed by the negative velocities. It is possible that the data is influenced by heating effects (thermal expansion and traction-fluid viscosity) and by mechanical run-in.

Measurements on shaft L1 (Figure 72) were more consistent. The low-speed datapoints agreed closely with the Coulomb friction observed from the cogging tests. The higher-speed datapoints showed a relatively weak and relatively symmetric velocity dependence. A least-squares fit of the velocity dependence yielded 1.6 N-m/(rad/sec). However, the data showed a higher-order dependence than a simple offset-plus-linear model. The linear term provides a reasonable approximation of the velocity dependence within the range of the data, but it should not be extrapolated beyond the measured speeds. At higher speeds, it appears that the velocity dependence becomes weaker.

Friction of shaft L2 (outer output, Figure 73) was harder to interpret. The low-speed friction

was approximately 45 N-m, significantly higher than the 36.8 N-m Coulomb friction of shaft L1. Although the torque meter for shaft L2 is not well sized to accurately measure such relatively low torques, the difference between the L2 and L1 Coulomb friction torques (8 N-m) is 0.7% of the L2 torque meter's range, which lies within the claimed 0.1% linearity. Thus, the measurements should be reliable in the result that shaft L2 Coulomb friction is approximately 20% higher than that of shaft L1.

There does appear to be a relatively weak dependence of the L2 friction on velocity. However, the data cannot support a reliable conclusion regarding the sensitivity. It is also noteworthy that the positive velocities showed a stronger velocity-dependent friction than the negative velocities. As with the input friction data, however, this may be due to slow thermal or mechanical wear variations during the data collection.

The relatively large Coulomb friction and relatively weak velocity-dependent friction behavior observed is consistent with traction-drive designs.

## Efficiency

Efficiency tests were performed on the DC-400 transmission under nearly 200 steady-state conditions of speed, input torque, and ratio of output torques. The data included power flow in both the "forward"condition (power into high-speed shaft, power out of low-speed shafts) and "reverse" (power into shafts L1 and L2, power out of shaft H).

Various constraints of the test equipment and of the DC-400 transmission limited the conditions to relatively low speeds and torques (roughly half the rated limits). The harmonic-drive load transmission limited the velocity of the tests to input speeds between -105 rad/sec and 105 rad/sec. Since the wave generator and flex spline of the harmonic drive were not adequately restrained in the axial direction, this transmission would bind up at higher speeds and under some conditions of direction of rotation and direction of power flow. In addition, axial drift of the harmonic-drive flex spline led to excessive friction under some test conditions of higher speeds and torques, corrupting the efficiency data. It was anticipated that the efficiency tests would be limited by the power limitations of the Compumotors used. The Compumotors were limited in both speed and torque to approximately half of the DC-400 rating. However, it was found that the Compumotors' speed limits were higher than the harmonic-drive speed constraint, so the Compumotors did not present a binding constraint on speed. In addition, although the Compumotors were not capable of exerting the full rated input torque of the DC-400, it was found experimentally

that the DC-400 could not accept input torques in excess of 17N-m (150 in-lbf), so the Compumotor torque limits were also not binding constraints.

The Uniq motor presented another constraint on the efficiency tests. This motor performed well as a power source, but it was not well behaved as a power sink. Some data was taken with this motor acting as a power sink, but the load torque provided was less well regulated. This constraint limited the measurements of forward efficiency (power in at shaft H and out at shafts L1 and L2).

The DC-400 design presented additional unexpected constraints on the torques which could be tested. Due to internal preloading limits at the grounded ring, it is most desirable to keep the two low speed shaft torques (L1 and L2 torques) within approximately 30% of each other to avoid the danger of slip at the grounded ring. A more surprising limit was the maximum input torque that the transmission could accept. Although it was rated for 36 N-m (320 in-lbf) input torque, it was found that the transmission misbehaved (appeared to induce roller slip) at input torques in excess of 17N-m (150 in-lbf).

The DC-400 was thus tested to the limits of the torques it could support, but the tests spanned only about 35% of the rated speed.

**Efficiency Test Procedure.-** For each condition of speeds and torques, the transmission was driven as follows. Shaft H (input) speed was regulated by driving the input Compumotor in synchronous mode. Shaft L1 torque was regulated by driving the second Compumotor (via the NAS-300A transmission) in torque mode. The Uniq motor was driven by a soft velocity-control loop. As the Uniq motor velocity control command was varied about the enforced L2 velocity, the resulting torque exerted by the Uniq motor (via the harmonic-drive load transmission) on L2 varied. Correspondingly, the torque on shaft H varied (by approximately 1/24 of the L2 torque change). Under such control, various combinations of shaft speeds and torques could be produced.

Data was acquired at steady-state input velocities of -105, -70, -35, 35, 70 and 105 rad/sec. At each speed, tests were performed at steady-state input torques ranging between approximately plus and minus 17N-m (150 in-lbf). At each combination of speed and input torque, torque conditions on shafts L1 and L2 were tested, typically for 5 conditions of output torque ratio ranging from approximately 0.7 to 1.4.

**Data.-** Figure 74 displays a summary of data for the transmission efficiency in "reverse"

operation (power input to L1 and L2, power output from H). Each of the curves displayed comprises a set of data taken at constant input velocity. The 6 curves represent input velocities of -105, -70, -35, 35, 70 and 105 rad/sec. For each curve, specific datapoints are noted, totaling 39 conditions. For each condition, the two output shafts (L1 and L2) were driven with approximately equal torques and speeds (and thus approximately equal power). The Compumotor on shaft H was used as a power sink. The power extracted at port H divided by the power input to shafts L1 and L2 is plotted as the efficiency.

Figure 75 displays corresponding data for conditions of "forward" power transfer (power into shaft H and out of shafts L1 and L2).

Figure 76 offers a different visualization of the data. Efficiencies are plotted vs shaft H torque, rather than vs input power. Lines on this plot are, again, groups of datapoints acquired at constant speed. All 12 lines from Figs 74 and 75 (both forward and reverse power flow data) are included on this common plot. From this figure, it is evident that the efficiency improves with higher input torques. This observation is consistent with a hypothesis that transmission losses are primarily attributable to Coulomb-type friction, likely due to roller preloading. Such friction seems to be independent of speed and of output torque. To further explore this hypothesis, the power loss for each condition was computed, and the equivalent friction torque which could account for this loss (with respect to shaft H) was computed. A display of the equivalent loss torques (computed from the reverse efficiency data) is given in Figure 77.

Additional tests were performed with imbalanced torques L1 and L2. At input speeds of plus and minus 35, 70 and 105 rad/sec, and at input torques of plus and minus 80 in-lbf, 110 in-lbf and 150 in-lbf, the torque ratio between output shafts L1 and L2 was varied .

Efficiency data is plotted for each input speed, displaying efficiency vs output torque ratio, for lines of constant input torque. Nine such plots are included. Figures 78 through 83 show the "reverse" efficiencies (power sources at L1 and L2, power sink at H) for input speeds of -105, -70, -35, +35, +70, and +105 rad/sec, respectively. Figures 84, 85 and 86 show similar tests for "forward" efficiency (power sourced to shaft H, power sinks at L1 and L2). These plots display the results for input speeds of +35, +70 and +105 rad/sec, respectively.

Due to axial drift of the harmonic-drive wave generator, tests could not be performed for forward power flow with a negative input velocity. In addition, the data for forward power flow at +105 rad/sec was limited to conditions of L1 torque less than L2 torque. Increasing

torque on L1 higher than the torque on L2 resulted in roller slip.

**Analysis.-** Figure 75, which displays the "forward" efficiency values, indicates efficiencies as high as 92%. (Even higher efficiencies were measured when the output shaft torques were not balanced, favoring power flow via shaft L2). Figure 75 indicates that it is typically true that higher power transfers result in greater efficiency. The curve corresponding to an input velocity of +35 rad/sec seems to be an exception to this trend. Note, though, that the anomalous points occur at relatively low torques and at the lowest speed, making the measurement sensitivity poorer and the susceptibility to noise (such as the EMI produced by the motor amps and picked up by the torque-sensor electronics) higher.

The trend to higher efficiencies at higher powers is indicative of an equivalent "fixed cost" of transmission losses, which is proportionately less important as input powers increase. To test such a model of efficiency, Fig 76 was generated, in which all 12 of the constant-speed data sets are plotted (both positive and negative input velocities, and positive and negative power flows) vs input torque, rather than vs input power. For the most part, the lines of Fig 76 converge. This suggests that the efficiency is primarily a function of input torque. As the input torque increases, the efficiency increases. This is consistent with having a fixed input friction, which represents a smaller percentage loss as the input torque increases.

Figure 77 shows the computed equivalent input-shaft friction which could account for the net power loss for each reverse-efficiency measurement. If the losses could be explained by pure Coulomb friction, then the loci of Fig 77 would appear as coincident, horizontal lines. The computed Coulomb friction, however, varies from less than 1 N-m to nearly 6 N-m. It is possible that the higher computed friction values reflect additional friction introduced by the harmonic-drive flex spline. The lower computed friction values are more nearly flat vs input power, and thesetorque values are closer to the measured input-shaft friction with unloaded output shafts. Overall, this plot suggests that the DC-400 efficiency at different speeds and torques can be reasonably estimated by considering losses due to Coulomb friction, essentially independent of load. In addition, this plot suggests that harmonic-drive friction did influence the measurements, and it suggests a range for this influence.

In both Figures 74 and 75, the data at positive input speeds indicates a higher efficiency than the corresponding data at negative input speeds. There is no obvious reason why the DC-400 transmission data should have a preferred direction of rotation, and no such asymmetry was observed in the friction. This phenomenon is likely attributable to the test-stand problem with the harmonic-drive components. The direction of axial drift of the harmonic-drive flex

spline was a function of the direction of rotation. When this component translated into contact with its confining thrust washers, the resulting friction would affect the measurements, yielding a lower apparent efficiency. It could not be observed when such internal friction arose. However, this flaw in the test rig could only decrease the apparent efficiency. Thus, the highest measured efficiencies are the most credible.

The highest measured efficiencies exceeded 95%. As expected, based on the measured Coulomb friction, the highest efficiencies typically occurred at the highest torque loading. Some exceptions are notable. For example, Fig 83 (reverse efficiency at input speed +105 rad/sec) shows an efficiency at 150 in-lbf input torque which is lower than that of the 80 and 110 in-lbf input torques. This condition likely indicates the onset of roller slip in the DC-400 at this condition of speed and torque.

The differential output torque measurements (Figs 78 through 86) gave a surprising result. Efficiencies were typically higher when shaft L2 (outer output) was driven harder than shaft L1 (inner output). The friction measurements indicated that shaft L2 had a higher friction than shaft L1 (when the remaining two shafts were free). Thus, it would seem that efficiencies should be higher when more power is transmitted through shaft L1 than through shaft L2. As the output torque ratio L1/L2 varied from about 0.7 to about 1.4, the efficiency fell by (typically) several percentage points.It may be that this variation is an artifact of the test-stand flaws (particularly the harmonic drive friction), or it may be that the effect is a result of the complex kinematic interactions among the differential rollers of the DC-400 drive.

Finally, the efficiency data also provides information regarding roller creep vs load. The data from Fig 74 was used to compute the speed ratio from input shaft H to output shaft L1 (output shaft L2 angle could not be measured directly under load). The ratio of input to output speed was seen to change as the torque on L1 increased. For the data of Fig 8, shaft L1 was driven with a power source. As a result, this shaft ran somewhat faster than predicted by the transmission ratio (as measured under unloaded conditions). Alternatively, the speed ratio from H to L1 decreased as the torque on shaft L1 increased. The result is shown in Fig 87. Creep between shafts H and L1 apparently changes linearly as a function of applied torque. The lone out-lying datapoint (at ratio=23.07) corresponds to an input torque in excess of 150 in-lbf. Thus, this datapoint likely includes some roller slipping.

## DISCUSSION OF RESULTS

Several comparisons can be made between the performance of the Differential Roller-Gear Drive (DC-700) and the Differential Roller Drive (DC-500). As expected, the linearity of the Roller Drive is superior to that of the Roller-Gear Drive because the transfer of motion through rollers is smoother than through gears. The standard deviation of non-linearity in the Differential Roller Drive was approximately half that in the Differential Roller-Gear Drive. Variations in linearity result in small variations in the ratio of incremental input angle to incremental output angle which give rise to velocity ripple of the output. Velocity ripple acting on a load inertia induces torque pulsations. In a similar vein, cogging or torque ripple tests showed that the Differential Roller Drive is smoother as a speed reducer than is the Differential Roller-Gear Drive. Additionally the Differential Roller-Gear Drive exhibited some stick-slip in a back driving mode. Attempts to conduct cogging tests driving the output or low speed shaft with both input shafts free were unsuccessful because of a significant breakaway torque. The Differential Roller Drive was smoother in a back driving mode. In any robotic application where variations of output velocity and torque are critical to performance acceptability, use of a roller drive would be advantageous.

For simplicity of design a varible preload system was not incorporated into the Differential Roller Drive. It is preloaded at assembly with shims. At first assembly the preload was set at 100% of rated torque. The resulting tare torque was quite high, so the preload was reset at approximately 80% with the view that, after run-in, the drive would relax allowing an increase of preload to full rating while still maintaining a reasonable level of tare torque. Tests were therefore limited to 80% of full torque rating to avoid risking roller slip. Although simpler mechanically, the Coulomb friction losses in a fully preloaded drive are almost constant regardless of the torque (or power) being transmitted so that efficiency losses are incurred whenever levels of torque transfer are less than full rating. Friction losses at zero power output were five times as great in the Roller Drive as in the Roller-Gear Drive when each drive was operated as a speed reducer. Details of friction losses through the various torque transfer paths at zero power output are shown in Table XI.

Differential Roller-Gear Drive efficiencies at the highest output speed at which measurements were taken (4.9 rad/sec) ranged from 87 to 94% at full rated torque, and 86 to 94.5% at 20 percent of full rated torque. (In a differential drive the efficiency (power out/power in) at a set value of output speed and torque depends on the combination of input speeds used to obtain the desired output speed). In contrast, Differential Roller Drive efficiencies were 75 to 83% at 80 percent of full rated torque, and 52 to 83% at 20 percent of

full rated torque. In assessing the performance of the Differential Roller Drive it appears that the higher friction losses and lower part load efficiencies incurred by use of a full preload system make the incorporation of a variable preload system mandatory in future designs. The efficiencies measured are strictly those associated with frictional losses. Losses in efficiency in differential drives can also result from recirculating power. When $\omega_{H1}$ and $\omega_{H2}$ are of the same sense, then the output speed will be less than the greater input speed divided by R. One of the two input torques will be negative (that input will be a power absorber or brake rather than a driver). There will then be a recirculating power loss. This will generally be the operating mode of the differential drive. It will be used with two unidirectional variable speed inputs to produce low magnitude bidirectional output speeds, with a non-rotating output achievable without having to stop either input. This eliminates the stick-slip uncertainties associated with starts and stops. Table XII shows the combinations of input and output angular velocities at which frictional efficiencies (defined as the ratio of power out to power in) were measured. Some of those combinations of angular velocity result in recirculating power losses. In those cases the system efficiency will be the product of frictional efficiency and differential efficiency.

One of the ideosyncracies of motion and torque transfer through preloaded rollers revealed itself in measurements of ratios between each high speed or input shaft and the low speed or output shaft (with the second high speed shaft fixed), and from one high speed shaft to the other high speed shaft (with the low speed shaft fixed) in the Differential Roller Drive. The nominal design ratio from either high speed shaft to the low speed shaft is 24:1. The ratio from shaft H1 (inner input shaft) to output shaft L was measured as 23.5:1 with zero torque restraint on output shaft L. The ratio from shaft H2 (the outer input shaft) to output shaft L was measured as 24.08:1 with zero torque restraint on output shaft L. These ratios differ by 2.5%. In preloaded rollers a loss in motion known as roller creep occurs in the contact between each roller pair. The torque transfer path from shaft H1 to shaft L goes through one set of sun-first planet, one set of first planet-second planet, and one set of second planet-ring contacts (in the rotating ring roller cluster) to shaft L. The torque transfer path from shaft H2 to shaft L goes through one set of sun-first planet, one set of first planet-second planet, and one set of second planet-ring contacts (in the stationary ring roller cluster), and thence through the second planet-ring contacts in the rotating ring cluster to shaft L. Creep in the additional set of roller contacts accounts for the 2.5% difference in ratios. The small difference in ratios means that identical counterrotating speeds of shafts H1 and H2 will not result in a stationary shaft L. The speeds of shafts H1 and H2 must differ by 2.5% to produce a stationary shaft L.

Kinematic behavior of the Momentum Balanced (Grounded Ring) Drive was very promising. It was the smoothest of the three drive tested exhibiting a standard deviation of incremental transmission ratio of only 0.03. Reduction ratios from the input to the counterrotating outputs (design value = 24) were 23.98 and 24.12 at zero load, and changed about 2% due to roller creep at the maximum load.. Cogging torques were low, and friction losses were predominantly due to Coulomb friction. Constraints of the test equipment limited test conditions to relatively low speeds, and an overestimate of the initial preload setting caused a roller slip at half the rated capacity, but test results were very promising within the bounds of the test conditions. As with the Differential Roller Drive, the penalties incurred by fixed preload were apparent. Efficiencies at low torques were low, and the uncertainties associated with setting the initial preload level led to roller slip. The 95% efficiency obtained at maximum torque is quite satisfactory , however. A modification of the procedure used for setting initial preload level is indicated.

The Momentum Balanced (Grounded Ring) Drive exhibited differences in efficiency with positive and negative input rotations although there is no asymmetryin the drive. The negative rotation direction resulted in lower efficiencies due to problems with extraneous friction in the L2 shaft caused by a thrust reactioon in the harmonic drive elements. Therefore only the efficiency data obtained from the positive rotation tests are considered valid.

## SUMMARY OF RESULTS

1. Two differential (dual input, single output) drives (or transmissions), each rated at 295 rad/sec (2800 rpm) input speed, 450 N-m (4,000 in-lbf) output torque, and 5.6 kW (7.5hp) were designed, fabricated, and tested. The Dual Input Differential Roller-Gear Drive (DC-700) has a planetary roller-gear system with a reduction ratio (one input driving the output with the second input fixed) of 29.23:1. The Dual Input Differential Roller Drive (DC-500) has a planetary roller system with a reduction ratio of approximately 24:1. Each of the differential drives features dual roller-gear or roller arrangements consisting of a sun, four first row planets, four second row planets, and a ring. Both drives are lubricated with a charge (non-recirculating) of commercial traction fluid. Test results reported for the two differential drives include angular and torque ripple (linearity and cogging), viscous and Coulomb friction, and forward and reverse power efficiency.

2. A momentum balanced drive ( single input with two counterrotating, equal speed outputs ) was also designed, fabricated and tested. The Momentum Balanced (Grounded Ring) Drive (DC-400) features a unique "grounded ring" design which makes possible a reduction in size and weight of approximately 40% when compared to a conventional design. The drive is rated at 302 rad/sec (2880rpm) input speed, dual output torques of 434Nm(3840 in-lbf) and 10.9kw (14.62hp). The drive features a planetary roller system with five first and second row planets and a reduction ratio from the input to the dual counterrotating outputs of 24:1.

3. Standard deviation in linearity of the Differential Roller-Gear Drive was 0.1, and that of the Differential Roller Drive was 0.05. As expected motion and torque transfer through rollers is smoother than through gears.

4. Cogging tests to measure torque variations were conducted by smoothly rotating one input by hand with the second input locked and zero torque applied to the output. The Differential Roller-Gear Drive had a mean torque of .26N-m (2.3 in-lbf) due to Coulomb friction with a standard deviation (torque ripple) of .12N-m (1.06 in-lbf) indicating cogging. The Differential Roller Drive had an average mean torque of 1.5N-m (13.3 in-lbf) due to Coulomb friction with an average standard deviation (torque ripple) of .11N-m (.97 in-lbf).

5. Frictional power loss was measured in both differential drives for all torque transfer paths through the drives. At 140 rad/sec input speed to one input with the second input locked and the output free, power losses were 35 W (.047 hp) in the Differential Roller-Gear Drive and 170 W (.227 hp) in the Differential Roller Drive.These values are, respectively, .63 and 3

percent of full rating. The relatively high values of cogging torque and zero power friction loss in the Differential Roller Drive are due to the use of a full roller preload system rather than a cam-acting variable preload system. This results in frictional losses at zero power output which approximate those at full rated power output.

6. Efficiency (defined as the ratio of power out to power in) was measured for both differential drives at four output speeds, four combinations of dual input speeds for each output speed, and four torque levels. For the Differential Roller-Gear Drive efficiencies ranged from 75% at near zero power throughput to 95% at the maximum power level. For the Differential Roller Drive efficiencies ranged from less than 10% at near zero power throughput to 86% at the maximum power level. The highest measured efficiencies were obtained with the drives operating as conventional speed reducers. The low efficiencies of the Differential Roller Drive at low power throughputs are the result of full preloading.

7. The momentum balanced drive performed as expected kinematically.The measured reduction ratios between the input and the counterrotating outputs were 23.98:1 and 24.12:1 at zero load. A change in ratio of 2% due to roller creep was noted as output torque was increased to 250Nm (2200 in-lbf) The standard deviation of incremental transmission ratio was 0.03. It was the smoothest of the threee drives tested. Because of kinematic constraints, cogging test were conducted by rotating one of the shafts manually with the other two shafts free. The input shaft mean cogging torque was 1.56Nm (13.8 in-lbf). The inner output shaft mean cogging torque was 36.8Nm (325.6 in-lbf) with a standard deviation of 4.8Nm (42.8 in-lbf). Nonlinearity was dominated by Coulomb friction, as expected. In friction tests, when torque was inputted to the high speed input shaft, there was only a small speed dependence.

8. The momentum balanced drive successfully equilibrated torques among its three shafts. A given input shaft torque could be balanced by a range of output shaft torques. While the ratio of output torques was varied from 0.55 to 1.8, the sum of the output torques remained nearly constant for a given input torque.

9. Efficiencies of the momentum balanced drive were determined in both the forward mode (speed reducer) and reverse mode (speed increaser). Data were taken at three input velocities (both positive and negative) with equal torques on the output shafts, and then with output shaft torque ratios, $T_{L1}/T_{L2}$, ranging from 0.55 to 1.8. Efficiency improved with increasing torque and generally decreased with increasing speed. At maximum torque effficiency approached 95%. The effect of output torque ratio $T_{L1}/T_{L2}$ was inconsistent. When operated in the reverse mode, efficiencies decreased slightly with increasing torque ratio; when in the

forward mode, torque ratio had little effect on efficiency.

10. Limitations in the test stand made it impossible to test the momentum balanced drive up to its full rated speed. The harmonic drive components developed thrust loads which were unexpected. A major redesign of the test stand would have been required to accomodate the thrust loads. This was not possible, but thrust washers were added to make possible testing over a reasonable speed range.

11. The disadvantages of fixed preload again became apparent in these tests . Part load efficiencies were low, and the level of initial preload was evidently set too low. The latter resulted in roller slip at approximately 50% of the drive rating.

## REFERENCES


1. Steinetz, Bruce M., Rohn, Douglas A., and Anderson, William J.: Evaluation of a High Torque Backlash-Free Roller Actuator. Presented at the 20th Aerospace Mechanisms Symposium, May 7-9, 1986. NASA CP2423, pp. 215-240.

2. Anderson, William J.: Dual Counterrotating Output Torque and Speed Matched Drives. Final Report for NASA Lewis Research Center, Contract NAS 3-25576, June, 1989.

3. Anderson, William J.: Traction Drives for Reaction Free and Momentum Balanced Systems, and Zero Stick-Slip Robotic Drives. Final Report for NASA Lewis Research Center, Contract NAS 3-26570, August, 1992.

4. Anderson, William J., and Shipitalo, William: Roller-Gear Drives for Robotic Manipulators. Final Report for NASA Lewis Research Center, Contract NAS 3-25282, August 1988.

5. Anderson, William J., and Shipitalo, William: Roller-Gear Drives for Robotic Manipulators: Design, Fabrication and Test. Final Report for NASA Lewis Resarch Center, Contract NAS 3-25803, September, 1991.

6. Buckingham, E.: "Manual of Gear Design". The Industrial Press, New York.

7. Roark, Raymond J., and Young, Warren C.: Formulas for Stress and Strain. McGraw-Hill, Inc., 1982.

TABLE I

| ROLLER-GEAR DRIVE CLUSTER GEOMETRIES | | | | | | | | |
|---|---|---|---|---|---|---|---|---|
| | Design 1 | | Design 2 | | Design 3 | | Design 4 | |
| α | 18 | | 11.25 | | 9 | | 9 | |
| γ | 27 | | 33.75 | | 36 | | 36 | |
| a+x1 | 28.575mm | 1.125in | 28.118mm | 1.107in | 28.575mm | 1.125in | 28.397mm | 1.118in |
| y1+x2 | 44.506 | 1.7522 | 35.786 | 1.4089 | 34.376 | 1.3534 | 34.163 | 1.345 |
| z | 47.716 | 2.3567 | 49.639 | 1.9543 | 48.016 | 1.8904 | 47.716 | 1.8786 |
| Diametral Pitch | | | | | | | | |
| a-x1 | 40 | | 34 | | 40 | | 40 | |
| y1-x2-c | 34 | | 34 | | 41 | | 43 | |
| Number of teeth | | | | | | | | |
| a | 28 | | 24 | | 28 | | 28 | |
| x1 | 62 | | 53 | | 62 | | 62 | |
| y1 | 20 | | 16 | | 20 | | 20 | |
| x2 | 100 | | 80 | | 90 | | 95 | |
| c | 260 | | 212 | | 244 | | 256 | |
| Operating Pitch Dias. | | | | | | | | |
| a | 17.78mm | .700in | 17.526 | .6900in | 17.78mm | .700in | 17.668mm | .6956in |
| x1 | 39.37 | 1.55 | 38.707 | 1.5239 | 39.37 | 1.55 | 39.124 | 1.5403 |
| y1 | 14.836 | 0.5841 | 11.928 | 0.4696 | 12.499 | 0.4921 | 11.905 | 0.4678 |
| x2 with y1 | 74.178 | 2.9204 | 59.644 | 2.3482 | 56.251 | 2.2146 | 56.44 | 2.2221 |
| x2 with c | 74.826 | 2.9559 | 60.168 | 2.3688 | 56.124 | 2.2096 | 56.312 | 2.217 |
| c | 194.55 | 7.6594 | 159.44 | 6.2773 | 152.16 | 5.9906 | 151.75 | 5.9743 |
| Cutting Pitch Dias. | | | | | | | | |
| a | 17.78mm | .700in | 17.93mm | .7059in | 17.78mm | .700in | 17.78mm | .700in |
| x1 | 39.37 | 1.55 | 39.594 | 1.5588 | 39.37 | 1.55 | 39.37 | 1.55 |
| y1 | 14.94 | 0.5882 | 11.953 | 0.4706 | 12.39 | 0.4878 | 11.814 | 0.4651 |
| x2 | 74.706 | 2.9412 | 59.764 | 2.3529 | 55.756 | 2.1951 | 56.116 | 2.2093 |
| c | 194.24 | 7.6471 | 158.38 | 6.2353 | 151.16 | 5.9512 | 151.22 | 5.9535 |
| Reduction Ratio | | | | | | | | |
| | 28.876 | | 29.26 | | 27.014 | | 28.34 | |
| Estimated OD | | | | | | | | |
| | 254mm | 10in | 219.13mm | 8.627in | 211.84mm | 8.34in | 211.33mm | 8.32in |

TABLE II

| GEAR DATA FOR DUAL INPUT ROLLER-GEAR DIFFERENTIAL DRIVE | | | | | |
|---|---|---|---|---|---|
| GEAR | a | x1 | y1 | x2 | c |
| Number of teeth | 28 | 62 | 20 | 100 | 264 |
| Diametral pitch | 32 | 32 | 28 | 28 | 28 |
| Pitch dia.,mm | 22.225 | 49.213 | 18.143 | 90.714 | 239.486 |
| in | 0.875 | 1.9375 | 0.7143 | 3.5714 | 9.4286 |
| Pressure angle, deg. | 20 | 20 | 20 | 20 | 20 |
| Base circle dia.,mm | 20.884 | 46.246 | 17.048 | 85.242 | 225.044 |
| in | 0.8222 | 1.8207 | 0.6712 | 3.356 | 8.86 |
| Circular tooth thickness, mm | 1.3183/1.3056 | .8585/.8458 | 1.684/1.6713 | 1.5596/1.5469 | 1.5545/1.5291 |
| in | .0519/.0514 | .0338/.0333 | .0663/.0658 | .0614/.0609 | .0612/.0602 |
| Major dia., mm | 24.0309/24.0157 | 49.6037/49.5783 | 20.6883/20.6629 | 92.9208/92.8954 | 241.1197/241.3 |
| in | .9461/.9455 | 1.9529/1.9519 | .8145/.8135 | 3.6583/3.6573 | 9.4929/9.5000 |
| Root dia.,mm | 20.6019/20.3784 | 46.3271/46.1035 | 16.7691/16.5151 | 89.0016/88.7476 | 237.998/238.049 |
| in | .8111/.8023 | 1.8239/1.8151 | .6602/.6502 | 3.5040/3.4940 | 9.370/9.372 |
| True involute form dia.,mm | 21.2573 | 47.3177 | 17.3888 | 89.9414 | 240.69 |
| in | 0.8369 | 1.8629 | 0.6846 | 3.541 | 9.476 |
| Meas. pin dia.,mm | 1.524 | 1.524 | 1.7417 | 1.7417 | 1.7417 |
| in | 0.06 | 0.06 | 0.06857 | 0.06857 | 0.06857 |
| Meas. over pins,mm | 24.8107/24.7828 | 50.7009/50.6654 | 21.3944/21.3716 | 93.9165/93.8860 | 236.136/236.210 |
| in | .9768/.9757 | 1.9961/1.9947 | .8423/.8414 | 3.6975/3.6963 | 9.2981/9.3010 |
| Operating center distance,mm | 35.306 | | 54.991 | | 73.9623 |
| in | 1.39 | | 2.0165 | | 2.9119 |
| Contact ratio | 1.69 | | 1.55 | | 1.48 |
| Backlash at Operating Center Distance,mm | .0254/.0508 | | .0330/.0584 | | .0318/.0762 |
| in | .001/.002 | | .0013/.0023 | | .0015/.003 |
| Operating Pitch dia.,mm | 21.9685 | 48.6435 | 18.3312 | 91.6508/90.1979 | 238.1225 |
| in | 0.8649 | 1.9151 | 0.7217 | 3.6083/3.5511 | 9.3749 |
| Mating roller dia,mm | 21.9685 | 48.6435 | 18.3312 | 91.6508/90.1979 | 238.1225 |

TABLE III

| ROLLER DATA FOR DUAL INPUT ROLLER-GEAR DIFFERENTIAL DRIVE | | | | | | |
|---|---|---|---|---|---|---|
| (20 percent torque transfer through rollers) | | | | | | |
| Coefficient of friction=.06 at Sun-First planet | | | | | | |
| | | | | | | |
| **Roller** | **a** | **x1** | **y1** | **x2** | | **c** |
| Nominal diameter,mm | 21.98116 | 48.65624 | 18.34388 | 90.21826 | 91.66352 | 238.0793 |
| in | 0.8654 | 1.9156 | 0.7222 | 3.5519 | 3.6088 | 9.3732 |
| Width, mm | 3.175 | | 4.775 | | 4.775 | |
| in | 0.125 | | 0.188 | | 0.188 | |
| Number of rollers(dual) | 1 | 4 | 4 | 4 | 4 | 1 |
| Contacts/roller | 4 | 2 | 2 | 2 | 1 | 4 |
| Torque/roller, Nm | 1.899 | 1.048 | | 5.243 | | 55.577 |
| inlbf | 16.8 | 9.276 | | 46.387 | | 491.7 |
| Tangential force, N | 27.087 | | 43.95 | | 87.14 | |
| lb | 6.087 | | 9.876 | | 19.582 | |
| Normal force, N | 451.45 | | 1157 | | 1924.2 | |
| lb | 101.45 | | 260 | | 432.4 | |
| Hertz stress, GPa | 0.92 | | 1.33 | | 0.55 | |
| psi | 134,000 | | 192,600 | | 79,700 | |
| Coefficient of friction | 0.06 | | 0.038 | | 0.045 | |
| Half contact width,mm | 0.196 | | 0.234 | | 0.937 | |
| in | 0.0077 | | 0.0092 | | 0.0369 | |
| Normal approach, mm | 0.00483 | | 0.0079 | | 0.0178 | |
| in | 0.00019 | | 0.00031 | | 0.0007 | |
| Inner fiber stress,GPa | | | | | | 0.136 |
| psi | | | | | | 19,720 |
| Load point deflection,mm | | | | | | 0.031 |
| in | | | | | | 0.0012 |
| Material | M-50 tool steel | | | | | 9310 steel |
| Heat treatment | Rc61-63 | | | | | Carburize, Rc59-63 |

TABLE IV

| DC 700 GEAR MEASUREMENTS OVER PINS | | | | | |
|---|---|---|---|---|---|
| GEAR | PRINT DIM.,in. | MEASURED | DIFFERENCE FROM HIGH | INDEX ERROR, in. | CLUSTER NO. |
| SUN "a" (input side) | .9768/.9757 | 0.9772 | 0.0004+ | | |
| SUN "a" (output side) | .9768/.9757 | 0.9772 | 0.0004+ | | |
| 1st. PLANET, y1 | .8423/.8414 | | | | |
| NOS. 1&2 | | .8424/.8423 | 0.0001+/0 | | |
| NOS. 3&4 | | .8425/8423 | 0.0002+/0 | | |
| NOS. 5&6 | | .8421/.8424 | 0.0002-/0.0001+ | | |
| NOS. 7&8 | | .8425/.8426 | 0.0002+/0.0003+ | | |
| NOS. 9&10 | | .8424/.8425 | 0.0001+/0.0002+ | | |
| NOS. 11&12 | | .8422/.8425 | 0.0001-/0.0002+ | | |
| NOS. 13&14 | | .8419/.8420 | 0.0004-/0.0003- | | |
| NOS. 15&16 | | .8418/.8419 | 0.0005-/0.0004- | | |
| 1st. PLANET , x1 | 1.9961/1.9947 | | | | |
| WITH 1&2 y1 | | 1.9954/1.9954 | 0.0007-/0.0007- | 0.0008 | 2 |
| WITH 3&4 y1 | | 1.9953/1.9954 | 0.0008-/0.0007- | 0.0002 | 2 |
| WITH 5&6 y1 | | 1.9934/1.9934 | 0.0007-/0.0007- | 0.0008 | 1 |
| WITH 7&8 y1 | | 1.9951/1.9954 | 0.001-/0.0007- | 0.0001 | 2 |
| WITH 9&10 y1 | | 1.9949/1.9951 | 0.0012-/0.001- | 0.0003 | 1 |
| WITH 11&12 y1 | | 1.9940/1.9945 | 0.0021-/0.0016- | 0.0018 | 1 |
| WITH 13&14 y1 | | 1.9958/1.9958 | 0.0003-/0.0003- | 0.0004 | 2 |
| WITH 15&16 y1 | | 1.9946/1.9950 | 0.0005-/0.0011- | 0.0006 | 1 |
| 2nd. PLANET, x2 | 3.6975/3.6963 | | | | |
| NOS. 1&2 | | 3.6968/3.6968 | 0.0007-/0.0007- | | 1 |
| NOS. 3&4 | | 3.6965/3.6964 | 0.001-/0.0009- | | 2 |
| NOS. 5&6 | | 3.6964/3.6964 | 0.0011-/0.0011- | | 2 |
| NOS. 7&8 | | 3.6966/3.6965 | 0.0009-/0.001- | | 1 |
| NOS. 9&10 | | 3.6965/3.6965 | 0.001-/0.001- | | 2 |
| NOS. 11&12 | | 3.6965/3.6965 | 0.001-/0.001- | | 2 |
| NOS 13&14 | | 3.6968/3.6968 | 0.0007-/0.0007- | | 1 |
| NOS. 15&16 | | 3.6968/3.6968 | 0.0007-/0.0007- | | 1 |
| RING, c | 9.2981/9.3010 | | | | |
| NO.1 | | 9.2989 | 0.0021- | | 1 |
| NO.2 | | 9.2987* | 0.0023- | | 2 |
| *Average of six readings | | | | | |

TABLE V

| DC 700 ROLLER MEASUREMENTS | | | | | |
|---|---|---|---|---|---|
| | | | | | |
| ROLLER | PRINT DIM.,in. | MEASURED | ROLLER | PRINT DIM., in. | MEASURED |
| | | | | | |
| SUN "a" (input side) | .8655/.8653 | .8655/.8655 | | | |
| SUN "a" (output side) | .8655/.8653 | .8655/.8655 | | | |
| | | | | | |
| 1st. PLANET, y1 | .7223/.7221 | | | | |
| NOS. 1&2 | | .7222/.7223 | | | |
| NOS. 3&4 | | .7223/.7222 | | | |
| NOS. 5&6 | | .7222/.7222 | | | |
| NOS. 7&8 | | .7223/.7223 | | | |
| NOS. 9&10 | | .7222/.7223 | | | |
| NOS. 11&12 | | .7222/.7222 | | | |
| NOS. 13&14 | | .7222/.7222 | | | |
| NOS. 15&16 | | .7222/.7222 | | | |
| | | | | | |
| 1st. PLANET , x1 | 1.9157/1.9155 | | | | |
| WITH 1&2 y1 | | 1.9157/1.9157 | | | |
| WITH 3&4 y1 | | 1.9157/1.9157 | | | |
| WITH 5&6 y1 | | 1.9156/1.9157 | | | |
| WITH 7&8 y1 | | 1.9157/1.9157 | | | |
| WITH 9&10 y1 | | 1.9157/1.9157 | | | |
| WITH 11&12 y1 | | 1.9157/1.9157 | | | |
| WITH 13&14 y1 | | 1.9157/1.9157 | | | |
| WITH 15&16 y1 | | 1.9158/1.9157 | | | |
| | | | | | |
| 2nd. PLANET, x2/y1 | 3.6089/3.6087 | | 2nd. PLANET, x2/c | 3.5520/3.5518 | |
| NOS. 1&7 | | 3.6089/3.6089 | NOS. 1&7 | | 3.5520/3.5519 |
| NOS. 3&5 | | 3.6089/3.6089 | NOS. 3&5 | | 3.5520/3.5521 |
| NOS. 2&6 | | 3.6090/3.6089 | NOS. 2&6 | | 3.5521/3.5521 |
| NOS. 4&8 | | 3.6089/3.6088 | NOS. 4&8 | | 3.5521/3.5521 |
| NOS. 9&10 | | 3.6089/3.6090 | NOS. 9&10 | | 3.5521/3.5520 |
| NOS. 11&12 | | 3.6089/3.6089 | NOS. 11&12 | | 3.5520/3.5520 |
| NOS. 13&14 | | 3.6089/3.6089 | NOS. 13&14 | | 3.5520/3.5521 |
| NOS. 15&16 | | 3.6089/3.6089 | NOS. 15&16 | | 3.5520/3.5520 |
| | | | | | |
| 2nd. PLANET,x2/c | 3.5520/3.5518 | | | | |
| | | | | | |
| RING, c | 9.3685/9.3689 | | | | |
| NOS. | | | | | |
| NOS. | | | | | |

TABLE VI

**DC-700 POST ASSEMBLY RING ROLLER MODIFICATION**

**Roller Data**

| Roller | Measured Diameter | Width | Contact | Operating PD |
|---|---|---|---|---|
| a | 0.8655 | 0.125 | Line | 0.8649 |
| x1 | 1.9157 | 0.136 | Line | 1.9151 |
| y1 | 0.7223 | 0.187 | Line | 0.7217 |
| x2 | 3.6089 | 0.195 | Line | 3.6083 |
| y2 | 3.552 | 0.2 | Point | 3.5511 |
| c | 9.3685 | 0.218 | Point | 9.3749 |

**Stress and Deflection Data**

Full input torque=137 in.lbs.

Assumed ax1 contact traction coefficient=.06

Dual roller contacts throughout

| Torque Fraction, % | Normal Roller Load, lb. | | | Stress and Deflection | | | | | | Ring Bending Deflection at Load Points, inxE4 | Ring Roller Inside Diameter, in. |
|---|---|---|---|---|---|---|---|---|---|---|---|
| | ax1 | y1x2 | y2c | ax1 | | y1x2 | | y2c | | | |
| | | | | Max. Hertz Stress, ksi | Hertz Deformation, inxE4 | Max. Hertz Stress, ksi | Hertz Deformation, inxE4 | Max Hertz Stress, psi | Hertz Deformation, inxE4 | | |
| 0 | 0 | 0 | 0 | 0 | 0 | 0 | 0 | 0 | 0 | 0 | 9.3775 |
| 5 | 32.97 | 53.35 | 95.08 | 68.1 | 0.67 | 70.5 | 0.75 | 117 | 2.2 | 3.6 | 9.3762 |
| 10 | 65.95 | 106.7 | 190.2 | 96.4 | 1.3 | 99.8 | 1.4 | 148 | 3.5 | 7.1 | 9.375 |
| 15 | 98.92 | 160.1 | 285.3 | 118 | 1.9 | 122 | 2.1 | 169 | 4.6 | 10.7 | 9.3739 |
| 20 | 131.9 | 213.5 | 380.4 | 136 | 2.4 | 141 | 2.7 | 186 | 5.5 | 14.2 | 9.3728 |
| 25 | 164.9 | 266.9 | 475.6 | 152 | 3 | 158 | 3.3 | 201 | 6.4 | 17.8 | 9.3717 |

TABLE VII

| ROLLER CLUSTER DATA FOR DUAL INPUT DIFFERENTIAL ROLLER DRIVE (DC-500) | | | | | | | | | | | | | | |
|---|---|---|---|---|---|---|---|---|---|---|---|---|---|---|
| BOTH NON-ROTATING AND ROTATING RING ROLLER CLUSTERS | | | | | | | | | | | | | | |
| CONTACT | NORMAL FORCE | | x RADIUS | | y RADIUS | | HERTZ CONTACT | | | | HERTZ COMP. | | HERTZ STRESS | |
| | | | | | | | a | | b | | | | | |
| | N | lb | mm | in | mm | in | mm | in | mm | in | mm | in | GPa | KSI |
| ax1 | 3048 | 685 | 11.064 | 0.4356 | 279.40 | 11.0 | 2.667 | 0.1050 | 0.279 | 0.0110 | 0.0175 | 0.00069 | 2.028 | 294. |
| | | | 24.041 | 0.9465 | 25400. | 1000. | | | | | | | | |
| y1x2 | 6510 | 1463 | 9.375 | 0.3691 | 264.16 | 10.4 | 5.461 | 0.2150 | 0.279 | 0.0110 | 0.0211 | 0.00083 | 2.076 | 301. |
| | | | 38.176 | 1.5030 | -378.46 | -14.9 | | | | | | | | |
| x2c | 11107 | 2496 | 38.176 | 1.5030 | -378.46 | -14.9 | 2.896 | 0.1140 | 1.321 | 0.0520 | 0.0368 | 0.00145 | 1.379 | 200. |
| | | | -103.56 | -4.0771 | 129.54 | 5.1 | | | | | | | | |
| Ring roller max. bending stress = .153 GPa (22,200 psi) | | | | | | | | | | | | | | |
| Ring roller bending deflection = .0559mm (.0022in.) | | | | | | | | | | | | | | |

TABLE VIII

| DC-500 ASSEMBLY | | | | | | |
|---|---|---|---|---|---|---|
| **Roller Inspection Data** | | | | | | |
| | | | | | | |
| (ENGLISH UNITS) | | | | | | |
| | | | | | | |
| Roller Gage Diameters | | | | | | |
| Sun: a=.8719in. | | | | | | |
| First Planet: x1=1.8937in.; y1=.7390in. | | | | | | |
| Second Planet: x2=3.0068in. | | | | | | |
| | | | | | | |
| Roller | Serial No. | Y Diameter at x= | | | | Set No. |
| | | x=.340in. | | x=1.840 | | |
| Input Sun | | 0.8711 | | 0.87145 | | |
| Output Sun | | 0.8715 | | 0.87155 | | |
| | | | | | | |
| First Planet | | Numbered Side | | Plain Side | | |
| | | x=.150 | x=.605 | x=.150 | x=.605 | |
| | 1 | 1.89375 | 0.73915 | 1.8938 | 0.73935 | 1 |
| | 2 | 1.8939 | 0.7393 | 1.894 | 0.73915 | 2 |
| | 3 | 1.894 | 0.73935 | 1.8938 | 0.73915 | 2 |
| | 4 | 1.89385 | 0.7392 | 1.89365 | 0.73935 | 2 |
| | 5 | 1.89375 | 0.7391 | 1.89385 | 0.73915 | 1 |
| | 6 | 1.8939 | 0.73915 | 1.8937 | 0.73905 | 2 |
| | 7 | 1.8938 | 0.7393 | 1.89375 | 0.73915 | 1 |
| | 8 | 1.8938 | 0.7389 | 1.8938 | 0.7393 | 1 |
| | | | | | | |
| Second Planet- Stationary Ring Roller | | Numbered Side | | Plain Side | | |
| | | x=.265 | | x=.265 | | |
| | 1 | 3.00715 | | 3.00725 | | |
| | 2 | 3.00725 | | 3.00715 | | |
| | 3 | 3.00735 | | 3.00695 | | |
| | 4 | 3.00675 | | 3.00705 | | |
| | | | | | | |
| Second Planet- Rotating Ring Roller | | Short end | | Long end | | |
| | | x=.265 | | x=.265 | | |
| | 1 | 3.0066 | | 3.00645 | | |
| | 2 | 3.0073 | | 3.00735 | | |
| | 3 | 3.0071 | | 3.00735 | | |
| | 4 | 3.0068 | | 3.00705 | | |

TABLE IX

| MOMENTUM BALANCED (GROUNDED RING ) DRIVE | | | | | | | | | | | | | | |
|---|---|---|---|---|---|---|---|---|---|---|---|---|---|---|
| DC-400 | | | | | | | | | | | | | | |
| ROTATING CLUSTER | | | | | | | | | | | | | | |
| CONTACT | NORMAL FORCE | | x RADIUS | | y RADIUS | | HERTZ CONTACT | | | | HERTZ COMP. | | HERTZ STRESS | |
| | | | | | | | a | | b | | | | | |
| | N | lb | mm | in | mm | in | mm | in | mm | in | mm | in | GPa | KSI |
| ax1 | 3564 | 801 | 14.503 | 0.5710 | 299.72 | 11.8 | 2.863 | 0.1127 | 0.290 | 0.0114 | 0.0191 | 0.00075 | 2.049 | 297. |
| | | | 18.613 | 0.7328 | 25400. | 1000. | | | | | | | | |
| y1x2 | 4343 | 976 | 9.309 | 0.3665 | 152.40 | 6.0 | 3.886 | 0.1530 | 0.257 | 0.0101 | 0.0188 | 0.00074 | 2.069 | 300. |
| | | | 29.873 | 1.1761 | -218.44 | -8.6 | | | | | | | | |
| x2c | 7538 | 1694 | 29.873 | 1.1761 | -218.44 | -8.6 | 2.540 | 0.1000 | 1.011 | 0.0398 | 0.0300 | 0.00118 | 1.400 | 203. |
| | | | -90.670 | -3.5697 | 101.60 | 4.0 | | | | | | | | |
| Ring roller max. bending stress = .148 GPa (21,400 psi) | | | | | | | | | | | | | | |
| Ring roller bending deflection = .0239mm (.00094in.) | | | | | | | | | | | | | | |
| GROUNDED RING CLUSTER | | | | | | | | | | | | | | |
| CONTACT | NORMAL FORCE | | x RADIUS | | y RADIUS | | HERTZ CONTACT | | | | HERTZ COMP. | | HERTZ STRESS | |
| | | | | | | | a | | b | | | | | |
| | N | lb | mm | in | mm | in | mm | in | mm | in | mm | in | GPa | KSI |
| ax1 | 1878 | 422 | 48.806 | 1.9215 | 25400. | 1000. | 1.445 | 0.0569 | 0.318 | 0.0125 | 0.0160 | 0.00063 | 1.945 | 282. |
| | | | 11.991 | 0.4721 | 104.14 | 4.1 | | | | | | | | |
| x1c | 3756 | 844 | 11.991 | 0.4721 | 104.14 | 4.1 | 1.748 | 0.0688 | 0.495 | 0.0195 | 0.0244 | 0.00096 | 2.069 | 300. |
| | | | -72.789 | -2.8657 | 25400. | 1000. | | | | | | | | |
| Sun roller max. bending stress = .0295 GPa (4270psi) | | | | | | | | | | | | | | |
| Sun roller bending deflection = .0043mm (.00017in) | | | | | | | | | | | | | | |
| Ring roller max. bending stress = .0292 GPa (4240psi) | | | | | | | | | | | | | | |
| Ring roller bending deflection = .0064mm (.00025in) | | | | | | | | | | | | | | |

TABLE X a

## DC-400 ROLLER INSPECTION DATA

I SUN ROLLER (DC-400-31)

SERIAL NO. 1

| STATION NO. | X-DIST. | PRINT DIM. | MEASURED |
|---|---|---|---|
| 1 | 1.240 | 1.1640 | 1.1641 |
| 3 | 1.350 | 1.1508 | |
| 4 | 1.410 | 1.1427G | 1.1428 |
| 5 | 1.470 | 1.1340 | |
| 15 | 2.720 | 1.1427G | 1.1428 |

SERIAL NO. 2

| STATION NO. | X-DIST. | PRINT DIM. | MEASURED |
|---|---|---|---|
| 1 | 1.240 | 1.1640 | 1.1639 |
| 3 | 1.350 | 1.1508 | |
| 4 | 1.410 | 1.1427G | 1.1427 |
| 5 | 1.470 | 1.1340 | |
| 15 | 2.720 | 1.1427G | 1.1428 |

II FIRST ROW PLANETS (DC-400-26)

A SERIAL NO. 1 NUMBERED SIDE

| STATION NO. | X-DIST. | PRINT DIM. | MEASURED |
|---|---|---|---|
| 2 | .050 | 1.4523 | |
| 4 | .150 | 1.4663G | 1.4665 |
| 6 | .250 | 1.4803 | |
| 13 | .455 | .7460 | |
| 15 | .555 | .7337G | .7338 |
| 17 | .655 | .7180 | |

PLAIN SIDE

| STATION NO. | X-DIST. | PRINT DIM. | MEASURED |
|---|---|---|---|
| 2 | .050 | 1.4523 | 1.4524 |
| 4 | .150 | 1.4663G | 1.4666 |
| 6 | .250 | 1.4803 | 1.4803 |
| 13 | .455 | .7460 | |
| 15 | .555 | .7337G | .7341 |
| 17 | .655 | .7180 | |

B SERIAL NO. 2 NUMBERED SIDE

| STATION NO. | X-DIST. | PRINT DIM. | MEASURED |
|---|---|---|---|
| 2 | .050 | 1.4523 | |
| 4 | .150 | 1.4663G | 1.46655 |
| 6 | .250 | 1.4803 | |
| 13 | .455 | .7460 | |
| 15 | .555 | .7337G | .7335 |
| 17 | .655 | .7180 | |

PLAIN SIDE

| STATION NO. | X-DIST. | PRINT DIM. | MEASURED |
|---|---|---|---|
| 2 | .050 | 1.4523 | |
| 4 | .150 | 1.4663G | 1.4665 |
| 6 | .250 | 1.4803 | |
| 13 | .455 | .7460 | |
| 15 | .555 | .7337G | .7336 |
| 17 | .655 | .7180 | |

C SERIAL NO. 3 NUMBERED SIDE

| STATION NO. | X-DIST. | PRINT DIM. | MEASURED |
|---|---|---|---|
| 2 | .050 | 1.4523 | |
| 4 | .150 | 1.4663G | 1.4665 |
| 6 | .250 | 1.4803 | |
| 13 | .455 | .7460 | |
| 15 | .555 | .7337G | .7339 |
| 17 | .655 | .7180 | |

PLAIN SIDE

| STATION NO. | X-DIST. | PRINT DIM. | MEASURED |
|---|---|---|---|
| 2 | .050 | 1.4523 | |
| 4 | .150 | 1.4663G | 1.46635 |
| 6 | .250 | 1.4803 | |
| 13 | .455 | .7460 | |
| 15 | .555 | .7337G | .73385 |
| 17 | .655 | .7180 | |

D SERIAL NO. 4 NUMBERED SIDE

| STATION NO. | X-DIST. | PRINT DIM. | MEASURED |
|---|---|---|---|
| 2 | .050 | 1.4523 | |
| 4 | .150 | 1.4663G | 1.46625 |
| 6 | .250 | 1.4803 | |
| 13 | .455 | .7460 | |
| 15 | .555 | .7337G | .7338 |
| 17 | .655 | .7180 | |

PLAIN SIDE

| STATION NO. | X-DIST. | PRINT DIM. | MEASURED |
|---|---|---|---|
| 2 | .050 | 1.4523 | |
| 4 | .150 | 1.4663G | 1.4666 |
| 6 | .250 | 1.4803 | |
| 13 | .455 | .7460 | |
| 15 | .555 | .7337G | .7337 |
| 17 | .655 | .7180 | |

E SERIAL NO. 5 NUMBERED SIDE

| STATION NO. | X-DIST. | PRINT DIM. | MEASURED |
|---|---|---|---|
| 2 | .050 | 1.4523 | |
| 4 | .150 | 1.4663G | 1.4667 |
| 6 | .250 | 1.4803 | |
| 13 | .455 | .7460 | |
| 15 | .555 | .7337G | .7342 |
| 17 | .655 | .7180 | |

PLAIN SIDE

| STATION NO. | X-DIST. | PRINT DIM. | MEASURED |
|---|---|---|---|
| 2 | .050 | 1.4523 | |
| 4 | .150 | 1.4663G | 1.4666 |
| 6 | .250 | 1.4803 | |
| 13 | .455 | .7460 | |
| 15 | .555 | .7337G | .7338 |
| 17 | .655 | .7180 | |

## TABLE Xa(concl.)

III SECOND ROW PLANETS (DC-400-7)

A SERIAL NO. 1

| STATION NO. | X-DIST.* | PRINT DIM. | MEASURED |
|---|---|---|---|
| 3 | .115 | 2.3401 | 2.3400 |
| 5 | .215 | 2.3529G | 2.3530 |
| 7 | .315 | 2.3681 | 2.3682 |
| 15 | .615 | 2.3681 | 2.3683 |
| 17 | .715 | 2.3529G | 2.3530 |
| 19 | .815 | 2.3401 | 2.3402 |

B SERIAL NO. 2

| STATION NO. | X-DIST.* | PRINT DIM. | MEASURED |
|---|---|---|---|
| 3 | .115 | 2.3401 | |
| 5 | .215 | 2.3529G | 2.3531 |
| 7 | .315 | 2.3681 | |
| 15 | .615 | 2.3681 | |
| 17 | .715 | 2.3529G | 2.3530 |
| 19 | .815 | 2.3401 | |

C SERIAL NO. 3

| STATION NO. | X-DIST.* | PRINT DIM. | MEASURED |
|---|---|---|---|
| 3 | .115 | 2.3401 | |
| 5 | .215 | 2.3529G | 2.3530 |
| 7 | .315 | 2.3681 | |
| 15 | .615 | 2.3681 | |
| 17 | .715 | 2.3529G | 2.3529 |
| 19 | .815 | 2.3401 | |

D SERIAL NO. 4

| STATION NO. | X-DIST.* | PRINT DIM. | MEASURED |
|---|---|---|---|
| 3 | .115 | 2.3401 | |
| 5 | .215 | 2.3529G | 2.3530 |
| 7 | .315 | 2.3681 | |
| 15 | .615 | 2.3681 | |
| 17 | .715 | 2.3529G | 2.3532 |
| 19 | .815 | 2.3401 | |

E SERIAL NO. 5

| STATION NO. | X-DIST.* | PRINT DIM. | MEASURED |
|---|---|---|---|
| 3 | .115 | 2.3401 | |
| 5 | .215 | 2.3529G | 2.3530 |
| 7 | .315 | 2.3681 | |
| 15 | .615 | 2.3681 | |
| 17 | .715 | 2.3529G | 2.3532 |
| 19 | .815 | 2.3401 | |

* MEASURED FROM NUMBERED SIDE

IV SECOND ROW PLANET SHAFTS (DC-400-11)

A SERIAL NO. 1

| STATION NO. | X-DIST. | PRINT DIM. | MEASURED |
|---|---|---|---|
| 3 | .225 | .9393 | .9395 |
| 6 | .375 | .9448G | .9452 |
| 9 | .525 | .9393 | .9394 |

B SERIAL NO. 2

| STATION NO. | X-DIST. | PRINT DIM. | MEASURED |
|---|---|---|---|
| 3 | .225 | .9393 | |
| 6 | .375 | .9448G | .94475 |
| 9 | .525 | .9393 | |

C SERIAL NO. 3

| STATION NO. | X-DIST. | PRINT DIM. | MEASURED |
|---|---|---|---|
| 3 | .225 | .9393 | |
| 6 | .375 | .9448G | .9449 |
| 9 | .525 | .9393 | |

D SERIAL NO. 4

| STATION NO. | X-DIST. | PRINT DIM. | MEASURED |
|---|---|---|---|
| 3 | .225 | .9393 | |
| 6 | .375 | .9448G | .9450 |
| 9 | .525 | .9393 | |

E SERIAL NO. 5

| STATION NO. | X-DIST. | PRINT DIM. | MEASURED |
|---|---|---|---|
| 3 | .225 | .9393 | |
| 6 | .375 | .9448G | .9450 |
| 9 | .525 | .9393 | |

V IDLER SUN ROLLER (DC-400-29)

A SERIAL NO. 1

| STATION NO. | X-DIST | PRINT DIM. | MEASURED |
|---|---|---|---|
| 3 | .075 | 3.8500 | |
| 5 | .125 | 3.8552G | 3.8554 |
| 7 | .175 | 3.8604 | |

B SERIAL NO. 2

| STATION NO. | X-DIST | PRINT DIM. | MEASURED |
|---|---|---|---|
| 3 | .075 | 3.8500 | |
| 5 | .125 | 3.8552G | 3.8550 |
| 7 | .175 | 3.8604 | |

VI GROUNDED RING

| PRINT DIM. | MEASURED |
|---|---|
| 5.7296 | 5.7305 |

TABLE Xb

# DC-400 ROLLER INSPECTION DATA

(Second set of First Row Planets)

I SUN ROLLER (DC-400-31)

SERIAL NO. 1

| STATION NO. | X-DIST. | PRINT DIM. | MEASURED |
|---|---|---|---|
| 1 | 1.240 | 1.1640 | |
| 3 | 1.350 | 1.1508 | |
| 4 | 1.410 | 1.1427G | |
| 5 | 1.470 | 1.1340 | |
| 15 | 2.720 | 1.1427G | |

SERIAL NO. 2

| STATION NO. | X-DIST. | PRINT DIM. | MEASURED |
|---|---|---|---|
| 1 | 1.240 | 1.1640 | |
| 3 | 1.350 | 1.1508 | |
| 4 | 1.410 | 1.1427G | |
| 5 | 1.470 | 1.1340 | |
| 15 | 2.720 | 1.1427G | |

II FIRST ROW PLANETS (DC-400-26)

A

SERIAL NO. 1 NUMBERED SIDE

| STATION NO. | X-DIST. | PRINT DIM. | MEASURED |
|---|---|---|---|
| 2 | .050 | 1.4523 | 1.4526 |
| 4 | .150 | 1.4663G | 1.4666 |
| 6 | .250 | 1.4803 | 1.4802 |
| 11 | .355 | .7550 | .7547 |
| 15 | .555 | .7337G | .7335 |
| 18 | .705 | .7089 | .7085 |

PLAIN SIDE

| STATION NO. | X-DIST. | PRINT DIM. | MEASURED |
|---|---|---|---|
| 2 | .050 | 1.4523 | 1.4524 |
| 4 | .150 | 1.4663G | 1.4664 |
| 6 | .250 | 1.4803 | 1.4804 |
| 11 | .355 | .7550 | .7548 |
| 15 | .555 | .7337G | .7334 |
| 18 | .705 | .7089 | .7084 |

B

SERIAL NO. 2 NUMBERED SIDE

| STATION NO. | X-DIST. | PRINT DIM. | MEASURED |
|---|---|---|---|
| 2 | .050 | 1.4523 | 1.4526 |
| 4 | .150 | 1.4663G | 1.4662 |
| 6 | .250 | 1.4803 | 1.4804 |
| 11 | .355 | .7550 | .7545 |
| 15 | .555 | .7337G | .7335 |
| 18 | .705 | .7089 | .7085 |

PLAIN SIDE

| STATION NO. | X-DIST. | PRINT DIM. | MEASURED |
|---|---|---|---|
| 2 | .050 | 1.4523 | 1.4524 |
| 4 | .150 | 1.4663G | 1.4662 |
| 6 | .250 | 1.4803 | 1.4804 |
| 11 | .355 | .7550 | .7547 |
| 15 | .555 | .7337G | .7335 |
| 18 | .705 | .7089 | .7085 |

C

SERIAL NO. 3 NUMBERED SIDE

| STATION NO. | X-DIST. | PRINT DIM. | MEASURED |
|---|---|---|---|
| 2 | .050 | 1.4523 | 1.4525 |
| 4 | .150 | 1.4663G | 1.4665 |
| 6 | .250 | 1.4803 | 1.4805 |
| 11 | .355 | .7550 | .7548 |
| 15 | .555 | .7337G | .7336 |
| 18 | .705 | .7089 | .7085 |

PLAIN SIDE

| STATION NO. | X-DIST. | PRINT DIM. | MEASURED |
|---|---|---|---|
| 2 | .050 | 1.4523 | 1.4523 |
| 4 | .150 | 1.4663G | 1.4662 |
| 6 | .250 | 1.4803 | 1.4802 |
| 11 | .355 | .7550 | .7548 |
| 15 | .555 | .7337G | .7336 |
| 18 | .705 | .7089 | .7086 |

D

SERIAL NO. 4 NUMBERED SIDE

| STATION NO. | X-DIST. | PRINT DIM. | MEASURED |
|---|---|---|---|
| 2 | .050 | 1.4523 | 1.4525 |
| 4 | .150 | 1.4663G | 1.4665 |
| 6 | .250 | 1.4803 | 1.4805 |
| 11 | .355 | .7550 | .7546 |
| 15 | .555 | .7337G | .7336 |
| 18 | .705 | .7089 | .7088 |

PLAIN SIDE

| STATION NO. | X-DIST. | PRINT DIM. | MEASURED |
|---|---|---|---|
| 2 | .050 | 1.4523 | 1.4528 |
| 4 | .150 | 1.4663G | 1.4666 |
| 6 | .250 | 1.4803 | 1.4806 |
| 11 | .355 | .7550 | .7550 |
| 15 | .555 | .7337G | .7338 |
| 18 | .705 | .7089 | .7090 |

E

SERIAL NO. 5 NUMBERED SIDE

| STATION NO. | X-DIST. | PRINT DIM. | MEASURED |
|---|---|---|---|
| 2 | .050 | 1.4523 | 1.4526 |
| 4 | .150 | 1.4663G | 1.4666 |
| 6 | .250 | 1.4803 | 1.4802 |
| 11 | .355 | .7550 | .7547 |
| 15 | .555 | .7337G | .7335 |
| 18 | .705 | .7089 | .7085 |

PLAIN SIDE

| STATION NO. | X-DIST. | PRINT DIM. | MEASURED |
|---|---|---|---|
| 2 | .050 | 1.4523 | 1.4524 |
| 4 | .150 | 1.4663G | 1.4664 |
| 6 | .250 | 1.4803 | 1.4804 |
| 11 | .355 | .7550 | .7548 |
| 15 | .555 | .7337G | .7334 |
| 18 | .705 | .7089 | .7084 |

TABLE XI

| DIFFERENTIAL DRIVE FRICTION LOSSES AT ZERO POWER OUTPUT | | | |
|---|---|---|---|
| TORQUE PATH | FIXED | FRICTION LOSS, N-m | |
| | | ROLLER-GEAR DRIVE (DC-700) | ROLLER DRIVE (DC-500) |
| H1 TO L | H2 | .2 to .25 | 1.2 |
| H1 TO H2 | L | .3 to .45 | 1.3 to 1.6 |
| H2 TO L | H1 | .1 to .24 | 0.7 |
| H2 TO L | L | .65 to .7 | 1.4 to 1.5 |
| L TO H1 | H2 | 4.5 to 5.5 | 24 to 26 |
| L TO H2 | H1 | 7.5 to 10 | 10 to 14 |

TABLE XII

| EFFICIENCY DATA SPECTRA | | | | |
|---|---|---|---|---|
| ANGULAR VELOCITIES, rad./sec | | | GREATER OF | DIFFERENTIAL EFFICIENCY, % |
| $\omega_{H1}$ | $\omega_{H2}$ | $\omega_L$ | $\omega_{H1}/\omega_L$ or $\omega_{H2}/\omega_L$ | |
| 35 | 35 | 0 | ∞ | 0 |
| 70 | 70 | 0 | ∞ | 0 |
| 105 | 105 | 0 | ∞ | 0 |
| 140 | 140 | 0 | ∞ | 0 |
| 35 | 0 | 1.2 | R | 100 |
| 70 | 35 | 1.2 | 2R | 33.3 |
| 105 | 70 | 1.2 | 3R | 20 |
| 140 | 105 | 1.2 | 4R | 14.3 |
| 35 | -35 | 2.4 | R/2 | 100 |
| 70 | 0 | 2.4 | R | 100 |
| 105 | 35 | 2.4 | 3R/2 | 50 |
| 140 | 70 | 2.4 | 2R | 33.3 |
| 35 | -70 | 3.59 | 2R/3 | 100 |
| 70 | -35 | 3.59 | 2R/3 | 100 |
| 105 | 0 | 3.59 | R | 100 |
| 140 | 35 | 3.59 | 4R/3 | 60 |
| 35 | -105 | 4.79 | 3R/4 | 100 |
| 70 | -70 | 4.79 | R/2 | 100 |
| 105 | -35 | 4.79 | 3R/4 | 100 |
| 140 | 0 | 4.79 | R | 100 |

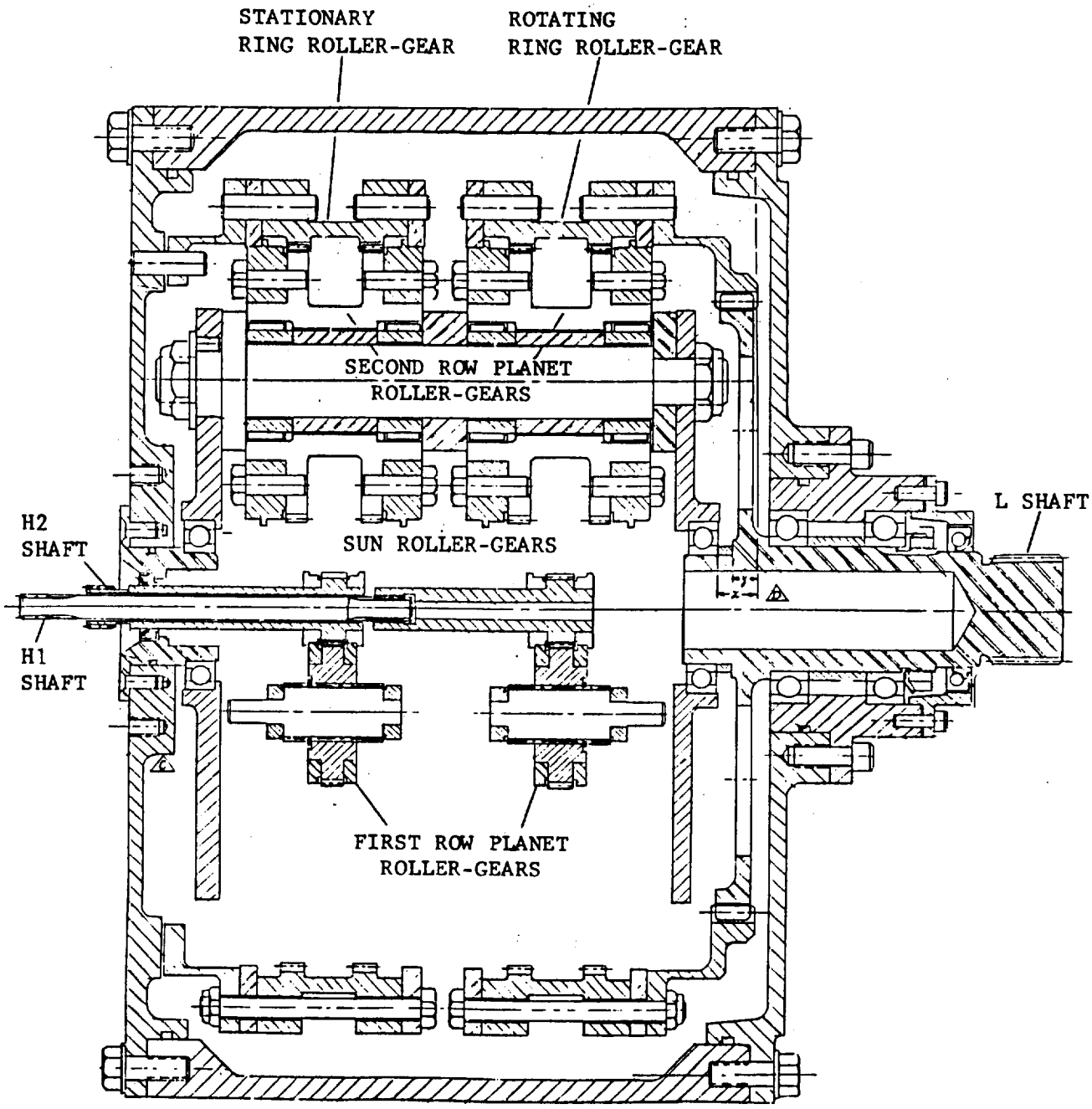


Figure 1. Dual Input Differential Roller-Gear Drive (DC-700).

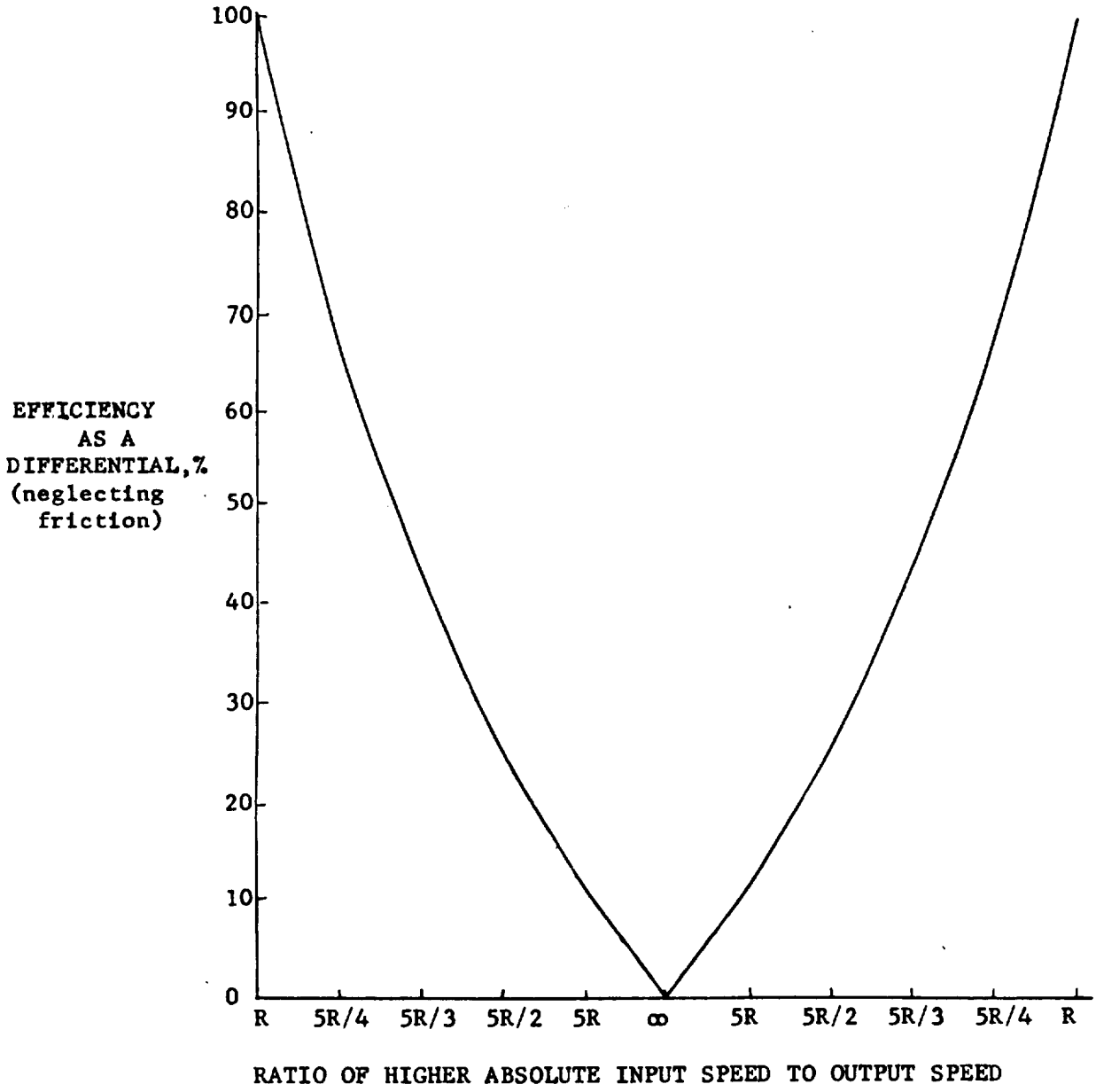


Figure 2. Differential drive efficiency loss caused by recirculating power. (R=reduction ratio from shaft H1 or H2 to shaft L).

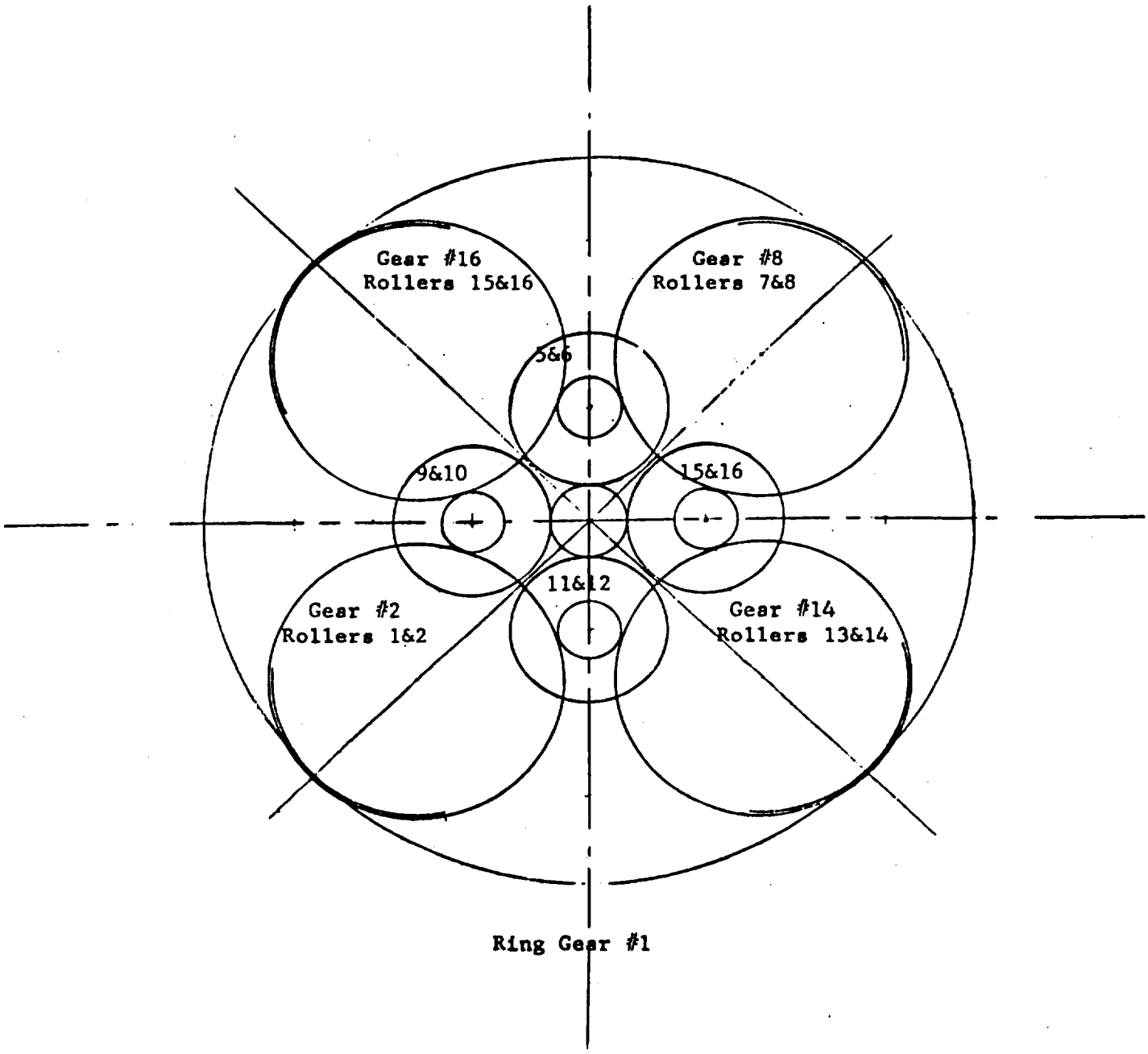


a) Input side cluster

Figure 3. Arrangement of first and second planet roller-gears as viewed from the input side (DC-700 drive).

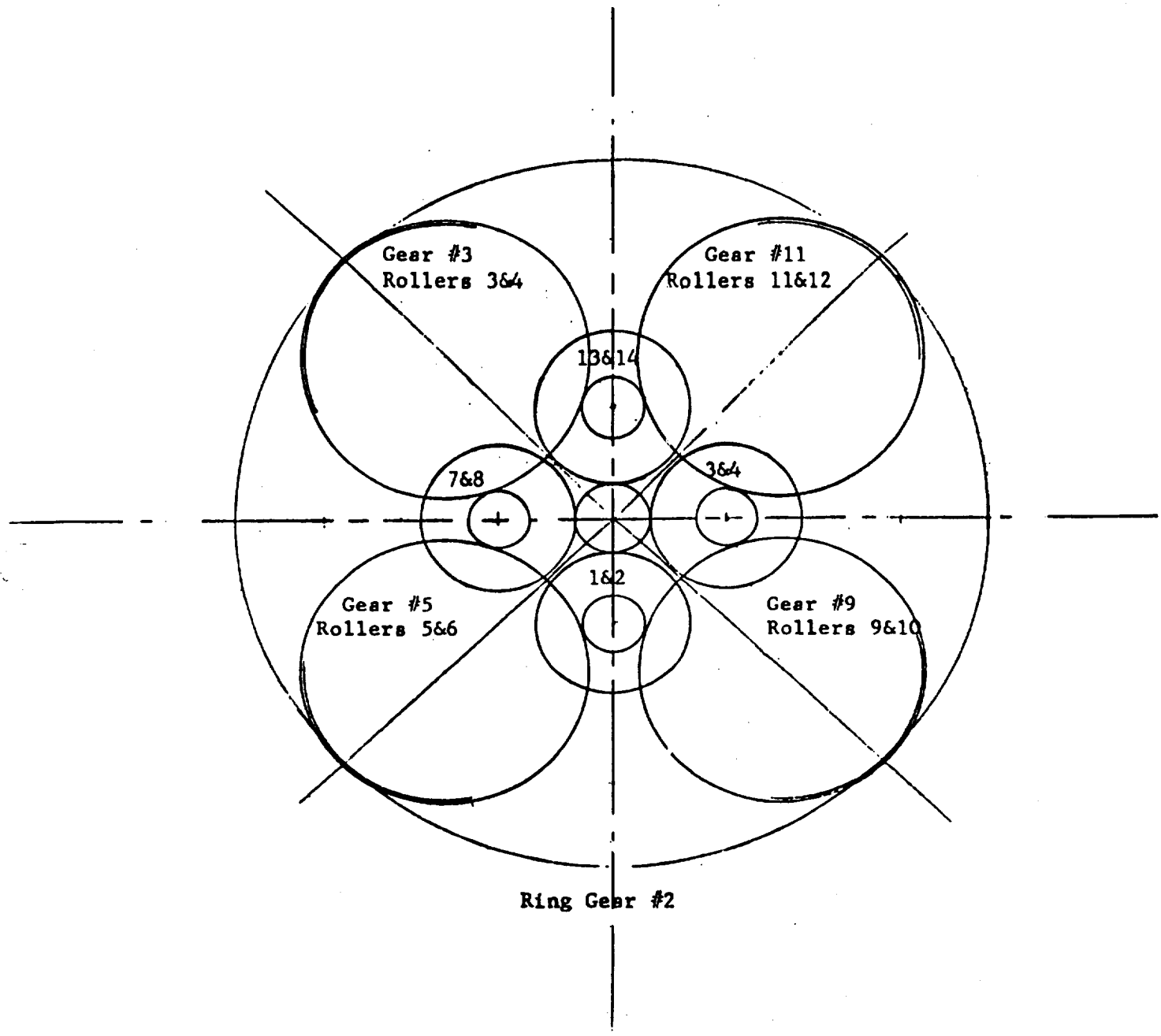


b) Output side cluster

Figure 3 (concl.). Arrangement of first and second planet roller-gears as viewed from the input side (DC-700 drive).

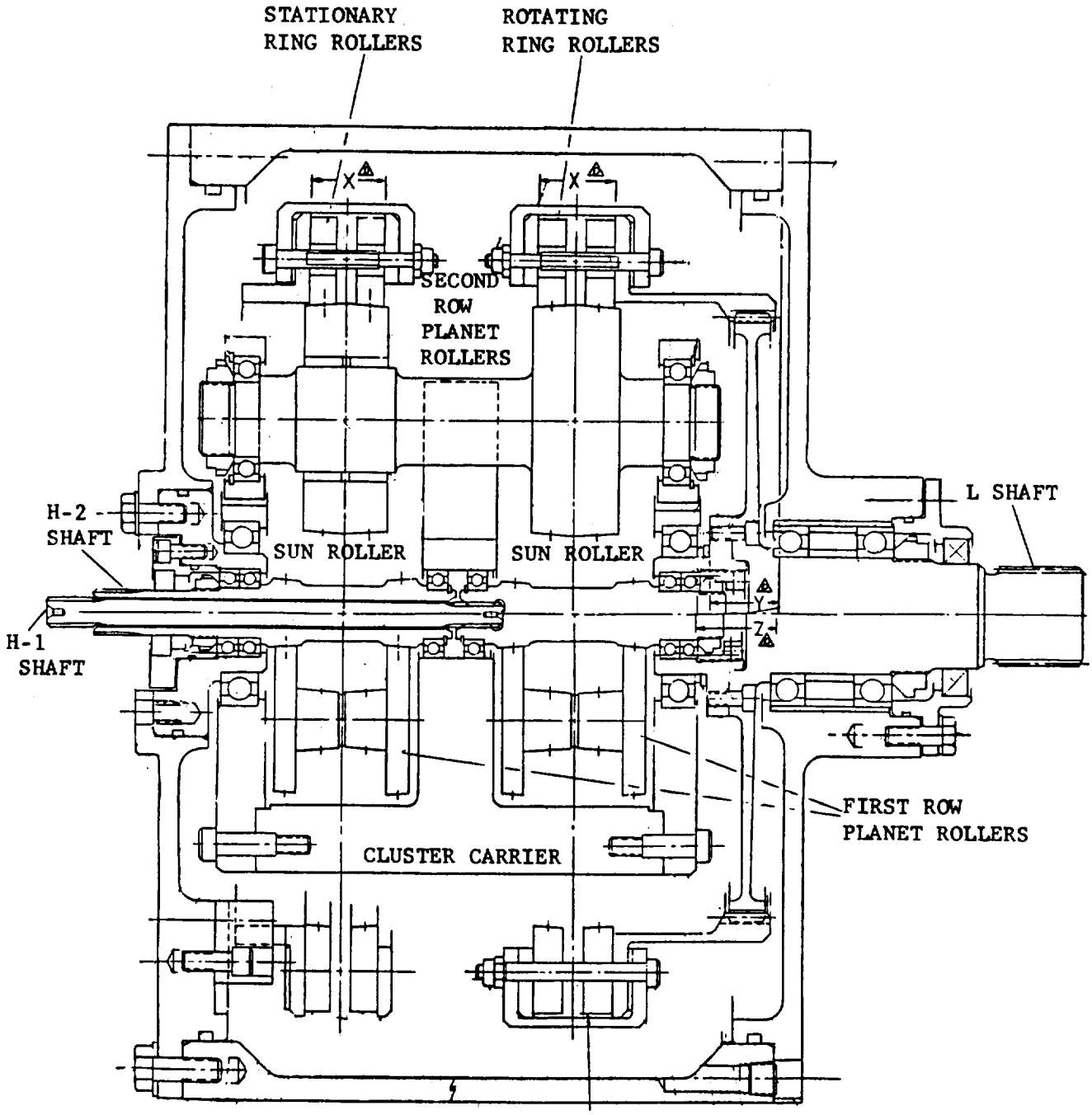


Figure 4. Dual Input Differential Roller Drive (DC-500).

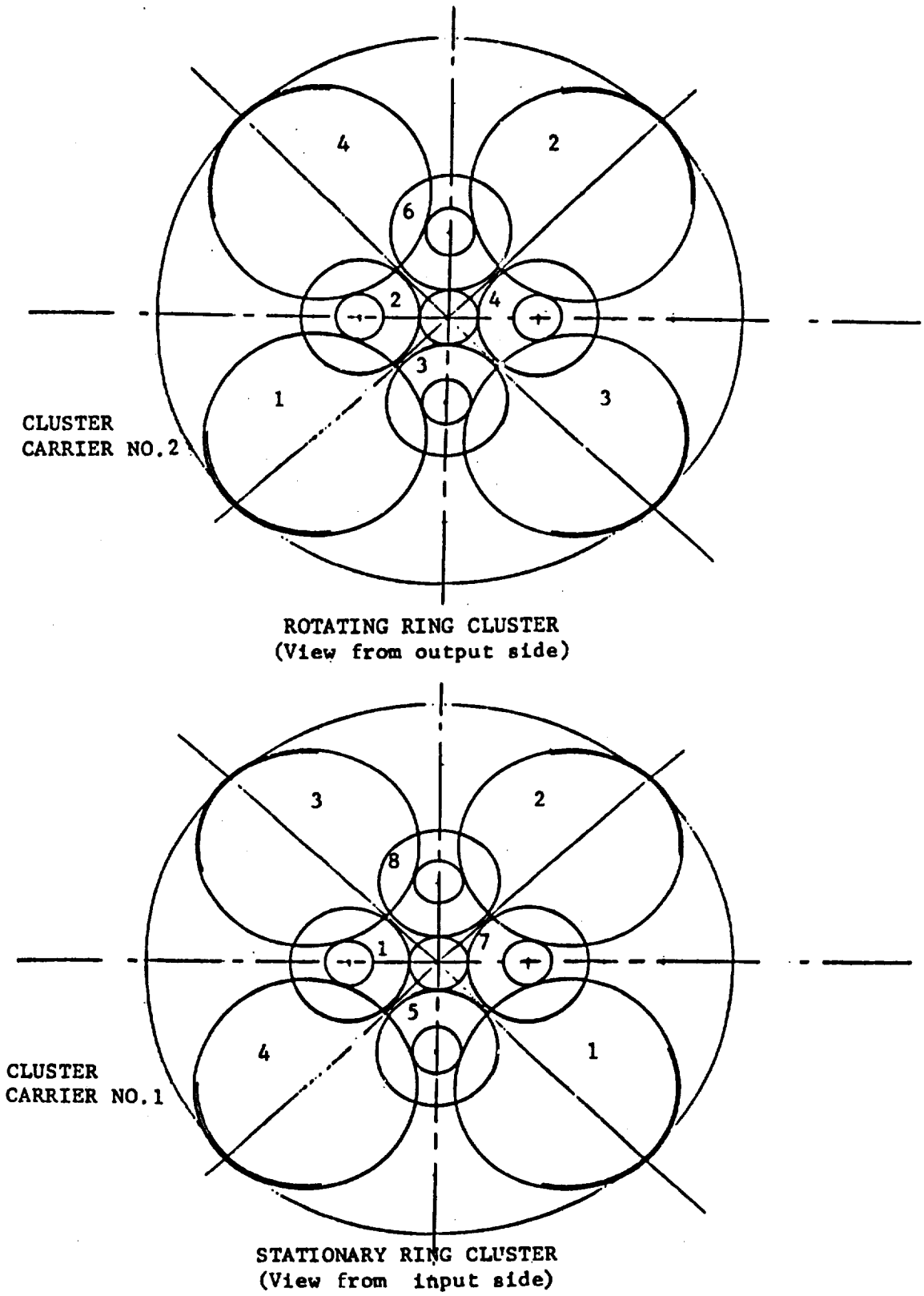


Figure 5. Arrangement of first and second planet rollers in two cluster assemblies (DC-500 drive). Viewed from the direction indicated.

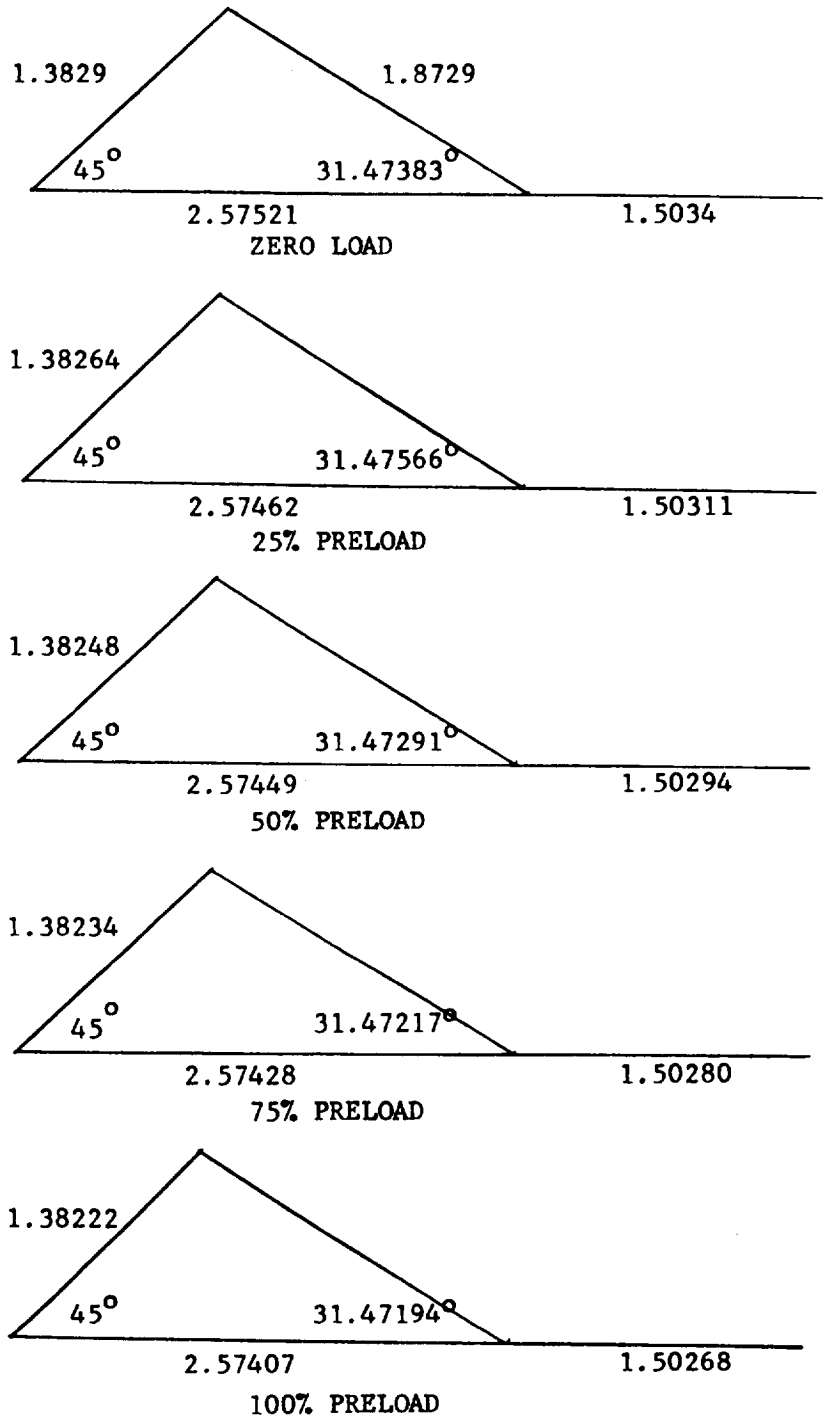


Figure 6. Roller spacing at different levels of preload (DC-500 drive).

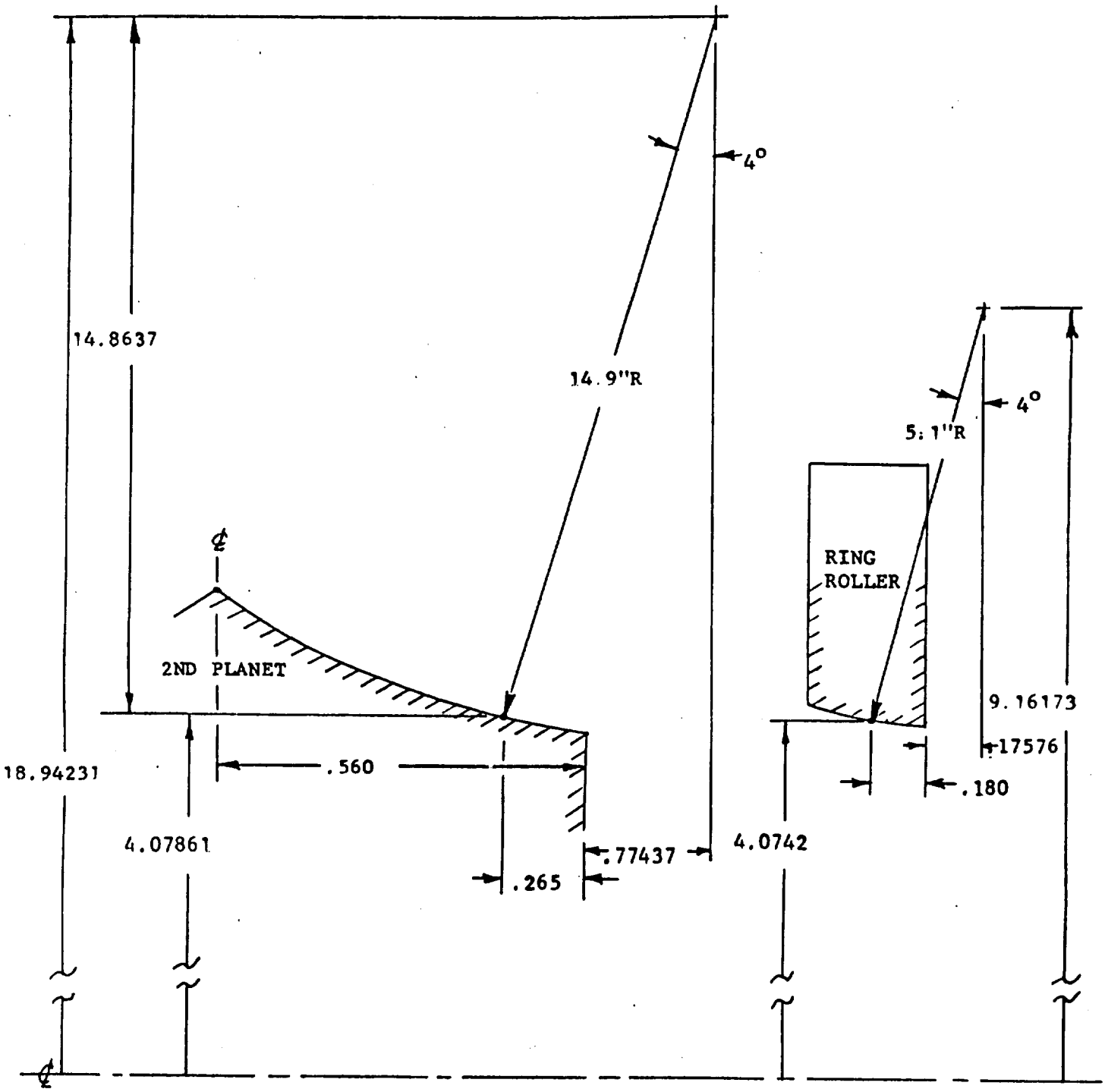


a) Initial setup

Figure 7. Second planet-ring roller engagement diagram (DC-500 drive).

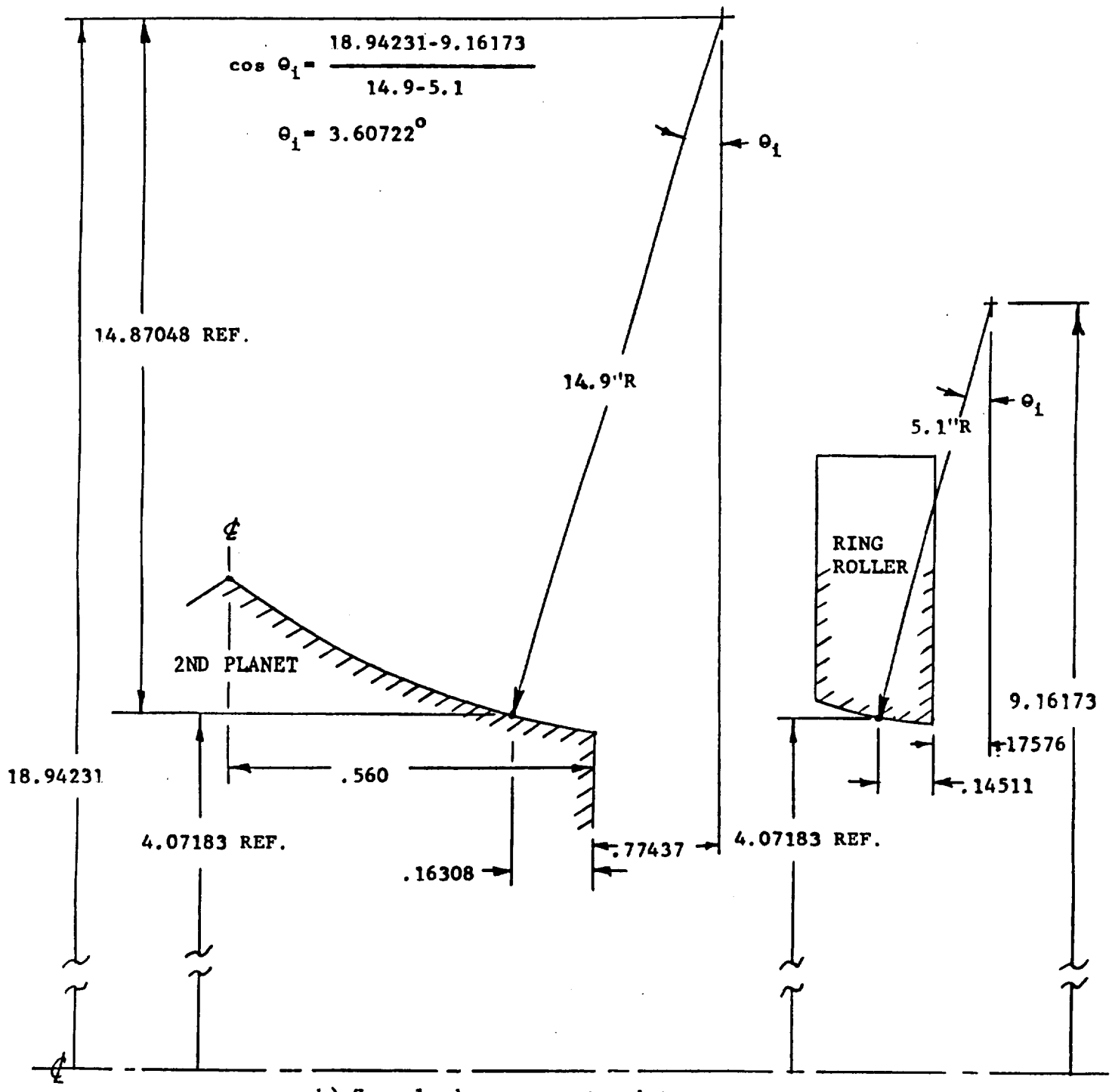


b) Zero load engagement point

Figure 7(cont.) Second planet-ring roller engagement diagram (DC-500 drive).

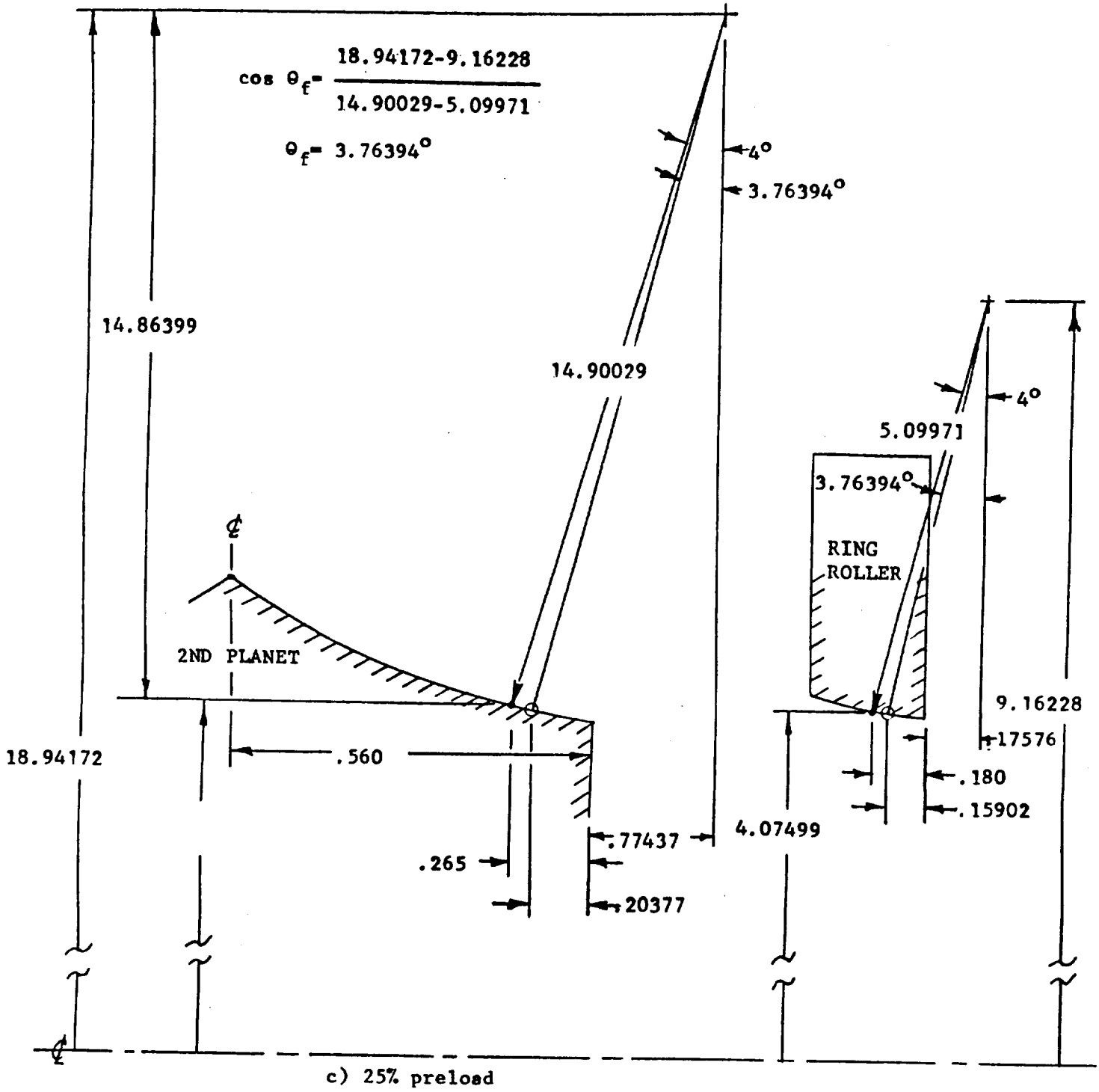


Figure 7(cont.) Second planet-ring roller engagement diagram (DC-500 drive).

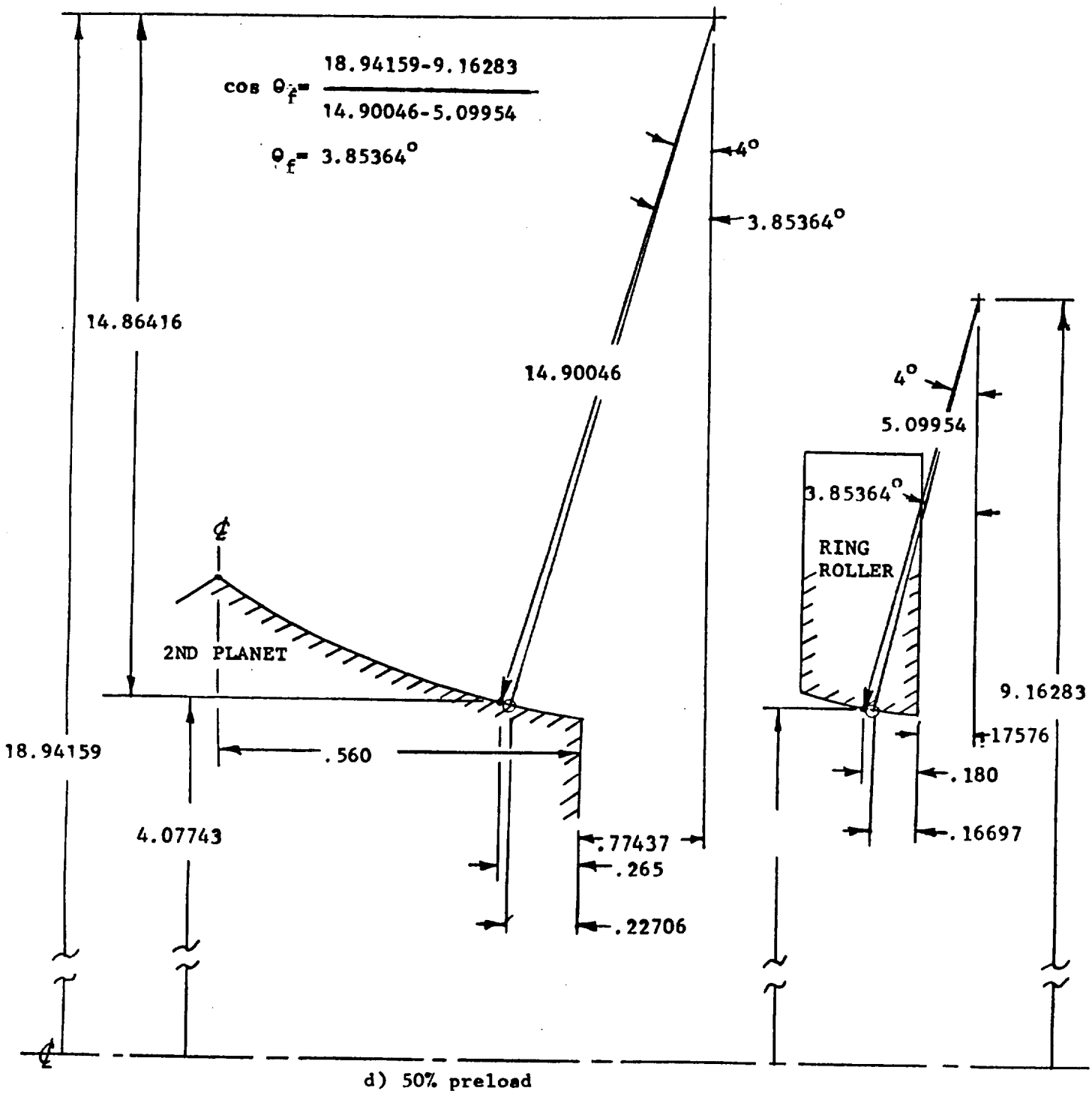


Figure 7(cont.) Second planet-ring roller engagement diagram (DC-500 drive).

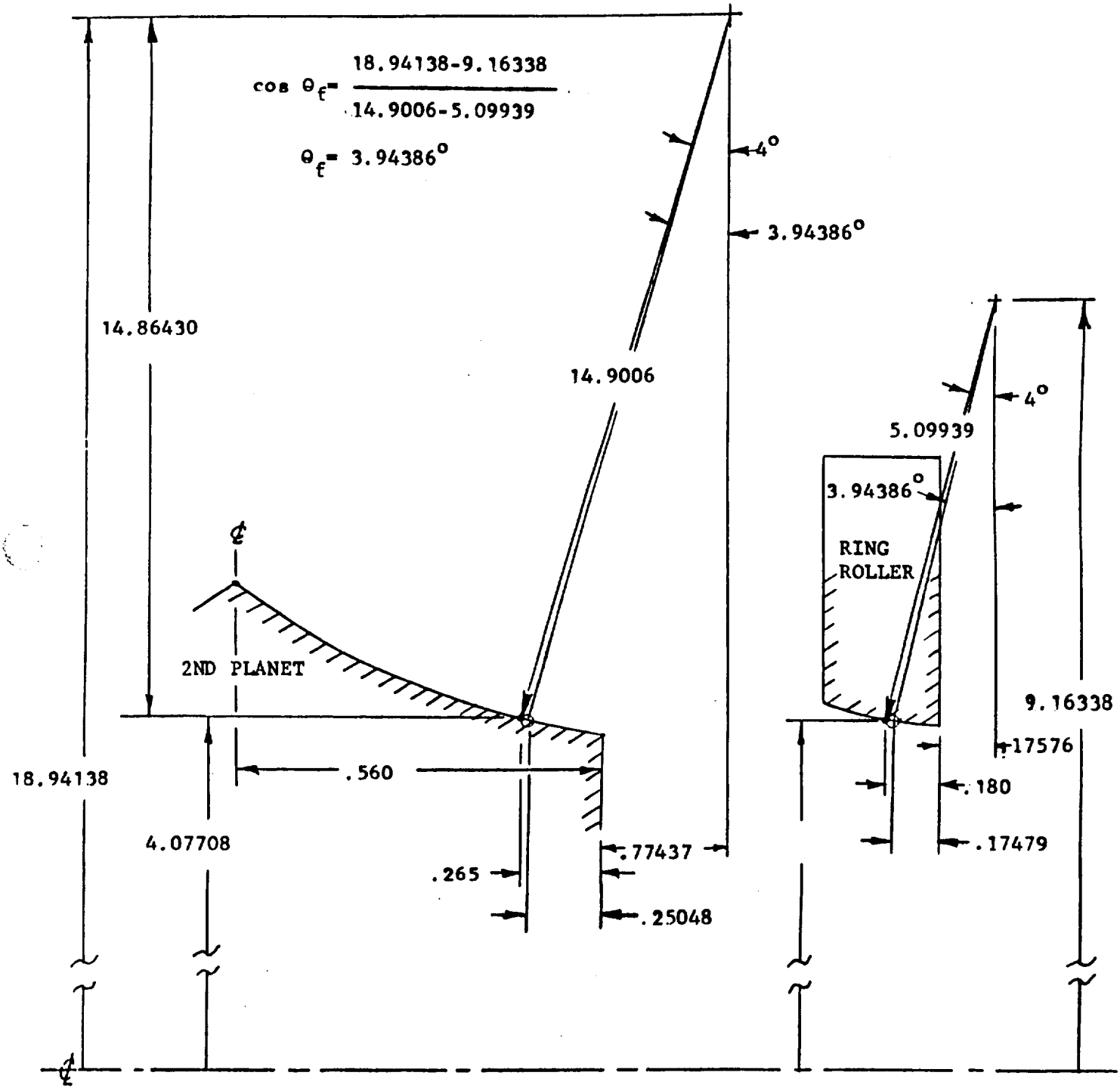


e) 75% preload

Figure 7(cont.) Second planet-ring roller engagement diagram (DC-500 drive).

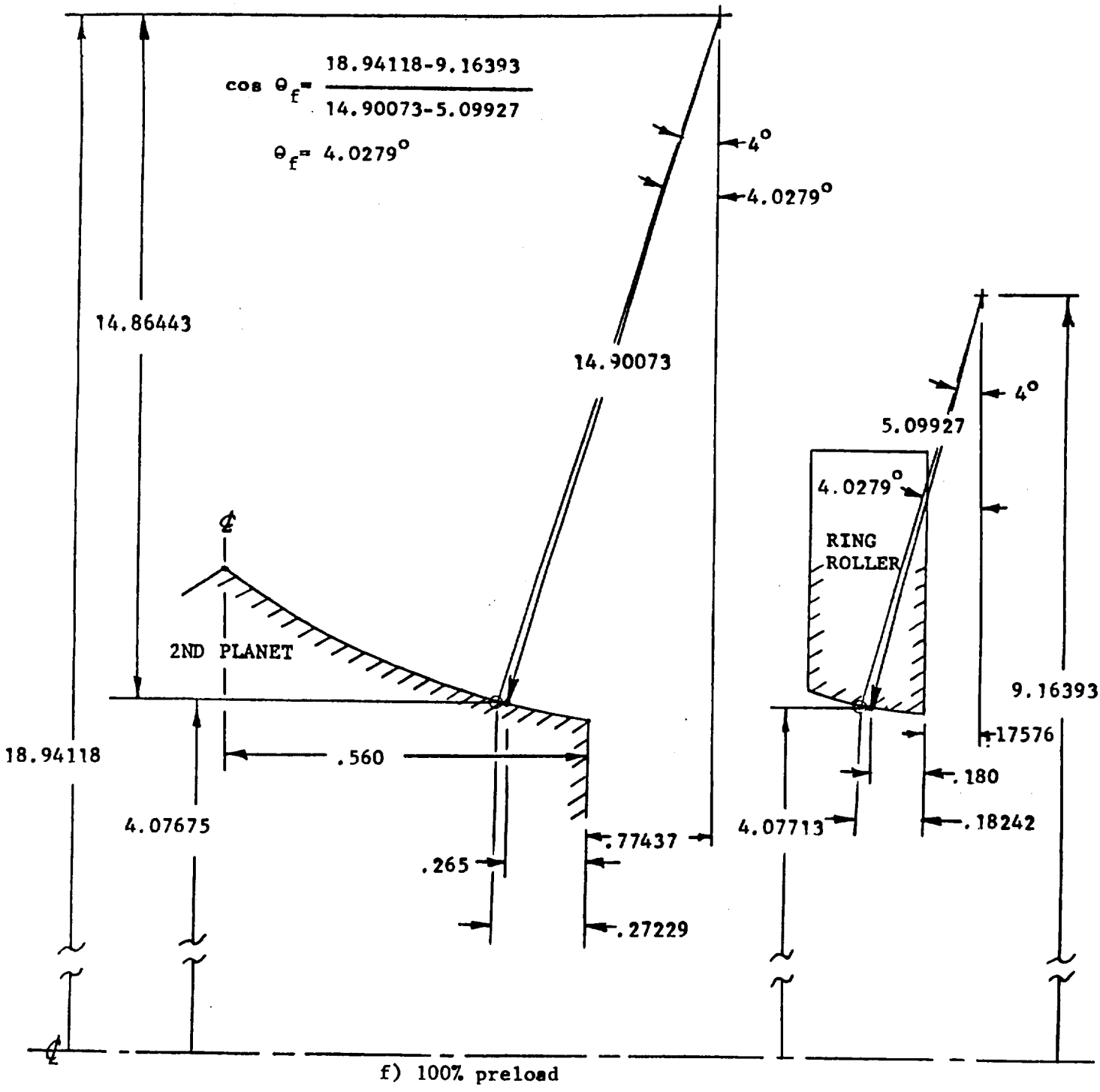


Figure 7(concl.) Second planet-ring roller engagement diagram (DC-500 drive).

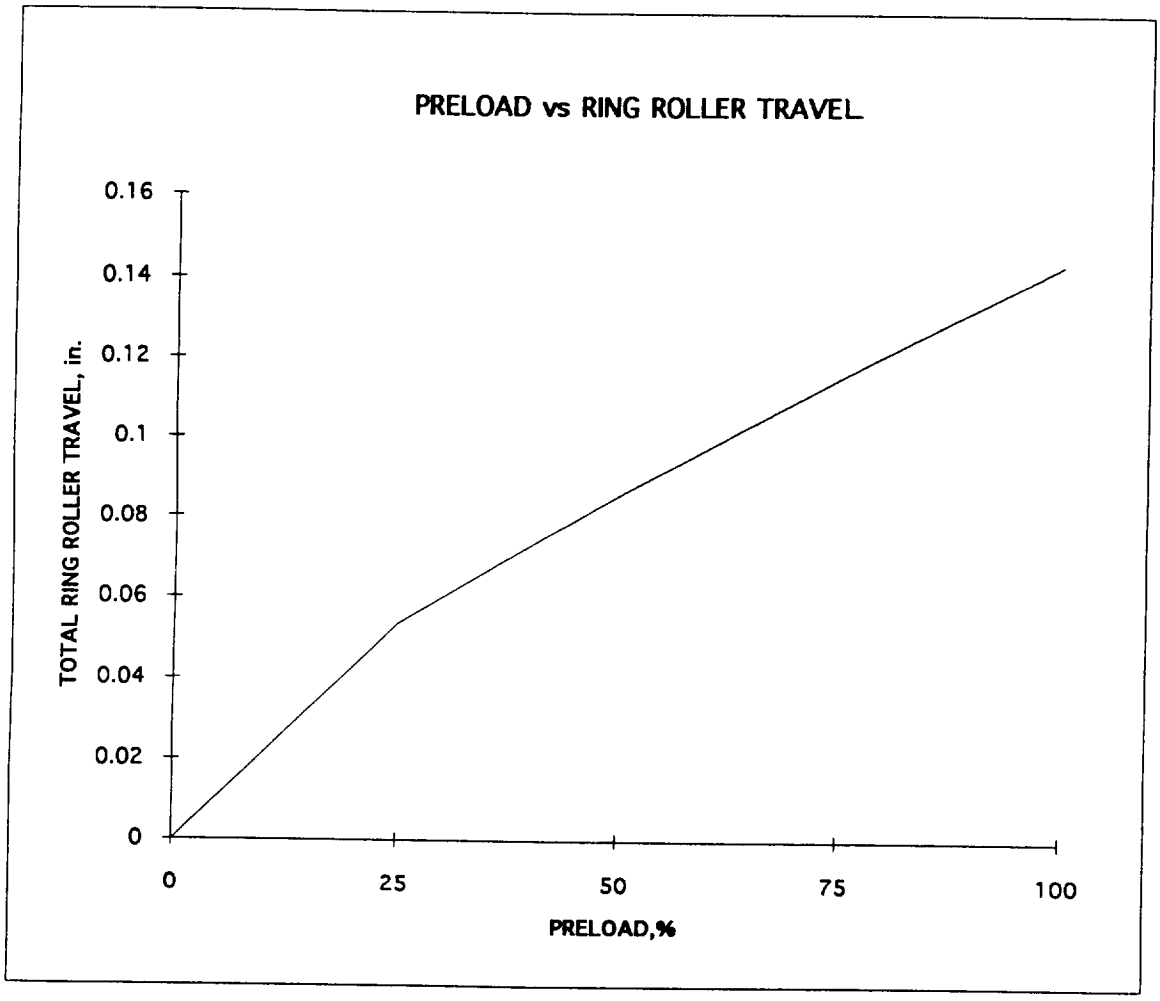


Figure 8. Preload level as a function of ring roller travel (DC-500 drive).

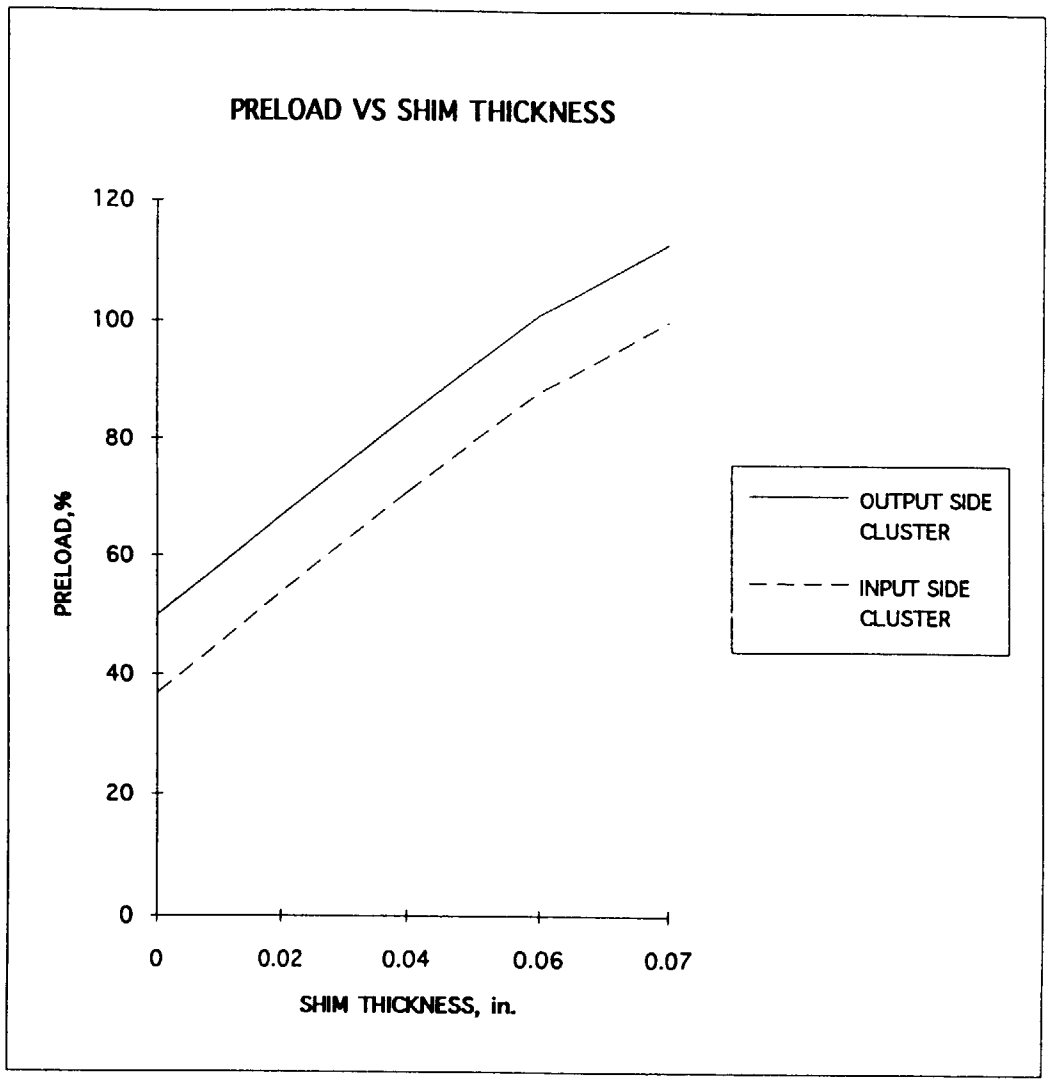


Figure 9. Preload level as a function of ring roller shim thickness (DC-500 drive)

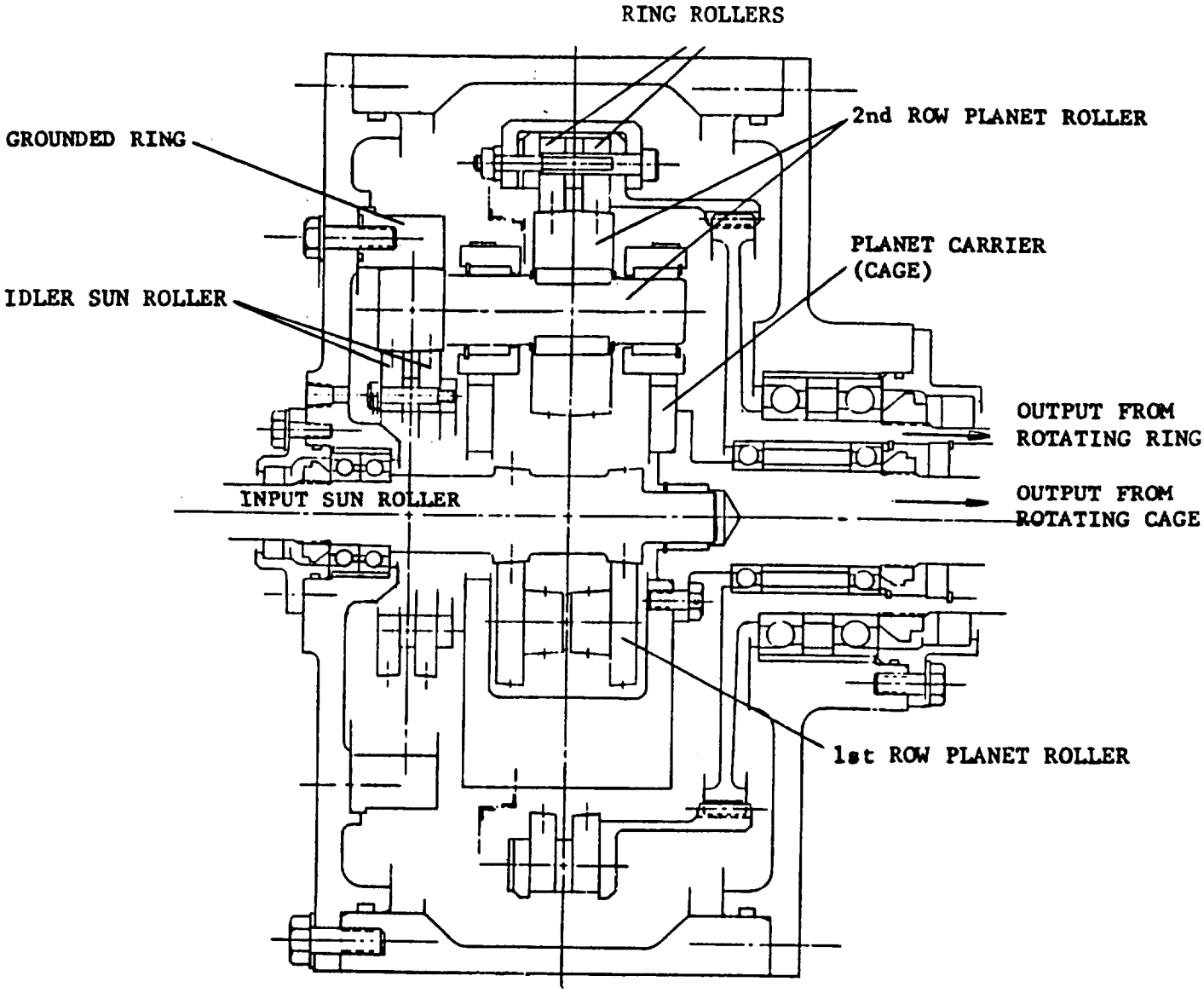


Figure 10. Grounded Ring (Momentum Balanced) Drive (DC-400).

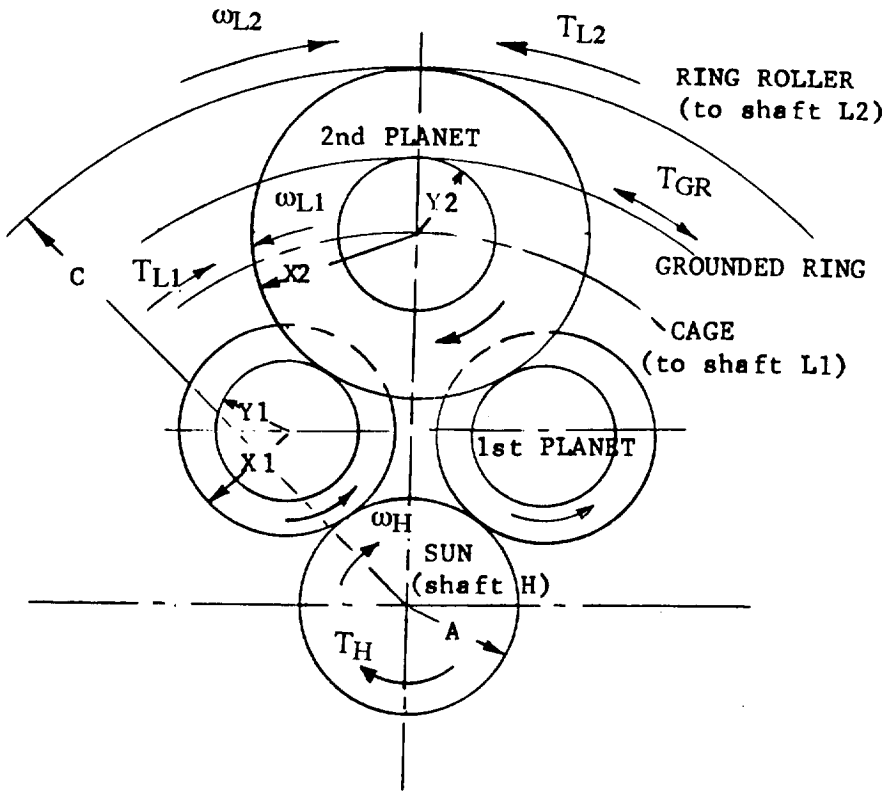


Figure 11. Torques and angular velocities in Grounded Ring (Momentum Balanced) Drive (DC-400). Torques are shown as inputted to the drive. Angular velocities are shown as viewed from one direction.

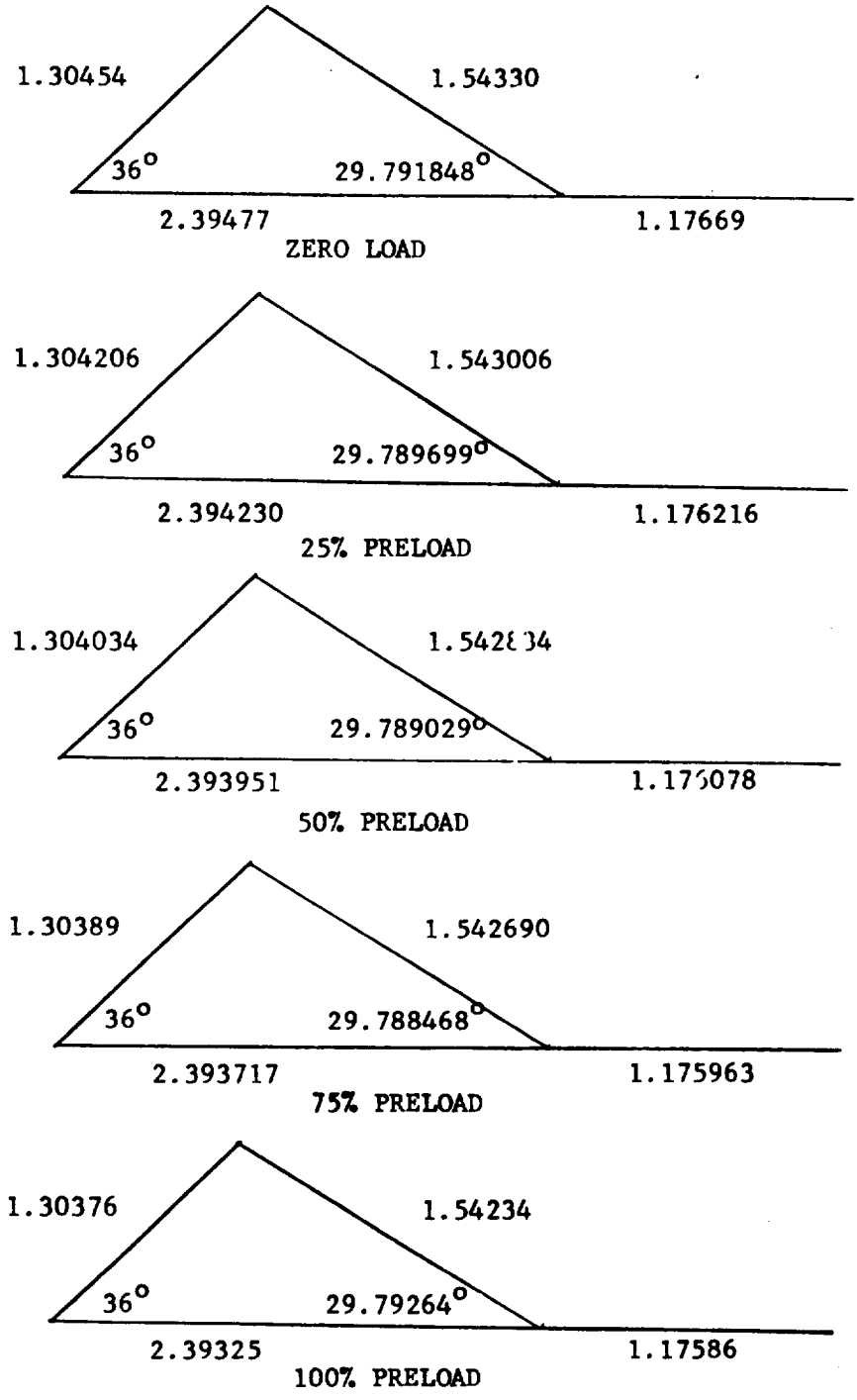


Figure 12.Roller spacing at different levels of preload (DC-400 drive).

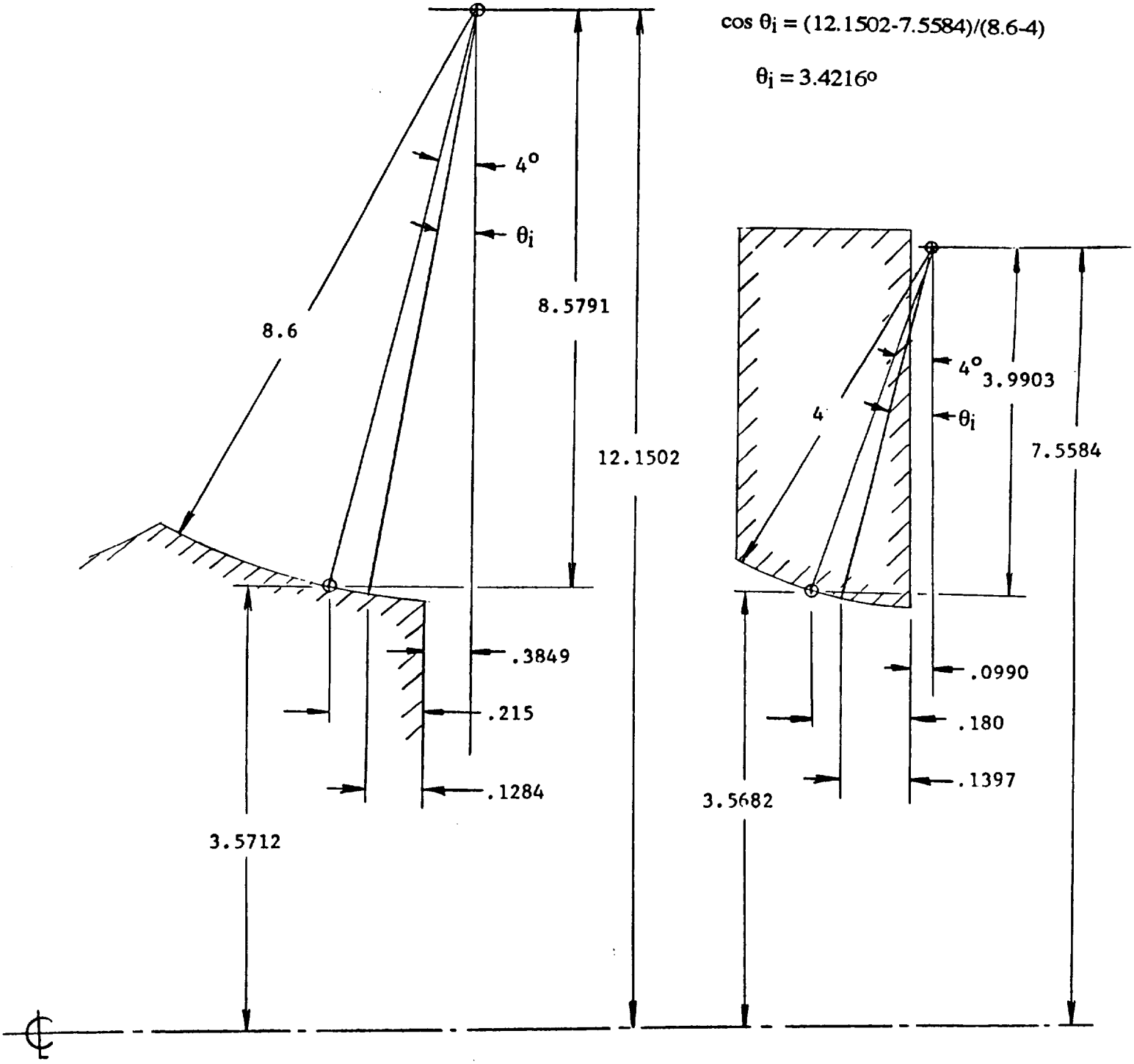


a) Initial setup, zero load

Figure 13. Second planet-ring roller engagement diagram (DC-400 drive).

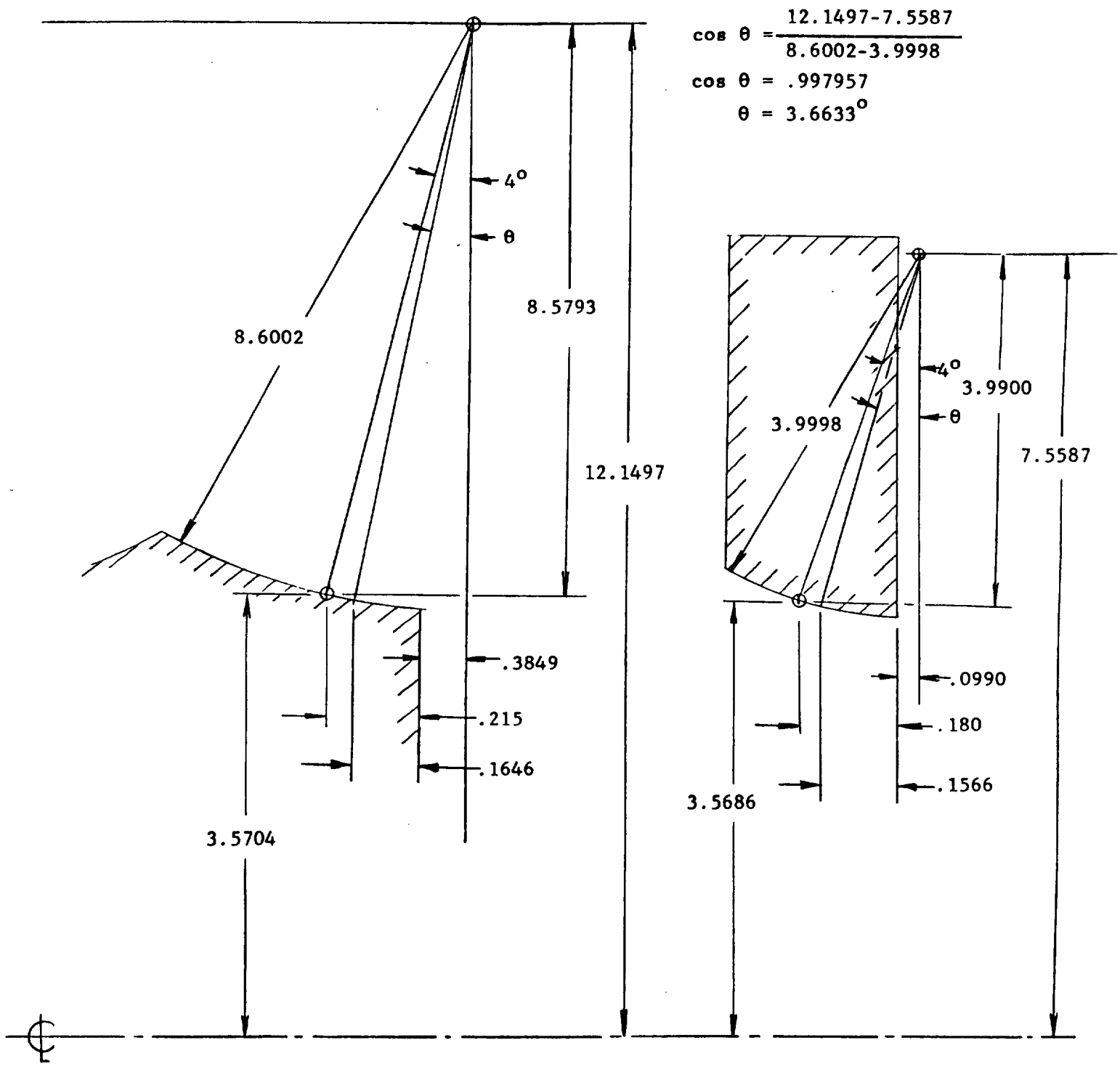


b) 25% preload

Figure 13(cont.) Second planet-ring roller engagement diagram (DC-400 drive).

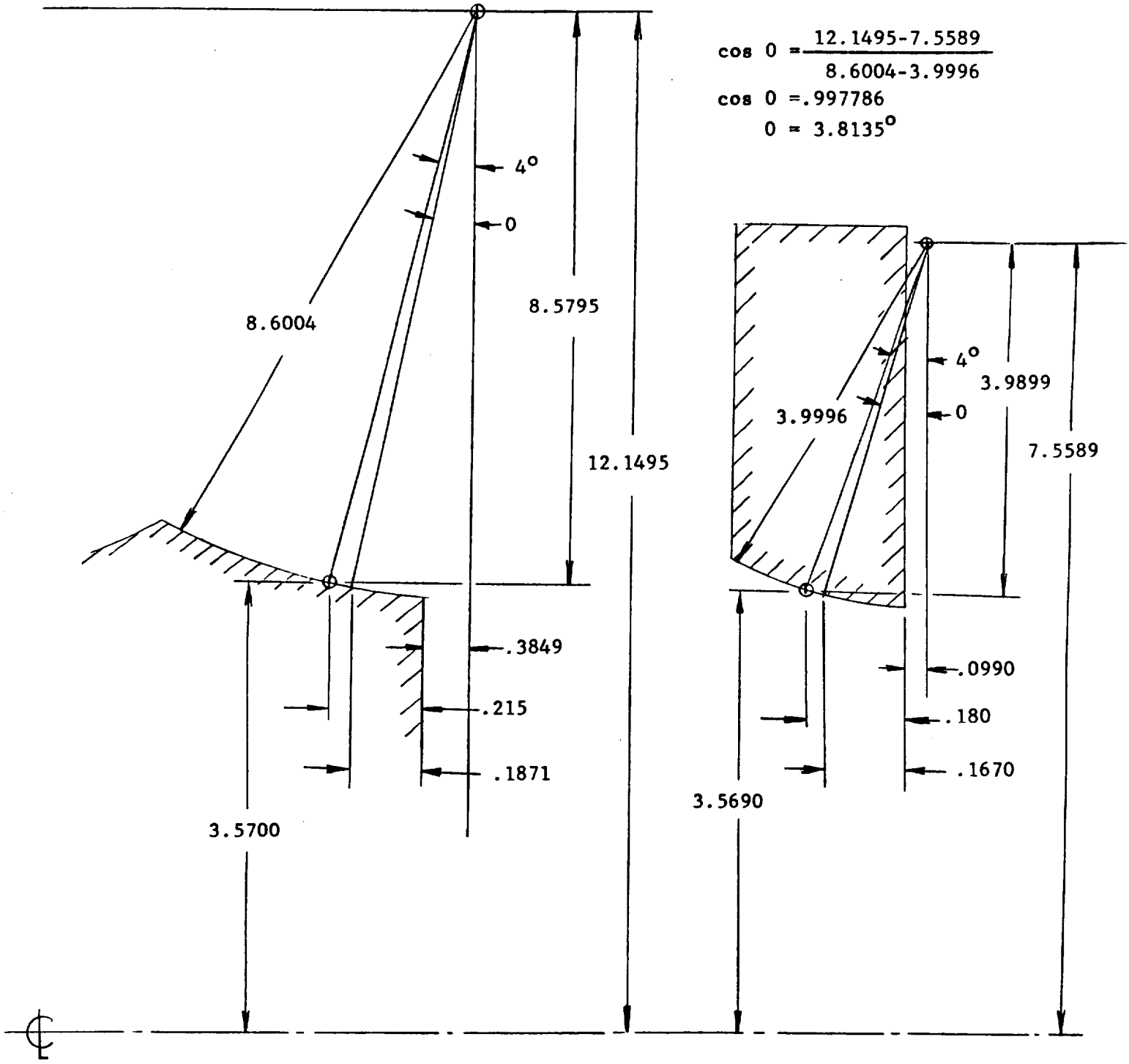


c) 50% preload

Figure 13(cont.) Second planet-ring roller engagement diagram (DC-400 drive).

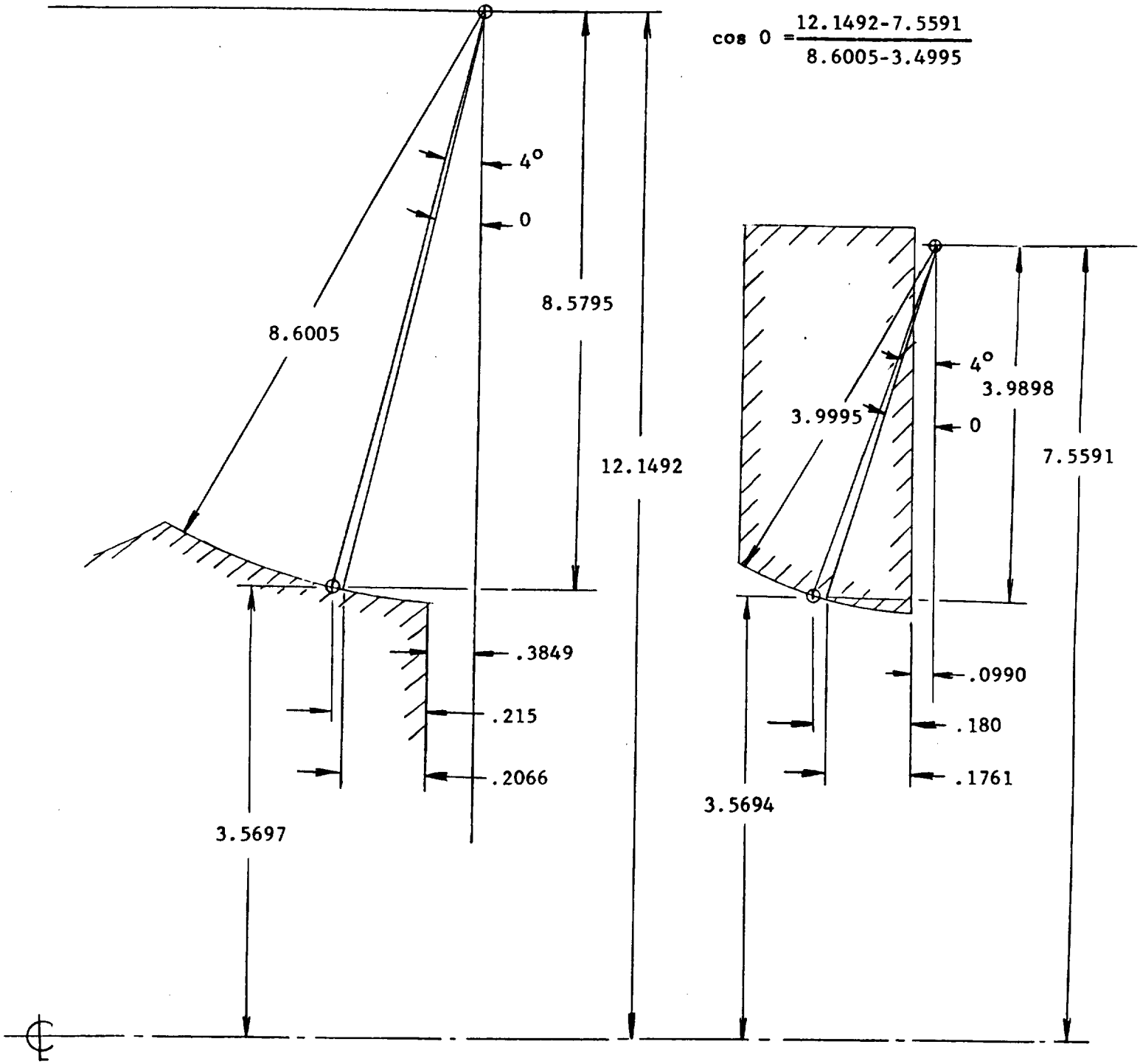


d) 75% preload

Figure 13(cont.) Second planet-ring roller engagement diagram (DC-400 drive).

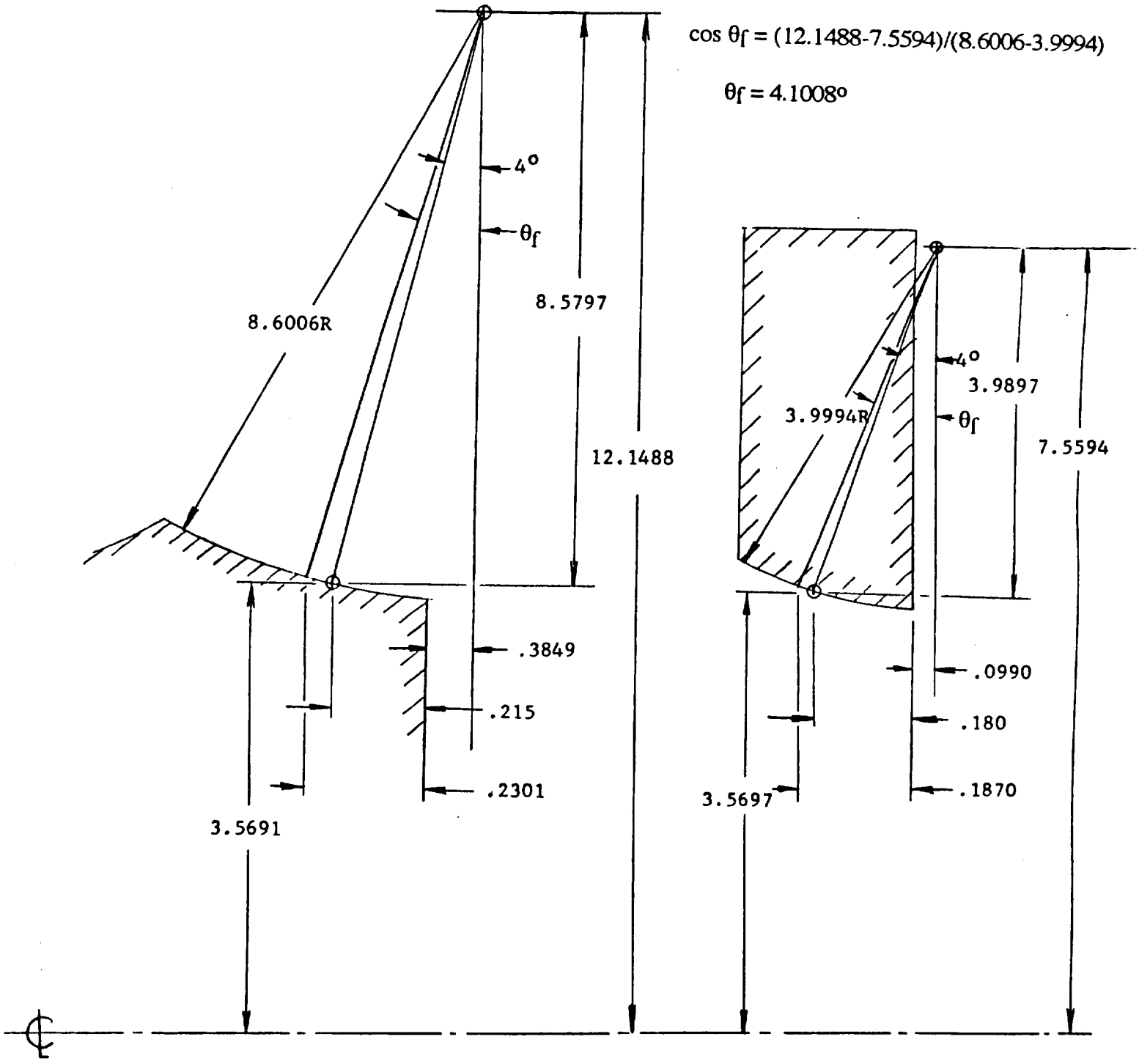


e) Full preload

Figure 13(concl.) Second planet-ring roller engagement diagram (DC-400 drive).

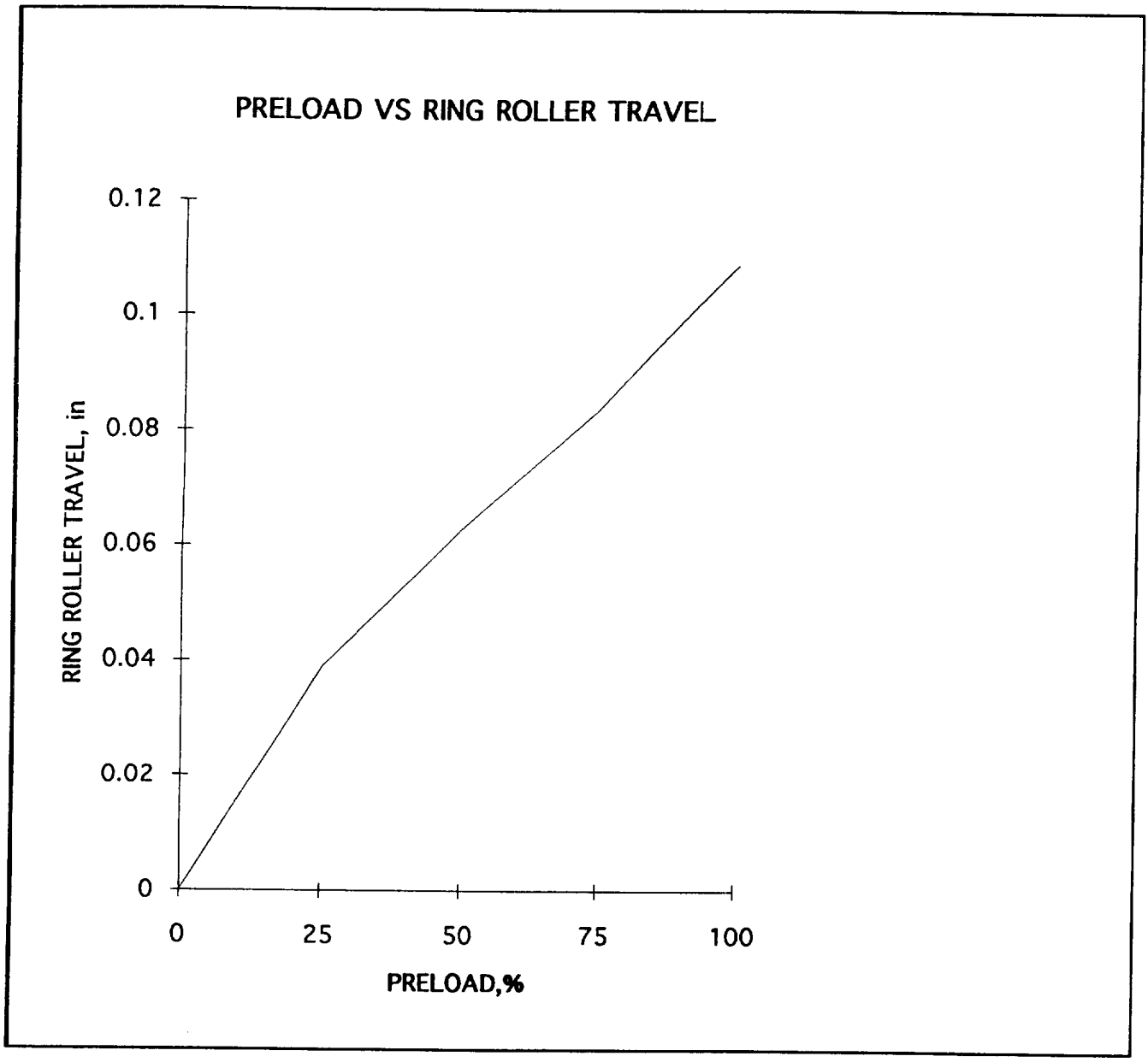


Figure 14. Preload level as a function of ring roller travel (DC-400 drive)

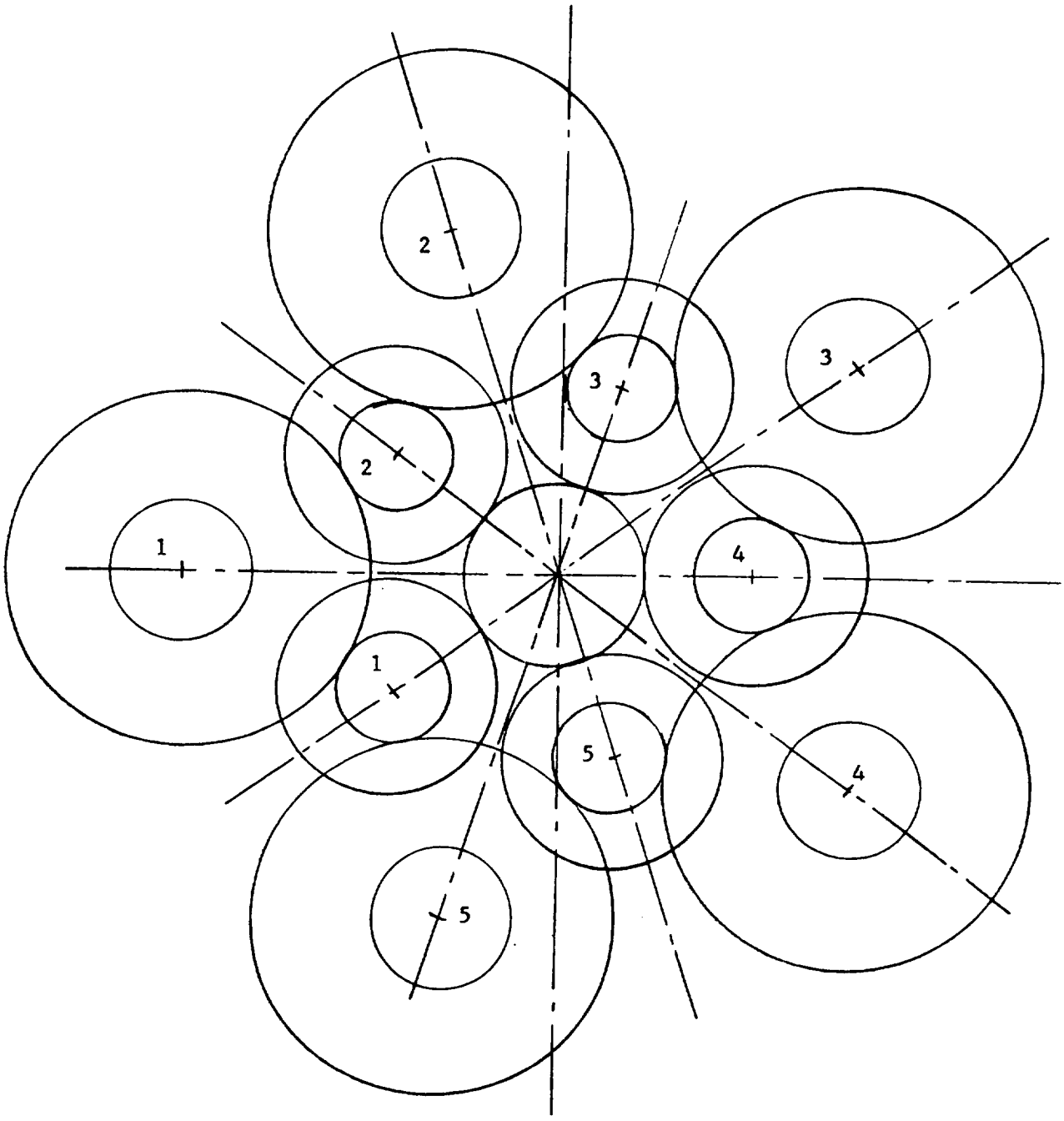


View from Input Side

Figure 15. Arrangement of first and second planet rollers as viewed from the input side (DC-400 drive).

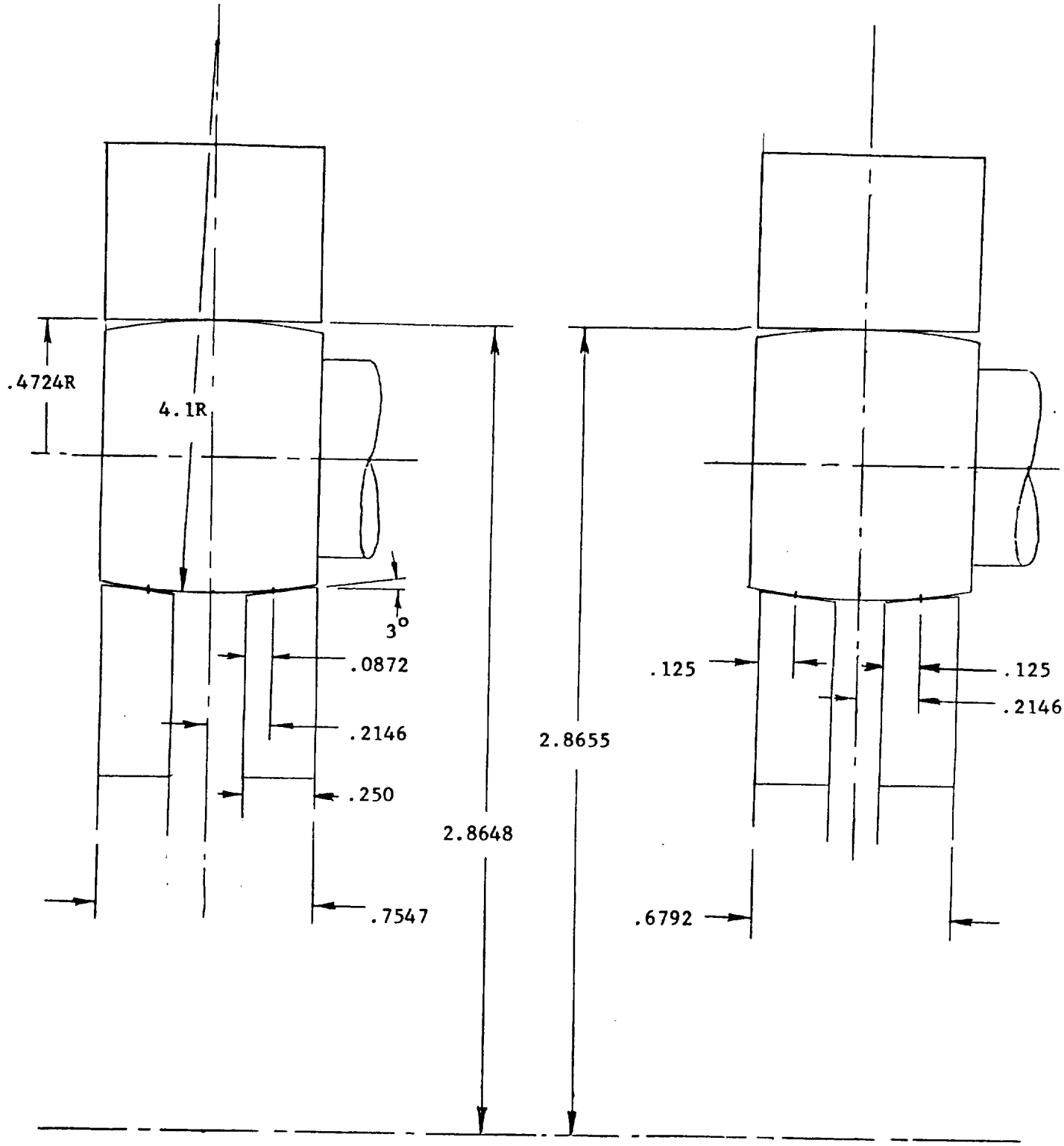


a) Initial engagement point
Zero preload

b) Final engagement point
100% preload

Figure 16. Initial and final engagement points in the grounded ring cluster ( DC-400 drive).

KEY

1 Encoder
2 Encoder- hollow shaft
3 Motor- KHX 740
4 Motor- hollow shaft
5 Torque meter- reactionless
6 Torque meter- reaction
7 Harmonic drive (80:1 ratio)
8 NAS 300A drive (29.23:1 ratio)
9 DC-500 or DC-700 Differential Drive
10 DC-400 Momentum Balanced Drive

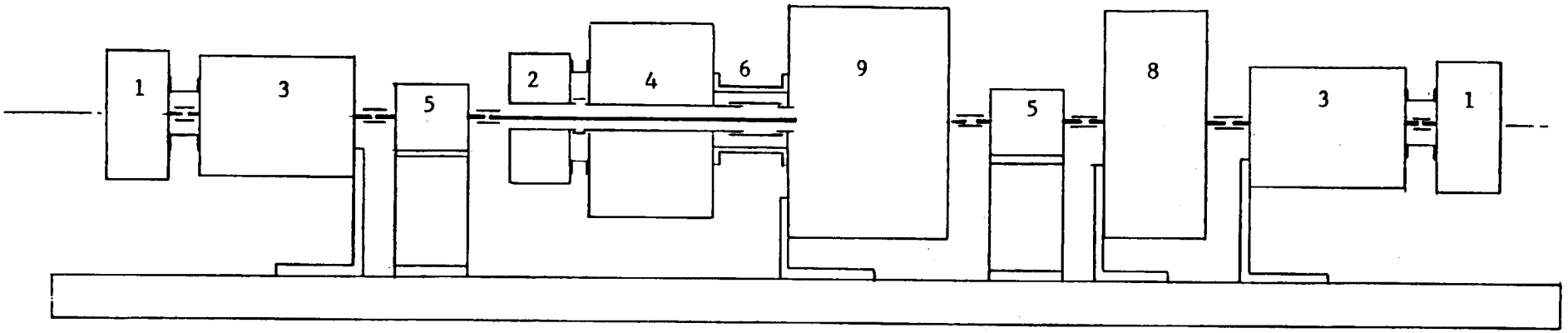


a) Test arrangement for DC-500 and DC-700 Differential Drives

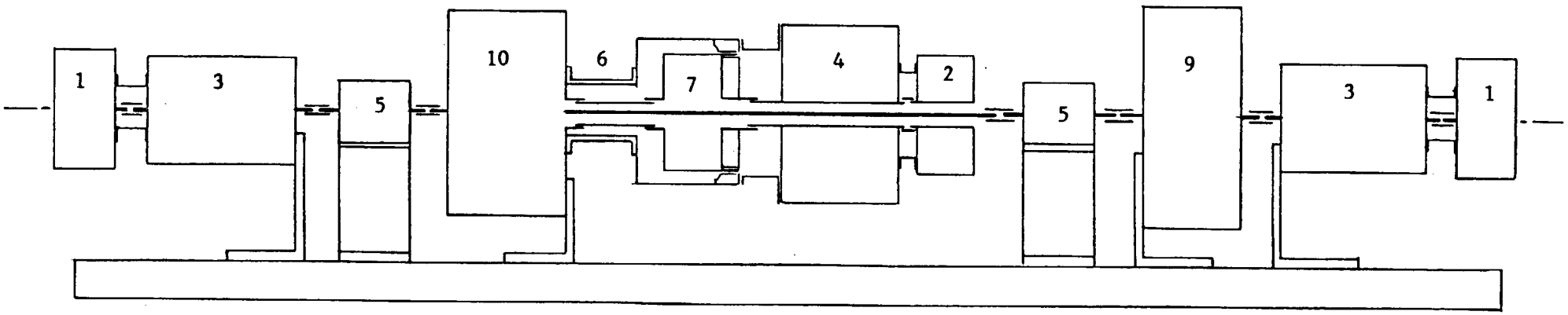


b) Test arrangement for DC-400 Momentum Balanced Drive

Figure 17. Arrangement of components in the test facility.

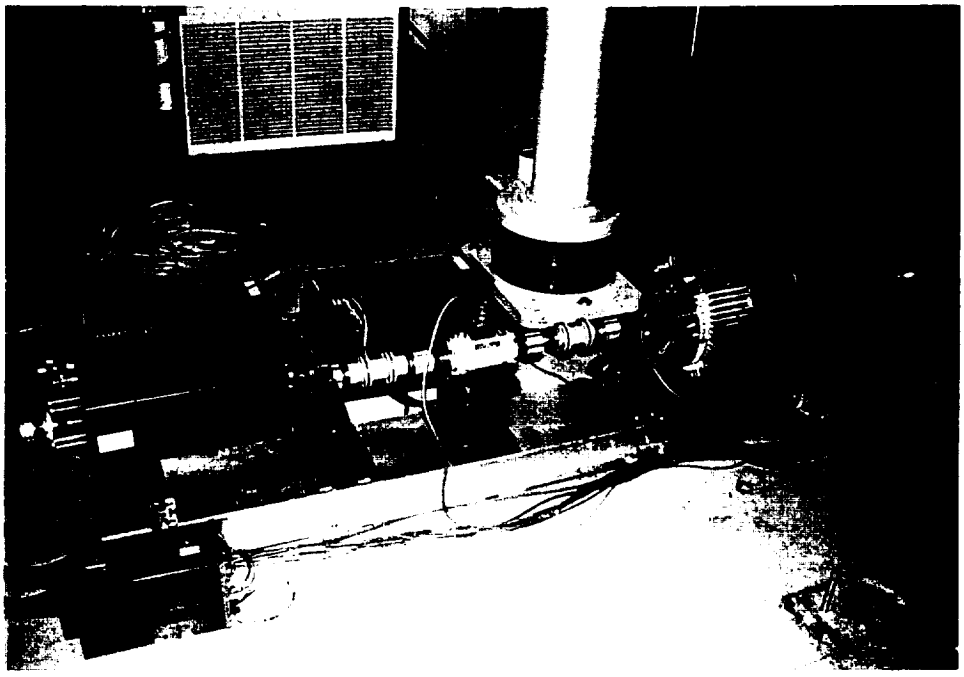

a) View showing KHX-740 motor, torquemeter, Uniq motor, and DC-500 drive.

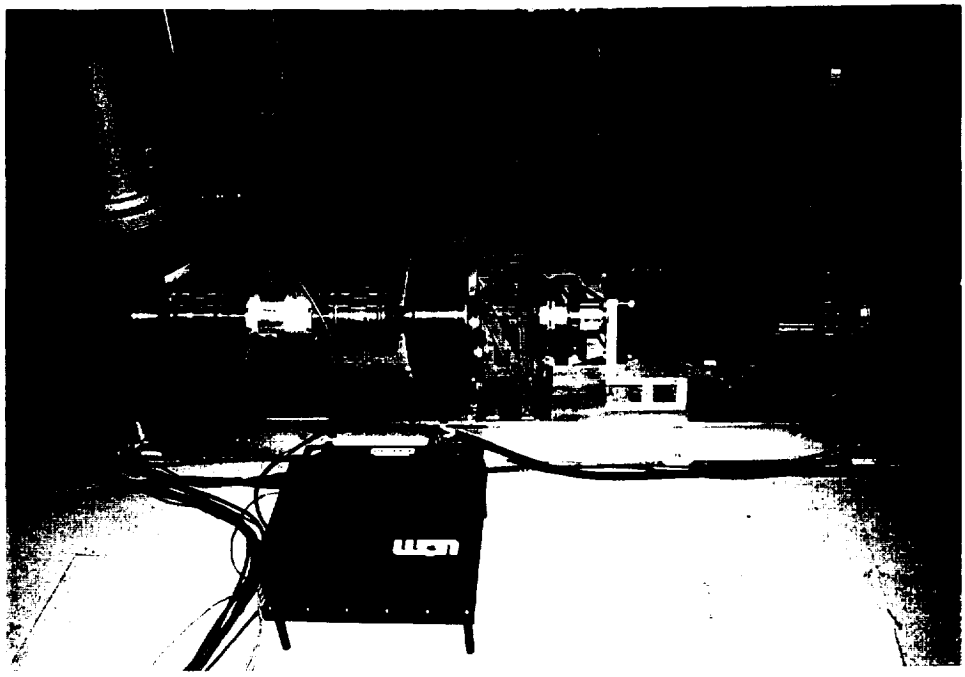

b) View showing DC-500 drive, torquemeter, MA-300 drive, and KHX-740 motor.

Figure 18. Views of test stand.

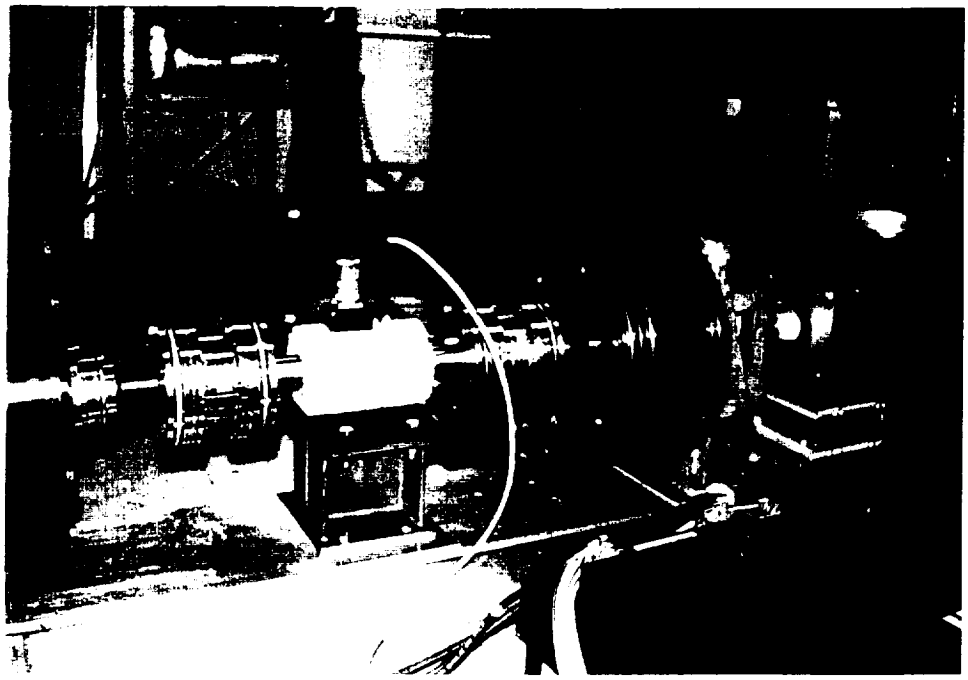

c) View showing DC-500 drive, torquemeter, and NA-300 drive.

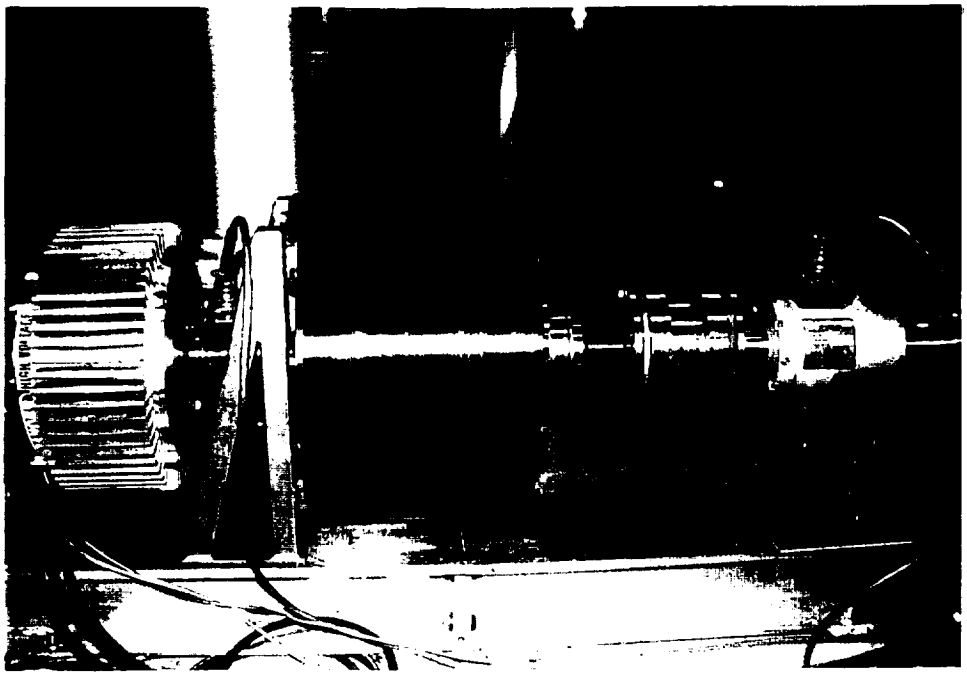

d) View showing Uniq motor, DC-500 drive, and torquemeter.

Figure 13(cont.). Views of test stand.

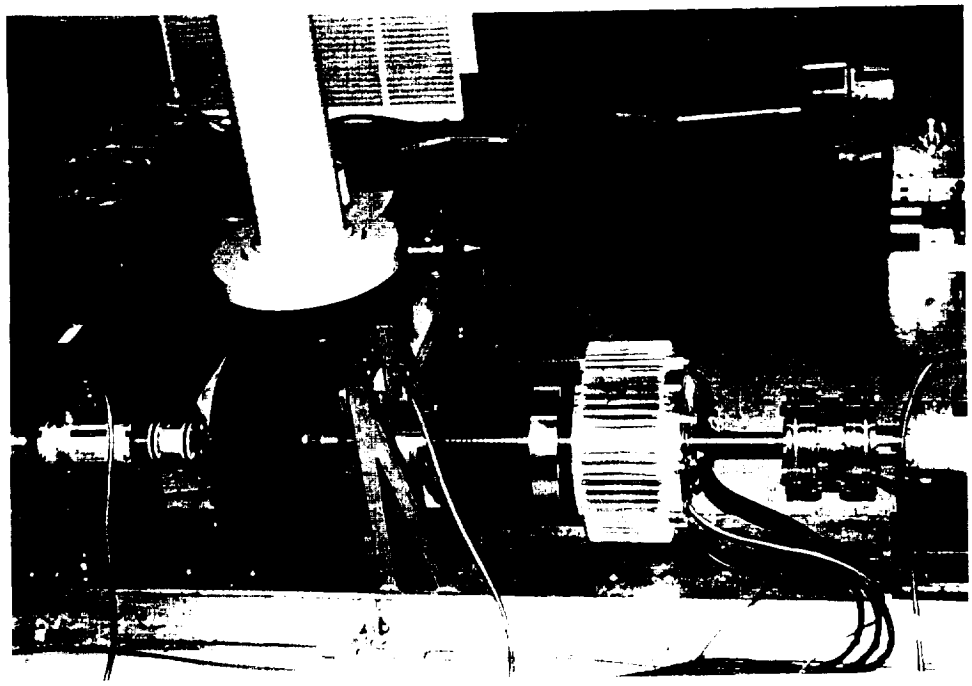

e) View showing torquemeter, DC-400 drive, Harmonic drive, and Uniq motor.

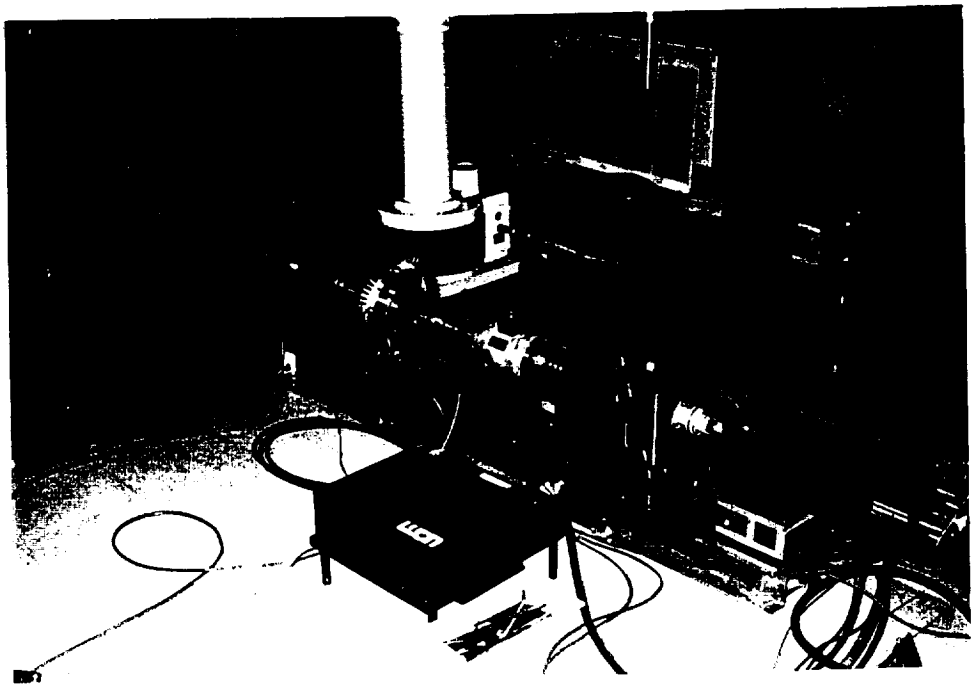

f) View showing Uniq motor, torquemeter, NA-300 drive, and KHX-740 motor.

Figure 18(concl.). Views of test stand.

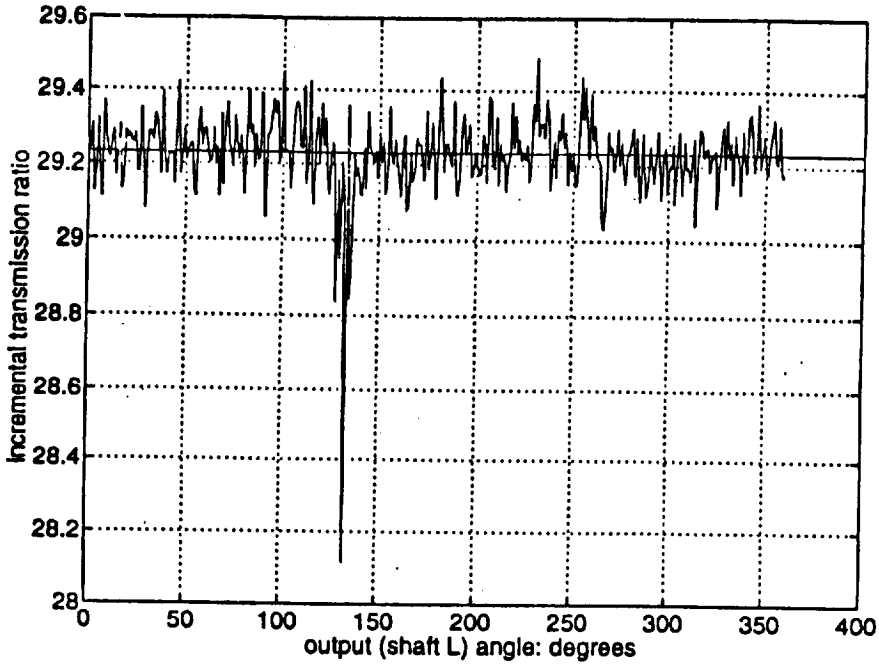


Figure 19. Angular linearity test for DC-700. H1 driven, H2 fixed, L free.

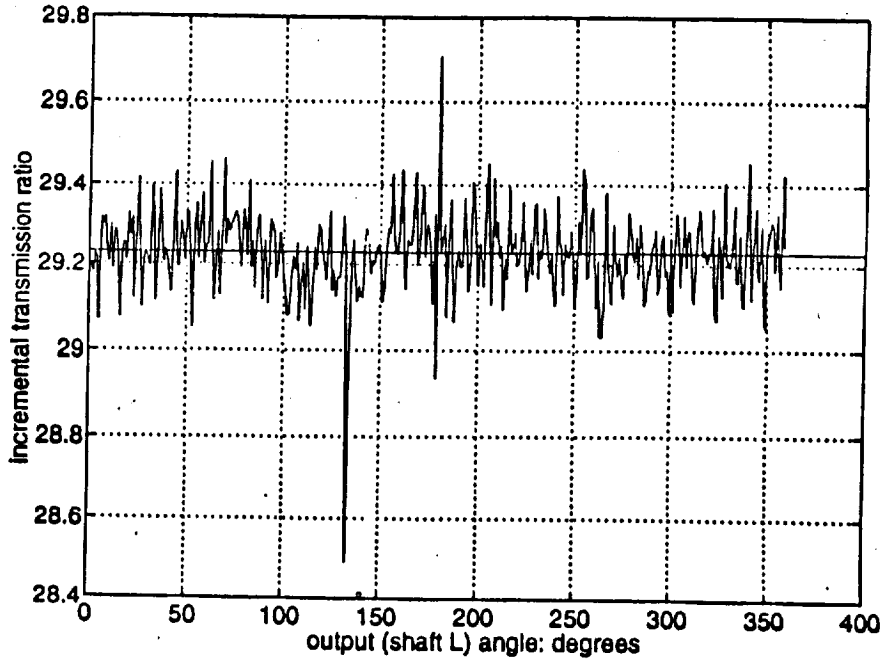


Figure 20. Repeat of angular linearity test of DC-700. H1 driven, H2 fixed, L free.

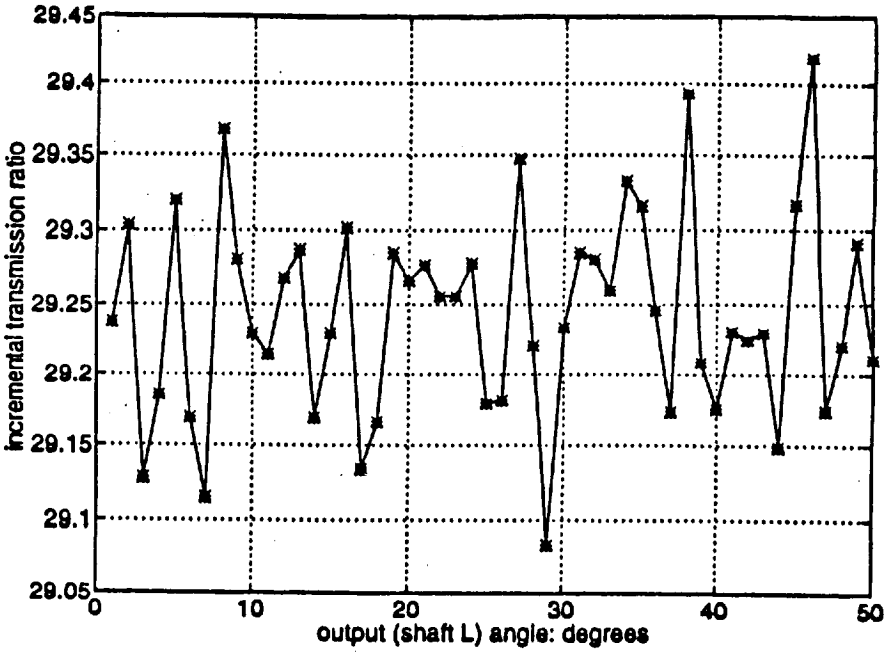


Figure 21. Zoom on 2nd angular linearity test for DC-700. H1 driven, H2 fixed, L free.

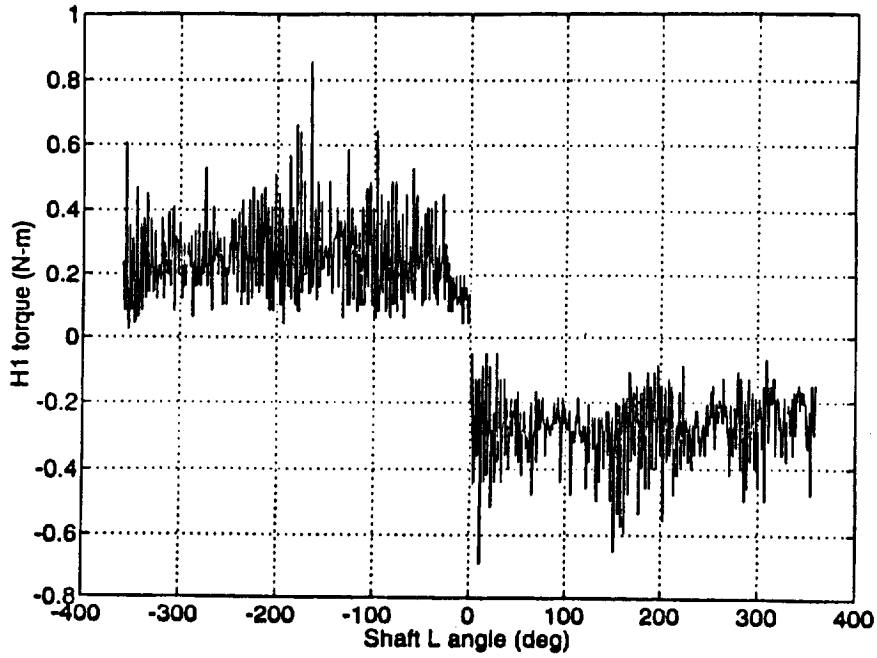


Figure 22. DC-700 shaft H1 input cogging torque. H2 fixed, L free.

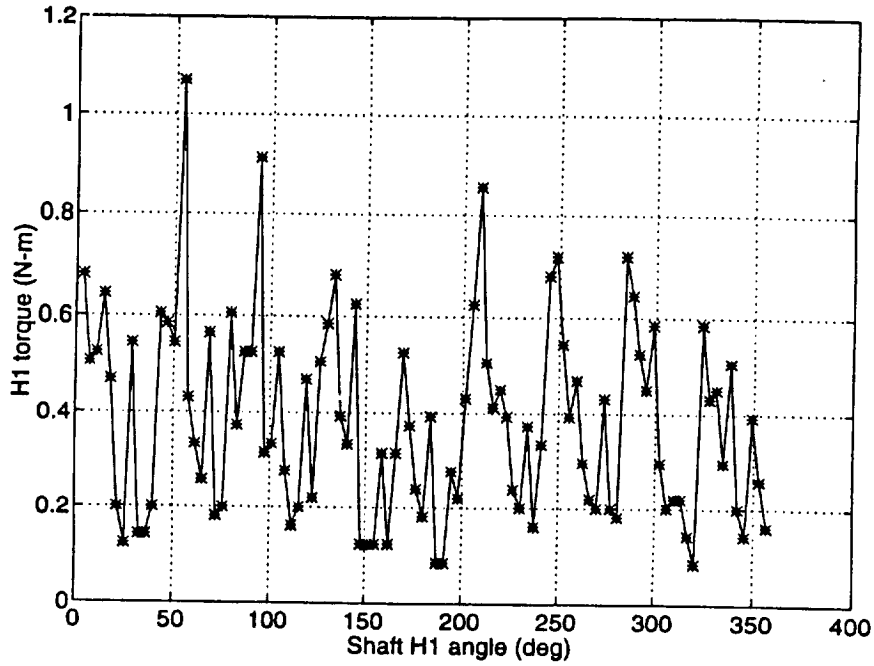


Figure 23. DC-700 shaft H1 input cogging torque (zoom). H2 fixed, L free.

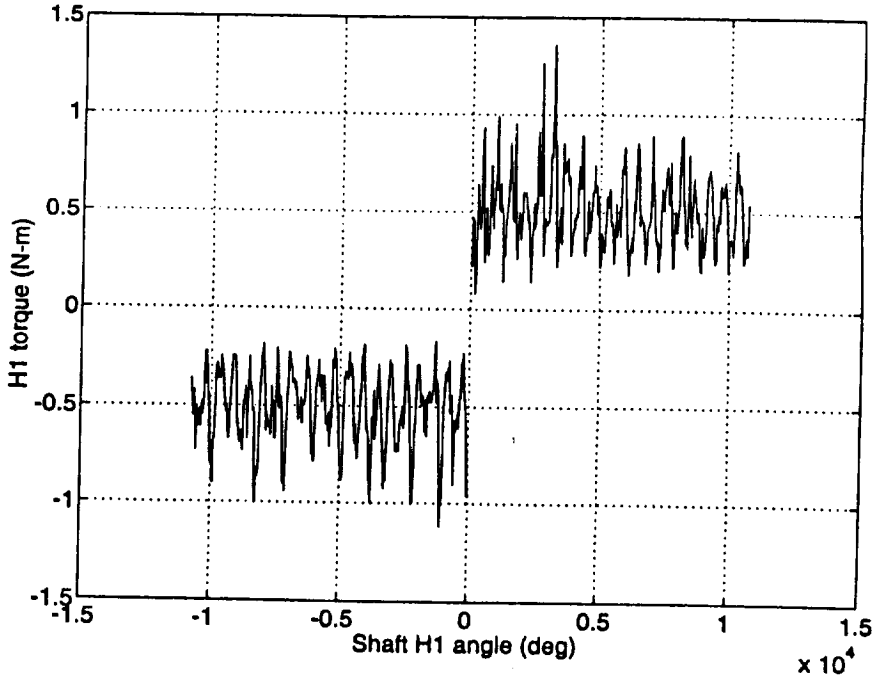


Figure 24. DC-700 shaft H2 input cogging torque. H2 free, L fixed.

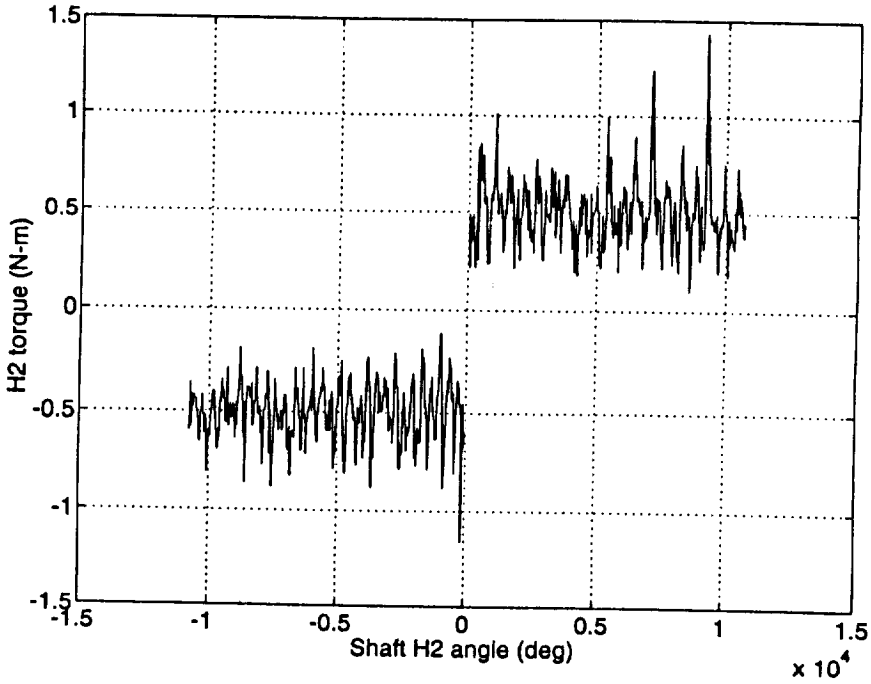


Figure 25. DC-700 shaft H2 input cogging torque. H1 free, L fixed.

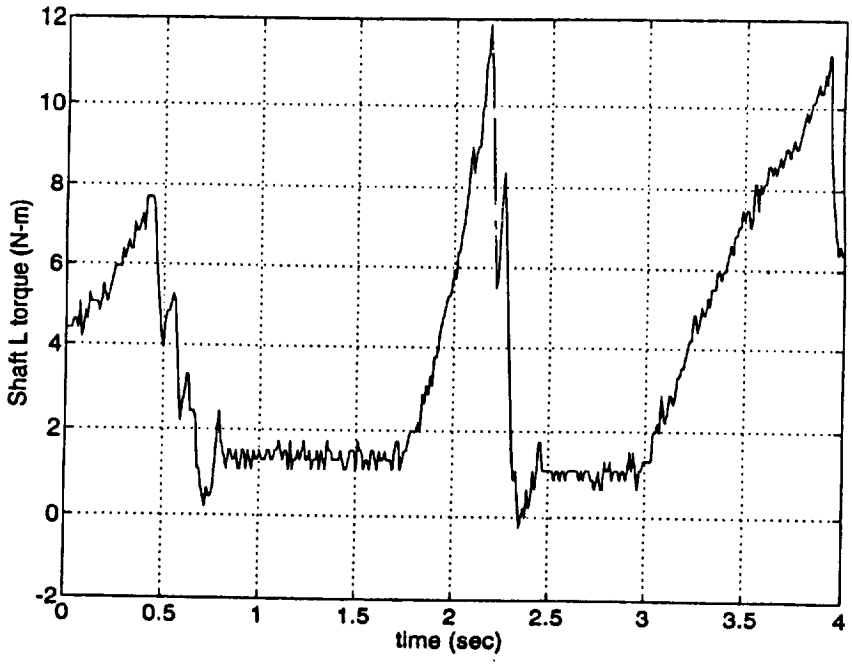


Figure 26. DC-700 shaft L break-away torque.

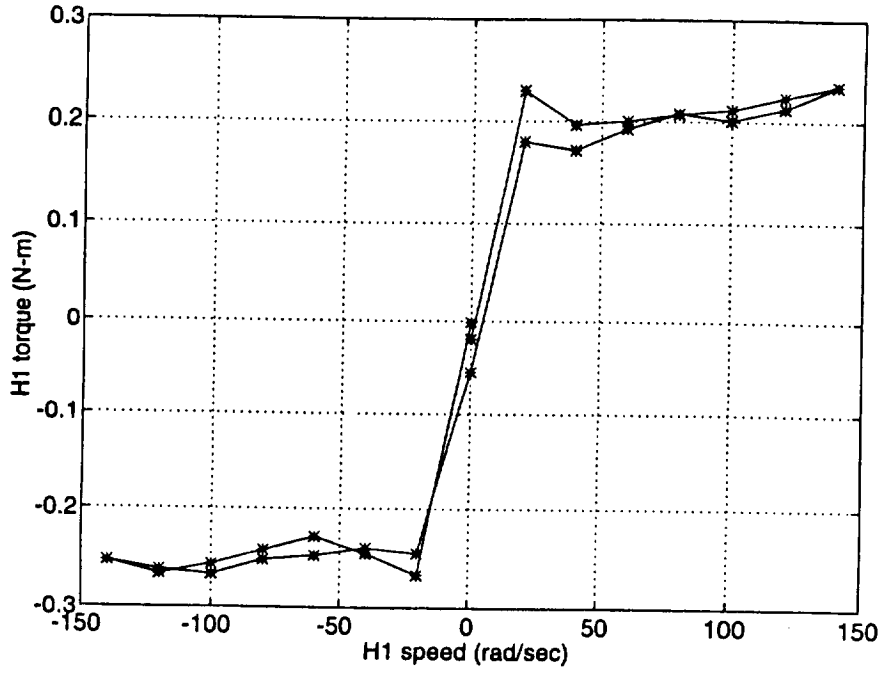


Figure 27. DC-700 unloaded drive friction. H1 driven, H2 fixed, L free.

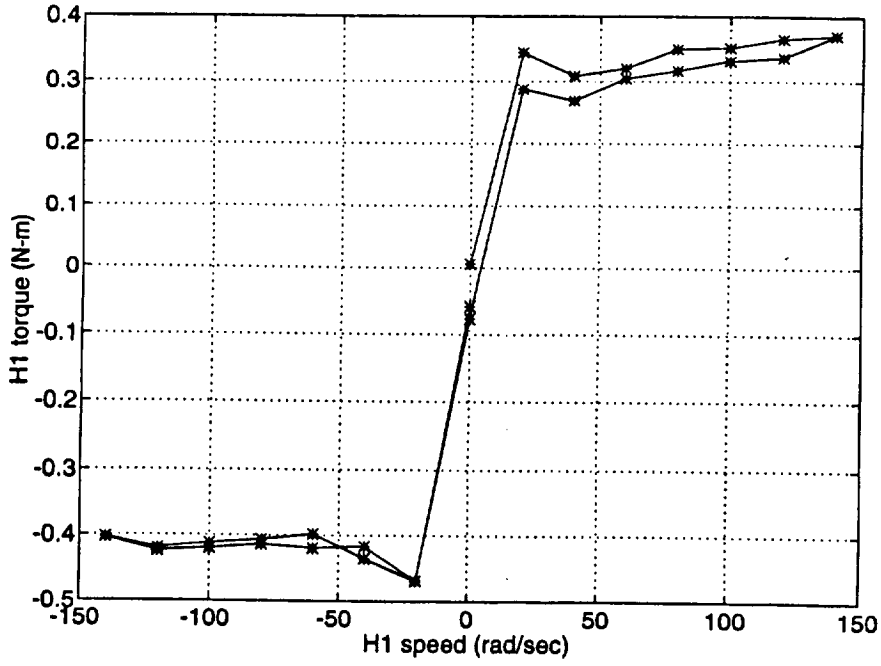


Figure 28. DC-700 unloaded drive friction. H1 driven, H2 free, L fixed.

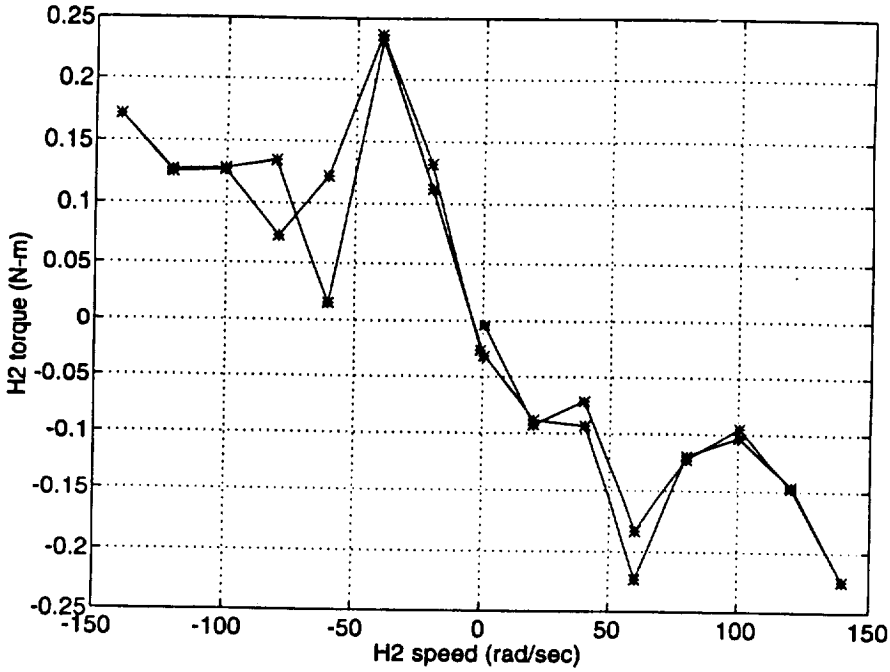


Figure 29. DC-700 unloaded drive friction. H2 driven, H1 fixed, L free.

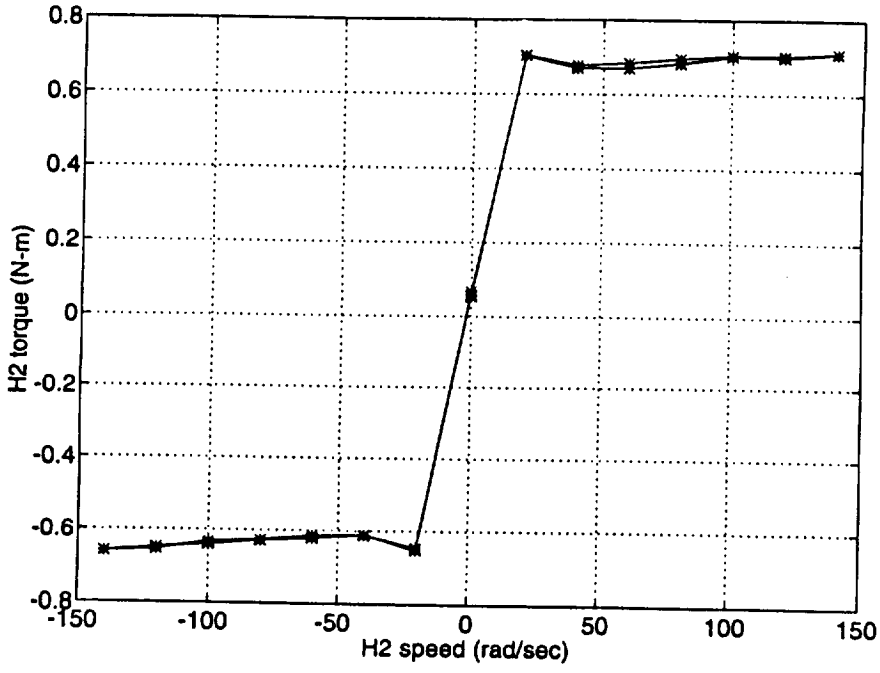


Figure 30. DC-700 unloaded drive friction. H2 driven, H1 free, L fixed.

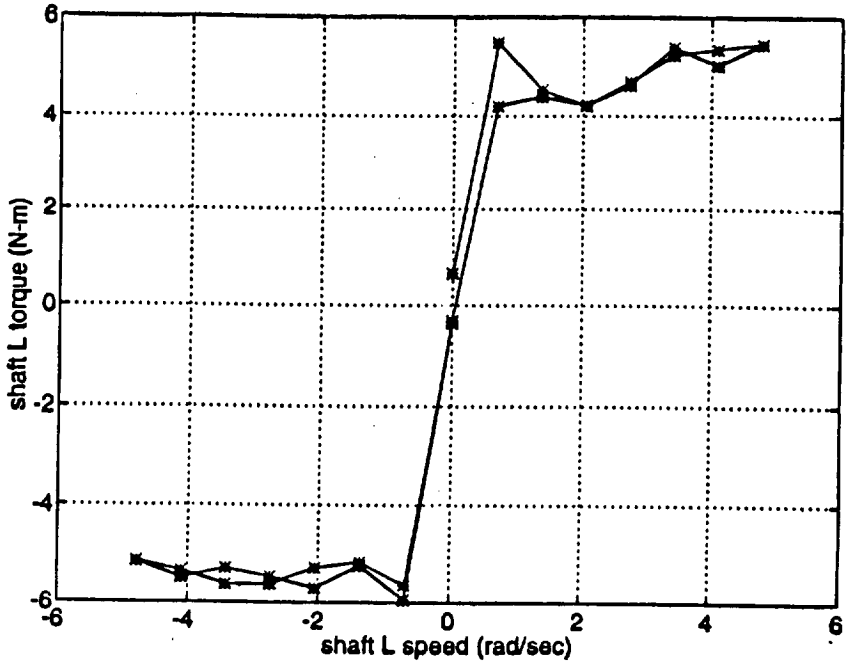


Figure 31. DC-700 unloaded drive friction. L driven, H1 free, H2 fixed.

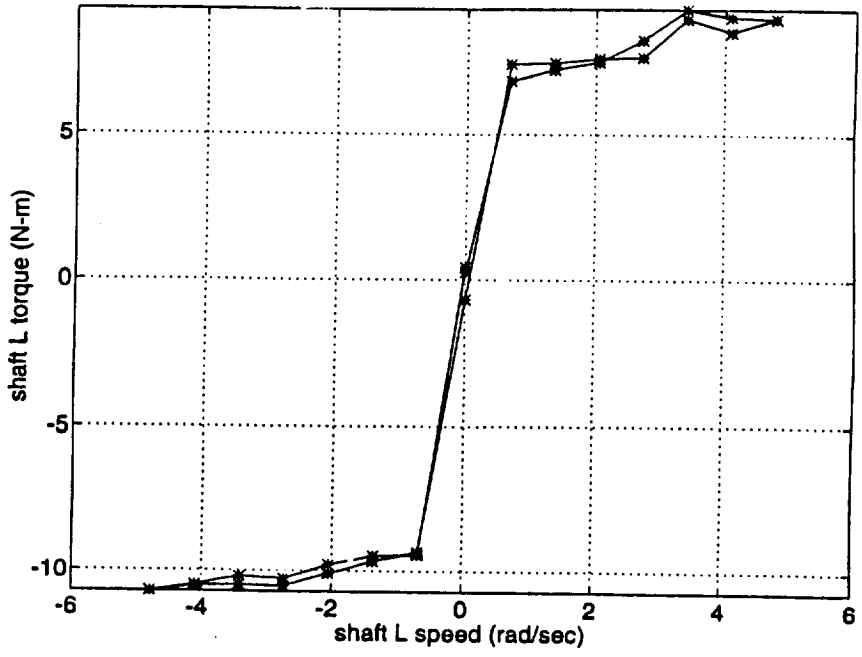


Figure 32. DC-700 unloaded drive friction. L driven, H2 free, H1 fixed.

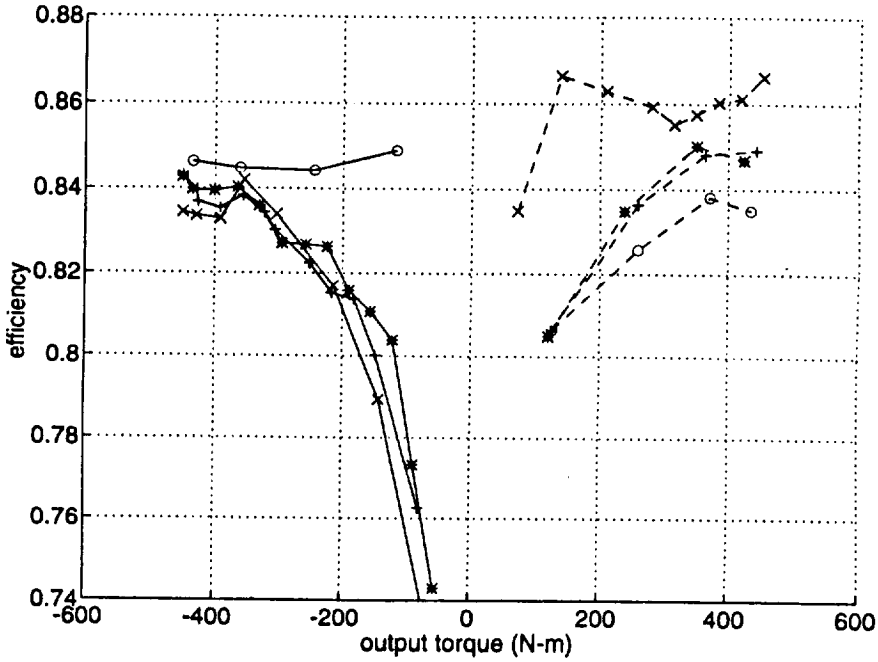


Figure 33. DC-700 efficiency at zero output speed.

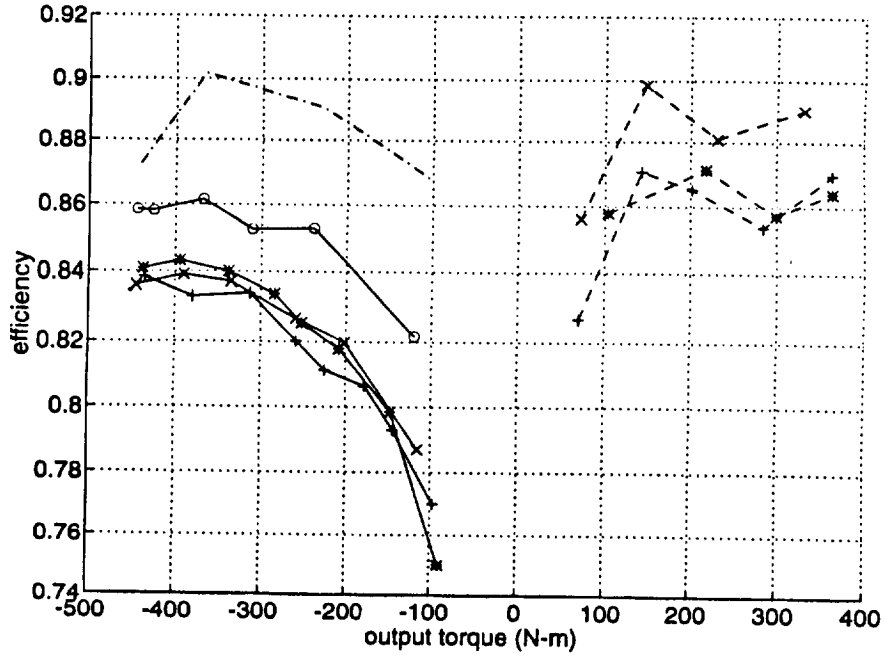


Figure 34. DC-700 efficiency at 1.2 rad/sec output speed (+35/R).

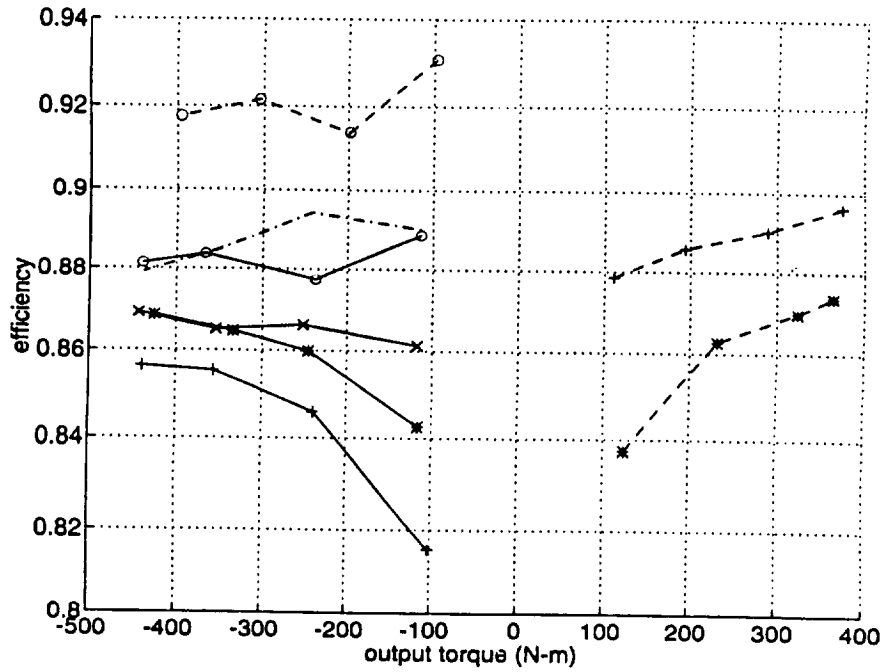


Figure 35. DC-700 efficiency at 2.4 rad/sec output speed (+70/R)

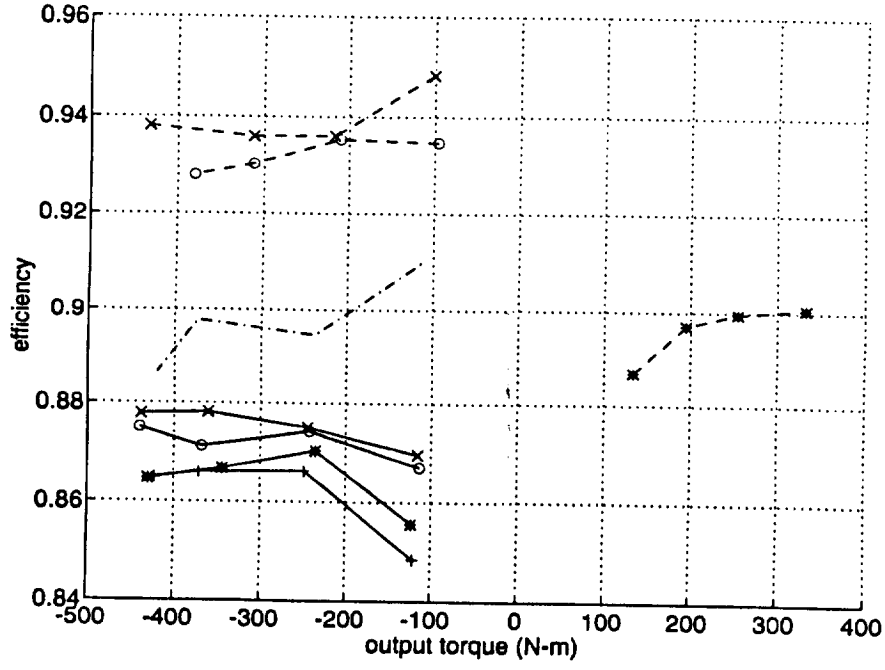


Figure 36. DC-700 efficiency at 3.59 rad/sec output speed (+105/R)

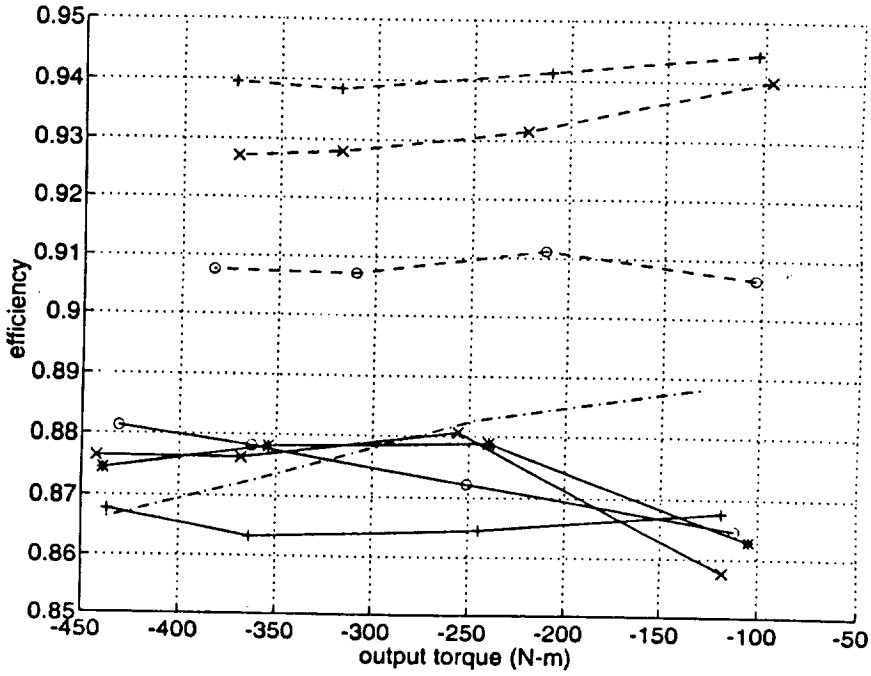


Figure 37. DC-700 efficiency at 4.79 rad/sec output speed (+140/R).

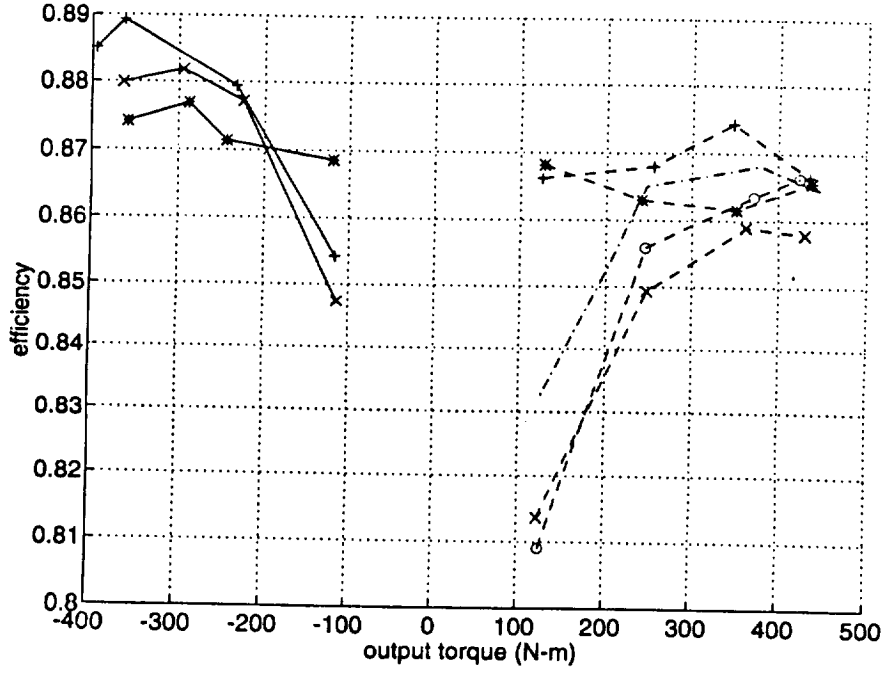


Figure 38. DC-700 efficiency at-1.2 rad/sec output speed (-35/R).

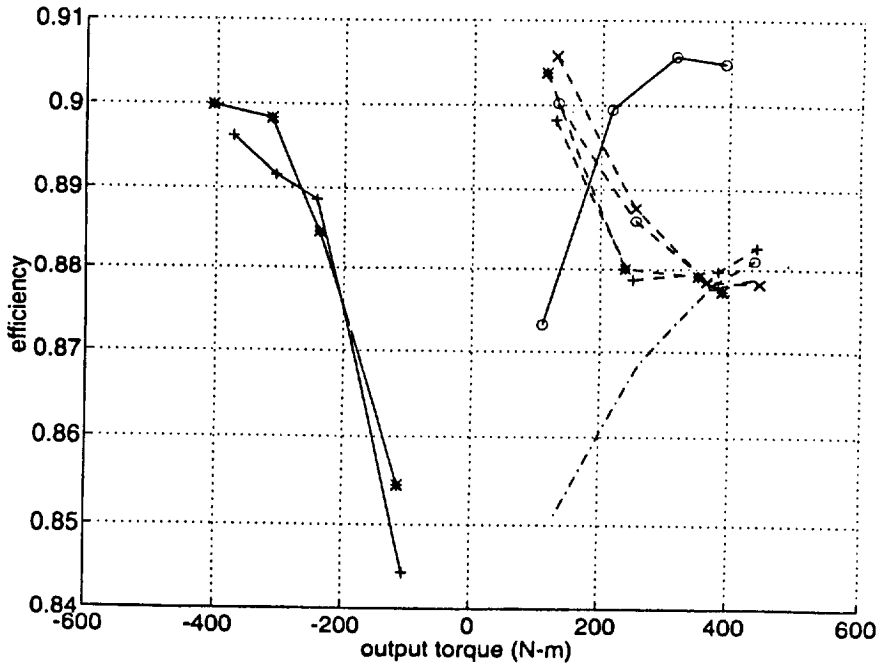


Figure 39. DC-700 efficiency at -2.4 rad/sec output speed (-70/R).

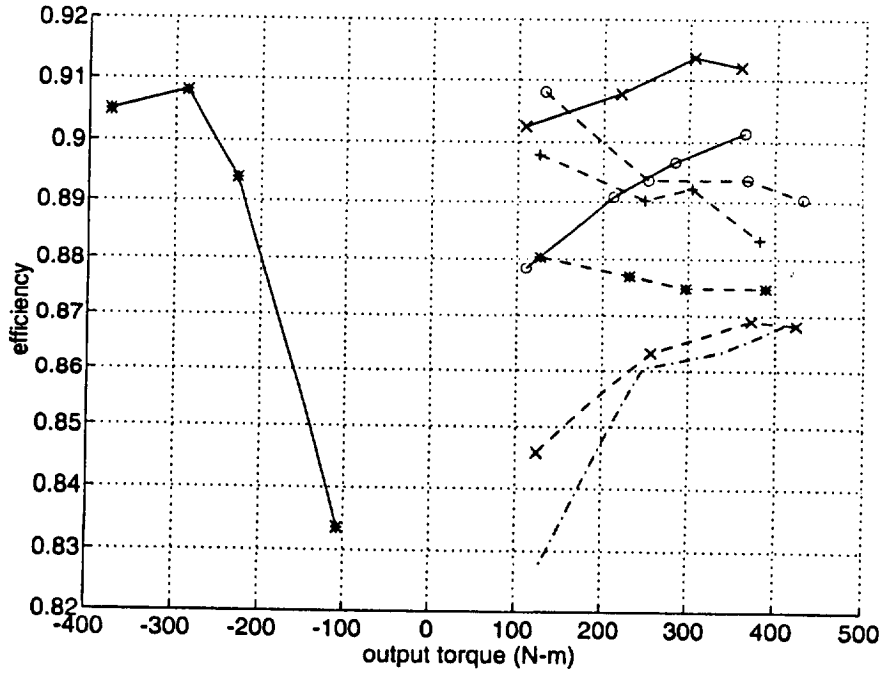


Figure 40. DC-700 efficiency at -3.59 rad/sec output speed (-105/R).

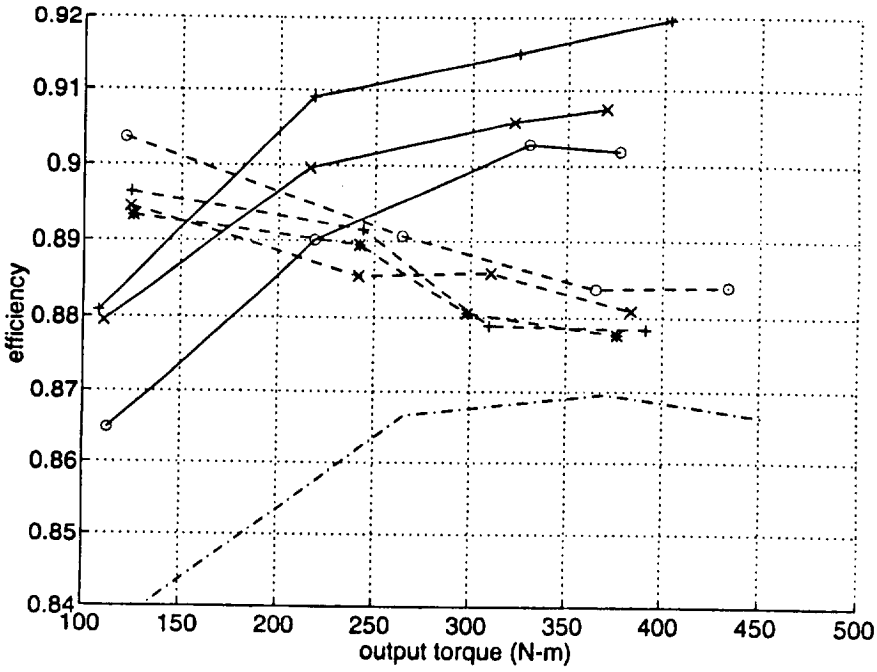


Figure 41. DC-700 efficiency at -4.79 rad/sec output speed (-140/R).

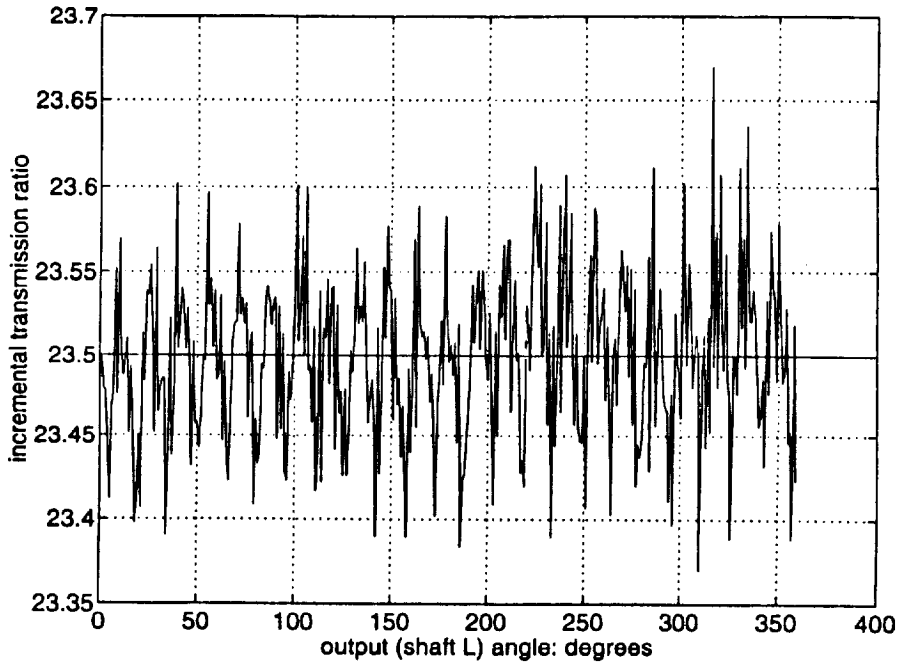


Figure 42. DC-500 ratio. H1 driven, L free, H2 fixed.

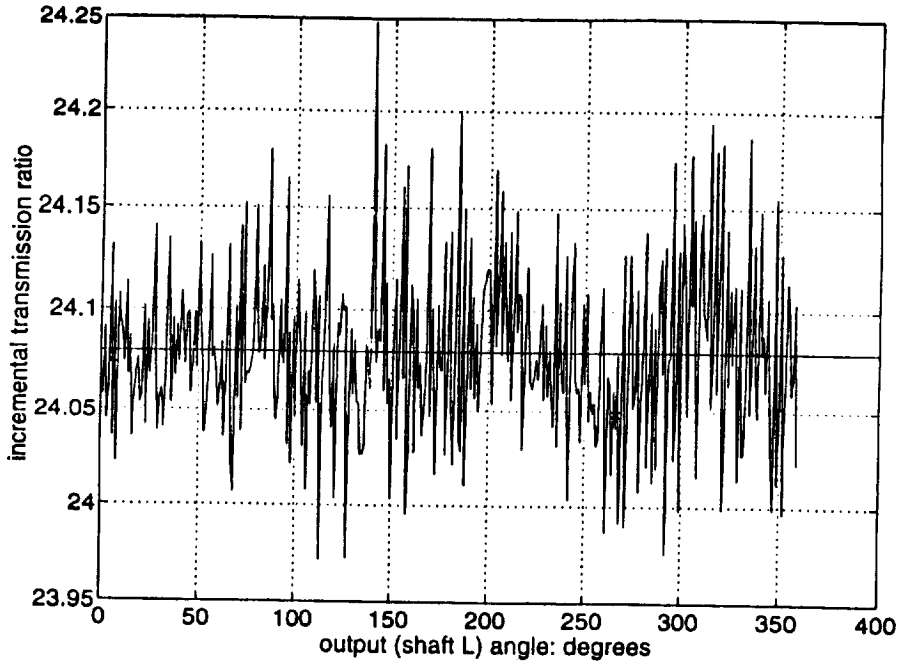


Figure 43. DC-500 ratio. H2 driven, L free, H1 fixed.

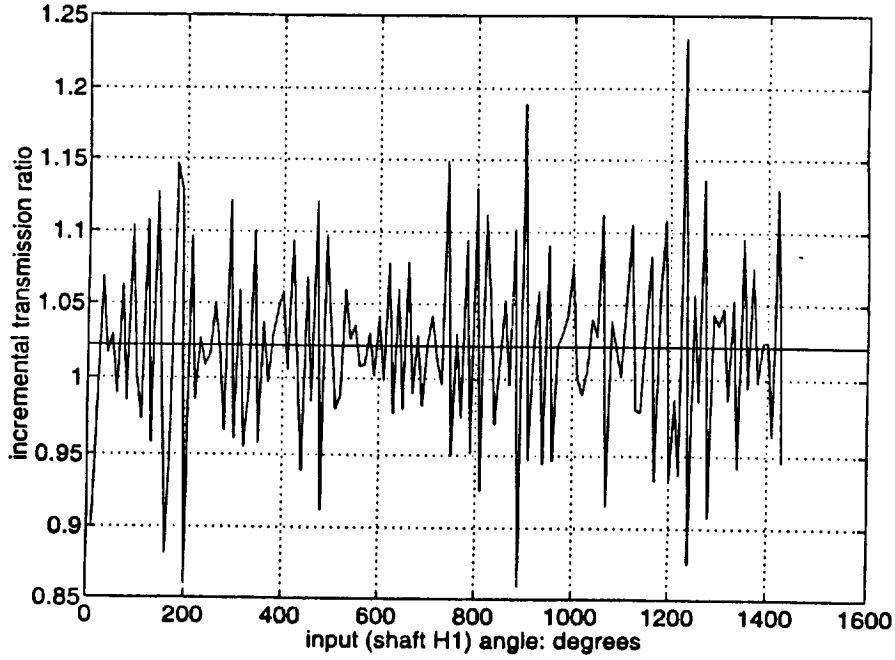


Figure 44. DC-500 ratio. H1 driven, H2 free, L fixed.

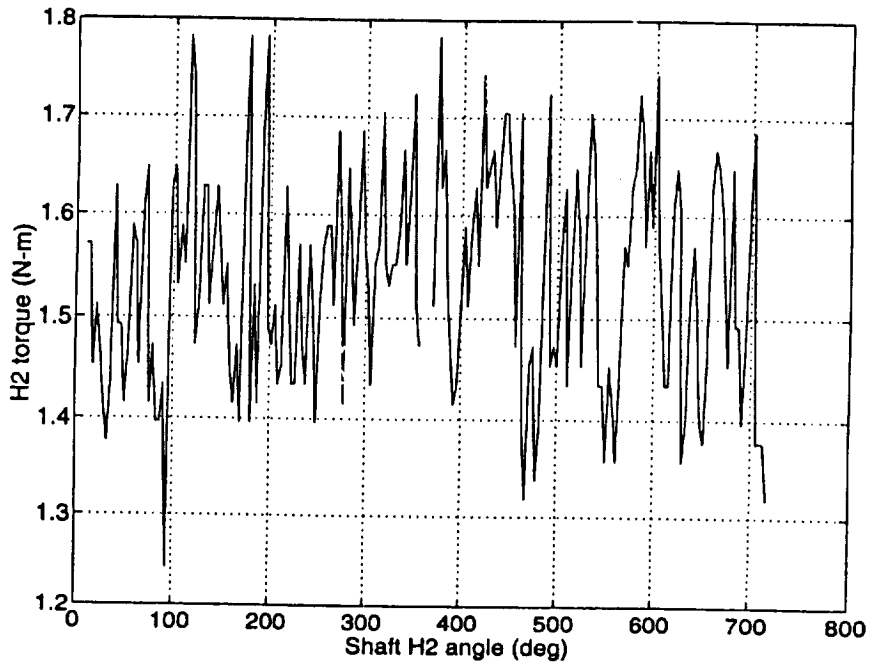


Figure 45. DC-500 H2 cogging torque. H1 free, L fixed.

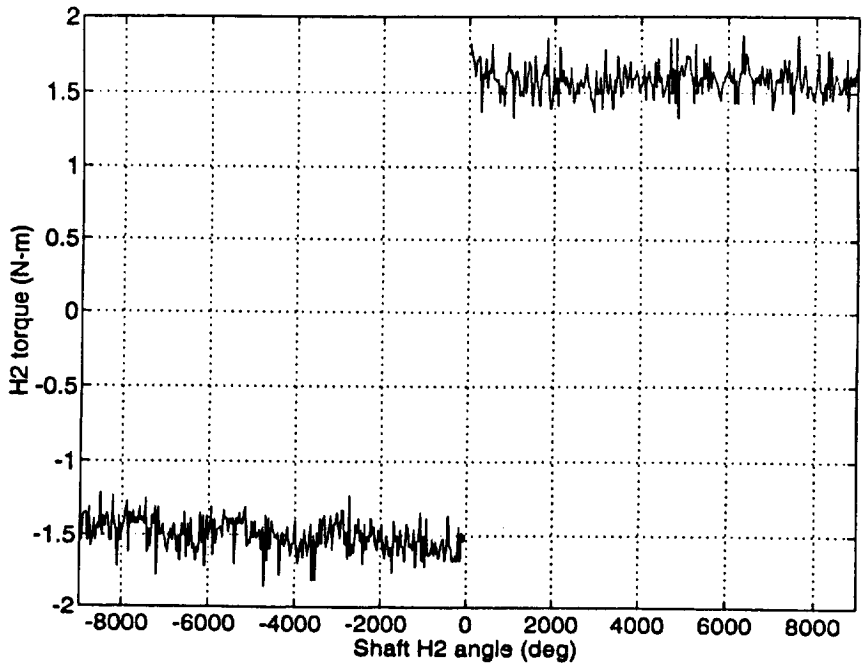


Figure 46. DC-500 H2 cogging torque. H1 free, L fixed.

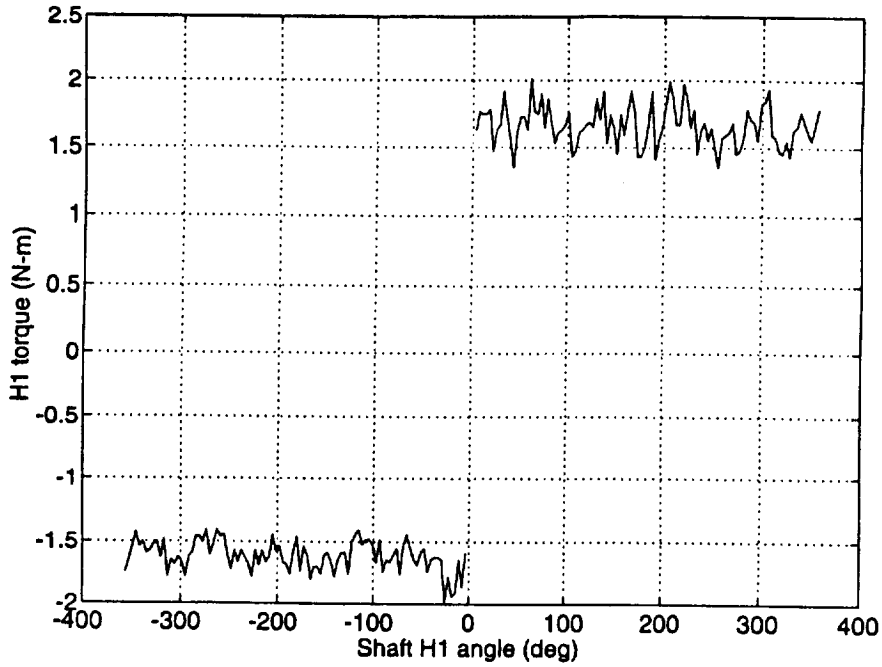


Figure 47. DC-500 H1 cogging torque. H2 free, L fixed.

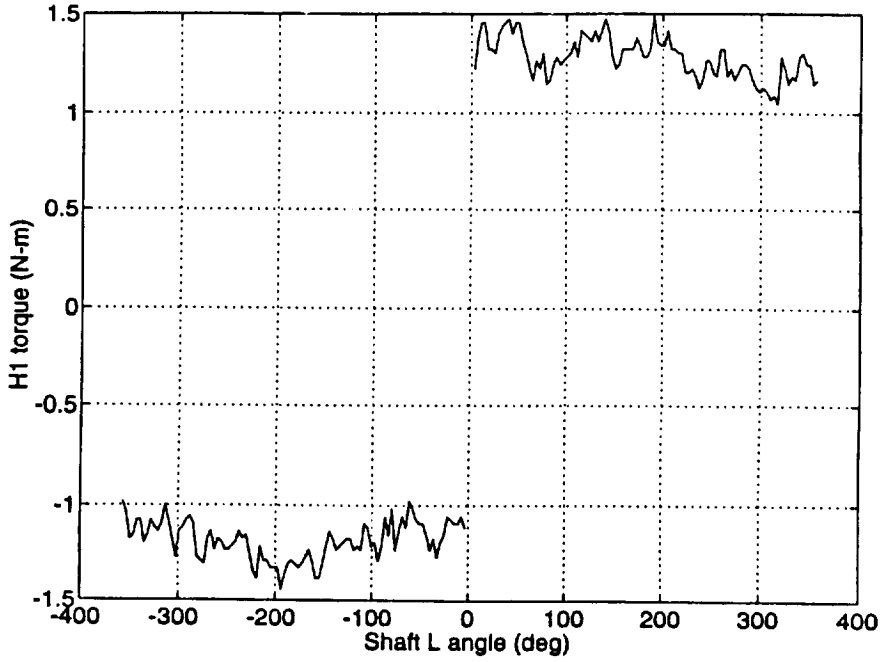


Figure 48. DC-500 cogging torque. L free, H2 fixed.

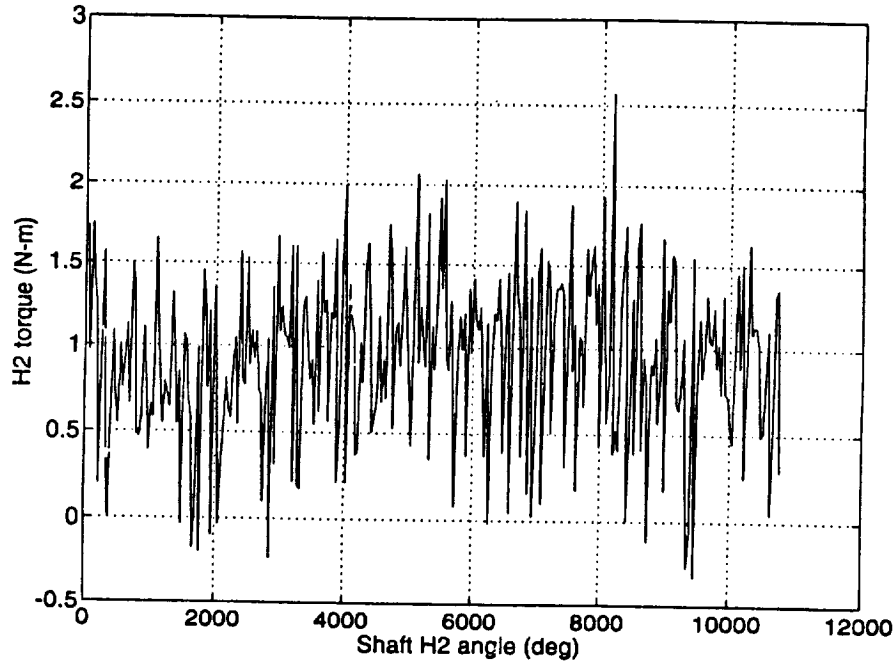


Figure 49. DC-500 H2 cogging torque. L free, H1 fixed.

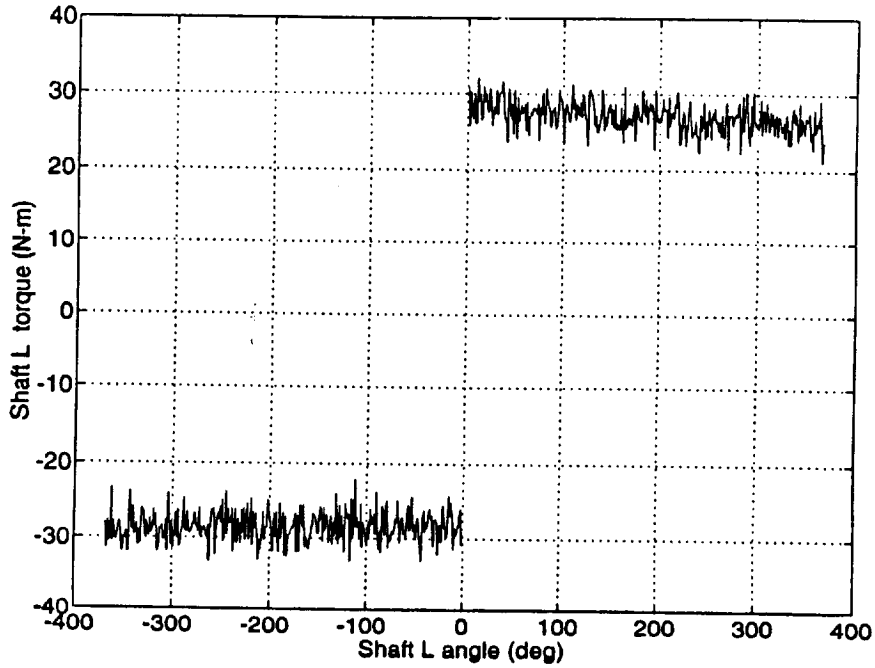


Figure 50. DC-500 shaft L cogging torque. H1 free, H2 fixed.

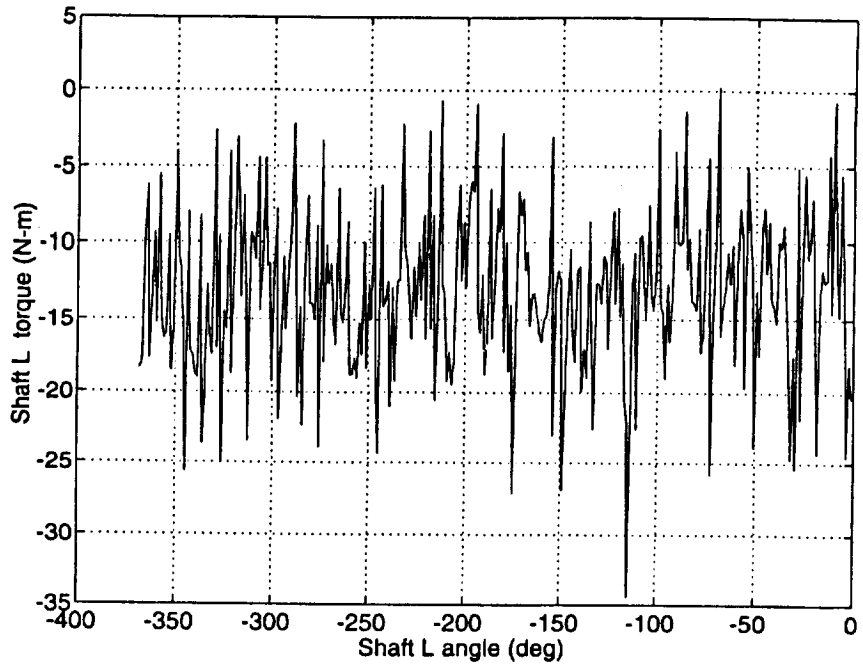


Figure 51. DC-500 shaft L cogging torque. H2 free, H1 fixed.

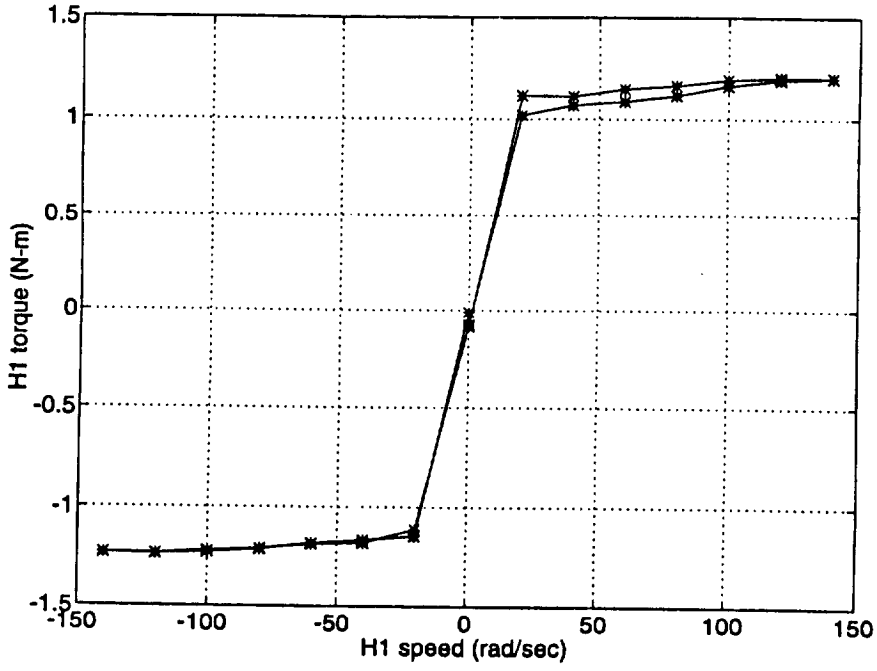


Figure 52. DC-500 friction. H1 driven, L free, H2 fixed.

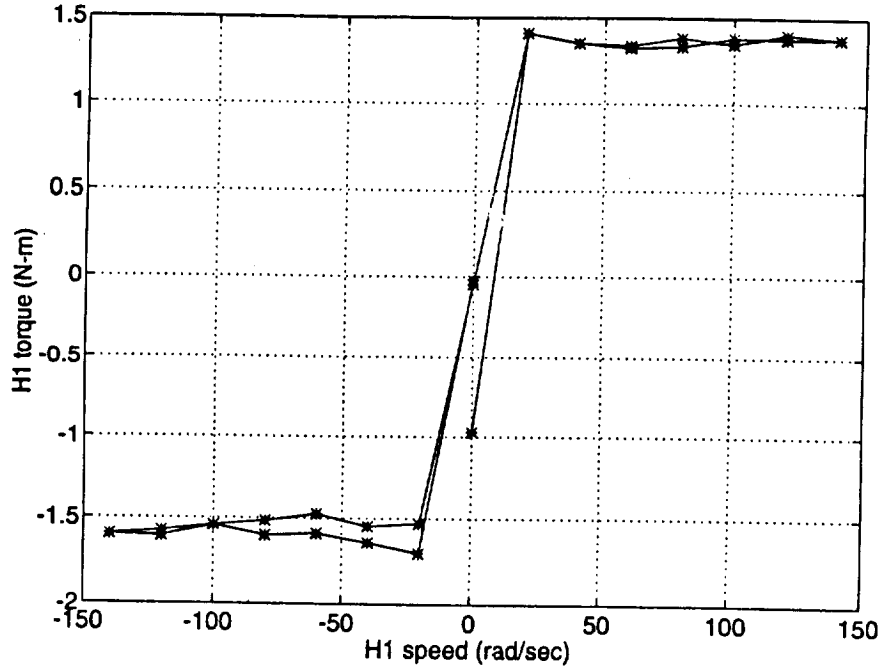


Figure 53. DC-500 friction. H1 driven, H2 free, L fixed.

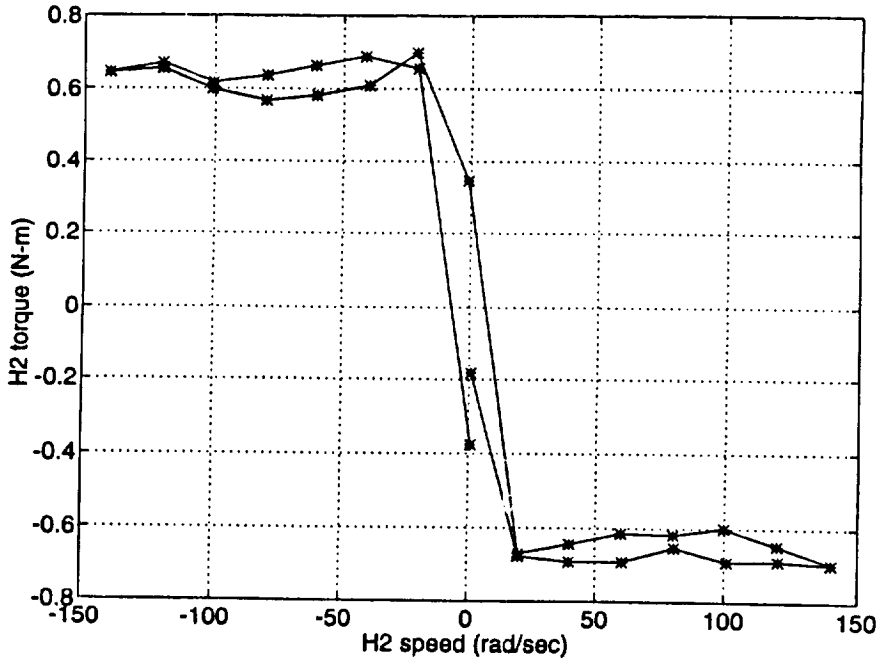


Figure 54. DC-500 friction. H2 driven, L free, H1 fixed.

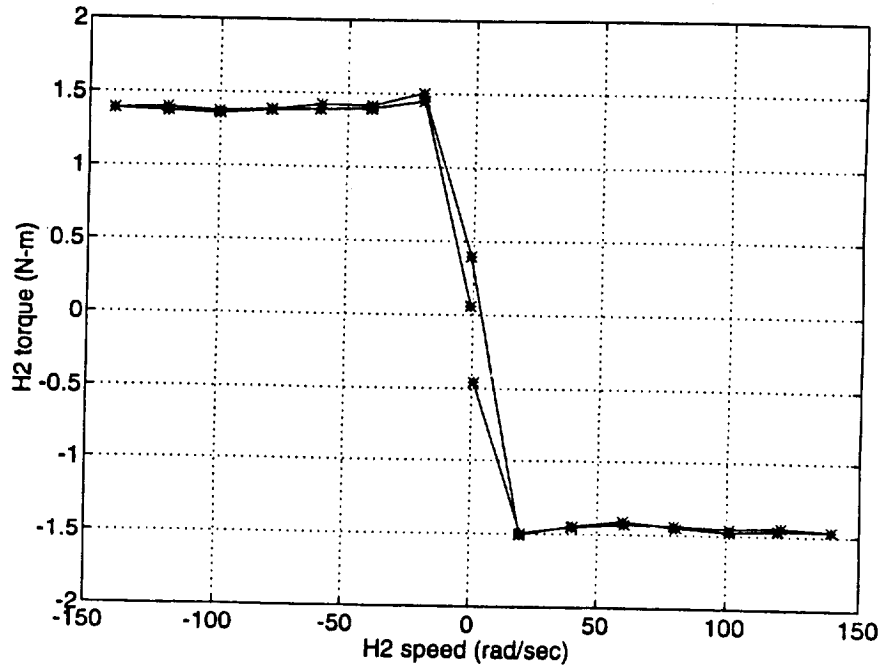


Figure 55. DC-500 friction. H2 driven, H1 free, L fixed.

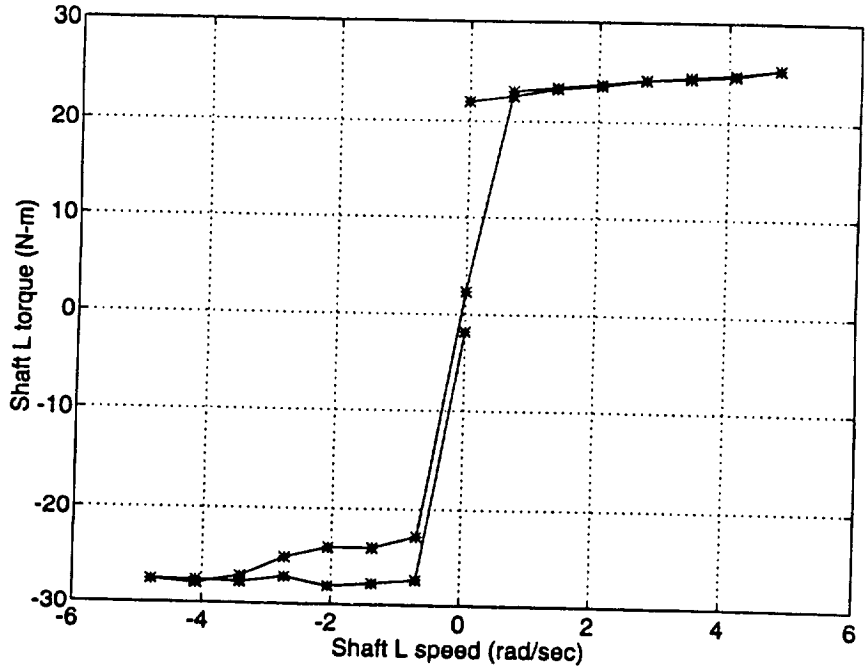


Figure 56. DC-500 friction. L driven, H1 free, H2 fixed.

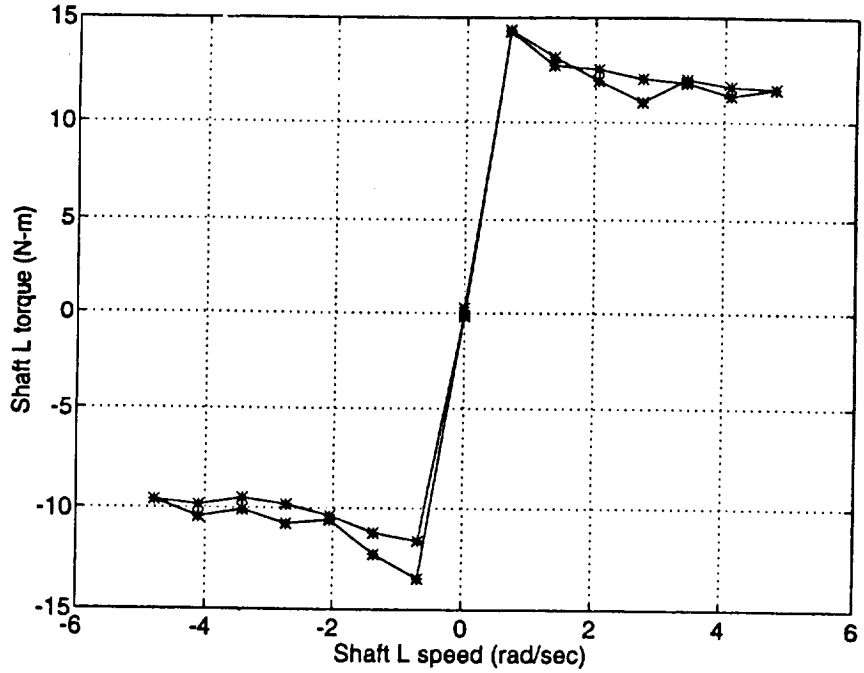


Figure 57. DC-500 friction. L driven, H2 free, H1 fixed.

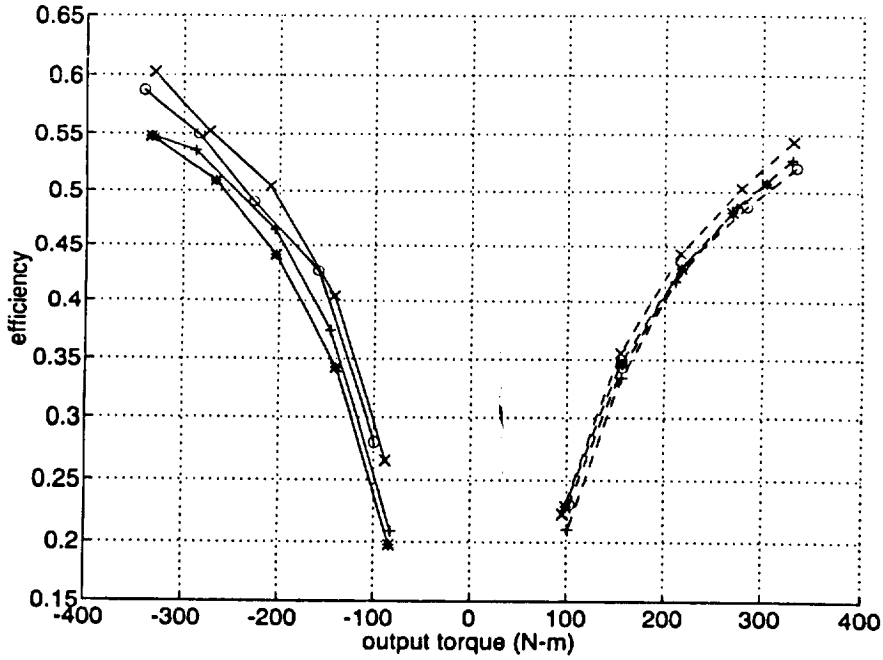


Figure 58. DC-500 efficiency at zero output speed.

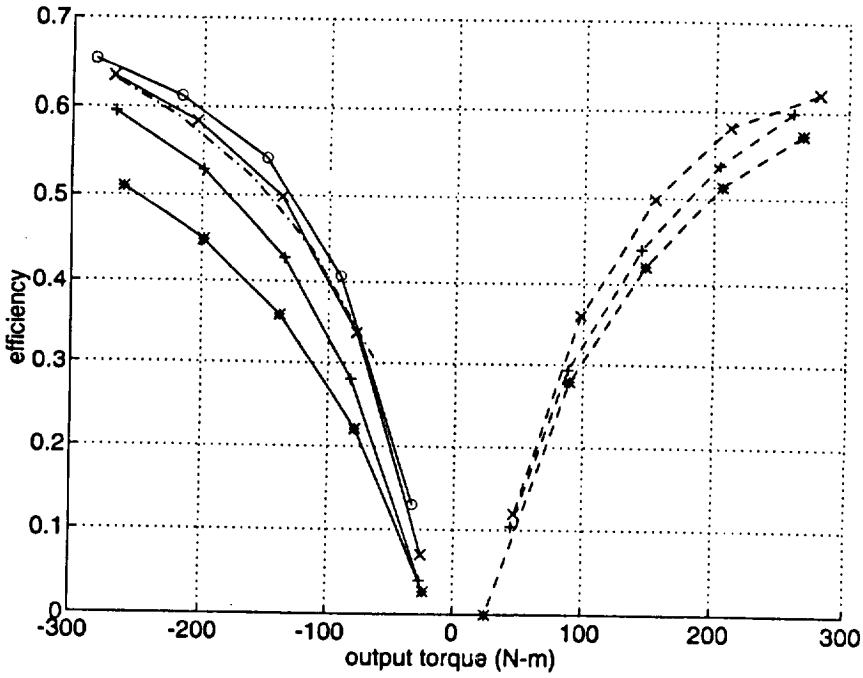


Figure 59. DC-500 efficiency at 1.2 rad/sec output speed (+28.8/R).

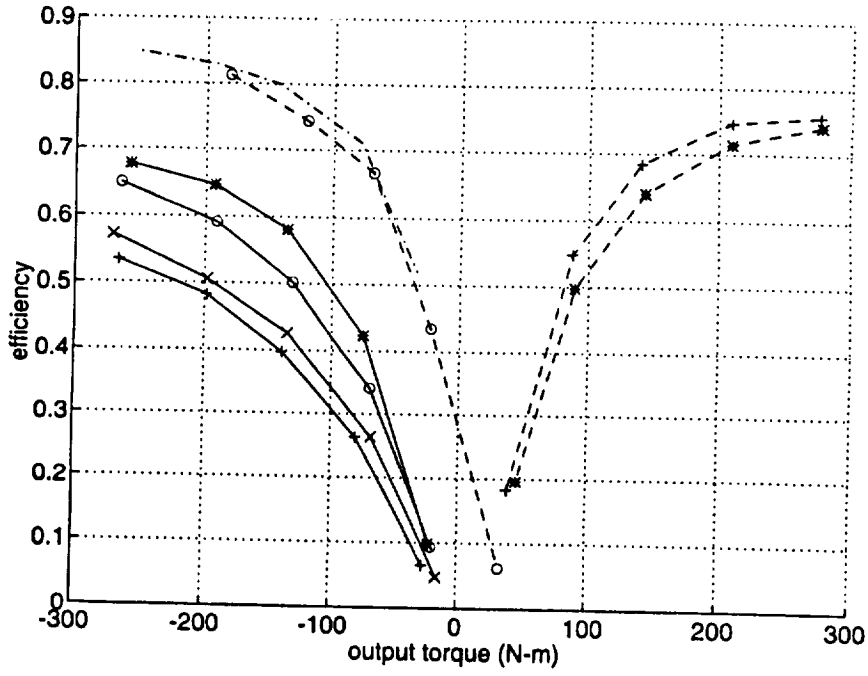


Figure 60. DC-500 efficiency at 2.4 rad/sec output speed (+57.6/R).

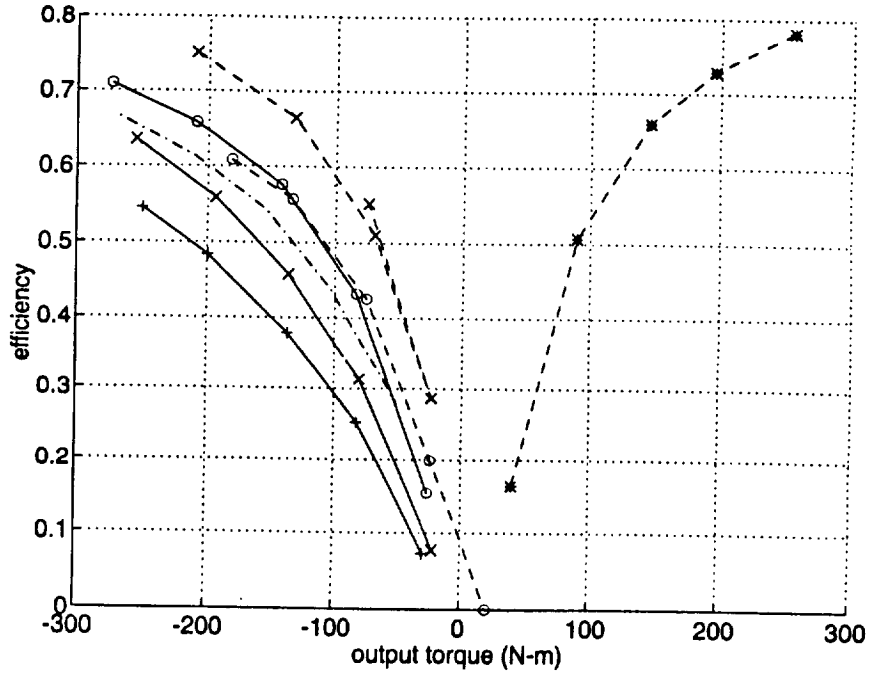


Figure 61. DC-500 efficiency at 3.59 rad/sec output speed (+86.2/R).

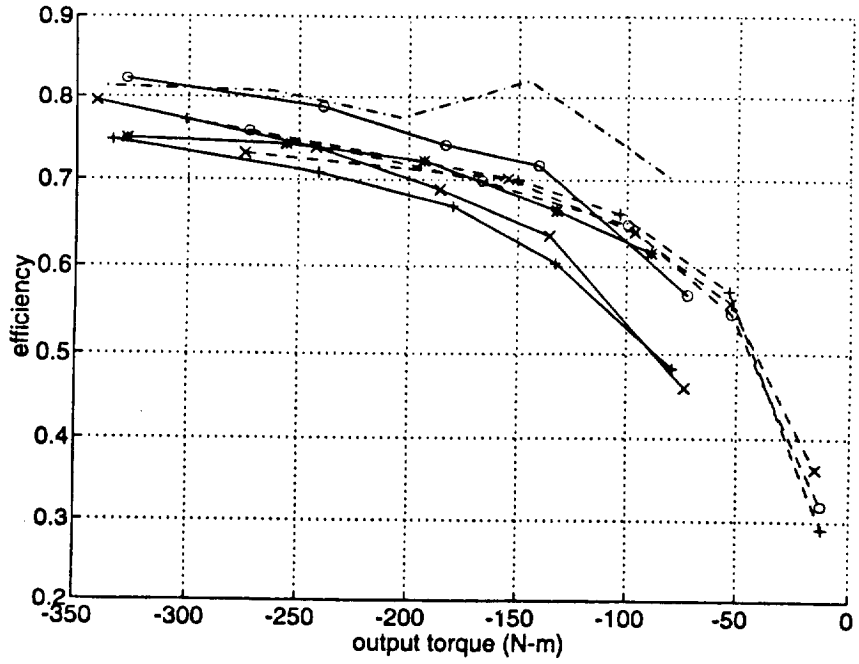


Figure 62. DC-500 efficiency at 4.79 rad/sec output speed (+115/R).

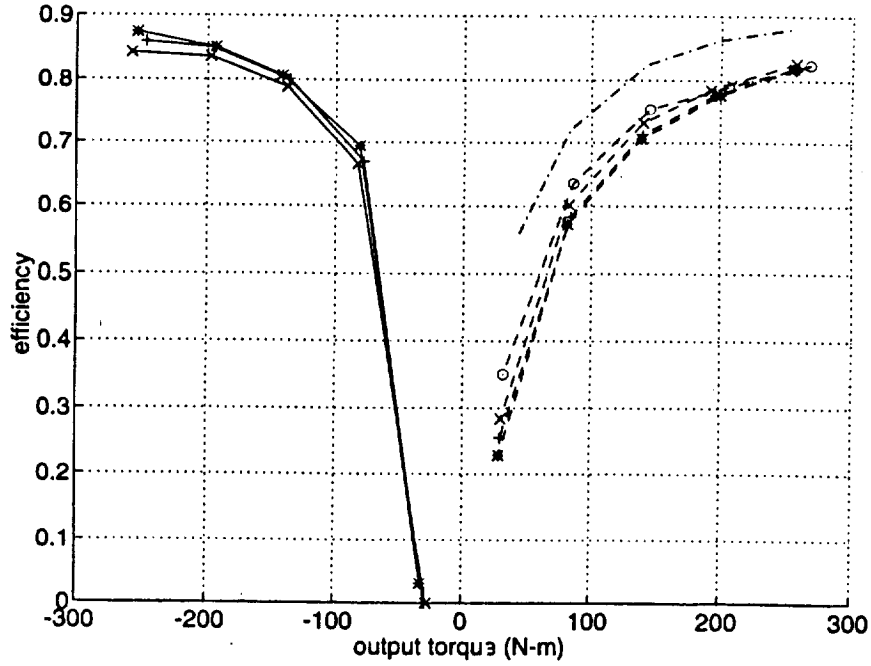


Figure 63. DC-500 efficiency at -1.2 rad/sec output speed (-28.8/R).

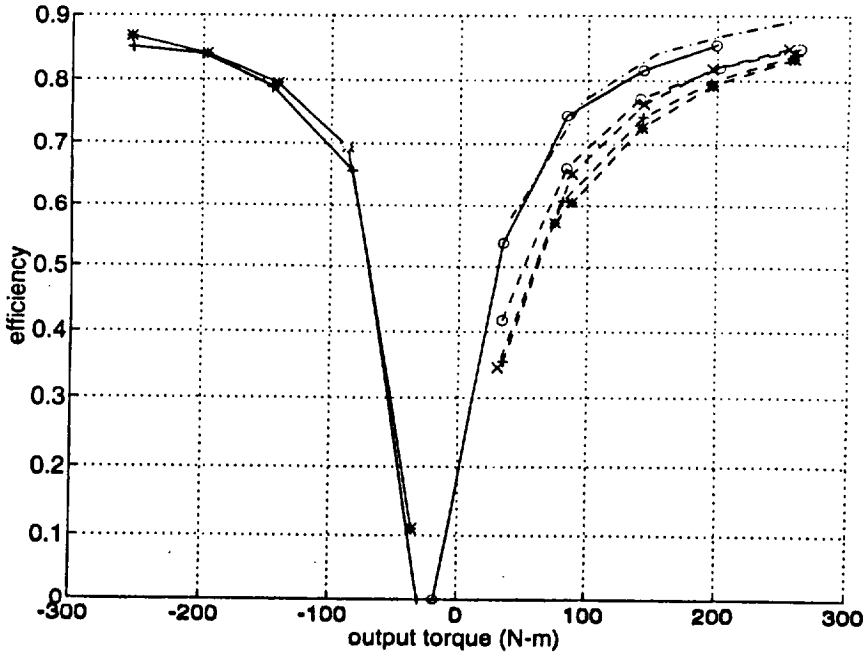


Figure 64. DC-500 efficiency at -2.4 rad/sec output speed (-57.6/R).

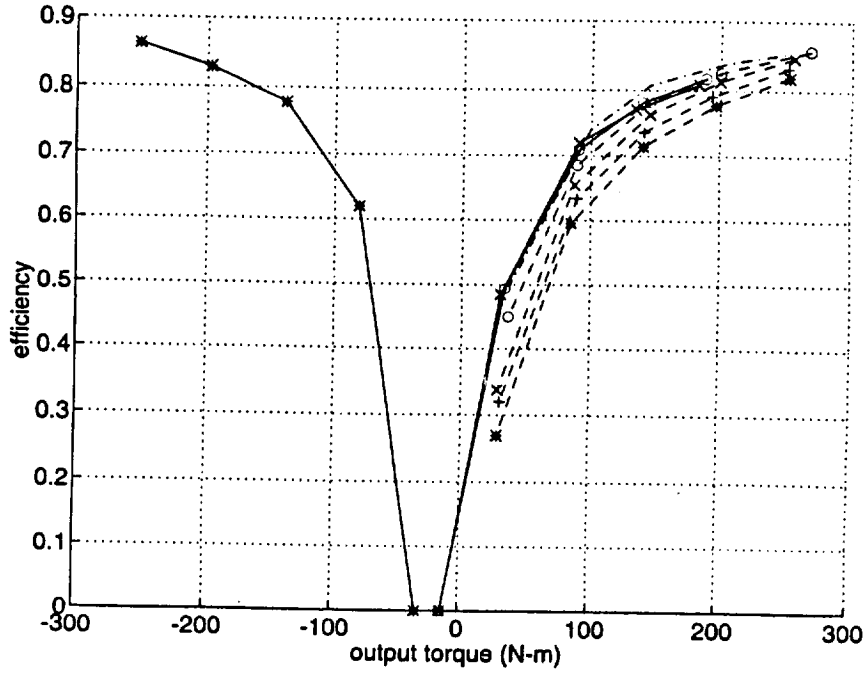


Figure 65. DC-500 efficiency at -3.59 rad/sec output speed (-86.2/R).

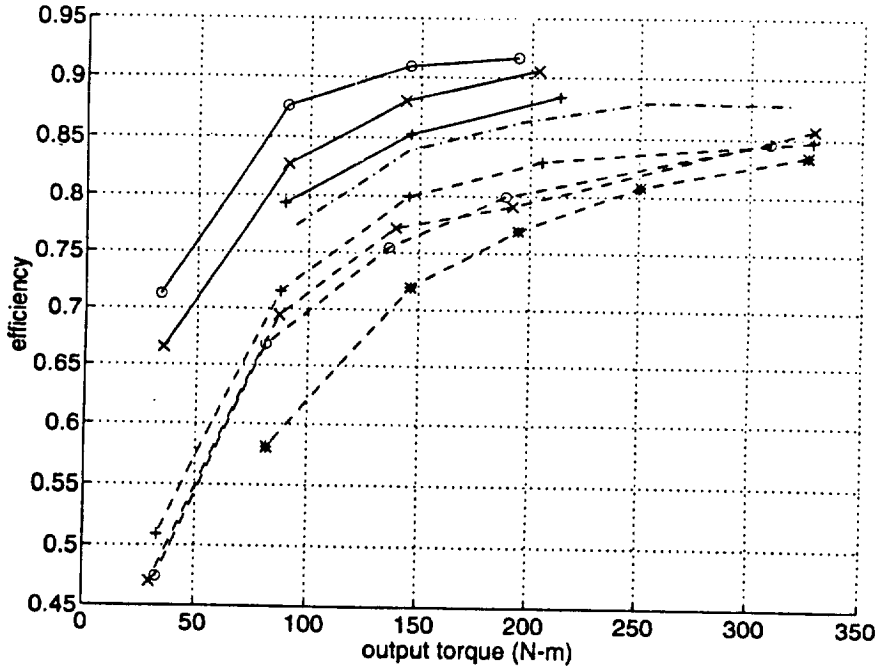


Figure 66. DC-500 efficiency at -4.79 rad/sec output speed (-115/R).

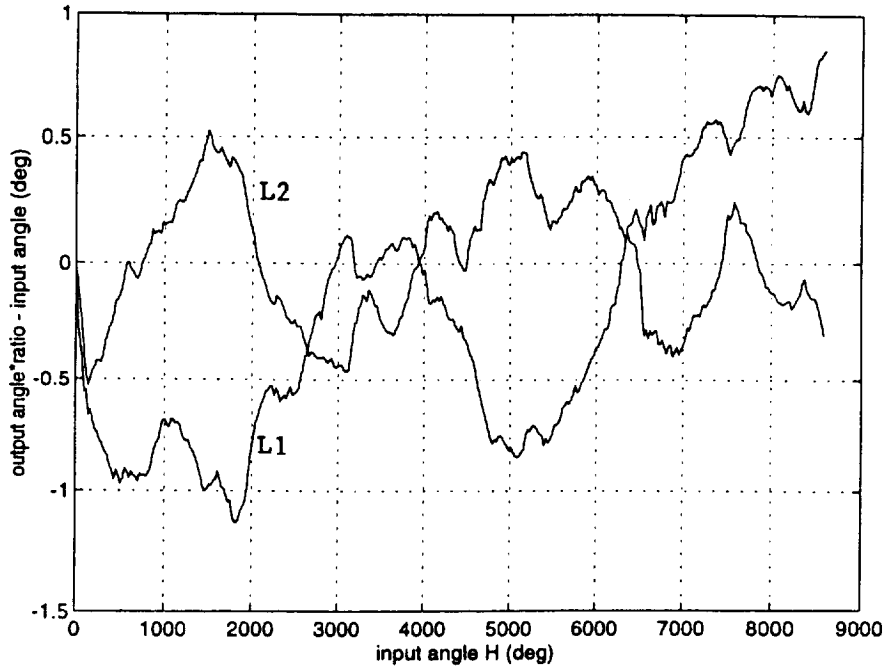


Figure 67. Ratio nonlinearity of DC-400. H=L1*R1; H=L2*R2. R1=23.98 and R2=24.12 (least squares analysis).

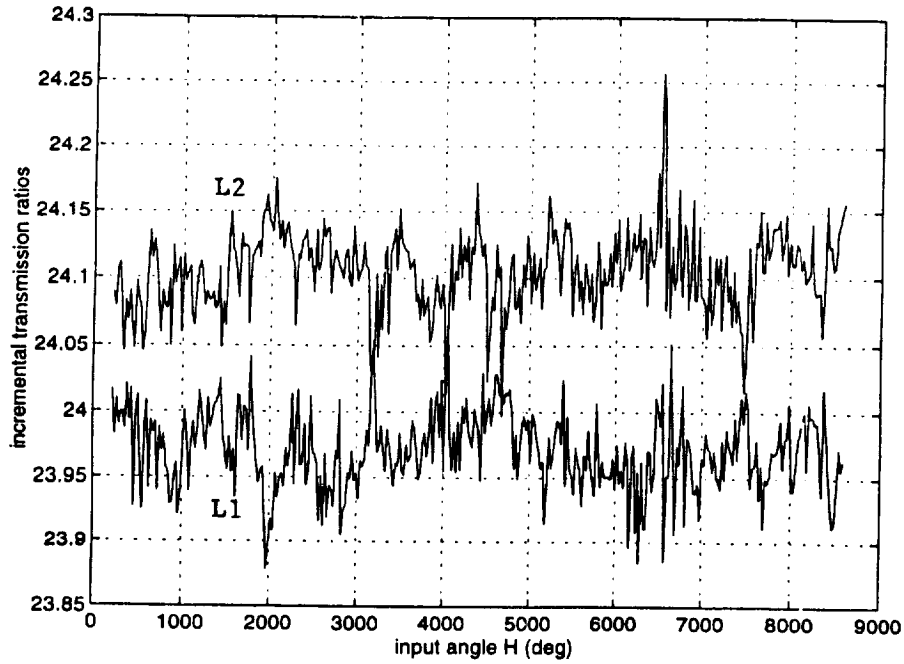


Figure 68. Linearity test of DC-400. H driven, L1 and L2 free.

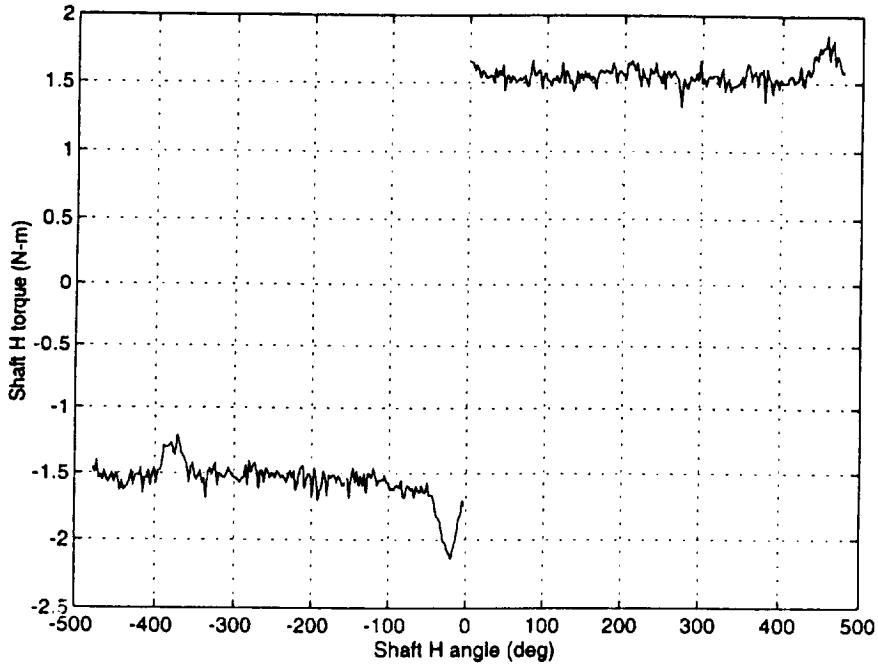


Figure 69. DC-400 shaft H input cogging torque. H driven,L1 and L2 free.

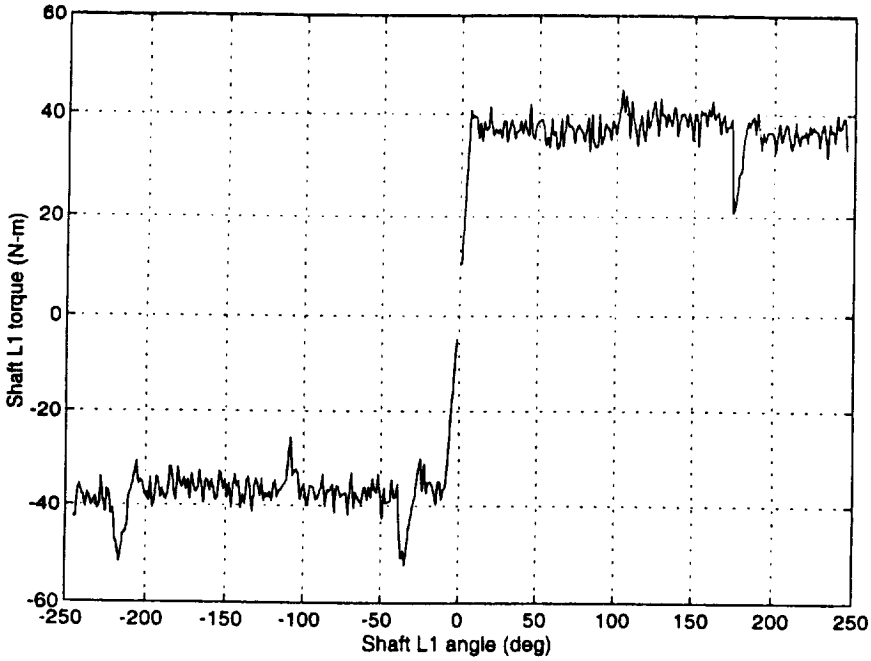


Figure 70. DC-400 shaft L1 input cogging torque. L1 driven, H and L2 free.

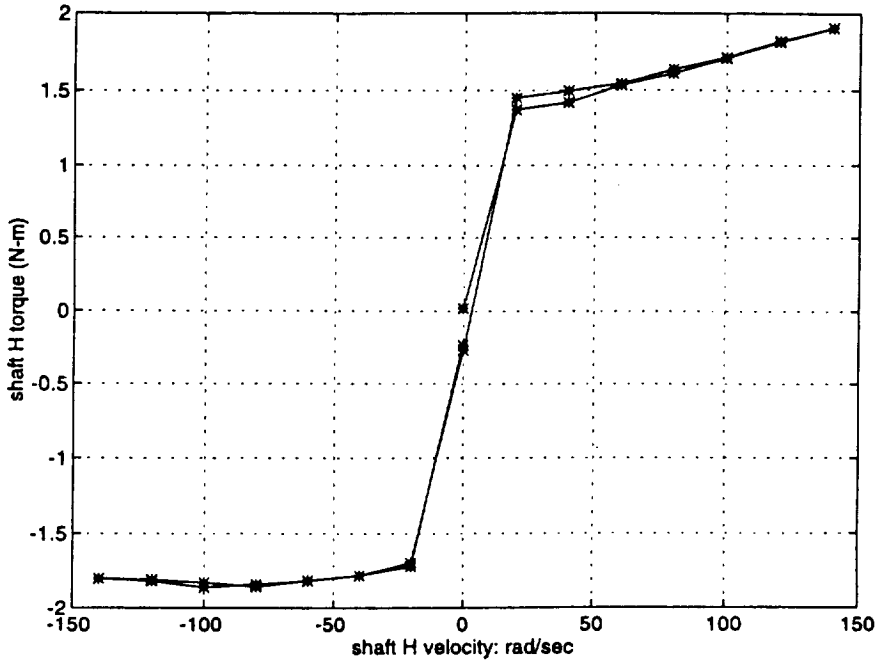


Figure 71. DC-400 unloaded drive friction. H driven, L1 and L2 free.

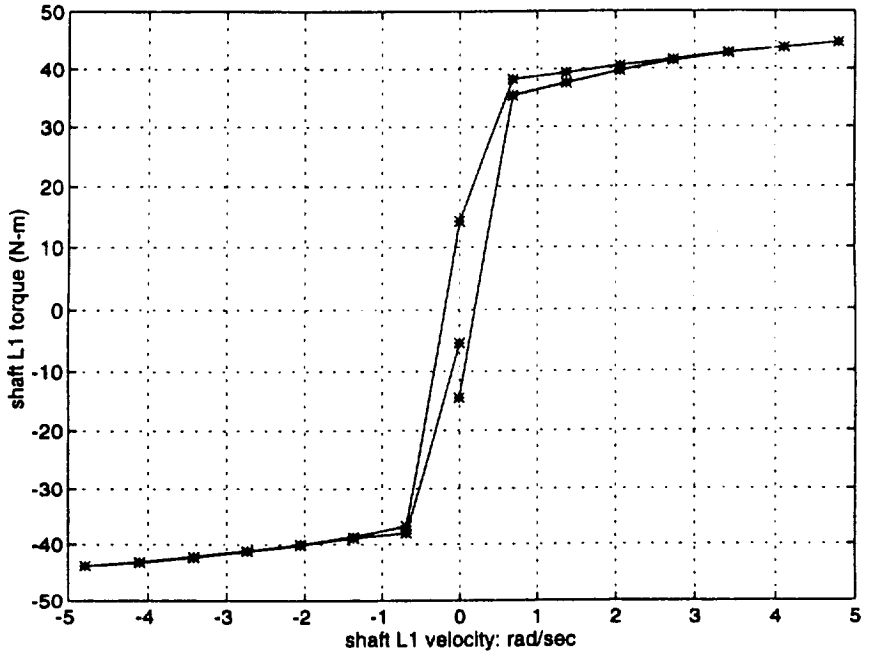


Figure 72. DC-400 unloaded drive friction. L1 driven, L2 and H free.

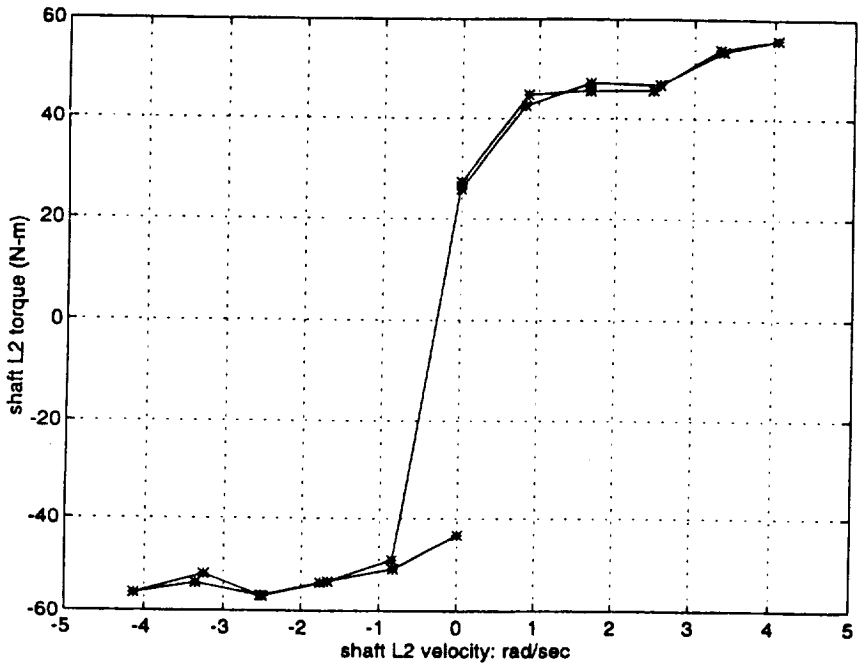


Figure 73. DC-400 unloaded drive friction. L2 driven, H and L1 free.

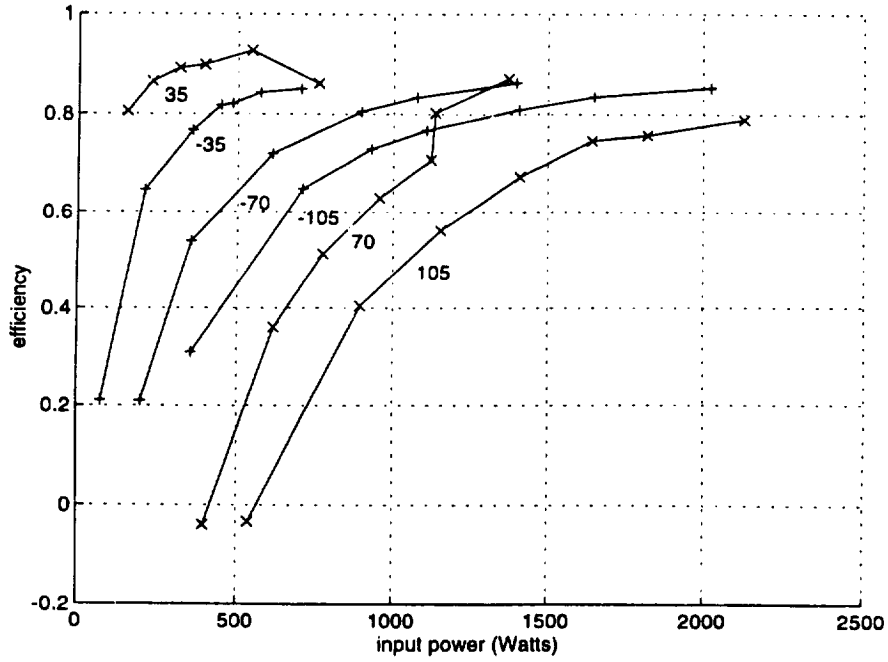


Figure 74. DC-400 reverse efficiency (power input to L1 and L2, power out of H. Velocities indicated in rad/sec.

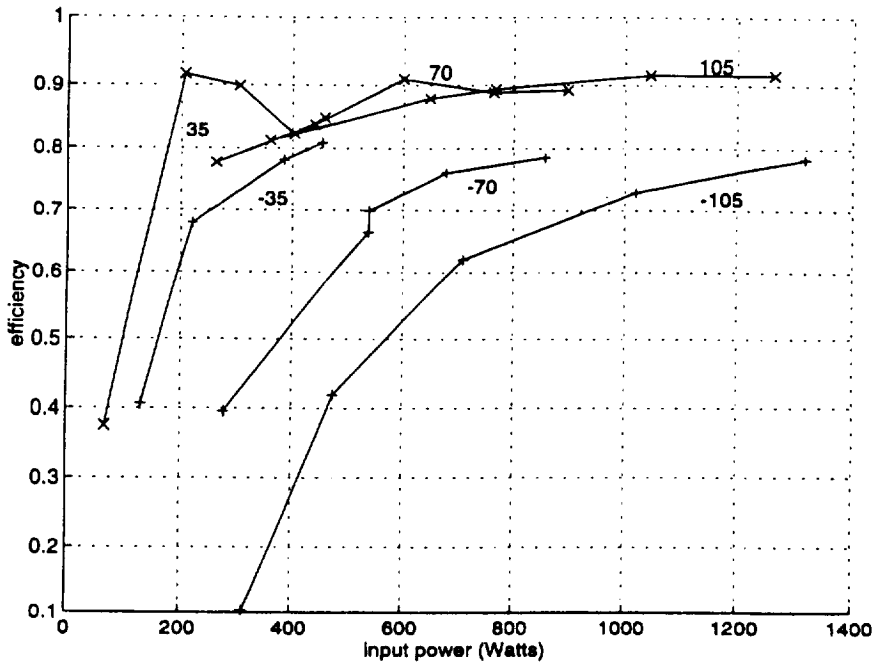


Figure 75. DC-400 forward efficiency (power input to H, power out of L1 and L2).Velocities indicated in rad/sec

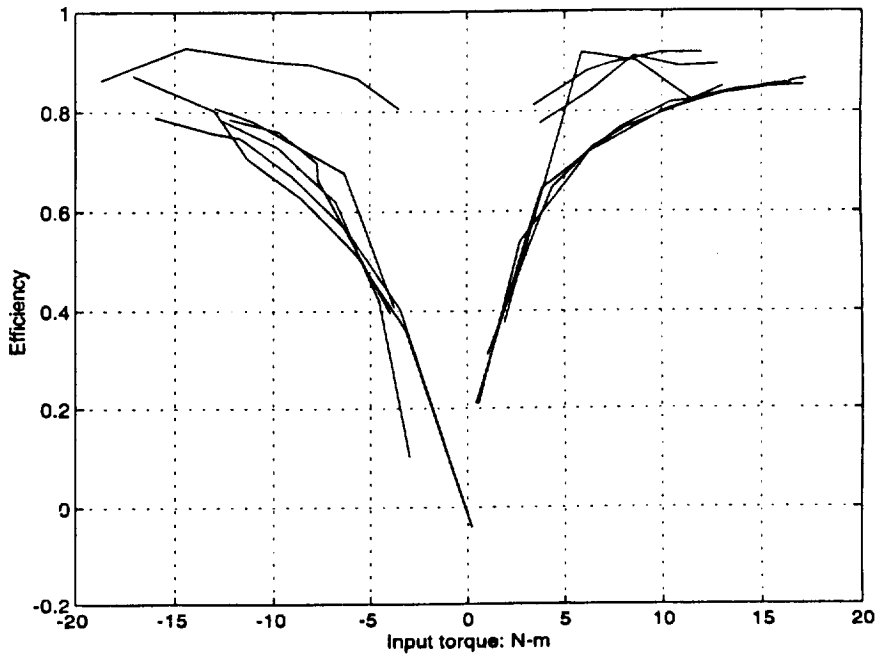


Figure 76. DC-400 efficiency as a function of input torque (forward and reverse operation, with three bidirectional input speeds). Data from figures 74 and 75.

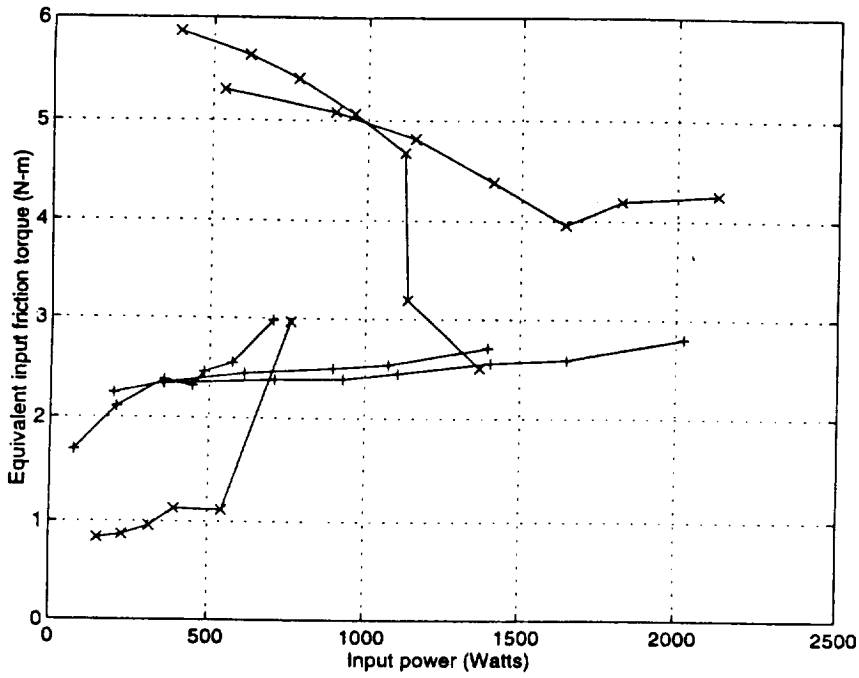


Figure 77. DC-400 shaft H input friction torque loss as a function of input power. (Computed from reverse efficiency data).

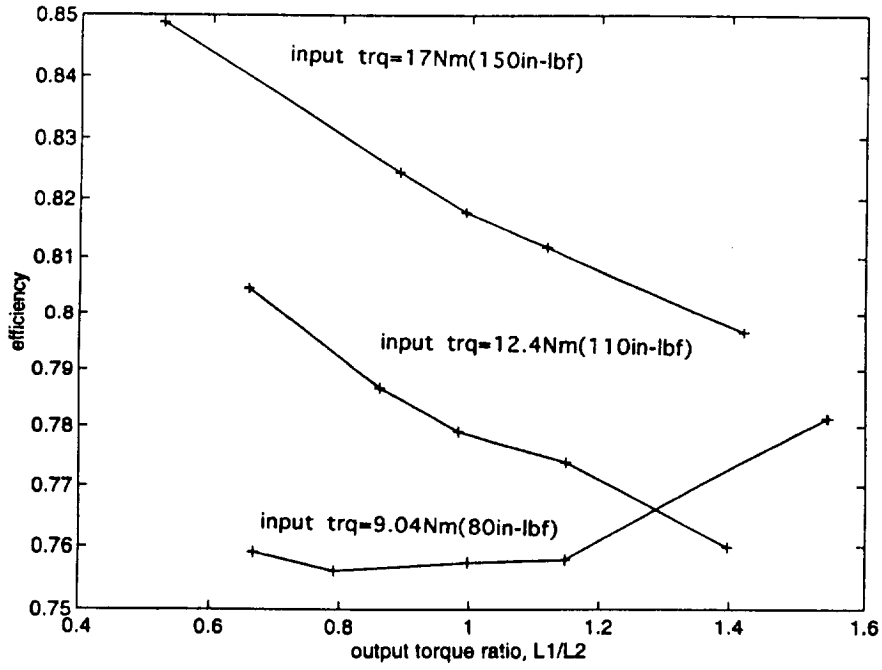


Figure 78. DC-400 reverse efficiency as a function of output torque ratio $T_{L1}/T_{L2}$. Shaft H speed, -105 rad/sec.

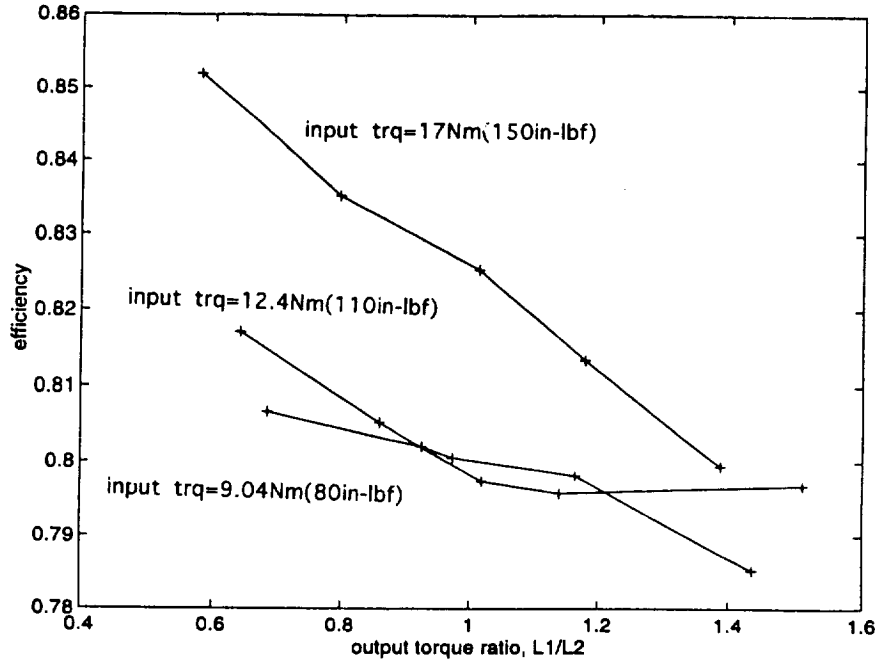


Figure 79. DC-400 reverse efficiency as a function of output torque ratio $T_{L1}/T_{L2}$. Shaft H speed, -70rad/sec.

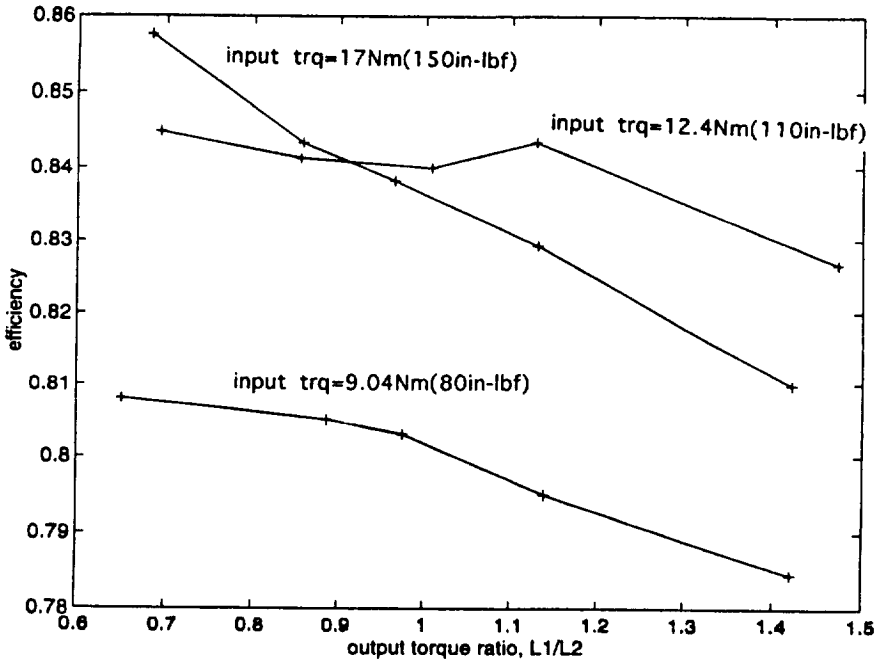


Figure 80. DC-400 reverse efficiency as a function of output torque ratio $T_{L1}/T_{L2}$. Shaft H speed, -35 rad/sec.

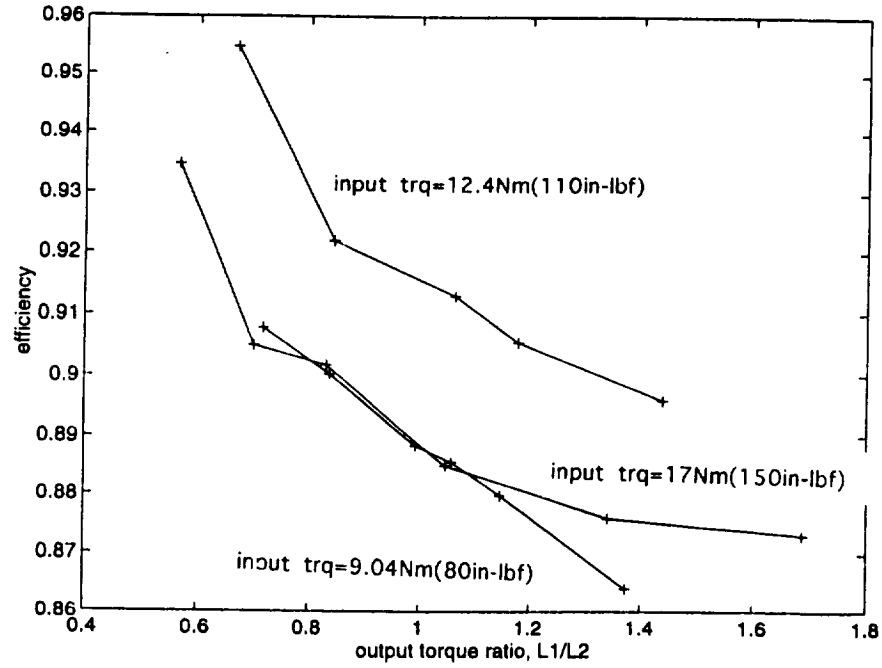


Figure 81. DC-400 reverse efficiency as a function of output torque ratio $T_{L1}/T_{L2}$. Shaft H speed, +35 rad/sec.

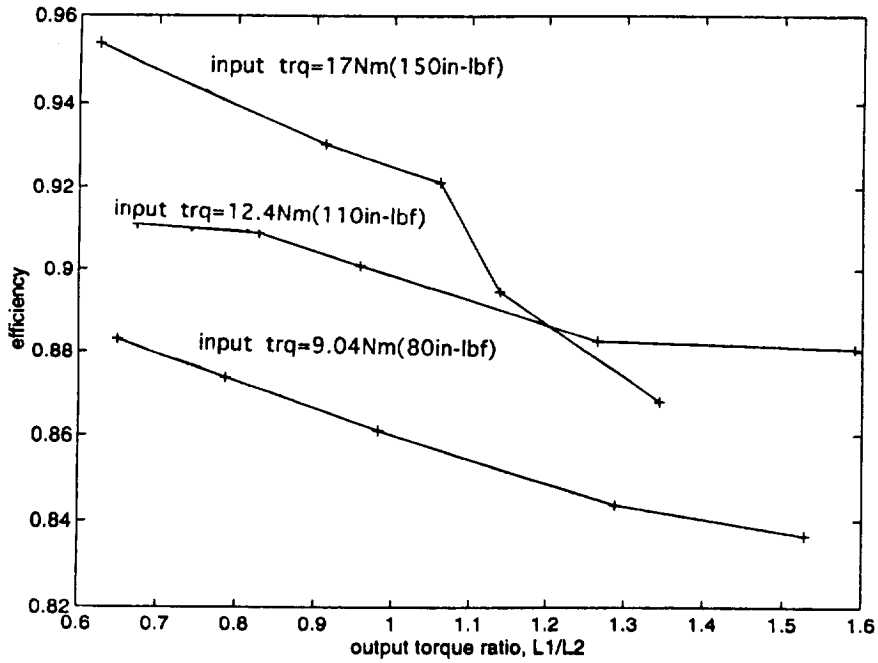


Figure 82. DC-400 reverse efficiency as a function of output torque ratio $T_{L1}/T_{L2}$. Shaft H speed,+70 rad/sec.

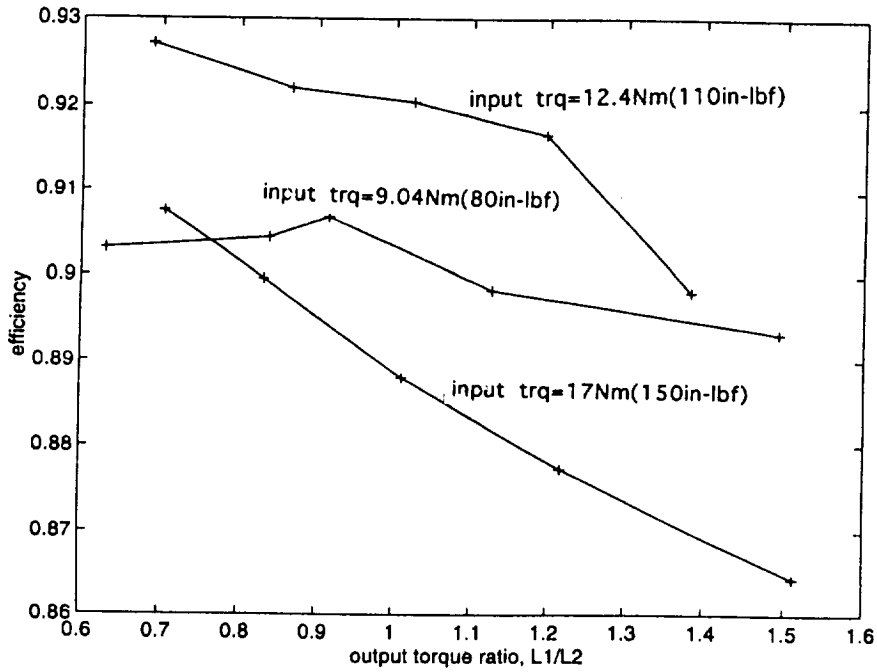


Figure 83. DC-400 reverse efficiency as a function of output torque ratio $T_{L1}/T_{L2}$. Shaft H speed, +105 rad/sec.

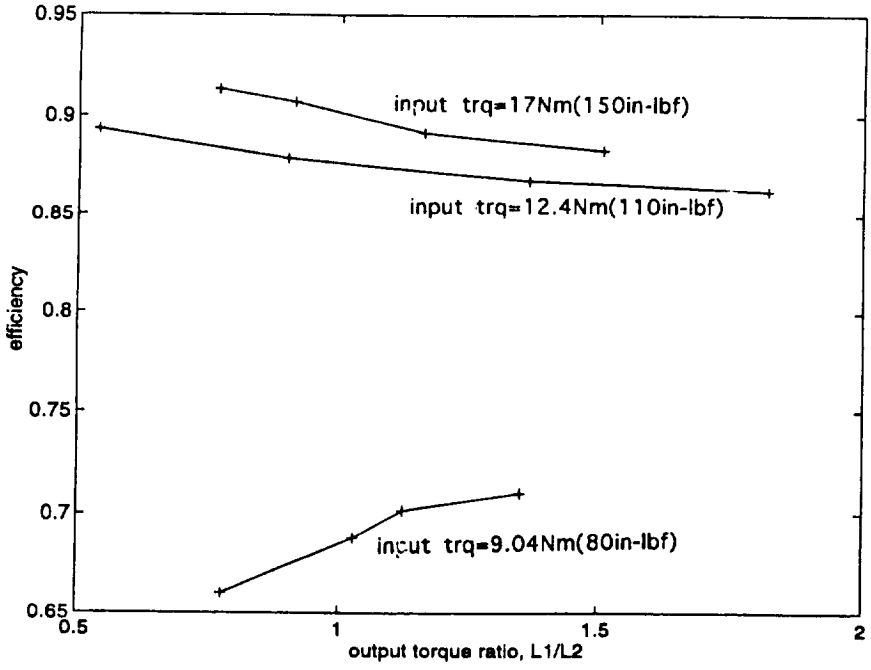


Figure 84. DC-400 forward efficiency as a function of output torque ratio $T_{L1}/T_{L2}$. Shaft H velocity, +35 rad/sec.

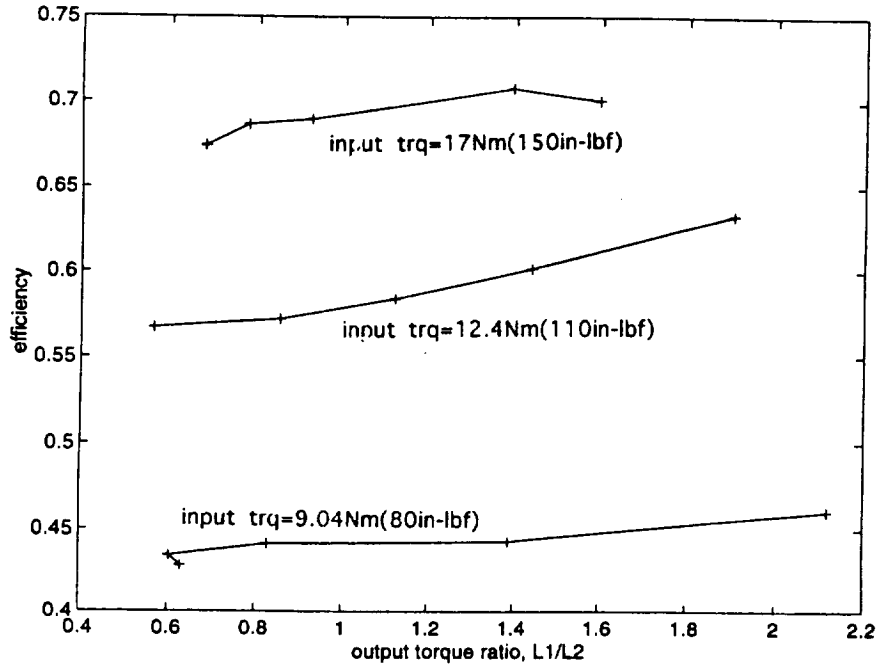


Figure 85. DC-400 forward efficiency as a function of output torque ratio $T_{L1}/T_{L2}$. Shaft H speed, +70 rad/sec.

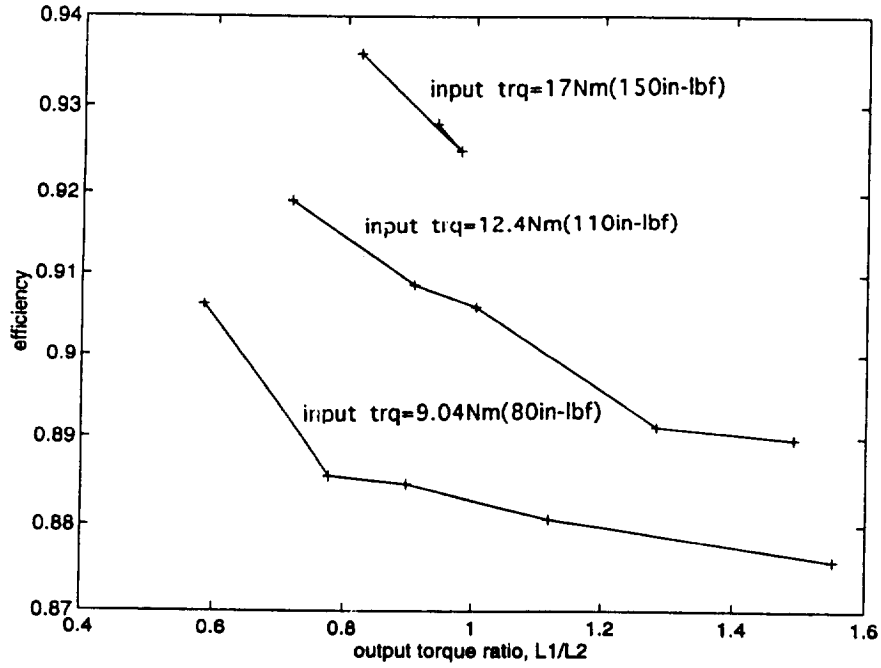


Figure 86. DC-400 forward efficiency as a function of output torque ratio $T_{L1}/T_{L2}$. Shaft H speed, +105 rad/sec.

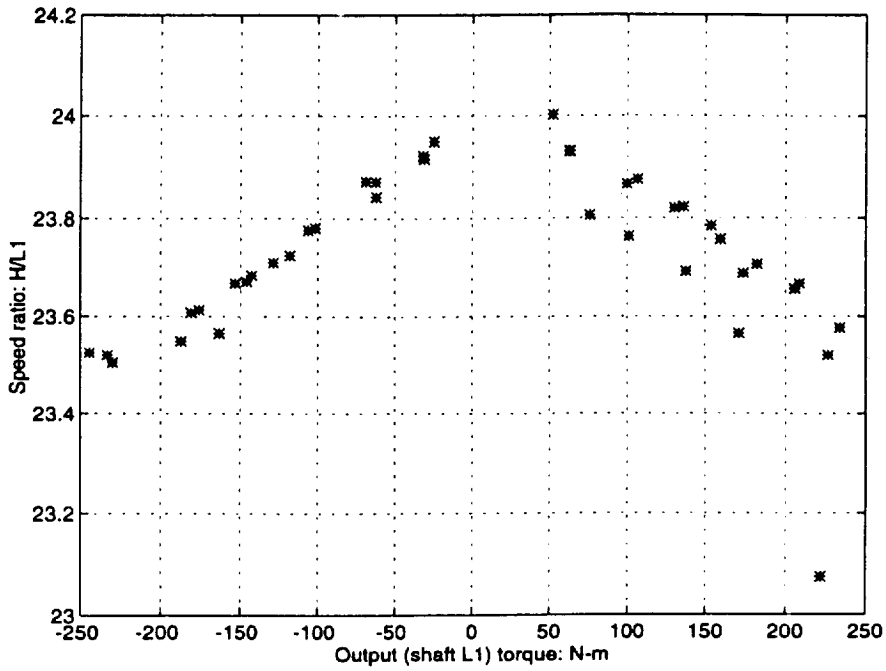


Figure 87. DC-400 speed ratio H/L1 as a function of shaft L1 torque. (Reverse operation as a speed increaser).

# APPENDICES

## APPENDIX A

### DUAL INPUT DIFFERENTIAL ROLLER-GEAR DRIVE (DC-700) GEAR DATA

#### Cluster Geometry

A cluster geometry that provides easy retrofittability into the Dual Input Differential Roller Drive (DC-500) housing with a sun roller amenable to a hollow design with a pass through quill shaft was sought. The geometry of the Hinge Joint Drive of [5] was suitable. To review briefly, the solution from [4]:

$\alpha = 18^o$ $\gamma = 27^o$

(2/5) $N_{y1}$ = integral number $N_{y1} = 20$ teeth

(3/20) $N_{x2}$ = integral number $N_{x2} = 100$ teeth

Selecting

$a + x_1 = 1.390in(35.306mm)$ $N_a = 28$ teeth (divisible by 4)

$N_{x1} = 62$ teeth $x_1/a = 62/28 = 2.2142in$ (56.243mm)

$x_1 = 2.2143in(56.243mm)$ $a = 1.390/3.2143 = .4324in$ (10.983mm)

$x_1 = .9576in(24.322mm)$

Operating P.D. $a = .8649in(21.969mm)$ $x_1 = 1.9151in(48.644mm)$

Selecting a cutter with P = 32 (20° pressure angle)

Max. permissible $x_1$ OD = 1.9151 + 2(.0188) = 1.9526in(49.596mm)

Clearance = 1.9658 - 1.9526 = .0132in(.3353mm)

From eq. (1): (All equations taken from [2] )

$(y_1 + x_2)/(a + x_1) = (\sin 45^o/\sin 27^o) = 1.5575in(39.561mm)$

$y_1 + x_2 = 2.1650in(54.991mm)$ $x_2/y_1 = 100/20 = 5$

$y_1 = .3608in(9.164mm)$ $x_2 = 1.8041in(45.824mm)$

Operating P.D. $y_1 = (.3608)(2) = .7217in(18.330mm)$

Operating P.D. $x_2 = (1.8041)(2) = 3.6083in(91.650mm)$

Selecting a cutter with P = 28 (20° pressure angle)

Cutting P.D. $y_1 = 20/28 = .7143in(18.143mm)$ $x_2 = 100/28 = .3.5714in$ (90.714mm)

From eq. (2):

$$z = ((y_1 + x_2)\sin(90^o + \alpha))/\sin\theta = 2.9119in(73.962mm)$$

Selecting $N_c = 264$ (divisible by 4)

Cutting P.D. $c = 264/28 = 9.4286in(239.486mm)$

$c/x_2 = 264/100 = 2.64$ $c - x_2 = 2.9119in(73.962mm)$

$x_2 = 1.7755in(45.099mm)$ $c = 4.6874in(119.061mm)$

Operating P.D. $x_2$ with c gear = 3.5511in(90.197mm)

Operating P.D. c with $x_2$ gear = 9.3749in(238.121mm)

Ratio = (62/28)(264/20) = 29.23

Gear Stresses (Methods of [6])

Since diametral pitches are in English units, stresses are calculated in English units and converted into SI units.

Max. input torque to each sun roller = 15.485Nm(137inlbf)

$ax_1$ contacts (4 contacts)

$F_T$ = (137/4)(1/.4324) = 79.2lb(352.48N)
with face width f = .312in(7.925mm), P = 32, and y = .344

Bending stress, $S_B = F_T P/fy$

$S_B$ = (79.2)(32)/(.312)(.344) = 23,600psi($162.8x10^6$Pa)

$m_G$ = 62/28 = 2.214 $(m_G + 1)/m_G = 1.45$

Compressive stress, $S_c = 5715[(F_T)(m_G + 1)/(m_G)(2af)]^{1/2}$

$S_c = 5715[(F_T)(1.45)/(2)(.4324)(.312)]^{1/2}$ = 118,500psi($817x10^6$Pa)

$y_1x_2$ contacts (8 contacts)

Torque = (137)(2.214)(1/4) = 75.8inlbf(8.57Nm)

$F_T$ = (75.8/2)(1/.361) = 105.1lb(467.5N)

Selecting 14.22mm(.56in) face width, P = 28, and y = .33

$S_B$ = (105.1)(28)/(.56)(.33) = 15,900psi($109.6x10^6$Pa)

$m_G$ = 100/20 = 5 $(m_G + 1)/m_G = 1.2$

K = (105.1)(1.2)/(2)(.361)(.56) = 312

$S_c = 5715[312]^{1/2}$ = 101,000psi($696x10^6$Pa)

$x_2$c contacts (4 contacts)

Torque = 4000inlbf(452Nm)

$F_T$ = (4000/4)(1/4.687) = 214lb(950N)

Selecting 14.22mm(.56in) face width (gear $x_2$), P = 28, and y = .38

$S_B = (214)(28)/(.56)(.38) = 28{,}100\text{psi}(194\text{x}10^6\text{Pa})$ in $x_2$

Selecting 15.24mm(.60in) face width (gear c), P = 28, and y = .38

$S_B = (214)(28)/(.60)(.38) = 26{,}200\text{psi}(181\text{x}10^6\text{Pa})$ in c

$m_G = 264/100 = 2.64$ $\qquad (m_G - 1)/m_G = .62$

$K = (214)(.62)/(2)(1.7755)(.56) = 66.4$

$S_c = 5715[66.4]^{1/2} = 46{,}700\text{psi}(322\text{x}10^6\text{Pa})$

With these levels of $S_B$ and $S_c$, all gears can be 4340 or 8620 steel or equivalent. Gears need not have hardened faces.

## APPENDIX B

### DUAL INPUT DIFFERENTIAL ROLLER-GEAR DRIVE (DC-700)

#### Sun Roller-Gear Design

Output Side

Input torque to each sun roller-gear = 15.485Nm (137inlbf)

Select an input spline:

11 teeth, 30° flat root side fit, 32/64 Pitch

P.D. = 8.731mm (.34375in)

Effective length, L = 9.52mm (.375in)

Tooth stress:

$$S = 2T/D^2L$$

$$S = (2)(15.485)/(.008731)^2(.00952)$$

$$S = 42.67 \times 10^6 Pa \ (6{,}187psi)$$

Stress level is OK with high strength steel and $R_C60$ tooth hardness.

Spline Data

| Internal Spline | External Spline |
|---|---|
| Major dia. = 9.9mm (.390in) max | Major dia. = 9.525/9.474mm (.375/.373in) |
| Minor dia = 8.052/8.179mm (.317/.322in) | Minor dia. = 7.34mm (.289in) min. |
| Form dia. = 9.627mm (.379in) | Form dia. = 7.925mm (.312in) |

This meets ANSI B 92.1 1970 standards.

Quill Shaft stress:

$$S_S = TC/J$$

$$C = 9.52/2 = 4.76mm \ (.1865in)$$

$$J = \pi d^4/32$$

$$J = \pi(.00476)^4/32 = 5.03977 \times 10^{-11} m^4 \ (.0019in^4)$$

$$S_S = 92.75 \times 10^6 Pa \ (13{,}450psi)$$

This is acceptable.

Shrink ring stresses for sun roller:

Roller width = 5.969mm (.235in)

Roller OD = 21.9837/21.9786mm (.8655/.8653in)

Shaft OD = 13.9229/13.9878mm (.5509/.5507in)

Roller ID = 13.970/13.9751mm (.5500/.5502in)

Min. dia. interference = .0127mm (.0005in)

Max. dia. interference = .02286mm (.0009in)

Max. ID Shear Stress = $E\delta d/4r$

$= (206.9)(.00002286)/(4)(.00699)$

$= .169GPa$ (24,500psi)

Min. fit pressure = $E\delta d(r_o^2-r_i^2)/4r_o^2a$

$= (206.9)(.01099^2-.00699^2)/4(.01099)^2(.00699)$

$= .056GPa$ (8,130psi)

Max. fit pressure = $(.056)(.02286)/(.0127)$

$= .101GPa$ (14,630psi)

Holding power (coefficient of friction = 0.1)

$HP = \pi r_i wpf$

$= \pi\ (.00699)(.005969)(.056)(.1)x10^9$

= 1,460N (328lb)

Min. torque trans. capability = $(HP)(r_i)$

$= (1,460)(.00699)$

= 10.2Nm (90.2inlbf)

Req'd. torque to be trans. = $(15.485/2)(.2)$

= 1.549Nm (13.7inlbf)

M-50 tool steel will be used for the rollers. If they are preheated to 600°F the bore expansion $\delta r$ will be

$\delta r = (6.3x10^{-6})(.00699)(600-70)(1000)$

$= .04572mm$ (.0018in)

This will be adequate for assembly.

Torsional stiffness of roller-gear and quill shaft

Angle of twist:

$\theta = Tl/GJ$

Torsional stiffness

$K_\theta = T/\theta$ Nm/rad (inlbf/rad)

$K_\theta = GJ/l$

For a series of shaft elements:

$$K_\theta = G / \sum_{i=1}^{n} l_i / J_i$$

Refer to Figure 2(b) and (c) for key dimensions

$$K_\theta = G/((.114)/(\pi/2)(.00952)^2 + (.0533)/(\pi/2)(.0139^2-.00635^2))$$

$= 6.391G$ Nm/rad (G in Giga Pascals)

$= .00039G$ inlb/rad (G in psi)

For steel

$G = 82.76$Giga Pascals

$\theta = T/K_\theta$

$\theta = 15.485/(6.391)(82.76)$

$\theta = .02928$rad

$= 1.68$deg

With an assumed backlash of .0508mm (.002in)

$\theta_b = .0508/11.11$

$\theta_b = .00457$rad

$= .262$deg

The "windup" in the output side sun roller-gear will thus be approximately 6 times the backlash in the sun-first planet mesh. Physically this means that the output speed will momentarily be slightly different from theoretical.

Input side

Select an input spline

17 teeth, 30° flat root side fit, 32/64 pitch

P.D. = 13.494mm (.53125in)

| Internal Spline | External Spline |
|---|---|
| Major dia. = 14.656mm (.577in) max | Major dia. = 13.919/13.868mm (.548/.546in) |
| Minor dia. = 12.725/12.852mm(.501/.506in) | Minor dia. = 12.090mm (.476in) min. |
| Form dia. = 14.402mm (.567in) | Form dia. = 12.598mm (.496in) |

This meets ANS B92.1 1970 spline standards.

Stresses will not be a problem in the spline or the shaft. They are stronger than those of the output side sun roller-gear.

Torsional Stiffness

Refer to Figure 2(a) fro key dimensions

$$K_\theta = G/((.00475)/(\pi/2)(.0121^2-.0099^2) + (.0667)/(\pi/2)(.0139^2-.0099^2))$$

$K_\theta = 34.741G$ Nm/rad (G in Giga Pascals)

$= .00212G$ inlbf/rad (G in psi)

For steel:

$$\theta = 15.485/(43.741)(82.76)$$

$$\theta = .00539\text{rad}$$

$$= .309\text{deg}$$

This is slightly more than the backlash in the sun-first planet mesh. The consequence of unequal torsional stiffnesses is simply that the output speed will not, momentarily, be as predicted theoretically. The torsional stiffness of the input side sun roller-gear could be reduced and made equal to that of the output side sun roller-gear, but there doesn't seem to be any particular advantage to that.

## APPENDIX C

DUAL INPUT DIFFERENTIAL ROLLER-GEAR DRIVE (DC-700)

Assembly Procedure

1) Lay Assembly Fixture, DC-700-37, flat on a table.

2) Using Dykem marking compound or equivalent, mark four equally spaced tooth spaces on the Input Side Sun Roller- Gear Assembly, DC-700-25.

3) Place this Input Side Sun Roller- Gear Assembly on the center post of the Assembly Fixture and insert the shaft extension of the Input Side Sun Roller-Gear Assembly into the center post hole. Orient the four equally spaced tooth spaces to face the four equally spaced holes in the Assembly Fixture.

4) Using the same Dykem marking compound, highlight the indexed tooth relationship on the large central gear of each of four 1st Row Planet Roller-Gear Assemblies, DC-700-14.

5) Radially assemble the four 1st Row Planet Roller-Gear Assemblies to the Input Side Sun Roller- Gear Assembly making sure that each marked index tooth goes into a marked tooth space on the Input Side Sun Roller- Gear Assembly. Index the Assembly Fixture on the table so that an Assembly Pin, DC-700-38, can be inserted onto the shaft extension of each of the 1st Row Planet Roller-Gear Assemblies. This assembled tooth relationship between the four 1st Row Planet Roller-Gear Assemblies and the Input Side Sun Roller- Gear Assembly must be maintained.

6) Press fit two Needle Bearings, item 46, into each of four 2nd Row Planet Gears, DC-700-03.

7) Assemble one 2nd Row Planet Roller, DC-700-01, to each of four 2nd Row Planet Gears, and fasten in place with Hex Head Screws, item 9.

8) On each of four Planet Shafts, DC-700-31, assemble two Bearing Races, DC-700-29, one Planet Shaft Spacer, DC-700-02, and one Planet Shaft Key, DC-700-30.

9) Insert each Planet Shaft assembly into a 2nd Row Planet Roller-Gear assembly with the 2nd Row Planet Roller toward the key end of the Planet Shaft assembly.

10) Radially insert the four Planet Shaft-2nd Row Planet Roller-Gear assemblies into the four slots of the Assembly Fixture. Each Planet Shaft Key must fit into the key slots on the Assembly Fixture. Make certain that gears are properly meshed and that proper roller contact is made.

11) Clamp each Planet Shaft-2nd Row Planet Roller-Gear assembly to the Assembly Fixture with Planet Shaft Nut, item 44.

12) Assemble two Ring Gear Dowels #1, item 7, and two Ring Gear Dowels #2, item

5, to Ring Gear, DC-700-12.

13) Assemble Ring Gear to the 2nd Row Planet Gears.

14) Assemble remaining four 2nd Row Planet Rollers to 2nd Row Planet Gears, and fasten in place with Hex Head Screws, item 9.

15) Assemble two Ring Rollers, DC-700-13, to the Ring Gear and the four 2nd Row Planet Rollers. It may be necessary to heat the Ring Rollers to be able to press them over the 2nd Row Planet Rollers. The Ring Rollers must make proper entry onto the projecting dowel pins.

16) Assemble Ring Gear Adaptor, DC-700-32, to the Roller-Gear cluster, making sure that the dowels are entered. The Ring Gear Adaptor can be bolted and clamped in place with Bolts, item 27, and Nuts, item 30.

17) Press fit Ball Bearing, item 35, into the Planetary Carrier Plate, DC-700-23.

18) Remove the Assembly Fixture from the Roller-Gear assembly by sliding the Fixture Plate from the unclamped Planet Shaft extensions.

19) Assemble the Planetary Carrier Plate assembly to the Planetary Shaft extensions and clamp this assembly with Washers, item 42, and Nuts, item 44. Assemble a Roller-Gear Spacer, DC-700-33, on each of the four Planet Shafts.

20) Lay the Assembly Fixture, DC-700-37, flat on a table.

21) Using Dykem marking compound or equivalent, mark four equally spaced tooth spaces on the Output Side Sun Roller-Gear Assembly, DC-700-20.

22) Insert Assembly Pin, DC-700-39, into the center hole of the Assembly Fixture, and place the Output Side Sun Roller-Gear Assembly (gear end down) on this center post. Orient the Output Side Sun Roller-Gear Assembly so that the four equally spaced tooth spaces face the four equally spaced holes in the Assembly Fixture.

23) Repeat steps 4,5,6, and 7.

24) On each of four Assembly Pins, DC-700-40, assemble two Bearing Races, DC-700-29, one Planet Shaft Spacer, DC-700-02, and one Planet Shaft Key, DC-700-30.

25) Repeat steps 9,10,11,12,13,14, and 15, noting that Assembly Pins, DC-700-40, are being used in place of Planet Shafts, DC-700-31.

26) Assemble Output Ring Gear Adaptor, DC-700-06, to the Roller-Gear cluster. making sure that the dowels are entered.This adaptor can be bolted in place with Bolts, item 27, and Nuts, item 30.

27) Place this fixture and roller-gear assembly on top of the four projecting planetary shafts of the previously assembled roller-gear assembly. Make certain that these planetary shaft extensions engage the bearing races correctly, and while applying a little downward pressure the assembly fixture and its pins will be axially displaced.

28) After press fitting Ball Bearing, item 35, into Planetary Support Ring, DC-700-04,

complete the Roller-Gear assembly by placing Washers, DC-700-34, on the planetary shaft extensions along with the Planetary Support Ring, and clamping in place with Nuts, item 44.

29) Into the Input Seal & Bearing Carrier, DC-700-28, press fit Seal, item 39, and install O-Ring, item 36. Grease the O-Ring to facilitate assembly.

30) Into the Input Housing End Plate, DC-700-24, press fit Dowels, item 7, , and install O-Ring, item 3. Grease the O-Ring to facilitate assembly.

31) Assemble the Input Seal & Bearing Carrier assembly into the Housing End Plate assembly and fasten with Screws, item 40. Lay this assembly flat on a table.

32) Take the Roller-Gear assembly and fit it to the Housing End Plate. Make certain that Ball Bearing, item 35, makes proper and full contact with the Input Seal & Bearing Carrier shaft support, and that the Input Side Sun Roller-Gear Assembly shaft has made proper entry into the Ring Gear Adaptor.

33) Assemble Main Housing, DC-500-02, to the Input Housing End Plate, and bolt in place with Bolts, item 1, and Washers, item 2.

34) From the end of the Main Housing surface, measure the distance marked "x" to the top surface of the Ball Bearing which is press fitted into the Planetary End Plate, DC-700-04.

35) Into Bearing Cartridge, DC-700-09, asssemble two Ball Bearings, item 24, and Bearing Spacer, DC-700-11. Insert Output Shaft, DC-700-07, into the Bearing Cartridge-Bearing assembly, and fasten with Bearing Lockwasher and Locknut, items 22 and 23. Assemble O-Ring, item 26, to the Bearing Cartridge. Grease the O-Ring to facilitate assembly.

36) Insert this Shaft and Bearing Cartridge assembly into the Output Housing End Plate, DC-700-05, and assemble O-Ring, item 3, into the End Plate. Grease the O-Ring to facilitate assembly.

37) From the flange of the Output Housing End Plate, DC-700-05, measure the distance marked "y" to the shoulder surface on the Output Shaft, DC-700-07.

38) Subtract distance "y" from distance "x" and make Output Shaft Spacer, DC-700-08, .010 in. less than this determined distance.

39) After push fitting this spacer on the Output Shaft, the Output Housing End Plate and Shaft Assembly can be fastened to the Main Housing. The spline on the Output Shaft must make proper entry into the female spline of the Output Ring Gear Adaptor and the Output Shaft must make proper entry into the Ball Bearing in the Planetary Support Ring. The Main Housing Bolts and Washer, items 1 and 2, complete the Main Housing assembly.

40) Into Output Seal Carrier, DC-700-10, assemble Seal, item 21, and Gasket, DC-700-35. Fasten this Seal Carrier Assembly to the Bearing cartridge with Screws, item 20.

41) Install 17.2 oz ( 1.14 pints) of Santotrac 50 fluid after positioning the two pipe

plugs ports in the Main Housing on a horizontal centerline.

42) The assembly is completed by inserting two Socket Pipe Plugs, Item 51, into the Main Housing, and Quill Shaft, DC-700-27, through the Input Side Sun Roller-Gear Assembly to make spline contact with the Output Side Sun Roller-Gear Assembly.

## APPENDIX D

### DUAL INPUT DIFFERENTIAL ROLLER DRIVE (DC-500)

#### Assembly Procedure

(Numbers in parentheses refer to callouts on drawing DC-500)

1) Install eight Screw Lock Inserts, (69), into Cluster Carrier Sub Assembly, DC-500-28, (26).

2) Install twenty four Screw Lock Inserts, (53), into Main Housing, DC-500-02, (2).

3) Install six Screw Lock Inserts, (58), into Output Housing, DC-500-10, (7).

4) Install eight Screw Lock Inserts, (83), into Bearing Housing, Input, DC-500-31, (32).

5) Install four Screw Lock Inserts, (79), into Bearing Housing, Input, DC-500-31, (32).

6) Install six Screw Lock Inserts, (79), into Housing, Sun Roller Brgs, DC-500-19, (1).

7) Install two Screw Lock Inserts, (51), into Input Housing, DC-500-01, (1).

8) Assemble two J-228 Needle Roller Bearings, (55), into each of four 2nd Row Planet Rollers, Sta. Ring, DC-500-06, (5).

9) Assemble one 1903S Deep Groove Ball Bearing, (81), and one Snap Ring, (71), onto Sun Roller, Sta. Ring, DC-500-15 (31).

10) Assemble one 1903S Deep Groove Ball Bearing, (81), and one Snap Ring, (71), onto Sun Roller, Rotating Ring, DC-500-20, (17).

11) Assemble one 1908S Deep Groove Ball Bearing, (59), into Cluster Carrier Plate A, DC-500-21A, (21A).

12) Assemble one 1908S Deep Groove Ball Bearing, (59), into Cluster Carrier Plate B, DC-500-21B, (21B).

13) Assemble one 1903H Duplex Ball Bearing Pair, (61), into Housing, Sun Roller Brgs., DC-500-19, (11). Fasten with Cup Nut, Sun Roller Brgs., DC-500-33, (33). Bearings are to be installed back to back.

14) Assemble one 1903H Duplex Ball Bearing Pair, (61), into Bearing Housing, Input, DC-500-31, (32). Temporarily lock bearings in place by installing Seal Carrier, Input, DC-500-32, (29) using Socket Head Cap Screws, (78). Bearings are to be installed back to back.

15) Assemble one 1905S Deep Groove Ball Bearing, (56), and one Snap Ring, (57),

into each of eight Brg. Carriers, 2nd Row Planet Rollers, DC-500-03, (6).

16) Assemble one 2nd Row Planet Roller, Sta. Ring, DC-500-06, (5), onto each of four 2nd Row Planet Roller, Rot. Ring, DC-500-11, (10). Complete 2nd Row Planet Roller assemblies by installing two of the Step 15 assemblies onto each of the 2nd Row Planet Rollers. Fasten in place with Locknuts, DC-500-09, (8).

17) Start assembly of the roller clusters by assembling the Cluster Carrier Plate asemblies from Steps 11 and 12 to Cluster Carrier, DC-500-27, (25). Fasten with Socket Head Shoulder Screws, (69).

18) Lay the assembly from Step 17 horizontally on a flat surface. Using .112in. thick washers as approximate locating spacers, place two sets of four 1st Row Planet Rollers, DC-500-22, (20), into the Cluster Carrier Sub Assembly, moving them radially inward until they touch (Sun Roller assemblies are not yet installed). Slide four 2nd Row Planet Roller assemblies from Step 16 into place, mating each bearing Carrier with its guide in a Cluster Carrier Plate. Position these 2nd Row Planet Roller assemblies solidly against the 1st Row Planet Rollers. It should now be possible to slip Ring Rollers, DC-500-21B, (21B), andDC-500-21C, (21C), and Load Rings A, DC-500-26A, (24A), and B, DC-500-26B, (24B) into place between the 2nd Row Planet Rollers, Rot. Ring, and 2nd Row Planet Rollers, Sta. Ring. Take care to orient these four parts correctly.

19) Move the four 2nd Row Planet Roller asemblies radially outward against the two pairs of captured Ring Rollers and Load Rings. Move one set of four 1st Row Planet Rollers radially outward against the inside diameter of the Cluster Carrier. Insert Sun Roller assemblies from Steps 9 and 10 into Cluster Carrier, (25). Bring two sets of four 1st Row Planet Rollers into contact with the Sun Rollers. Bring two sets of four 2nd Row Planet Roller assemblies into contact with the 1st Row Planet Rollers. It may be necessary to adjust the axial positions of the two Sun Roller assemblies to establish proper contact. Final positioning of rollers relative to the Cluster Carrier will not be established until the Ring Rollers are in position and preloaded.

20) Bring Ring Rollers DC-500-23A, (22A), and DC-500-23B, (22B), into place on the output side roller cluster. Measure the distance "X" across the outer faces when the cluster is snugged up. The theoretical nominal dimension is 1.0834in. To apply full preload the Ring Rollers must approach each other .144in. from the zero preload position. Calculate the thickness to grind Preload Fitted Shim, DC-500-23A, (22A), as follows:

Shim thickness = 1.375 - .187 -.187 -X + .144

The nominal theoretical value for the shim thickness is .0834in. After grinding the shim to its proper thickness, apply preload to the Ring Rollers with C-Clamps until their zero preload

distance X has been reduced by .144in. Assemble Load Ring A, Ring Rollers A and B, Preloaded Fitted Shim A, and Ring Roller Carrier, DC-500-07, (9), with two Clamping Lugs A, DC-500-05A, (4A), four Clamping Lugs B, DC-500-05B, (4B), Socket Head Shoulder Screws, (70), Shoulder Bolts, (3), and Locknuts, (54).

21) Repeat Step 20 for the input side cluster. Assemble Load Ring B, Ring Rollers,C and D, Preloaded Fitted Shim B, and Grounded Load Ring, Sta. Ring, DC-500-29, (27), with two Clamping Lugs A, four Clamping Lugs B, Socket Head Shoulder Screws, (70), Shoulder Bolts, (3), and Locknuts, (54).

22) Assemble Stop Block, Grounded Load Ring, DC-500-30, (28), and Input Housing, DC-500-01, (1), with two each Socket Head Cap Screws, (74).

23) Assemble Input Housing, DC-500-01, (1), and Bearing Housing, Input, DC-500-31, (32), with Hex Head Cap Screws, (80), and Plain Washers, (67). "O" Ring, (25), must be in place and properly greased for assembly.

24) Assemble Housing, Sun Roller Brgs., DC-500-19, (11), and Output Spindle, DC-500-12, (18), using Socket Head Cap Screws, (78).

25) Install one each 1908H Duplex Ball Bearing Pair, (62), with one each Cup Spacer, Output Brgs., DC-500-13, (14), and one each Cone Spacer, Output Brgs., DC-500-14, (15), into Output Housing, DC-500-110, (7). Lock the bearings temporarily in place with Seal CArrier, Output, DC-500-16, (16), and Cap Screws, (66). Insert the assembly from Step 24, disassemble Seal Carrier, Output, (16), install Locknut, (64), and reassemble Seal Carrier, Output, (16). Measure the distance "Y" on this assembly.

26) Lay the assembly from Step 23 on parallel bars with the input side face of the Input Housing down. Carefully mate the roller cluster assembly from Step 21 with the Input Housing assembly. The Sun Roller, Sta. Ring, must enter the Stop Block, Grounded Load Ring, (28).

27) Assemble the Main Housing, DC-500-02, (2), and the assembly from step 26 with Hex Head cap screws, (72), and Plain Washers, (73). Make certain that "O" Ring, (52), is in place and properly greased for assembly. Measure distance "Z" from the face of the Main Housing to the inner race face of the 1908S Ball Bearing in Cluster Carrier Plate A. Grind the Fitted Spacer, Cluster Carrier Brg., (34), to a thickness T, where

$$T = Z - Y - .078$$

This will insure that the Wave Spring, (60), is compressed to its proper working height of .078in.

28) Disassemble Seal Carrier, Output, (16), Locknut, ((64), Output Housing, (7), Output Spindle, (18), and Housing, Sun Roller Brgs, (11).

29) Place Wave Spring, (60), and Fitted Spacer, (34), on Housing, Sun Roller Brgs., (11). Assemble onto Sun Roller, Rotating Ring, (17), and into 1908S Ball Bearing in Cluster Carrier Plate A, (21A). Remove Cup Nut, (33), install Locknut, (12), reinstall Cup Nut, (33), and install Jam Nut, Sun Roller Brgs., DC-500-08, (13). Assemble Output Spindle, (18), with Socket Head Cap Screws, (78), making certain that splines engage properly. Assemble Output Housing, (7), with Hex Head Cap Screws, (72), and Plain Washers, (73). Make certain that "O" Ring, (52), is in place and properly greased for assembly.

30) Disassemble Seal Carrier, Output, (16). Install Locknut, (64). Assemble Seal Carrier, Output, (16), with Seal, (65), and "O" Ring, (63). Make certain that the "O" Ring is properly greased for asembly. Install this assembly with Hex Head Cap Screws, (66), and Plain Washers, (67).

31) Remove Seal Carrier, Input, (29). Install Locknut, (12). Assemble "O" Ring, (76), properly greased for assembly, and Seal, (77), into Seal Carrier, Input, (29). Install this asembly using Socket Head Cap Screws, (78).

32) Install 31.4 oz ( 2.1 pints) of Santotrac 50 fluid after positioning the two pipe plug ports in the Output Housing on a horizontal centerline.

33) Install two Socket Pipe Plugs, (82). Use nylon pipe thread sealer on each plug.

## APPENDIX E

GROUNDED RING (MOMENTUM BALANCED) DRIVE (DC-400)

Assembly Procedure

( Callouts on drawing DC-400 correspond to part numbers))

1) Lap the .7874" diameter on Sun Roller, DC-400-31, for an easy push fit into 1904H Angular Contact Bearings, Part 69.

2) Lap the 1.1811" diameter on Output Spindle, Inner, DC-400-16, for an easy push fit into 1906H Angular Contact Bearings, Part 60.

3) Install twenty Screw Lock Inserts, Part 82, in Main Housing, DC-400-2.

4) Install six Screw Lock Inserts, Part 84, and five Screw Lock Inserts, Part 54, in Output Housing, DC-400-8.

5) Install four Screw Lock Inserts, Part 81, in Input Housing, DC-400-1.

6) Install ten Screw Lock Inserts, Part 82, in Grounded Ring, DC-400-3.

7) Install five Screw Lock Inserts, Part 65, in Cluster Carrier, DC-400-25.

8) Install ten Screw Lock Inserts, Part 68, in Idler Cluster Retaining Ring, DC-400-27.

9) Install one Needle Roller Bearing, Part 79, in each of five Front Bearing Carriers, 2nd Row Planet, DC-400-4.

10) Install one Needle Roller Bearing, Part 53, in each of five Rear Bearing Carriers, 2nd Row Planet, DC-400-10.

11) Install one Needle Roller Bearing, Part 64, in Output Spindle, Inner, DC-400-16.

12) Assemble two Retaining Rings, Part 52, one Planet Roller, 2nd Row, DC-400-7, and two Keys, 2nd Row Planet Roller, DC-400-36, on each of five Shafts, 2nd Row Planet, DC-400-11. Measure the gap between the 2nd Row Planet face and the Retaining Ring on the short side of the shaft. Grind each of five Fitted Spacers, 2nd Row Planet, DC-400-21, for a no shake fit. (The nominal thickness is .050"). Install the Retaining Ring, and mount the Bearing Carriers from steps 9 and 10 to complete the 2nd Row Planet Roller assemblies.

13) Install two 1906H Angular Contact Bearings, Part 60, Cup Spacer, Inner Output Bearings, DC-400-13, Cone Spacer, Inner Output Bearings, DC-400-14, and Retaining Ring, Part 57, into Output Spindle, Outer, DC-400-20. Bearings are to be installed back to back.Measure the gap between the bearing face and the Retaining Ring. Grind Fitted Cup Spacer, Inner Output Bearings, DC-400-35, for a no shake fit. (The nominal thickness is .066"). Remove Retaining Ring, Part 57, install the Fitted Cup Spacer, and reinstall the Retaining Ring. Install Retaining Ring, Part 58.

14) Install 1912H Angular Contact Bearings, Part 55, Cup Spacer, Outer Output Bearings, Part DC-400-12, Cone Spacer, Outer Output Bearings, Part DC-400-19, into Housing, Output, DC-400-08. Bearings are to be installed back to back. Install Seal Carrier, Output, DC-400-18, with five Screws, Part 62, and five Washers, Part 63. At this time do not install O-Ring, Part 56.

15) Assemble the Output Spindle, Inner, DC-400-16, to the Cluster Carrier, DC-400-25. Fasten with five Screws, Part 66.

16) Begin assembly of the cluster by placing the assembly from Step 15 with the Cluster Carrier on top and the asssembly axis vertical. Insert five Planet Rollers, 1st Row, DC-400-26, into the Cluster Carrier, resting them on spacers approximately .095" thick. Lay the Idler Cluster Retaining Ring, DC-400-27, on spacers aproximately .125" thick placed on the upper surface of the Cluster Carrier. Place one Idler Sun Roller, DC-400-29, properly oriented, on the the Idler Cluster Retaining Ring. Insert five 2nd Row Planet Roller assemblies from step 12 into the Cluster Carrier.

17) Place the Ring Rollers, DC-400-22A and DC-400-22B, over the 2nd Row Planets and move them gently toward each other. Hold them in place with C-clamps. Remove the spacers between the 1st Row Planet Rollers and the Cluster Carrier. Snug up the Ring Rollers and measure the "X" dimension on drawing DC-400. The Preload Fitted Shim, DC-400-24, is to be ground to a thickness of 1.013-X inches.

18) Using C-clamps on the Ring Rollers, slowly bring them together while oscillating or rotating the roller cluster until the separation of the outer faces is X-.109 inches. Place the Grounded Ring, DC-400-3, on the Front Bearing Carriers using spacers approximately .187" thick. Bring the second Idler Sun Roller into place and, using Shoulder Screws, Part 75, gently pull the two Idler Sun Rollers toward each other until positive contact is made with the 2nd Row Planets and the Grounded Ring. Measure the "Y" dimension on drawing DC-400. Remove the input side Idler Sun Roller and the Grounded Ring from this assembly. Grind the Preload Spacer, Idler Sun Roller, DC-400-28, to thickness Y-.576 inches.

19) Slide the step 13 assembly onto the Output Spindle, Inner, Part 16 to engage the spline in the Ring Roller Carrier to make certain that concentricity is maintained during the assembly of the main cluster. Complete the main cluster assembly by installing Load Ring, Ring Rollers, DC-400-23, Preload Fitted Shim, DC-400-24, Ring Roller Carrier, DC-400-09, three Clamping Lugs, Ring Rollers, DC-400-5A, and one each Clamping Lug, Ring Rollers, DC-400-5B and DC-400-5C. Fasten with two Shoulder Bolts, Ring Roller Clamp, DC-400-06, eight Shoulder Screws, Part 78, two Nuts, Part 50, and eight Nuts, Part 51. It may be necessary to join the output assembly from Step 14 to the Output Spindle, Inner, Part 16.

20) Install the Preload Spacer, Idler Sun Rollers, DC-400-28, and the input side Idler Sun Roller, DC-400-29. Fasten loosely with ten Shoulder Screws, Part 75. Do not torque the

screws tightly.

21) Assemble Housing, Input, DC-400-01, and Grounded Ring, DC-400-03, with ten O-Rings, Part 77, in place (properly greased), ten Cap Screws, Part 76, and ten Washers, Part 63. Install 1904H Angular Contact Bearings, Part 69. Bearings are to be installed face to face. Install Seal Carrier, Input, DC-400-32, using four Screws, Part 72, and four Washers, Part 73. At this time do not install O-Ring, Part 70, or Rotary Seal, Part 71.

22) Place the assembly from step 21 on blocks about 2" thick, with the input side face down. Join the assembly from steps 19 and 20, by inserting the Sun Roller into the 1904 Angular Contact Bearings, and the five Second Row Planet Roller Shafts inside the Grounded Ring. Turn the assembly over and remove the Seal Carrier, Input, DC-400-32. Install Locknut, Input Bearing, DC-400-30. Install O-Ring, Part 70, properly greased, in Seal Carrier, Input. Reinstall the Seal Carrier, Input, into Housing, Input.

23) Install one each O-Ring, Part 80, properly greased, into Housing, Input, (step 21 assembly) and Housing, Output, (step 14 assembly).

24) Join the input assembly from steps 21, 22 and 23 with the Main Housing, DC-400-02. Fasten with Screws, Part 67, and Washers, Part 63.

25) Join the output assembly (steps 14 and 23) with the Main Housing. Remove Seal Carrier, Output, and install Locknut, Outer Output Bearings, DC-400-15. Install O-Ring, Part 56, properly greased, in Seal Carrier, Output, and reinstall into Housing, Output.
Fasten with Screws, Part 67, and Washers, Part 63. Install Locknut, Inner Output Bearings, DC-400-17.

26) Apply torque to Idler Sun Roller Shoulder Screws, Part 75, using the access ports in the Input Housing. Torque each screw sequentially. Rotate or oscillate the drive while torqueing, until each screw is solidly bottomed. Check for smooth , counterrotation of the outputs when the Sun Roller is rotated. Install ten Socket Pipe Plugs, Part 74. Use nylon pipe thread sealer on each plug.

27) Install Rotary Seals, Parts 59, 61, and 71..

28) Install 18 oz ( 1.2 pints) of Santotrac 50 fluid after positioning the two pipe plug ports in the Output Housing on a horizontal centerline. Install two Pipe Plugs, Part 83. Use nylon pipe thread sealer on each plug.